

## ΔΙΠΛΩΜΑΤΙΚΗ ΕΡΓΑΣΙΑ ΜΕ ΤΙΤΛΟ :

# Σχεδιασμός και κατασκευή εισαγωγής κινητήρα μονοθέσιου αγωνιστικού οχήματος τύπου FSAE



Υπεύθυνος φοιτητής : Δημητράνopoulos Μενέλαος

A.M. : 18392137

Επιβλέπων καθηγητής : Δρ. Θεοδωρακάκος Ανδρέας

Αθήνα, 2/24

## Diploma Thesis:

# Design and manufacturing of the engine's inlet plenum and runners for an FSAE formula car



Student Responsible: Dimitranopoulos Menelaos

Registration Number (R.N.): 18392137

Supervisor: Dr. Theodorakakos Andreas

Athens, 2/24

## Μέλη Εξεταστικής Επιτροπής συμπεριλαμβανομένου και του Εισηγητή

Η πτυχιακή/διπλωματική εργασία εξετάστηκε επιτυχώς από την κάτωθι Εξεταστική Επιτροπή:

Α/α	ΟΝΟΜΑ ΕΠΩΝΥΜΟ	ΒΑΘΜΙΔΑ/ΙΔΙΟΤΗΤΑ	ΨΗΦΙΑΚΗ ΥΠΟΓΡΑΦΗ
1	ΝΙΚΑΣ Κ.Σ.	ΚΑΘΗΓΗΤΗΣ	
2	ΘΕΟΔΩΡΑΚΑΚΟΣ Α.	ΑΝΑΠΛΗΡΩΤΗΣ ΚΑΘΗΓΗΤΗΣ	
3	ΤΣΟΛΑΚΗΣ Α.	ΑΝΑΠΛΗΡΩΤΗΣ ΚΑΘΗΓΗΤΗΣ	

### ΔΗΛΩΣΗ ΣΥΓΓΡΑΦΕΑ ΔΙΠΛΩΜΑΤΙΚΗΣ ΕΡΓΑΣΙΑΣ

Ο κάτωθι υπογεγραμμένος Δημητρανόπουλος Μενέλαος του Αναστασίου, με αριθμό μητρώου 18392137 φοιτητής του Πανεπιστημίου Δυτικής Αττικής της Σχολής Μηχανικών του Τμήματος Μηχανολόγων Μηχανικών, δηλώνω υπεύθυνα ότι:

«Είμαι συγγραφέας αυτής της διπλωματικής εργασίας και ότι κάθε βοήθεια την οποία είχα για την προετοιμασία της είναι πλήρως αναγνωρισμένη και αναφέρεται στην εργασία. Επίσης, οι όποιες πηγές από τις οποίες έκανα χρήση δεδομένων, ιδεών ή λέξεων, είτε ακριβώς είτε παραφρασμένες, αναφέρονται στο σύνολό τους, με πλήρη αναφορά στους συγγραφείς, τον εκδοτικό οίκο ή το περιοδικό, συμπεριλαμβανομένων και των πηγών που ενδεχομένως χρησιμοποιήθηκαν από το διαδίκτυο. Επίσης, βεβαιώνω ότι αυτή η εργασία έχει συγγραφεί από μένα αποκλειστικά και αποτελεί προϊόν πνευματικής ιδιοκτησίας τόσο δικής μου, όσο και του Ιδρύματος.

Παράβαση της ανωτέρω ακαδημαϊκής μου ευθύνης αποτελεί ουσιώδη λόγο για την ανάκληση του πτυχίου μου».

\*Επιθυμώ την απαγόρευση πρόσβασης στο πλήρες κείμενο της εργασίας μου μέχρι ..... και έπειτα από αίτηση μου στη Βιβλιοθήκη και έγκριση του επιβλέποντα καθηγητή.

Ο/Η Δηλών/ούσα



\* Ονοματεπώνυμο /Ιδιότητα

(Υπογραφή)

Ψηφιακή Υπογραφή Επιβλέποντα

\* Σε εξαιρετικές περιπτώσεις και μετά από αιτιολόγηση και έγκριση του επιβλέποντα, προβλέπεται χρονικός περιορισμός πρόσβασης (embargo) 6-12 μήνες. Στην περίπτωση αυτή θα πρέπει να υπογράψει ψηφιακά ο/η επιβλέπων/ουσα καθηγητής/τρια, για να γνωστοποιεί ότι είναι ενημερωμένος/η και συναινεί. Οι λόγοι χρονικού αποκλεισμού πρόσβασης περιγράφονται αναλυτικά στις πολιτικές του Ι.Α. (σελ. 6):

[https://www.uniwa.gr/wp-content/uploads/2021/01/%CE%A0%CE%BF%CE%BB%CE%B9%CF%84%CE%B9%CE%BA%CE%B5%CC%81%CF%82\\_%CE%99%CE%B4%CF%81%CF%85%CE%BC%CE%B1%CF%84%CE%B9%CE%BA%CE%BF%CF%85%CC%81\\_%CE%91%CF%80%CE%BF%CE%B8%CE%B5%CF%84%CE%B7%CF%81%CE%B9%CC%81%CE%BF%CF%85\\_final.pdf](https://www.uniwa.gr/wp-content/uploads/2021/01/%CE%A0%CE%BF%CE%BB%CE%B9%CF%84%CE%B9%CE%BA%CE%B5%CC%81%CF%82_%CE%99%CE%B4%CF%81%CF%85%CE%BC%CE%B1%CF%84%CE%B9%CE%BA%CE%BF%CF%85%CC%81_%CE%91%CF%80%CE%BF%CE%B8%CE%B5%CF%84%CE%B7%CF%81%CE%B9%CC%81%CE%BF%CF%85_final.pdf)

## Περίληψη-Εισαγωγή

Η παρούσα διπλωματική εργασία πραγματεύεται τον τρόπο με τον οποίο μελετάται, καταγράφεται και μοντελοποιείται ένας 4χρονος κινητήρας ΜΕΚ με σκοπό να χρησιμοποιηθεί σε πρωτότυπο αγωνιστικό μονοθέσιο τύπου formula SAE. Παρακάτω παρουσιάζεται η προσέγγιση που ακολούθησε η φοιτητική ομάδα Poseidon Racing team για την αγωνιστική σεζόν 2022-2023. Αρχικά πραγματοποιήθηκε προσεκτική μελέτη τόσο στους κανονισμούς του διαγωνισμού όσο και στο απαραίτητο θεωρητικό υπόβαθρο που χρησιμοποιήθηκε. Έπειτα, εφόσον τέθηκαν οι στόχοι της ομάδας, πραγματοποιήθηκε μελέτη του προγράμματος μοντελοποίησης Ricardo καθώς και κατανόηση τόσο του τρόπου λειτουργίας του σε βάθος με σκοπό την ακριβέστερη προσέγγιση του κινητήρα όσο και των μεγεθών που χρησιμοποιούνται. Με την επιλογή του κινητήρα, μετρήθηκαν τα απαιτούμενα μεγέθη για την κατάλληλη προσομοίωση του και δημιουργήθηκε το πρότυπο μοντέλο. Στην συνέχεια, πάνω στο πρωτότυπο μοντέλο αυτό διαστασιολογήθηκαν πρώτα το plenum (δεξαμενή αέρα) και στην συνέχεια οι αυλοί (runners) με σκοπό την μεγιστοποίηση του ογκομετρικού βαθμού απόδοσης και της ομαλοποίησης της καμπύλης ροπής στις στροφές (RPM) ενδιαφέροντος. Καταληκτικά, πραγματοποιείται σύγκριση των παραγόμενων διαγραμμάτων με τα αντίστοιχα του πρωτότυπου μοντέλου του κινητήρα. Τέλος, επιλέγονται οι τελικές διαστάσεις, σχεδιάζεται η τελική εισαγωγή στον τρισδιάστατο μοντελοποιητή και αξιολογείται ροϊκά και στατικά με την χρήση προγραμμάτων CFD και FEA αντίστοιχα. Επιλέγεται το τελικό σχέδιο, κατασκευάζεται και τοποθετείται στο όχημα. Η διπλωματική ολοκληρώνεται με συνολικά συμπεράσματα και παρατηρήσεις.

## Summary

This diploma thesis deals with the way in which a 4-stroke MEK engine is studied, recorded and modeled in order to be used in a prototype formula SAE racing car. Below is presented the approach followed by the student team Poseidon Racing team for the 2022-2023 racing season. Initially, careful study was carried out both in the competition regulations and in the necessary theoretical background used. Then, once the goals of the team were set, a study of the Ricardo modeling program was carried out as well as an understanding of how it works in depth in order to approach the engine more accurately and the sizes used. With the selection of the engine, the required sizes for its proper simulation were measured and the standard model was created. Then, on this prototype model, first the plenum (air tank) and then the intake runners were dimensioned in order to maximize the volumetric efficiency and the normalization of the torque curve at revs (RPM) of interest. Finally, the produced diagrams are compared with those of the original engine model. Finally, the final dimensions are selected, the final input to the three-dimensional modeler is designed and evaluated flowingly and statically using CFD and FEA programs respectively. The final design is selected, manufactured and installed on the vehicle. The thesis concludes with comprehensive conclusions and observations.

### Πρόλογος – Ευχαριστίες

Η παρούσα διπλωματική εργασία αναφέρεται σε ένα κομμάτι της προσπάθειας μιας ομάδας φοιτητών για την κατασκευή ενός πρωτότυπου μονοθέσιου οχήματος τύπου formula SAE. Το αυτοκίνητο που κατασκευάστηκε αποτελεί προϊόν αρκετού κόπου, προσωπικής προσπάθειας, αμέτρητων θησείων και αφοσίωσης πολλών ατόμων. Από το 2017-2018 που άρχισε η συστηματική αναδιάρθρωση της ομάδας, το αυτοκίνητο σχεδιάστηκε σε ένα φύλλο χαρτί και βήμα βήμα κατασκευάστηκε και εκπλήρωσε τον στόχο του. Να συμμετάσχει στον διαγωνισμό formula SAE της Ουγγαρίας το 2023. Ως μέλος της ομάδας από τα πρώτα έτη μου στο πανεπιστήμιο θα ήθελα σε αυτό το κομμάτι της διπλωματικής μου να ευχαριστήσω κάποιους ανθρώπους που συνέβαλαν τόσο στον σχεδιασμό και την κατασκευή του οχήματος αλλά και της ομάδας άμεσα και έμμεσα όσο και στην προσωπική μου πρόοδο ως μηχανικός αλλά και ως άνθρωπος.

Πρώτα από όλα θα ήθελα να ευχαριστήσω την οικογένεια μου και τους φίλους μου για την ακατάπαυστη ψυχολογική υποστήριξη που μου έδωσαν και την υπομονή τους με την ελλιπή παρουσία μου από κοντά τους. Θα ήθελα επίσης να ευχαριστήσω τον Κ. Κωνσταντίνο Στεργίου που ήταν πάντα δίπλα μας ως επιστημονικός υπεύθυνος της ομάδας. Τον Κ. Ανδρέα Θεοδωρακάκο, επιβλέπον καθηγητή της παρούσας διπλωματικής, για τις πολύτιμες συμβουλές του και την ατελείωτη όρεξή του να συμβάλει στο έργο της ομάδας με οποιονδήποτε τρόπο. Αντιστοίχως, θα ήθελα να ευχαριστήσω και τους Κ. Παναγιώτη Τσολάκη, Κ. Μάριο Τσαϊνή, Κ. Δημήτρη Παπαγεωργίου, καθηγητές μας αλλά και σύμβουλοί μας, πίστεψαν και υποστήριξαν το έργο της ομάδας μέχρι την ολοκλήρωση του στόχου της και συνεχίζουν να την υποστηρίζουν.

Δεν θα μπορούσα να παραλείψω να ευχαριστήσω τα μέλη της ομάδας αυτής, παλιά και νέα. Μαζί ονειρευτήκαμε, σχεδιάσαμε, κατασκευάσαμε, μαλώσαμε, γελάσαμε, μάθαμε, κοιμηθήκαμε...φάγαμε και μοιραστήκαμε αυτό το υπέροχο ταξίδι γεμάτο όμορφες εμπειρίες. Ειδικές ευχαριστίες θα ήθελα να δώσω στον αρχηγό – υπεύθυνο του project Αλέξανδρο Καραβίτη για τον επαγγελματισμό του και την υποδειγματική διαχείριση της ομάδας, τον Βασίλειο Γιολδάση για τον δυναμισμό και το πείσμα που προσέφερε, τον Γεώργιο Μιχαλόπουλο για τις ατελείωτες ώρες μηχανουργικών κατεργασιών και γνώσεων προσέφερε, τον Στράτο Παππά για την εργατικότητα που έδειξε από την πρώτη στιγμή, τον Παναγιώτη Παπαδημητρίου για τις απέραντες γνώσεις ηλεκτρολογικών και την όρεξη να τις μοιραστεί και τον Γεώργιο Παπανδρέου για την εφευρετικότητα και την υπομονή του στην ολοκλήρωση του στόχου της ομάδας. Ακόμα, θα ήθελα να ευχαριστήσω τους Φίλιππο Κουκλάκη, Γιάννη Μαύρο, Γιάννη Μπόκα, Χάρη Κοντονάσιο, Αργύρη Καστανιώτη και Θοδωρή Γκότση οι οποίοι άλλοτε συμβουλευτικά και άλλοτε έμπρακτα πρόσφεραν απλόχερα τις γνώσεις τους και τις ιδέες τους. Τέλος, ευχαριστώ όλα τα μέλη της ομάδας που συνεργαστήκαμε όλα αυτά τα χρόνια.

Ολοκληρώνοντας, θα ήθελα να ευχαριστήσω τους χορηγούς της ομάδας, τους ανθρώπους εκείνους δηλαδή που μας αφουγκράστηκαν, μας πίστεψαν και απλόχερα μας παρείχαν είτε τα προϊόντα τους είτε τις υπηρεσίες τους χωρίς να αναλογιστούν τα έξοδά τους και μας βοήθησαν να κάνουμε το όνειρά μας πραγματικότητα. Ευχαριστώ όμως και αυτούς που αρνήθηκαν να μας βοηθήσουν καθώς μας έκαναν πιο δυνατούς και παρόλη την στεναχώρια, μας έκαναν να δουλέψουμε πιο σκληρά.

## Contents

ΔΗΛΩΣΗ ΣΥΓΓΡΑΦΕΑ ΔΙΠΛΩΜΑΤΙΚΗΣ ΕΡΓΑΣΙΑΣ .....	4
Περίληψη-Εισαγωγή .....	5
Summary .....	5
Πρόλογος – Ευχαριστίες .....	6
List of Tables .....	10
List of Figures .....	10
1. Introduction .....	14
1.1. The Formula Student Competition (FSAE) .....	14
1.2. Poseidon Racing Team.....	15
1.3. Rules – Objectives – Limitations.....	16
1.4. Delimitations – Clarifications .....	21
1.5. Methodology.....	22
2. Basic Engine Theory Principals.....	22
2.1. Introduction, Historical Perspective and Engine classifications .....	22
2.2. Engine Operating Cycles.....	23
2.3. Spark-Ignition Engine Operation .....	24
2.4. Combustion .....	26
2.5. Heat Transfer .....	29
2.6. Power and Torque .....	30
2.7. Volumetric Efficiency.....	31
2.8. Other significant operating parameters.....	31
2.8.1. Mean Effective Pressure.....	31
2.8.2. Specific fuel consumption and efficiency.....	32
2.8.3. Air/Fuel and Fuel/Air Ratios .....	32
2.9. Friction and Lubrication .....	32
2.10. General Engine Design Goals – Theory Summary.....	33
3. Ricardo Program – Air flow Theory .....	34
3.1. The Ricardo Program - Engine Simulation.....	34
3.2. Intake Fundamentals.....	35

3.2.1. Frictional Losses .....	36
3.2.2. Heat Transfer .....	36
3.2.3. Valve timing.....	36
3.2.4. Airflow Chocking .....	37
3.2.5. Tuning - Reverse flow into the intake.....	37
3.3. Basic Program Parameters .....	38
3.3.1. Discharge Coefficient .....	39
3.3.2. Friction correlation.....	40
3.3.3. Discretization length .....	41
3.3.4. Heat Transfer Model .....	42
3.3.5. Combustion Model.....	42
3.3.6. Complex Y-Junction .....	44
4. Engine Selection – Specifications Identification.....	46
4.1. Engine Choice-Engine Specifications.....	46
4.2. Real life Measurements .....	48
4.3. Data insert into Engine Model .....	52
4.3.1. Simulation Controls.....	52
4.3.2. Intake Ambient.....	53
4.3.3. Ducts (Valve ports) .....	53
4.3.4. Fuel Injectors.....	56
4.3.5. Cylinder - Engine .....	58
4.3.6. Variables.....	62
5. Stock Engine Ricardo Model .....	63
5.1. Model Overview.....	66
5.2. Run Data – Diagrams.....	67
5.3. Comments.....	68
5.4. Final Results .....	68
6. Restrictor and Throttle-body Implementation.....	69
6.1. Restrictor Model Overview .....	69
6.2. Throttle-body Model Overview.....	71



7.	Final Engine Model.....	73
7.1.	Model Overview.....	74
7.2.	Runners.....	74
7.3.	Plenum.....	75
7.4.	Run Data – Diagrams.....	76
7.5.	Final Results & Comments.....	84
8.	Model Data Comparison.....	84
8.1.	Key Differences between Stock and Race engine.....	84
8.2.	Goal Assessment.....	88
9.	Final Dimensioning and CFD study.....	88
9.1.	General Limitations.....	88
9.2.	Final Design Choices and Dimensions.....	89
9.3.	Basic Parameters for ANSYS Study and ANSA pre-processing.....	91
9.4.	Meta Analysis.....	94
10.	Manufacturing, FEA Analysis and vehicle placement.....	97
10.1.	Manufacturing Method.....	97
10.2.	Material Choice.....	98
10.3.	FEA Analysis.....	104
10.4.	Final Assembly and First Tests.....	106
11.	Results.....	107
11.1.	Competition Results.....	107
11.2.	Acknowledgments – Comments.....	108
12.	Appendix.....	111
12.1.	Ricardo Diagrams.....	111
	References.....	121

## List of Tables

Table 1 Competition Points Table .....	16
Table 2 Engine Type Evaluation Table .....	47
Table 3 Yamaha R6 2006 Engine Specifications .....	48
Table 4 Yamaha R6 2006 Intake Flange Data.....	48
Table 5 Yamaha R6 2006 Intake Throttle body Data.....	49
Table 6 Intake Valve Port Data for Ducts and Y-Junction .....	49
Table 7 Exhaust Valve Port Data for Ducts and Y-Junction.....	50
Table 8 Variables Table for each case in the Ricardo Program .....	62
Table 9 Variables Table for each case in the Ricardo Program .....	63
Table 10 Restrictor Data Table .....	69
Table 11 Basic parameters for Ansys software .....	91

## List of Figures

Figure 1 PR-23 at Hungaroring .....	15
Figure 2 Skid-Pad Track Configuration .....	17
Figure 3 Surface Envelope (Dotted Black Line).....	18
Figure 4 Intake Configuration Allowed for the competition.....	19
Figure 5 Rollover Protection Envelope .....	19
Figure 6 Basic Geometric Values of an Engine .....	23
Figure 7 An Illustration of the 4 Strokes of an ICE Engine .....	24
Figure 8 Types of Injection Systems a) Single Point b) Multi Point c) Direct Injection .....	25
Figure 9 Sequence of events in four-stroke spark-ignition engine operating cycle. Cylinder pressure $p$ , Cylinder Volume ( $V/V_{max}$ ) and mass fraction burned $x_b$ are plotted against crank angle .....	25
Figure 10 Energy Distribution for engines at Maximum Power .....	29
Figure 11 Brake Power, Coolant Load, Sensible Exhaust Enthalpy and Miscellaneous Energy Transfers as Percent of Flow x Heating Value at Road-Load Operating Conditions .....	30
Figure 12 Two Different Engines Producing the Same Torque at the End of the Crankshaft .....	30
Figure 13 Comparison of Major Categories of Friction Loses .....	33
Figure 14 Operation Process for Dimensions in Ricardo Software .....	35
Figure 15 Effect of Intake Runner Length on V.E. on four-cylinder Engine .....	37
Figure 16 Reference Geometry for Discharge Coefficient Calculation .....	40
Figure 17 Discretization Length Basic Explanation with Different Number of Elements.....	41
Figure 18 SI Wiebe Combustion Model in WAVE and Table of Properties.....	44
Figure 19 Complex Y-Junction Illustration of Intake (Left) and Exhaust (Right) of the Yamaha R6 Engine .....	45
Figure 20 Complex Y-Junction Modeling Dimensions.....	46
Figure 21 Yamaha R6 2006 Stock Intake Flange .....	48
Figure 22 Yamaha R6 2006 Throttle Body.....	49
Figure 23 Schematic of Intake and Exhaust Port Geometrical Analysis .....	49
Figure 24 Intake Ports of the Yamaha R6 Cylinder Head.....	49
Figure 25 Exhaust Ports of Yamaha R6 Cylinder Head .....	50
Figure 26 Top View of Yamaha R6 Cylinder Head .....	50
Figure 27 Intake Valve Lift - Crank Angle Diagram .....	50
Figure 28 Intake and Exhaust Camshafts of Yamaha R6 Cylinder Head.....	51
Figure 29 Exhaust Valve Lift-Crank Angle Diagram.....	51
Figure 30 Valve Overlap Diagram .....	51
Figure 31 Simulation Control Settings for Ricardo Program .....	52

Figure 32 Ambient Settings for Ricardo Program .....	53
Figure 33 Coefficients and Initial Conditions for Valve Port Ducts .....	54
Figure 34 Duct (Intake Valve Port Settings) for Ricardo Program .....	54
Figure 35 Duct (Exhaust Valve Port Settings) for Ricardo Program.....	55
Figure 36 Intake and Exhaust Valve Y-junction Settings.....	55
Figure 37 Injector Settings for Ricardo Program .....	56
Figure 38 Duct Data and Injector Placement on Duct Port .....	57
Figure 39 Throttle Valve Settings for Ricardo Program .....	57
Figure 40 Injector Properties for Ricardo Program .....	57
Figure 41 Engine Settings and Geometrical Data for Ricardo Program .....	58
Figure 42 Cylinder and Valve Settings for Ricardo Program .....	59
Figure 43 Piston and Cylinder Settings for Ricardo Program .....	59
Figure 44 Intake Valve Lift Profile .....	60
Figure 45 Piston and Cylinder Settings for Ricardo Program .....	60
Figure 46 Exhaust Valve Lift Profile.....	61
Figure 47 Flow Coefficient Diagrams for Intake (left) and Exhaust (right).....	61
Figure 48 Hydraulic Dynamometer Flange Design .....	63
Figure 49 Yamaha R6 Engine Dyno Diagram .....	64
Figure 50 Brake Power and Torque Diagrams of a 0.6L SuperSport Motorbike Engine .....	65
Figure 51 Simulated Model of Stock Engine made by the Team (Throttle Body) .....	66
Figure 52 Power and Torque Diagrams of the Team's Model .....	67
Figure 53 Comparison between Team's Model and 0.6L SuperSport Model.....	67
Figure 54 Taper Angle implementation in Ricardo Software .....	69
Figure 55 Bell-Mouth Modeling in Ricardo Software.....	70
Figure 56 Team's Modeled Restrictor.....	70
Figure 57 Duct Data used in Restrictor Model .....	71
Figure 58 Throttle Valve Geometry Settings for Final Model .....	72
Figure 59 Final Intake System Model .....	72
Figure 60 Final Team's Engine Model .....	74
Figure 61 Power Diagram for 3L Plenum and Different Length Runners. The last number refers to the length of the tested runner in mm. ....	76
Figure 62 Torque Diagram for 3L Plenum and Different Length Runners. The last number refers to the length of the tested runner in mm. ....	77
Figure 63 Comparison for 3L plenum and the two best runner options regarding torque and power. The last number refers to the length of the tested runner in mm. ....	78
Figure 64 Power Diagram for optimal runner option and different plenum volumes. The first number refers to the volume of the tested plenum in L.....	79
Figure 65 Torque Diagram for optimal runner option and different plenum volumes. The first number refers to the volume of the tested plenum in L.....	79
Figure 66 Max Power Differential at 7500rpm between the best runner options. The two numbers correspond to the different length in mm. ....	80
Figure 67 Peak Power Differential between the best runner options. The two numbers correspond to the different length in mm.....	80
Figure 68 Max Power Differential at 7500rpm between the best runner options. The two numbers correspond to the different length in mm. ....	81
Figure 69 Peak Torque Differential between the best runner options. The two numbers correspond to the different length in mm.....	81

Figure 70 Volumetric Efficiency Diagram for a Range of Different Plenums Between the Best Runner Options. The first number corresponds to plenum volume in L whilst the last to runner length in mm. ....	82
Figure 71 Volumetric Flow Along the Intake for 180mm (Left) and 240mm (Right) Runners .....	83
Figure 72 Comparison for Optimal Runner Diameter.....	83
Figure 73 Comparison between Stock R6 Ricardo Model vs Modified Ricardo Model.....	85
Figure 74 Comparison of Volumetric Efficiency Between Stock and Modified R6 Model.....	86
Figure 75 BMEP and BSFC Comparison Between Stock and Modified Model.....	87
Figure 76 Envelope Visualization on Cad Software .....	89
Figure 77 Intake Assembly Design Evolution Diagram.....	90
Figure 78 Batch Meshing Scenarios for Different Intake Parts and Meshing Visualization from Cut Plane.....	92
Figure 79 Basic Mesh Parameters for Each Intake Part. Restrictor, Inlet and Outlet (Left), Runners (Middle), Plenum (Right). ....	93
Figure 80 Velocity Magnitude (Left) and Turbulent Intensity (Right) for Ball Geometry.....	94
Figure 81 Vorticity Magnitude Diagram for Cone Geometry .....	94
Figure 82 Pressure Diagram for Disc Geometry.....	94
Figure 83 Velocity Magnitude Diagram for Final Intake on a Selected Plane (Left) and Turbulent Kinetic Energy on a Selected Plane (Right).....	96
Figure 84 Vorticity Diagram for Final Intake on a Selected Plane (Left) and with Flow Line Visualization (Right).....	96
Figure 85 Velocity Diagram for Final Intake on a Selected Plane (Left) and with Flow Line Visualization (Right) .....	96
Figure 86 Total Pressure on a Selected Plane (Left) and Vorticity Magnitude with Flow Line Visualization (Right) ....	97
Figure 87 Different 3D Printing Methods Available for the Intake Assembly.....	99
Figure 88 Mechanical Properties for PAHTCF15 Material.....	100
Figure 89 Process of Assessing the PAHTCF15 Material with the Help of Test Pieces.....	101
Figure 90 Issues of PAHTCF15 Components After Printing.....	102
Figure 91 ASTM D638-14 Test Piece Dimensions .....	103
Figure 92 Mechanical Properties for PA12 Material .....	103
Figure 93 Meshing Parameters for FEA Model .....	104
Figure 94 Factor of Safety Visualization on Intake Assembly.....	105
Figure 95 Equivalent Stress Visualization on Intake Assembly.....	105
Figure 96 Deformation Visualization on Intake Assembly.....	105
Figure 97 Final Intake Assembly in Cad Software .....	106
Figure 98 Post Processing and Testing of Final Manufactured Assembly on Engine.....	106
Figure 99 Plenum Redesign on Cad Software and Issue Area.....	107
Figure 100 The PR-23 Race car During the Dynamic and Static Events of the Competition .....	108
Figure 101 Dyno Diagram for PR-23 Post Competition.....	109
Figure 102 Torque Diagram for 3L Plenum and Different Length Runners. The last number refers to the length of the tested runner in mm. ....	111
Figure 103 Power Diagram for 3L Plenum and Different Length Runners. The last number refers to the length of the tested runner in mm. ....	111
Figure 104 Power Diagram for 3.5L Plenum and Different Length Runners. The last number refers to the length of the tested runner in mm. ....	112
Figure 105 Torque Diagram for 3.5L Plenum and Different Length Runners. The last number refers to the length of the tested runner in mm. ....	112
Figure 106 Power Diagram for 4L Plenum and Different Length Runners. The last number refers to the length of the tested runner in mm. ....	113
Figure 107 Torque Diagram for 4L Plenum and Different Length Runners. The last number refers to the length of the tested runner in mm. ....	113

<i>Figure 108 Power Diagram for 4.5L Plenum and Different Length Runners. The last number refers to the length of the tested runner in mm. ....</i>	<i>114</i>
<i>Figure 109 Torque Diagram for 4.5L Plenum and Different Length Runners. The last number refers to the length of the tested runner in mm. ....</i>	<i>114</i>
<i>Figure 110 Torque Diagram for 5L Plenum and Different Length Runners. The last number refers to the length of the tested runner in mm. ....</i>	<i>115</i>
<i>Figure 111 Power Diagram for 5L Plenum and Different Length Runners. The last number refers to the length of the tested runner in mm. ....</i>	<i>115</i>
<i>Figure 112 Power Diagram for 240mm and 180mm Runners and Different Plenum Volumes.....</i>	<i>116</i>
<i>Figure 113 Torque Diagram for 240mm and 180mm Runners and Different Plenum Volumes.....</i>	<i>116</i>
<i>Figure 114 Pressure Diagram at Runner No1. The Red Vertical Lines Indicate the Intake Stroke. ....</i>	<i>117</i>
<i>Figure 115 Pressure Diagram at Runner No2. The Red Vertical Lines Indicate the Intake Stroke. ....</i>	<i>117</i>
<i>Figure 116 Pressure Diagram at Runner No4. The Red Vertical Lines Indicate the Intake Stroke. ....</i>	<i>118</i>
<i>Figure 117 Pressure Diagram at Runner No3. The Red Vertical Lines Indicate the Intake Stroke. ....</i>	<i>118</i>
<i>Figure 118 Volumetric Flow vs Crank Angle for Runners 1 (Above) and 2 (Below) .....</i>	<i>119</i>
<i>Figure 119 Volumetric Flow vs Crank Angle for Runners 3 (Above) and 4 (Below) .....</i>	<i>120</i>

## 1. Introduction

### 1.1. The Formula Student Competition (FSAE)

Formula SAE is a student design competition organized by SAE International (known as the Society of Automotive Engineers, SAE). SAE International is a global association of more than 128,000 engineers and related technical experts in the aerospace, automotive and commercial-vehicle industries. Their core competencies are life-long learning and voluntary consensus standards development. (Wikipedia, n.d.)

The competition started in 1980 by the SAE student branch at the University of Texas at Austin. Ron Matthews, then an untenured Assistant Professor at the University of Texas, started the UT student branch of SAE in January of 1980. A month later, three of the new officers (Mike Best, Robert Edwards, and John Tellkamp) told him they had decided to enter SAE's Mini Indy competition which was asphalt racing using a 5-hp small Briggs & Stratton engine); unfortunately, the competition was no longer being organized. The four of them discussed their options and decided that they wanted to start a new asphalt racing competition with a new name (Formula SAE, coined by Professor Matthews) and new rules, the most important of which was that the teams could choose any 4-stroke engine including Wankels and Diesels but the intake was restricted to one inch (25.4 mm) in diameter. Engine modifications were not only allowed but encouraged. Professor Matthews called Bob Sechler, Manager of Collegiate Design Series competitions to ask whether SAE would support this new competition and Mr. Sechler enthusiastically gave his approval. In 2010, after years of the Formula SAE competitions seeing growth not only in the United States but internationally, SAE International recognized three more international competitions as part of the Official Series; Formula Student Japan, Formula Student Germany, and Formula Student Austria. (SAE International, n.d.)

Students build a single seated formula style car with which they can compete against teams from all over the world. The international design competition is not won solely by the team with the fastest car, but rather by the team with the best overall package of construction, performance, and financial and sales planning.

Formula Student challenges the team members to go the extra step in their education by incorporating into its intensive experience in building and manufacturing as well as considering the economic aspects of the automotive industry. Teams take on the assumption that they are a manufacturer developing a prototype to be evaluated for production. The car must show very good driving characteristics such as acceleration, braking and handling. It should be offered at a very reasonable cost and be reliable and dependable. Additionally, the car's market value increases through other factors such as aesthetics, comfort and the use of readily available, standard purchase components.

The challenge the teams face is to compose a complete package consisting of a well-constructed single seated formula style car and a sales plan that best matches these given criteria. The decision is made by a jury of experts from the motorsport, automotive and supplier industries. The jury will judge every team's car and sales plan based on construction, cost planning and sales presentation. The rest of the judging will be done out on the track, where the students demonstrate in a number of performance tests how well their self-built cars fare in their true environment. (Formula Student Germany, n.d.)

## 1.2. Poseidon Racing Team

Poseidon team is a research student group from the University of Western Attica, the third largest university in Greece, that designs and builds single-seater vehicles. The team started as a simple idea in 2012 from two mechanical engineering students named Trireme, participating in competitions such as the SHELL ECO-MARATHON, while also preparing for entry into the world of the Formula Student competition.

The vehicles it has created so far are the Dominator 1 and its follower Dominator 2 (vehicles that participated in competitions without recorded performance due to construction problems), "RENA" with which the team competed for 4 years and collected enough data that helped it design and build the "ORCA". The vehicle "ORCA" managed to be awarded both for its design and its performance on the track finishing 1<sup>st</sup> in the eastern Europe competition. It also holds the Panhellenic Record in the Prototype Battery Electric category of the competition which was set at 507km/kWh this year.

In 2021 Poseidon participated for the very first time in the Concept Class category of the UK Formula Student competition, where it claimed 51st position among 72 teams. In 2023 the team made its maiden appearance in the world of Formula Student, where it participated in Formula Student East with the very first vehicle made named "Orion - PR23". After the event was completed, it claimed the 10th position in the overall standings, claiming 5<sup>th</sup> place at the endurance event and 6<sup>th</sup> place at the Engineering Design event.



Figure 1 PR-23 at Hungaroring

For the 2023-2024 season the goal is to successfully participate in the Formula Student 2024 competition, with a new, electric vehicle, as well as in the Shell Eco-Marathon 2024, having completed the necessary studies and the reconstruction of the components of the single-seater vehicle "ORCA".

### 1.3. Rules – Objectives – Limitations

As mentioned previously, the competition challenges teams of university students to conceive, design, fabricate, develop and compete with small, formula style, race cars. It is split into the following classes:

- Internal Combustion Engine Vehicle (CV)
- Electric Vehicle (EV)

All vehicles must meet particular requirements defined in the rulebook which is published and renewed every year for each competition. The competition starts with a series of technical inspections to check the vehicle for safety and compliance with the rules. After the inspection, the competition is divided into a series of static and dynamic events, each one with a different scoring formula and procedure. The maximum points awarded to each event, the points total and some further information for each event can be seen below and in the following table. The team with the most overall points will win the competition for its class.

*Table 1 Competition Points Table*

	CV & EV
Static Events:	
Business Plan Presentation	75 Points
Cost & Manufacturing	100 Points
Engineering Design	150 Points
Dynamic Events:	
Skidpad	50 Points
DV Skidpad	75 Points
Acceleration	50 Points
DV Acceleration	75 Points
Autocross	100 Points
DV Autocross	-
Endurance	250 Points
Efficiency	75 Points
Trackdrive	-
Overall	<b>1000 Points</b>

**Business Plan Presentation (BPP):** The objective of the BPP is to evaluate the team’s ability to develop and deliver a comprehensive business model. The judges should be treated as if they were potential investors or partners for the presented business model.

**Cost & Manufacturing:** The objective of the cost and manufacturing event is to evaluate the team’s understanding of the manufacturing processes and costs associated with the construction of a prototype race car. This includes trade off decisions between content and cost, make or buy decisions and understanding the differences between prototype and mass production.

**Engineering Design Event:** The concept of the design event is to evaluate the student’s engineering process and effort that went into the design of a vehicle, meeting the intent of the competition.



Proprietary components and systems that are incorporated into the vehicle design as finished items are not evaluated as a student designed unit, but are only assessed on the team's selection and application of that unit.

**Skidpad:** The skidpad track consists of two pairs of concentric circles in a figure of eight pattern. The vehicle will enter perpendicular to the figure of eight and will take one full lap on the right circle to establish the turn. The next lap will be on the right circle and will be timed. Immediately following the second lap, the vehicle will enter the left circle for the third lap. The fourth lap will be on the left circle and will be timed. Immediately upon finishing the fourth lap, the vehicle will exit the track perpendicular to the figure of eight and moving in the same direction as entered.

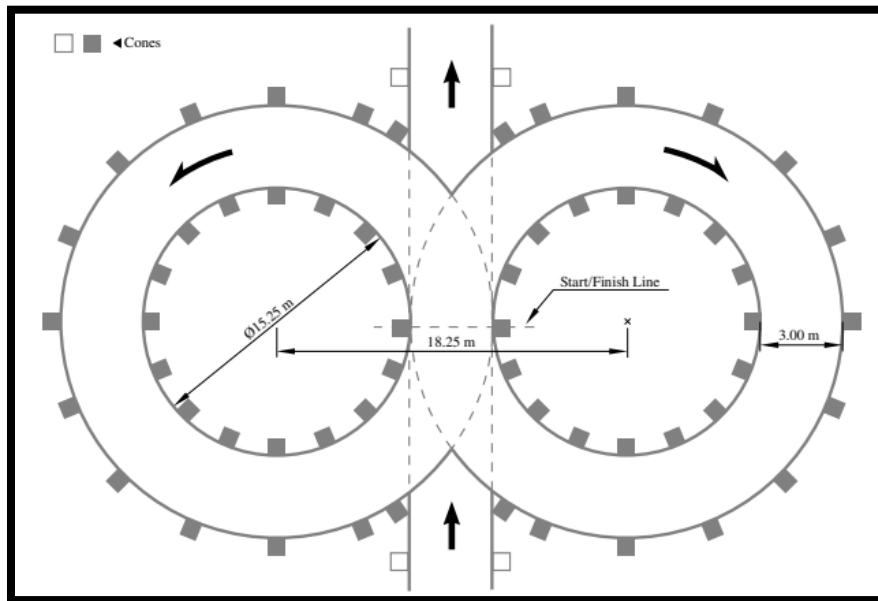


Figure 2 Skid-Pad Track Configuration

**Acceleration:** The acceleration track is a straight line with a length of 75 m from starting line to finish line. The track is at least 3 m wide. Cones are placed along the track at intervals of about 5 m. Cone locations are not marked on the pavement.

**Autocross:** The autocross track layout is a handling track built to the following guidelines:

- Straights: No longer than 80 m
- Constant Turns: up to 50 m diameter
- Hairpin Turns: Minimum of 9 m outside diameter (of the turn)
- Slaloms: Cones in a straight line with 7.5 m to 12 m spacing
- Miscellaneous: Chicanes, multiple turns, decreasing radius turns, etc. The minimum track width is 3 m.
- The length of the autocross track is less than 1.5 Km.

**Endurance:** The endurance track layout is a closed lap circuit built to the same guidelines as the Autocross event. The length of one lap of the endurance track is approximately 1km. The complete length of the track is approximately 22km.

Vehicles entered into the competition must be conceived, designed and maintained by the student team members without direct involvement from external professional engineers, racers, machinists or related professionals. However, the student team may use any information from professionals or from academics as long as the information is given as a discussion of alternatives with their pros and cons. It should also be mentioned that for the 2023 year, the Formula Student Germany (FSG) rules that most European competitions follow included the driverless dynamic events into the points scoring board therefore making the maximum points available only for driverless vehicles.

In order to succeed, a newly formed team should carefully read and understand in depth the rules document that is provided. The knowledge of these rules will be tested throughout the competition. Based on the 2023 document, the basic limitations for the CV category will be mentioned as well as some paragraphs from the technical inspection for further understanding of the competition.

**Engine Limitation:** The engine used to power the vehicle must be a **piston engine**, using a **four-stroke primary heat cycle** with a displacement not exceeding **710 cm<sup>3</sup>** per cycle. Hybrid powertrains, such as those using electric motors running off stored energy, are prohibited. Water-cooled engines must only use plain water.

**Air Intake System:** All parts of the engine air and fuel control systems (including the throttle and the complete air intake system, including the air filter and any air boxes) must lie within the surface envelope.

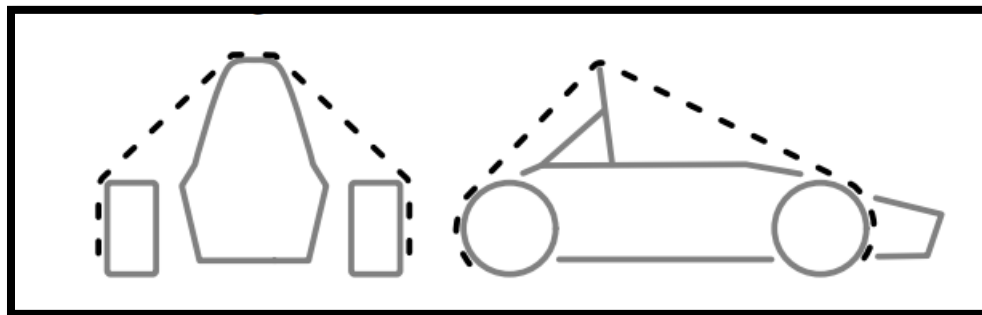


Figure 3 Surface Envelope (Dotted Black Line)

Any portion of the air intake system that is less than 350 mm above the ground must be shielded from side and rear impact collisions.

The intake manifold must be securely attached to the engine block or cylinder head with brackets and mechanical fasteners. The vehicle must be equipped with a throttle body of any size or design. The throttle should be actuated mechanically by a foot pedal i.e. via cable or a rod system.

In order to limit the power capability from the engine, a single circular restrictor must be placed in the intake system and all engine airflow must pass through this restrictor. The maximum restrictor diameters which must be respected at all times during the competition are 20mm for gasoline fueled vehicles and 19mm for E85 (15% gasoline and 85% ethanol fuel blend) fueled vehicles. The restrictor must be located

to facilitate measurement during the inspection process. The only allowed intake configuration is displayed below.

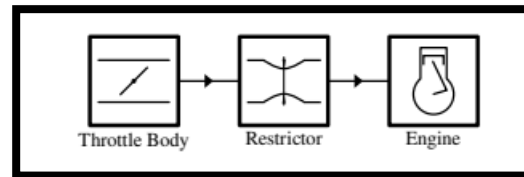


Figure 4 Intake Configuration Allowed for the competition

**Fuel System:** No agents other than fuel and air may be induced into the combustion chamber. The temperature of fuel introduced into the fuel system may not be changed with the intent to improve calculated efficiency.

The fuel tank must be located within the rollover protection envelope and must not touch any part of the vehicle other than its mounting and parts of the fuel system at any time.

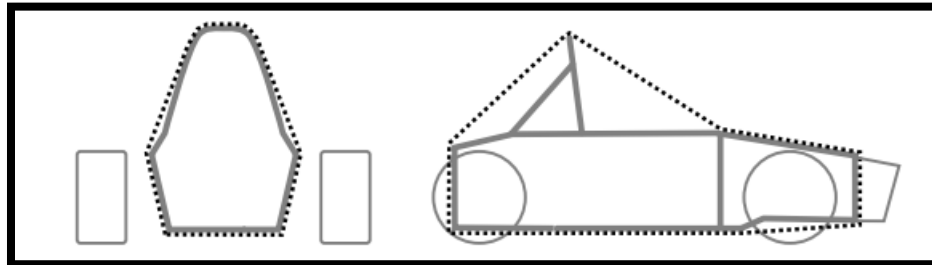


Figure 5 Rollover Protection Envelope

Fuel lines between fuel tank and fuel rail and return lines must have reinforced rubber fuel lines with an abrasion protection with a fuel hose clamp which has a full 360° wrap, a nut and bolt system for tightening and rolled edges to prevent the clamp cutting into the hose, or metal braided hoses with crimped-on or reusable, threaded fittings. Fuel lines must be securely attached to the vehicle and/or engine. All fuel lines must be shielded from possible rotating equipment failure or collision damage.

**Exhaust System:** The maximum sound level test speed for a given engine will be the engine speed that corresponds to an average piston speed of 15.25 m/s. The calculated speed will be rounded to the nearest 500 rpm. The maximum permitted sound level up to this calculated speed is 110 dB(C), fast weighting.

The idle test speed for a given engine will be up to the team and determined by their calibrated idle speed. If the idle speed varies then the vehicle will be tested across the range of idle speeds determined by the team. At idle the maximum permitted sound level is 103 dB(C), fast weighting.

The exhaust outlet(s) must not extend more than 450 mm behind the centerline of the rear axle and shall be no more than 600 mm above the ground.

**Drive Train:** Exposed rotating final drivetrain parts, such as gears, clutches, chains and belts must be fitted with scatter shields. Scatter shields and their mountings must:

- Be constructed of non-perforated 2 mm steel or 3 mm aluminum alloy 6061-T6.
- Be attached with 6mm metric grade 8.8 or stronger.



For the better management of the team, it was divided into different sub teams each one focusing on a different aspect of the vehicle. In this particular thesis, the intake system and the engine simulation will be thoroughly studied therefore the Engine & Drivetrain Sub team and its decisions will be the primary focus.

After some careful research, it was decided that the engine used for the vehicle was to be kept as close to the manufacturer specifications as possible without further enhancements for reliability reasons. Moreover, on the dynamic events, the team noticed based on previous year's data that the track was defined in such a way that vehicles cannot reach speeds above 120 km/h. The track had continuous and closed turns as well as tight slaloms. The conclusion was that the vehicle had to be able to accelerate almost instantaneously until the driver had to apply the brakes and take the upcoming tight corner at low speed.

Finally, taken into consideration the 20mm diameter of the air restrictor, the sub team understood the engine should produce the same torque or more than the stock one, with a smoother curve. Basically, the goal was to increase the torque at low speeds and increase the kW of power at high speeds compared to the stock engine and using the manufacturers data as basis for comparison.

#### 1.4. Delimitations – Clarifications

The purpose of an intake system in a combustion engine is to provide clean air to the engine, and, except for direct-injection and diesel engines, facilitate the mixing of the air-fuel mixture prior to entering the combustion chamber. The restrictor also dictates much of the intake design, as designing a restricted intake carries different challenges and limitations than for a regular, non-restricted intake.

The main components of an intake system in FSAE are: the air filter, throttle body, restrictor, plenum and runners. The throttle body controls the amount of air flow into the intake system and therefore into the engine, the restrictor restricts the maximum airflow into the system and the plenum acts as 'air storage' which the engine draws from during the intake stroke. Finally, the runner transports air from the plenum to the engine and its length is chosen to take advantage of resonance effects. All these components should be designed to work together to minimize pressure loss through the system and mitigate the effects of the restrictor as much as possible.

On this particular thesis, the focus will mainly be around the dimensioning and design of the plenum and the runners. The air filter, throttle body and the restrictor have already been carefully investigated and optimized separately and were considered to remain unchanged unless something indicated the opposite. Poseidon Racing team owns only one engine which was placed on a handmade test bench. Several tries were made from the team to place the engine onto a hydraulic dynamometer to compare those results with the ones from the 1D program which however proved to not be possible due to time constrains. In addition, the final exhaust system on the engine used in the competition is not identical to the one that will be simulated for the car and will therefore not provide any data to be confirmed or dismissed. Therefore, in order to evaluate the results of the program accordingly, parts of the software will undergo investigation to confirm that the algorithms provide correct results.

## 1.5. Methodology

In the following chapters, the methods followed to optimize the engine performance will be described in as much detail as possible in order to design and manufacture an intake system as accurate to the one visioned. In the second chapter a brief description of the basic theoretical background of a 4-stroke engine is given. In the third chapter the theory behind the Ricardo Engine simulation is discussed. In the fourth chapter the engine choice of the vehicle and some basic measurements are being shown. In the next 3 chapters the different 1D models are being created and data diagrams are collected. In the eighth chapter the final comparison between stock and modified engine is being made. In the ninth chapter the final dimensioning of the runners and plenum is being made with the help of a flow study and an FEA study. In the final two chapters the manufacturing of the intake system is being shown as well as the final results of the whole study and thesis as well as some acknowledgements.

## 2. Basic Engine Theory Principals

### 2.1. Introduction, Historical Perspective and Engine classifications

The purpose of internal combustion engines (ICE) is the production of mechanical power from the chemical energy contained in the fuel. In internal combustion engines, as distinct from external combustion engines, this energy is released by burning or oxidizing the fuel inside the engine. The fuel-air mixture before combustion and the burned products after combustion are the actual working fluids.

The internal combustion engines are spark-ignition engines (sometimes called Otto engines, or gasoline or petrol engines, though other fuels can be used) and compression-ignition or diesel engines. Because of their simplicity, ruggedness and high power to weight ratio, these two types of engines have found wide application in transportation (land, sea, and air) and power generation. It is the fact that combustion takes place inside the work-producing part of these engines that makes their design and operating characteristics fundamentally different from those of other types of engines.

Practical heat engines have served mankind for over two and a half centuries. For the first 150 years, water, raised to steam, was interposed between the combustion gases produced by burning the fuel and the work-producing piston in-cylinder expander. It was not until the 1860s that the internal combustion engine became a practical reality. J. J. E. Lenoir was the first to develop an ICE. Gas and air were drawn into the cylinder during the first half of the piston stroke. The charge was then ignited with a spark, the pressure increased, and the burned gases then delivered power to the piston for the second half of the stroke. The cycle was completed with an exhaust stroke. Nicolaus A. Otto later proposed a more efficient engine model, very similar to the one most of our vehicles use today, based on the one Lenoir first introduced. This was the breakthrough that effectively founded the internal combustion engine industry. Further developments followed fast once the full impact of what Otto had achieved became apparent. Several engineers followed with their own patent paving the way for new types of internal combustion engines like Rudolf Diesel with liquid fuel injection and initiating combustion solely by compression and James Atkinson who made an engine with a longer expansion than compression stroke, which had a high efficiency but due to many mechanical weaknesses it did not stick.

It can be easily understood that through the years a lot of different types of internal combustion engines have been manufactured and used in a variety of applications. All these engines can be distinguished and

classified by their different characteristics. Some of the most notable are the fuel, the working cycle and the engine design:

**Fuel.** Gasoline (or petrol), fuel oil (or diesel fuel), natural gas, liquid petroleum gas, alcohols (methanol, ethanol), hydrogen, dual fuel.

**Working cycle.** Four-stroke cycle: naturally aspirated (admitting atmospheric air), supercharged (admitting pre-compressed fresh mixture), and turbocharged (admitting fresh mixture compressed in a compressor driven by an exhaust turbine), two-stroke cycle: crankcase scavenged, supercharged, and turbocharged.

**Basic engine design.** Reciprocating engines (in turn subdivided by arrangement of cylinders: e.g., in-line, V, radial, opposed), rotary engines (Wankel and other geometries)

Due to the rules of the competition, for this thesis, a gasoline engine with pistons, a 4-stroke working cycle and spark ignition will be studied.

## 2.2. Engine Operating Cycles

Before analyzing the operating cycle of the 4-stroke engine, the basic piston geometry must be presented and understood in depth. The steady rotation of the crankshaft produces a cyclical piston motion. The piston comes to rest at the top dead center (TDC or TC) crank position and bottom dead center (BDC OR BC) crank position when the cylinder volume is a minimum or maximum, respectively. The minimum cylinder volume is called the clearance volume  $V_c$ . The volume swept out by the piston, the difference between the maximum or total volume  $V_t$  and the clearance volume  $V_c$ , is called the displaced or swept volume  $V_d$ . The ratio  $V_t$  to  $V_c$  is the compression ratio  $r_c$ . Typical values of compression ratio are 8 to 12 for SI engines. As the rules of the competition state, the engine displacement must not exceed  $720\text{cm}^3$ . To calculate the displacement  $D$  for the whole engine some simple calculations are necessary :

$$V_d = \text{Stroke}(\text{Distance travelled by piston}) * \text{Bore}(\text{Diameter of piston})$$

$$D = V_d * \text{Number of Cylinders}$$

The majority of reciprocating engines operate on what is known as the four-stroke cycle. Each cylinder requires four strokes of its piston—two revolutions of the crankshaft—to complete the sequence of events which produces one power stroke:

1. **An intake stroke**, which starts with the piston at TDC and ends with the piston at BDC, which draws fresh air mixture into the cylinder. To increase the mass inducted, the inlet valve opens shortly before the stroke starts and closes after it ends.

2. **A compression stroke**, which starts when both valves are closed and the piston is at BDC and ends with the piston at TDC. The mixture inside the cylinder is compressed to a small fraction of its initial volume. Toward the end of the compression stroke, combustion is initiated and the cylinder pressure rises more rapidly.

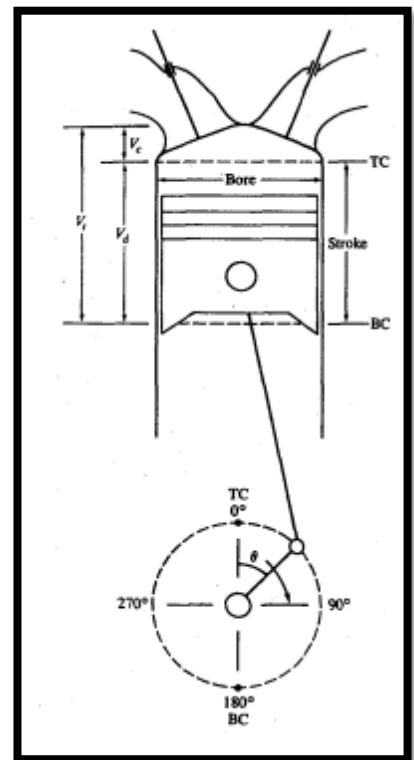


Figure 6 Basic Geometric Values of an Engine

3. **A power stroke**, or expansion stroke, which starts with the piston at TDC and ends at BDC as the high-temperature, high-pressure, gases push the piston down and force the crank to rotate. About five times as much work is done on the piston during the power stroke as the piston had to do during compression. As the piston approaches BDC the exhaust valve opens to initiate the exhaust process and drops the cylinder pressure close to the exhaust pressure.

4. **An exhaust stroke**, which starts with the piston at BDC and ends at TDC where the remaining burned gases exit the cylinder. This happens because the cylinder pressure may be substantially higher than the exhaust pressure. The exhaust gases are swept out by the piston as it moves toward TDC. As the piston approaches TDC the inlet valve opens. Just after TDC the exhaust valve closes and the cycle starts again.

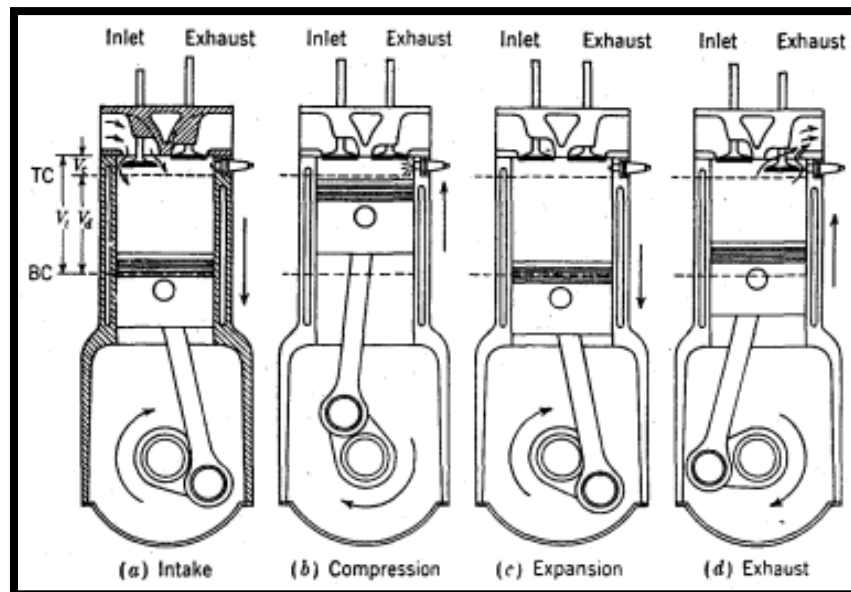


Figure 7 An Illustration of the 4 Strokes of an ICE Engine

### 2.3. Spark-Ignition Engine Operation

In SI engines the fuel must be vented and properly mixed with the air entering the cylinder before combustion. Fuel and air are usually mixed together in the intake system prior to entry to the engine cylinder, using a carburetor or fuel-injection system.

Into the intake assembly there is a throttle valve or plate which controls the combined air flow, and thus the engine output. The intake flow is throttled to below atmospheric pressure by reducing the flow area when the power required (at any engine speed) is below the maximum which is obtained when the throttle is wide open. The intake manifold is usually heated to promote faster evaporation of the liquid fuel and obtain more uniform fuel distribution between cylinders.



Fuel injection into the intake manifold or inlet port is an increasingly common alternative to a carburetor. With port injection, fuel is injected through individual injectors from a low-pressure fuel supply system into each intake port. There are several different types of systems: mechanical injection using an injection

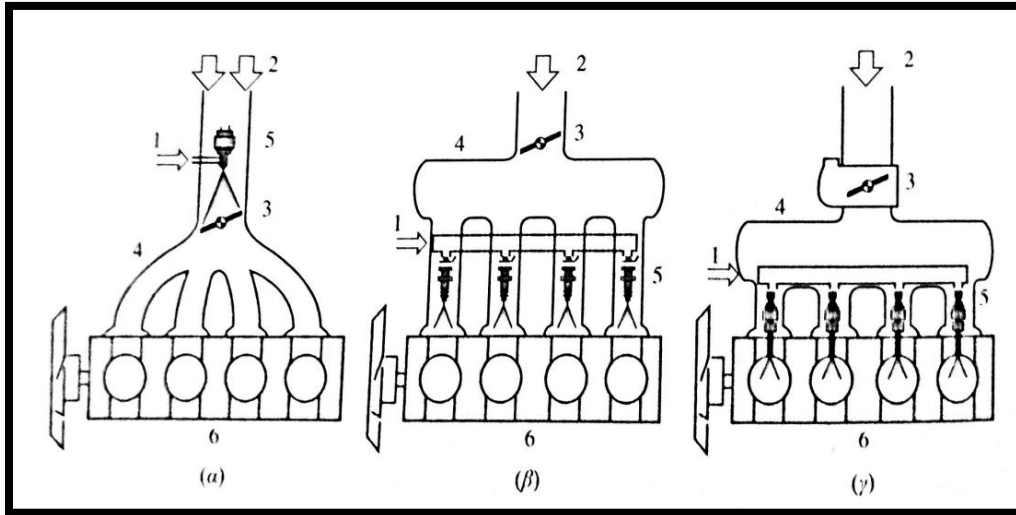


Figure 8 Types of Injection Systems a) Single Point b) Multi Point c) Direct Injection

pump driven by the engine; mechanical, driverless, continuous injection; electronically controlled, driverless, injection. In this system, the air flow rate is measured directly; the injection valves are actuated twice per cam shaft revolution by injection pulses whose duration is determined by the electronic control unit (ECU) to provide the desired amount of fuel per cylinder per cycle.

The sequence of events which take place inside the engine cylinder is illustrated in the figure below. Several variables are plotted against crank angle through the entire four-stroke cycle. Crank angle is a useful independent variable because engine processes occupy almost constant crank angle intervals over

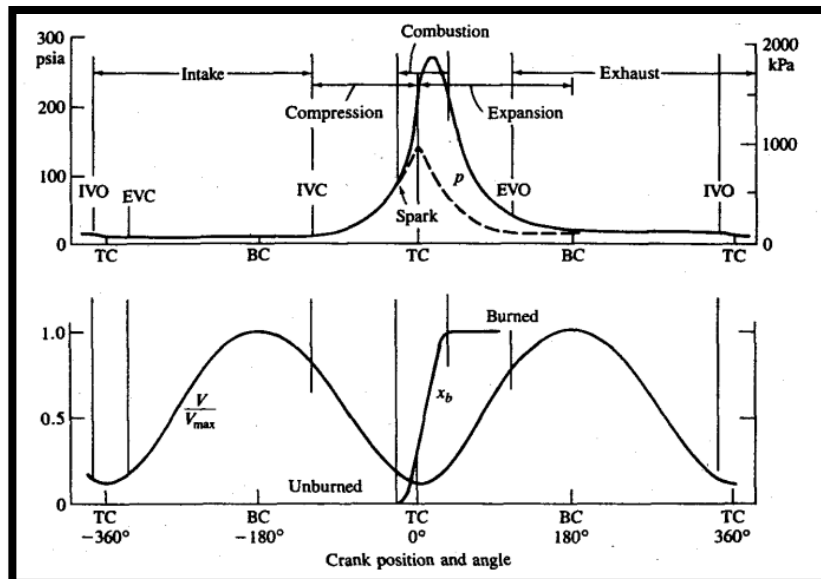


Figure 9 Sequence of events in four-stroke spark-ignition engine operating cycle. Cylinder pressure  $p$ , Cylinder Volume ( $V/V_{max}$ ) and mass fraction burned  $x_b$  are plotted against crank angle

a wide range of engine speeds. The figure shows the valve timing and volume relationship for a typical automotive spark-ignition engine. To maintain high mixture flows at high engine speeds (and hence high-power outputs) the inlet valve, which opens before TDC, closes substantially after BDC. During intake, the inducted fuel and air mix in the cylinder with the residual burned gases remaining from the previous cycle. After the intake valve closes, the cylinder contents are compressed to above atmospheric pressure and temperature as the cylinder volume is reduced. Some heat transfer to the piston, cylinder head, and cylinder walls occurs but the effect on unburned gas properties is modest.

Between 10 and 40 crank angle degrees before TDC an electrical discharge across the spark plug starts the combustion process. A turbulent flame develops from the spark discharge, propagates across the mixture of air, fuel, and residual gas in the cylinder, and extinguishes at the combustion chamber wall. The duration of this burning process varies with engine design and operation, but is typically 40 to 60 crank angle degrees. As the fuel-air mixture burns in the flame, the cylinder pressure (solid line) rises due to compression alone. Note that due to differences in the flow pattern and mixture composition between cylinders, and within each cylinder cycle-by-cycle, the development of each combustion process differs somewhat. As a result, the shape of the pressure versus crank angle curve in each cylinder, and cycle-by-cycle, is not exactly the same.

There is an optimum spark timing which, for a given mass of fuel and air inside the cylinder, gives maximum torque. More **advanced** (earlier) timing or **retarded** (later) timing than this optimum gives lower output. It is called maximum brake-torque (MBT) timing, and is an empirical compromise between starting combustion too early in the compression stroke (when the work transfer is to the cylinder gases) and completing combustion too late in the stroke (and so lowering peak expansion stroke pressures).

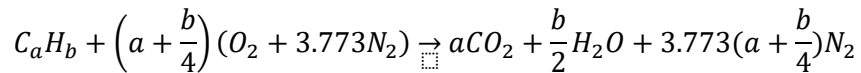
About two-thirds of the way through the expansion stroke, the exhaust valve starts to open. The cylinder pressure is greater than the exhaust manifold pressure and a blowdown process occurs. The burned gases flow through the valve into the exhaust port and manifold until the cylinder pressure and exhaust pressure equilibrate. The duration of this process depends on the pressure level in the cylinder. The piston then displaces the burned gases from the cylinder into the manifold during the exhaust stroke. The exhaust valve opens before the end of the expansion stroke to ensure that the blowdown process does not last too far into the exhaust stroke. The actual timing is a compromise which balances reduced work transfer to the piston before BDC against reduced work transfer to the cylinder contents after BDC. The exhaust valve remains open until just after TDC and the intake opens just before TDC. To ensure the valves are fully open when piston velocities are at their highest, the valve open periods often overlap. **If the intake flow is throttled to below exhaust manifold pressure, then backflow of burned gases into the intake manifold occurs when the intake valve is first opened.** (Heywood, Βασικές Αρχές Μηχανών Εσωτερικής Καύσης, 2021)

## 2.4. Combustion

Combustion of the fuel-air mixture inside the engine cylinder is one of the processes that controls engine power, efficiency, and emissions. Some background in relevant combustion phenomena is therefore a necessary preliminary to understanding engine operation. In spark-ignition engines, the fuel is normally mixed with air in the engine intake system. Following the compression of this fuel-air mixture, an electrical discharge initiates the combustion process; a flame develops created by the spark discharge and

propagates across the cylinder to the combustion chamber walls. At the walls, the flame is "quenched" or extinguished as heat transfer and destruction of active species at the wall become the dominant processes. An undesirable combustion phenomenon-the "spontaneous" ignition of a substantial mass of fuel-air mixture ahead of the flame, before the flame can propagate through this mixture can also occur. This autoignition or self-explosion combustion phenomenon is the cause of spark-ignition engine knock which, due to the high pressures generated, can lead to engine damage.

This section develops relations between the composition of the reactants (fuel and air) of a combustible mixture and the composition of the products. Since these relations depend only on the conservation of mass of each chemical element in the reactants, only the relative elemental composition of the **fuel** and the relative proportions of **fuel and air** are needed. If sufficient oxygen is available, a hydrocarbon fuel can be completely oxidized. The carbon in the fuel is then converted to carbon dioxide  $CO_2$  and the hydrogen to water  $H_2O$ . However, air contains nitrogen, but when the products are at low temperatures the nitrogen is not significantly affected by the reaction. Consider the complete combustion of a general hydrocarbon fuel of average molecular composition  $C_aH_b$ , with air. The overall complete combustion equation is



The equation above, defines the stoichiometric (or chemically correct or theoretical) proportions of fuel and air; i.e., there is just enough oxygen for conversion of all the fuel into completely oxidized products.

The stoichiometric air/ fuel or fuel/air ratios depend on fuel composition. Using the molecular weights of each particle present in the equation we can calculate the air mass and fuel mass for stoichiometric combustion.

In reality, the air fuel mixture cannot be stoichiometric. Usually, the air mass could be less or more than the one necessary. Fuel-air mixtures with more than or less than the stoichiometric air requirement can be burned too. With excess air or fuel-lean combustion, the extra air appears in the products in unchanged form. With less than the stoichiometric air requirement, i.e., with fuel-rich combustion, there is insufficient oxygen to oxidize fully the fuel C and H to  $CO_2$ , and  $H_2O$ . The products are a mixture of  $CO_2$  and  $H_2O$  with carbon monoxide CO and hydrogen  $H_2$  (as well as  $N_2$ ).

Because the composition of the combustion products is significantly different for fuel-lean and fuel-rich mixtures, and because the stoichiometric fuel/air ratio depends on fuel composition, the ratio of the actual fuel/air ratio (F) to the stoichiometric ratio ( $F_s$ ), is a more informative parameter for defining mixture composition: The fuel/air equivalence ratio  $\phi$  can be defined as follows:

$$\phi = \frac{F}{F_s}$$

An important advantage of the equivalence ratio is that it always has the same value whether it is expressed in terms of moles or mass. In the equivalence ratio, a mixture is characterized as fuel lean if  $\phi < 1$ , fuel rich if  $\phi > 1$  while when  $\phi = 1$  then the mixture is considered stoichiometric.

The inverse of  $\phi$ , the relative air/fuel ratio  $\lambda$ , is also sometimes used. In that occasion,  $\lambda > 1$  corresponds to fuel lean mixture and  $\lambda < 1$  to fuel rich mixture.

Mixture requirements are different for full-load (wide-open throttle) and for part-load operation. At the former operating condition, **complete utilization of the inducted air** to obtain maximum power for a given displaced volume is the critical issue. Where **less than the maximum power** at a given speed is required, **efficient utilization of the fuel** is the critical issue. At wide-open throttle, maximum power for a given volumetric efficiency is obtained with rich-of-stoichiometric mixtures,  $\lambda = 0.9$ .

This occurs because the burned gas temperatures after combustion decrease, decreasing the burned gas **specific heat** (the amount of energy required by one gram of gas to raise the temperature by unit degree Celsius) and thereby increasing the effective value of  $\gamma$  over the expansion stroke. The efficiency increases because, for a given volume-expansion ratio, the burned gases expand through a larger temperature ratio prior to exhaust; therefore, per unit mass of fuel, the expansion stroke work is increased. Mixtures that are richer still are sometimes used to increase volumetric efficiency by increasing the amount of charge cooling that accompanies fuel vaporization, thereby increasing the inducted air density.

At part-load (or part-throttle) operating conditions, it is advantageous to dilute the fuel-air mixture, either with excess air or with recycled exhaust gas. This dilution improves the fuel conversion efficiency for three reasons:

(1) the expansion stroke work for a given expansion ratio is increased as a result of the change in thermodynamic properties of the burned gases, (2) for a given mean effective pressure, the intake pressure increases with increasing dilution, so pumping work decreases, (3) the heat losses to the walls are reduced because the burned gas temperatures are lower

It should also be mentioned that SI engines with stoichiometric operation have exhaust temperatures of approximately 650°C (925K). When operating with a fuel lean mixture the exhaust temperatures decrease e.g. for  $\lambda = 1.4$  by about 50°C. For mixtures richer than the stoichiometric, the exhaust temperatures increase slightly, with maximum values occurring around  $\lambda = 0.95$  and then decreasing again.

Finally, Regarding the operation of engines, the most important properties of gasoline are its volatility and resistance to self-ignition (or impact combustion) during the last part of the combustion process. The volatility of gasoline is characterized by the distillation curve, that is, the volume fraction evaporated at atmospheric pressure as a function of temperature. Usually, 10% of gasoline evaporates below 50°C. The resistance of the fuel to impact combustion is characterized by the octane number. There are two standard fuel test procedures that determine the octane number: Research Octane Number (RON) and Motor Octane Number (MON). The impact resistance requirements of modern engines are best correlated with the octane number RON, which is the octane number of fuel widely used in Europe. At least two grades of gasoline are usually available, a standard one with an octane number of RON92, while superior quality gasoline has a higher number up to RON 98. The competition for the 2023 year provided RON 100 fuel.

## 2.5. Heat Transfer

The peak burned gas temperature in the cylinder of an internal combustion engine can reach up to 2500 K. Maximum metal temperatures for the inside of the combustion chamber space are limited to much

<b>Energy balance for automotive engines at maximum power</b>					
	$P_b$	$Q_{cool}$	$Q_{misc}$	$H_{e,ic}$	$\dot{m}h_{e,s}$
(percentage of fuel heating value)					
SI engine	25–28	17–26	3–10	2–5	34–45
Diesel	34–38	16–35	2–6	1–2	22–35

Sources: From Khovakh,<sup>3</sup> Sitkei,<sup>4</sup> and Burke *et al.*<sup>5</sup>

Figure 10 Energy Distribution for engines at Maximum Power

lower values by a number of considerations, and cooling for the cylinder head, cylinder, and piston must therefore be provided. These conditions lead to heat fluxes to the chamber walls that can reach as high as 10 MW/m<sup>2</sup> during the combustion period. However, during other parts of the operating cycle, the heat flux is essentially zero. The flux varies substantially with location: regions of the chamber that are contacted by rapidly moving high-temperature burned gases generally experience the highest fluxes. In regions of high heat flux, thermal stresses must be kept below levels that would cause fatigue cracking (so temperatures must be less than about 400°C for cast iron and 300°C for aluminum alloys). The gas-side surface of the cylinder wall must be kept below about 180°C to prevent deterioration of the lubricating oil film. Spark plug and valves must be kept cool to avoid knock and preignition problems which result from overheated spark plug electrodes or exhaust valves. Solving these engine heat-transfer problems is obviously a major design task.

Heat transfer affects engine performance, efficiency, and emissions. For a given mass of fuel within the cylinder, higher heat transfer to the combustion chamber walls will lower the average combustion gas temperature and pressure and reduce the work per cycle transferred to the piston. Thus, specific power and, efficiency is affected by the magnitude of engine heat transfer. Heat transfer between the unburned charge and the chamber walls in spark-ignition engines affects the onset of knock which, by limiting the compression ratio, also influences power and efficiency.

An overall first law energy balance for an engine provides useful information on the disposition of the initial fuel energy. For a control volume which surrounds the engine, the steady-flow energy-conservation equation is

$$\dot{m}_f h_f + \dot{m}_a h_a = P_b + \dot{Q}_{cool} + \dot{Q}_{misc} + (\dot{m}_f + \dot{m}_a) h_e$$

where  $P_b$ , is the brake power,  $Q_{cool}$  is the heat-transfer rate to the cooling medium,  $Q_{misc}$  is the heat rejected to the oil (if separately cooled) plus convection and radiation from the engine's external surface.

For a spark-ignition engine, the conversion to useful work is lower compared to a compression ignition engine, because the compression ratio is lower. However, as shown in the diagram **above** the heat losses at part-load (an important operating regime for automobile use) are a substantially larger fraction of the fuel heating value. Studies with computer simulations of the spark-ignition engine operating cycle indicate that at typical part-load conditions a proportional reduction in combustion-chamber-wall heat losses of 10% results in a proportional increase (improvement) in brake fuel conversion efficiency of about 3%.

## 2.6. Power and Torque

Engine torque is normally measured with a dynamometer. Torque  $M$  is defined as the product  $M=F*d$  (where  $d$  is the distance) and relates to the application of force to a body rotating relative to a point and measured in Nm. The torque of an engine is the product of the force (from exhaust gas expansion through the piston) exerted on the engine crankshaft by the distance of the application point from the axis of rotation (the perpendicular distance of the connecting rod from the crank, e.g. in the TDC, is zero). The torque in an engine is not constant and varies in the operating speed range per engine cycle.

Power  $P$  is a physical quantity used as a comparison measure for the performance of various machines. From the relation  $P=W/t$  it is understood that the power comes from the work produced at a given moment, i.e. It shows us the rate at which the work is produced (the faster it is produced, the faster the acceleration). It is measured in watts (W) and it is often used with other units such as the metric horsepower (1 PS= 0.736 kW) and the British horsepower (1 HP = 0.746 kW).

Power and specifically horsepower is what in an engine expresses the total work of combustion per unit of time. In other words, torque shows us the ability of the engine at a particular moment, how easily it can overcome resistances such as increased weight in the car, instant acceleration, comfort on uphill routes. On the other hand, horsepower shows us how quickly a certain task can be carried out, how fast an engine can accelerate a car.

The first and most important thing to remember is that horsepower and torque are connected ( $HP = \text{Torque} * \text{RPM}/\text{Const.}$ ). If we look at the horsepower at any particular rev point, we can calculate the torque value. Respectively for torque. The torque shows us the torsion force exerted by the crankshaft on the drivetrain. If we use a bike as an example, torque is how hard you push with your foot on the pedal.

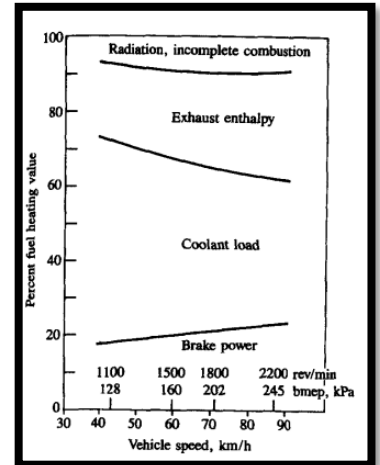


Figure 11 Brake Power, Coolant Load, Sensible Exhaust Enthalpy and Miscellaneous Energy Transfers as Percent of Flow x Heating Value at Road-Load Operating Conditions

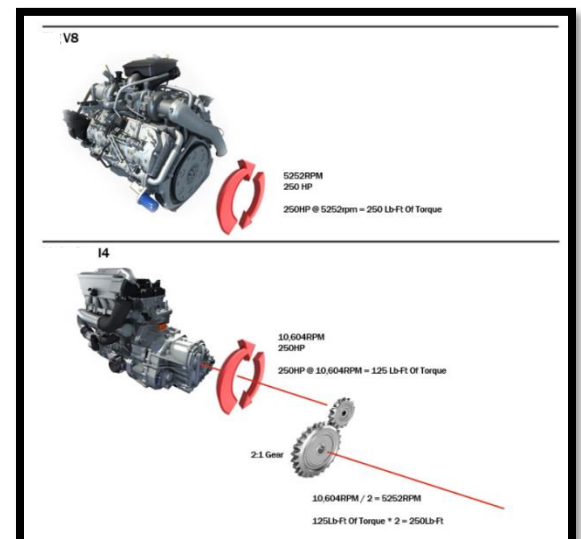


Figure 12 Two Different Engines Producing the Same Torque at the End of the Crankshaft

The horsepower shows us the energy produced by the engine. The energy produced by the motor is torque multiplied by the speed of the motor.

In other words, we can get the same horsepower either by rotating the engine very quickly with little torque (think motorcycle engine), or by rotating the engine slowly but creating a lot of torque (think V8). The energy (or power) generated can be the same, even with very different torque numbers.

Finally, the term load (e.g. medium load) is often used to denote at which point in the torque range (from zero to maximum) the engine is operating.

## 2.7. Volumetric Efficiency

The intake system (the air filter, throttle plate, intake manifold, intake port, intake valve) restricts the amount of air which an engine of given displacement can induct. The parameter used to measure the effectiveness of an engine's induction process is the volumetric efficiency  $n_v$ . Volumetric efficiency is only used with four-stroke cycle engines which have a distinct induction process. It is defined as the volume flow rate of air into the intake system divided by the theoretical maximum volume that can enter the cylinder:

$$n_v = \frac{\dot{m}_{\text{πραγμ.}}}{\dot{m}_{\text{θεωρ.}}} = \frac{\dot{m}_{\text{πραγμ.}}}{\rho_{a,i} * V_d}$$

The inlet density may either be taken as atmosphere air density (in which case  $n_v$  measures the pumping performance of the entire inlet system) or may be taken as the air density in the inlet manifold (in which case  $n_v$  measures the pumping performance of the inlet port and valve only). Typical maximum values of  $n_v$  for naturally aspirated engines are in the range 80 to 90 percent.

## 2.8. Other significant operating parameters

### 2.8.1. Mean Effective Pressure

While torque is a valuable measure of a particular engine's ability to do work, it depends on engine size. A more useful relative engine performance measure is obtained by dividing the work per cycle by the cylinder volume displaced per cycle. The parameter obtained has units of force per unit area and is called the mean effective pressure (mep):

$$mep \text{ (kPa)} = \frac{P \text{ (kW)} * n_R * 10^3}{V_d \text{ (dm}^3\text{)} * N \left(\frac{rev}{s}\right)}$$

where  $n_R$  is the number of crank revolutions for each power stroke per cylinder (two for four-stroke cycles and one for two-stroke cycles). Mean effective pressure (mep) is defined by the location measurement and method of calculation. Mean effective pressure calculated from measured brake torque is called brake mean effective pressure and is one of the most commonly used.

The maximum brake mean effective pressure of good engine designs is well established, and is essentially constant over a wide range of engine sizes. Thus, the actual bmep that a particular engine develops can

be compared with this norm, and the effectiveness with which the engine designer has used the engine's displaced volume can be assessed.

$$bmep (kPa) = \frac{T(Nm) * n_R * 2\pi}{V_d(dm^3)}$$

### 2.8.2. Specific fuel consumption and efficiency

In engine tests, the fuel consumption is measured as a flow rate, mass flow per unit time  $\dot{m}_f$ . A more useful parameter is the specific fuel consumption (sfc) the fuel flow rate per unit power output. It measures how efficiently an engine is using the fuel supplied to produce work:

$$sfc \left( \frac{mg}{J} \right) = \frac{\dot{m}_f \left( \frac{g}{s} \right)}{P(kW)}$$

Low values of sfc are obviously desirable. For SI engines typical best values of brake specific fuel consumption are about 75  $\mu g/J$ .

### 2.8.3. Air/Fuel and Fuel/Air Ratios

In engine testing, both the air mass flow rate  $\dot{m}_a$  and the fuel mass flow rate  $\dot{m}_f$  are normally measured. The ratio of these flow rates is useful in defining engine operating conditions:

$$AFR = \frac{\dot{m}_a}{\dot{m}_f}, \quad FAR = \frac{\dot{m}_f}{\dot{m}_a}$$

The normal operating range for a conventional SI engine using gasoline fuel is  $12 < AFR < 18$  ( $0.056 < FAR < 0.083$ ).

## 2.9. Friction and Lubrication

Not all the work transferred to the piston from the gases contained inside the cylinder is available at the drive shaft for actual use. That portion of the work transferred which is not available is usually termed friction work. It is dissipated in a variety of ways within the engine and engine auxiliaries. The friction work or power is a sufficiently large fraction of the indicated work or power-varying between about 10% at full load and 100% at idle or no-load. Friction losses affect the maximum brake torque and minimum brake specific fuel consumption directly; often the difference between a good engine design and an average engine is the difference in their frictional losses. A large part of the friction losses appears as heat in the coolant and oil which must be removed in the radiator and oil cooler system. Thus, friction losses influence the size of the coolant systems. A knowledge of friction power is required to relate the combustion characteristics of an engine which influence the indicated power-and the useful output-the brake power.

The friction work, defined as the difference between the work delivered to the piston while the working fluid is contained within the cylinder (i.e., during the compression and expansion strokes) and the usable work delivered to the drive shaft, is expended as follows:

1. To draw the fresh mixture through the intake system and into the cylinder, and to expel the burned gases from the cylinder and out of the exhaust system. This is usually called the pumping work.



2. To overcome the resistance to relative motion of all the moving parts of the engine. This includes the friction between the piston rings, piston skirt, and cylinder wall; friction in the wrist pin, big end, crankshaft, and camshaft bearings; friction in the valve mechanism; friction in the gears, or pulleys and belts, which drive the camshaft and engine accessories.
3. To drive the engine accessories. These can include: the fan, the water pump, the oil pump, the fuel pump, the generator, a secondary air pump for emission control, a power-steering pump, and an air conditioner.

All this work is eventually dissipated as heat. The friction losses outlined in the figure below can be classified into two groups, depending on the type of dissipation which occurs. One type is friction between two metal surfaces in relative motion, with a lubricant in between. The other type is turbulent dissipation.

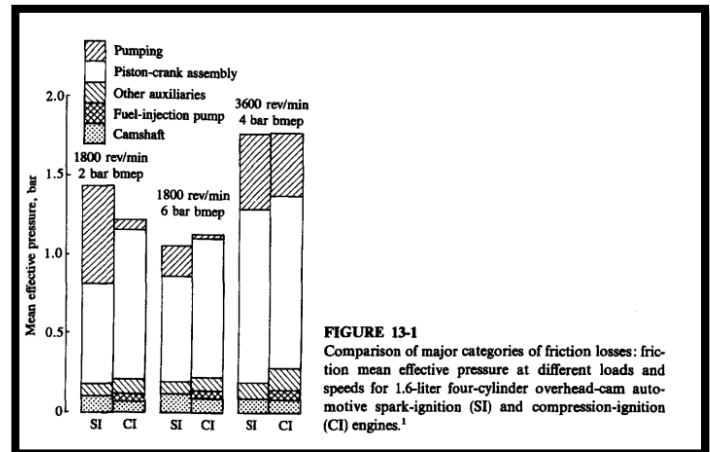


Figure 13 Comparison of Major Categories of Friction Losses

## 2.10. General Engine Design Goals – Theory Summary

Engine ratings usually indicate the highest power at which manufacturers expect their products to give satisfactory economy, reliability, and durability under service conditions. Maximum torque, and the speed at which it is achieved, is usually given also. The following measures, at the operating points indicated, have most significance:

**At all speeds at which the engine will be used with full throttle or with maximum fuel-pump setting:** *Brake mean effective pressure*. It measures the ability to obtain/provide high air flow and use it effectively over the full range.

**At all useful regimes of operation and particularly in those regimes where the engine is run for long periods of time:** *Brake specific fuel consumption*

Having mentioned all the basic theory principals that they will be used throughout this thesis, each one will be studied and analyzed further for the engine the team opted to use for the 2023 competition. Each principal will be studied and evaluated based on the team's goals for the competition. Additionally, further emphasis will be placed on those that the team considers of higher importance. As mentioned before the team needs a reliable vehicle that can withstand every dynamic event. Similarly to the engine ratings the manufacturers use for their engine, the team is going to follow a similar path in its evaluation process with sfc and bmep playing a vital role. Horsepower and torque curves along with volumetric efficiency are also going to be monitored in depth and compared between the stock engine and with the manufactured intake. To perform all these measurements, the team is going to utilize a 1D modeler which is discussed further in the next chapter along with some basic theory principals that affect the intake system which is the main focus of this thesis.

### 3. Ricardo Program – Air flow Theory

In this chapter the Ricardo 1D program is going to be discussed and analyzed along with basic fluid principals and phenomenon that take place inside the intake. Moreover, some basic parameters are going to be decided regarding the program setup. The help of the theory principals mentioned in the previous chapter is also going to be utilized.

#### 3.1. The Ricardo Program - Engine Simulation

As of August 2022, Realis Simulation is the new name for Ricardo Software following the purchase from Ricardo plc by FOG Software Group, a division of Constellation Software Inc. based in Toronto, Canada. This only applies to Ricardo Software only; all other parts of Ricardo plc remained unchanged.

Realis Simulation, formerly known as Ricardo Software, deliver advanced virtual engineering tools, supported by a team of technical experts, to global partners across automotive, rail, motorcycle, off-highway, defense, energy and environment industries. Based on nearly 30 years of software expertise, Realis focuses on delivering highly tailored tools and application engineering support to provide fast, repeatable, and predictive results across existing and emerging technologies. Their products model all major propulsion technologies, reducing the requirement for expensive hardware testing. The variety of leading-edge simulation tools facilitate design and calibration programs as the world transitions into the future, supporting clean combustion fuels, sustainable powertrain systems, efficient vehicle transmission and optimized hybrid internal combustion/electric solutions.

WAVE, or formerly known as Ricardo Wave, is a state-of-the-art 1D gas dynamics simulation tool. It is used worldwide in industry sectors including ground transportation, rail, motor sport, marine and power generation. WAVE enables performance and acoustic analyses to be performed for virtually any intake, combustion and exhaust system configuration. WAVE simulation software solves the 1D form of the Navier-Stokes equations governing the transfer of mass, momentum and energy for compressible gas flows, and includes sub-models for combustion and emissions. It is used throughout the engine design process such as improving volumetric efficiency, designing complex boosting systems, improving transient response or extracting the maximum performance from a race engine. It also contains advanced combustion models for diesel and spark ignition (SI) engines and includes secondary models specifically for the study of direct injection, SI turbulent flame propagation, engine-out emissions and knock.

Wave consists of three primary types of programs:

- 1) **Pre-processors** are programs used to set up the simulation/analysis. They are GUI (Graphical user interface)-based, where the user is provided with an input window on the computer screen and prompted for a series of values, inputs, and parameters required to describe the simulation and perform the analysis.
- 2) **Solvers** are programs used to analyze the data provided by the pre-processors. They are largely non-interactive and print text output to the screen detailing the progress of the simulation.
- 3) **Post-processors** are programs used to view and interpret the results provided by the solvers for the simulation. Again, post-processors are primarily GUI-based with user input required to produce 2-D/3-D graphs, pictures of results, and simple text-reporting of significant numerical values.

The complicity of the software can be reduced for the user. Default and tutorial values are available for basically every required input. This lowers the entry level for beginners and also makes it possible to run simulations even if some data is missing. The software includes an extended tutorial package split in basic, intermediate and advance levels. The quality and trustworthiness of the results gained from the post-processing part of the software (Wave Post) are a direct consequence of the tolerance and quality of the inserted data and how well defined the engine is.

A combustion engine is a 3D-phenomenon in respect to combustion, ducts, valves etc. In order to

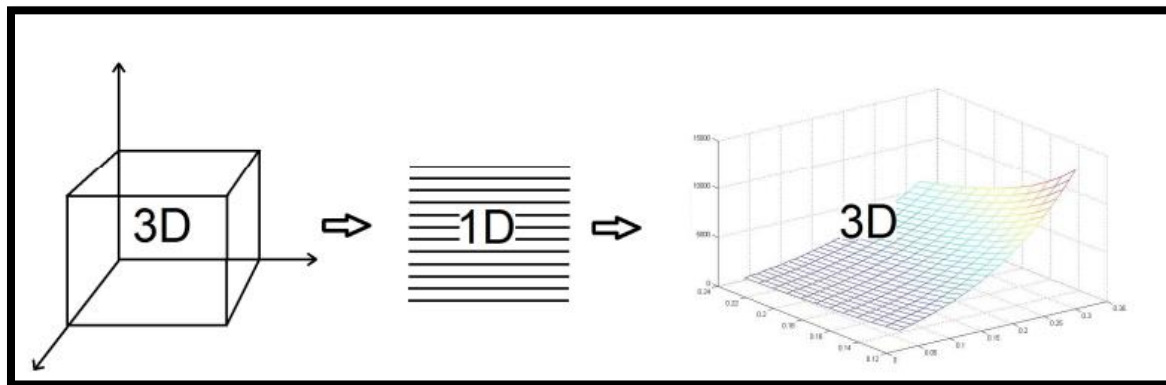


Figure 14 Operation Process for Dimensions in Ricardo Software

investigate the concept of representing a combustion engine in 1D in Wave, some additional information is required. The procedure is to split the three dimensions into multiple one dimension of data and keep track of how each dimension corresponds to one another. This is all done with equations pre-programmed in the software. For the software to be able to solve given tasks, coefficients and advanced sub-models are implemented. With user-provided data, pre-programmed equations and governing laws of physics like momentum, energy- and mass conservation, different aspects of the particular engine can be solved.

Engine simulation software is developed to reduce cost of development by shortening testing time and effort required to reach desired results. Both Ricardo Wave and GT-Power to mention the ones leading engine simulation software manufactures can provide valuable results on several hundred parameters for optimization of components not yet created in reality. The plenum chamber for example which is one of the main components that will require extended research can easily be studied with simulation software. By dragging a complex Y-junction from the menu into the canvas attaching it properly to the engine and providing all geometries for the plenum, the simulation can provide results. No real dynamometer required and no need to manufacture the plenum to find its performance or efficiency.

### 3.2. Intake Fundamentals

When gas flows unsteadily through a system of pipes, chambers, ports, and valves, both friction, pressure, and inertial forces are present. The relative importance of these forces depends on gas velocity and the size and shape of these passages and their junctions. As mentioned before, an intake system in Formula SAE will consist primarily of an air filter, throttle body, restrictor, plenum and the runner(s), in that order. Within the scope of Formula SAE, where an intake system must always be designed and manufactured to accommodate the rules-mandated restrictor, the intake system is the most effective way to increase

volumetric efficiency by minimizing not only the negative effects of the restrictor but other several separate phenomena that occur simultaneously. Those separate phenomena that affect volumetric efficiency can be identified as:

### 3.2.1. Frictional Losses

During the induction process, due to friction in each part of the intake system, the pressure in the cylinder  $p_c$  is less than the atmospheric pressure  $p_{atm}$ , by an amount dependent on the square of the speed. This total pressure drop is the sum of the pressure loss in each component of the intake system: air filter, throttle, manifold, inlet port, and inlet valve. Each loss is a few percent, with the port and valve contributing the largest drop. As a result, the pressure in the cylinder during the period in the intake process when the piston is moving at close to its maximum speed can be 10 to 20 percent lower than atmospheric. For each component in the intake (and the exhaust) system, Bernoulli's equation gives:

$$\Delta p_j = \xi_j \rho v_j^2$$

where  $\xi$  is the resistance coefficient for that component which depends on its geometric details and  $v_j$  is the local velocity. Assuming the flow is quasi-steady,  $v_j$  is related to the mean piston speed  $S_p$  by:

$$v_j A_j = S_p A_p$$

where  $A_j$  and  $A_p$  are the component minimum flow area and the piston area respectively. Hence the total quasi-steady pressure loss due to friction is:

$$P_{atm}(P_i) - P_c = \Sigma \Delta p_j = \Sigma \xi_j \rho v_j^2 = \rho \overline{S_p^2} \Sigma \xi_j \left(\frac{A_p}{A_j}\right)^2$$

The equation above, indicates the importance of large component flow areas for reducing frictional losses, and the dependence of these losses on engine speed.

### 3.2.2. Heat Transfer

As air flows through the intake runners (about 90°C) and crosses the surface of the intake valve (around 150°C), it gets heated. Such heating decreases volumetric efficiency by around 2-3%. This proportion is determined by both engine rpm and air temperature. Furthermore, interaction with hot exhaust gases and high temperatures of internal components can result in a loss in volumetric efficiency of up to 2%.

### 3.2.3. Valve timing

The pressure in the inlet manifold varies during each cylinder's intake process due to the piston velocity variation, valve open area variation, and the unsteady gas-flow effects that result from these geometric variations. The mass of air inducted into the cylinder, and hence the volumetric efficiency, is almost entirely determined by the pressure level in the inlet port during the short period before the inlet valve is closed. At higher engine speeds, the inertia of the gas in the intake system as the intake valve is closing increases the pressure in the port and continues the charging process as the piston slows down around BDC and starts the compression stroke. This effect becomes progressively greater as engine speed is increased. The inlet valve is closed some 40 to 60° after BDC, in part to take advantage of this so-called ram effect phenomenon.

### 3.2.4. Airflow Chocking

A significant pressure drop occurs along the intake port and valve as well as the restrictor which is mandatory from the competition to further limit the power output of the engine. As the intake valve opens, the minimum flow area is an annular surface between the valve head and seat. The flow of air passes through the valve system and the intake lumen to the cylinder due to the downward movement of the piston. At high speeds during the first stage of the intake stroke, the valve opening area is much smaller than the piston surface, therefore the flow velocity in the minimum cross section becomes very large. More specifically, the speed at that point approaches or exceeds that of sound. Then we say that the flow is strangled. As the flow rate increases, at full load and especially at high speeds the air supply decreases more and more because friction losses increase with the square of the speed. In a similar way acts the rules-mandatory restrictor. When the air travels through the restrictor at high velocity, near 1 Mach, very low-pressure values occur, making it harder for the engine to suction air into the cylinders. In order to overcome this additional pressure loss, a smooth restrictor design that avoids flow separation and effectively recovering this pressure prior to the plenum is essential for an efficient intake system.

### 3.2.5. Tuning - Reverse flow into the intake

The time-varying inlet flow to the cylinder causes expansion waves to be propagated back into the inlet manifold. These expansion waves can be reflected at the open end of the manifold (at the plenum) causing positive pressure waves to be propagated toward the cylinder. If the timing of these waves is appropriately arranged, the positive pressure wave will cause the pressure at the inlet valve at the end of the intake process to be raised above the nominal inlet pressure. This will increase the inducted air mass. Such an intake system is described as **tuned**.

Because the inlet valve closes after the start of the compression stroke, a reverse flow of fresh charge from the cylinder back into the intake can occur as the cylinder pressure rises due to piston motion toward TDC. This reverse flow is largest at the lowest engine speeds. It is an inevitable consequence of the inlet valve closing time chosen to take advantage of the ram effect at high speeds.

An example of the effect on volumetric efficiency of tuning the intake manifold runner is shown in the figure below. In an unsteady flow calculation of the gas exchange processes of a four-cylinder spark-ignition engine, the length of the intake manifold runners was increased successively by factors of 2.

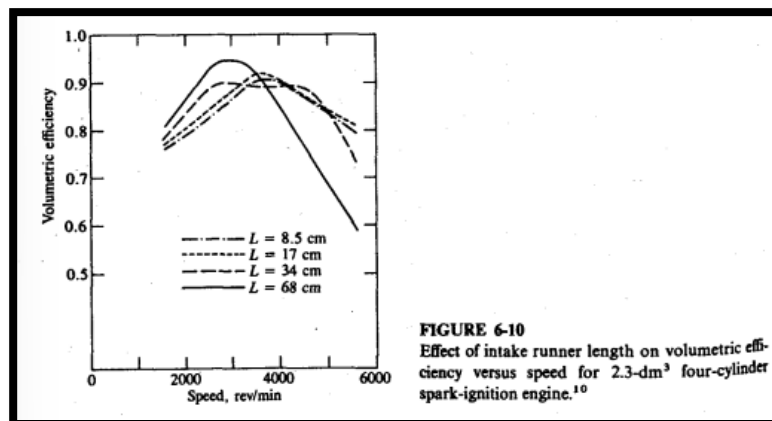


Figure 15 Effect of Intake Runner Length on V.E. on four-cylinder Engine

The 34-cm length produces a desirable "tuned " volumetric efficiency curve with increased low-speed air flow and flat mid-speed characteristics. While the longest runner further increases low-speed air flow, the loss in  $n_v$ , at high speed would be unacceptable.

Keeping all the above phenomenon in mind, several intake design considerations must be made in order to limit all the forementioned pressure losses in the system and maximize the volumetric efficiency of the engine. The amount of air introduced into each cylinder limits the amount of fuel that can be burned. Thus, the ability of the engine intake system to supply the maximum amount of air to each cylinder, i.e. the ability to suction at a given rotational speed, **is the key design goal**.

### 3.3. Basic Program Parameters

As mentioned in paragraph 3.1 the engine simulation program Ricardo, utilizes several parameters that make the simulation process more effortless. Some basic parameters are going to be described into this paragraph that are going to affect the whole simulation process and become the default settings for the stock engine simulation which is going to be described in a following chapter.

Before diving into more detail about the different parameters, Ricardo wave utilizes different elements in order to aid the user to simulate the desired engine. There are 3 different categories of elements:

1. Flow Elements: Flow elements are used to construct the flow network, which is the primary part of any WAVE model.
2. Control Elements: Control elements are used to construct a control network. The control network is not a required portion of the WAVE model, but can be used to control aspects of the flow network when required.
3. Mechanical Elements: Mechanical elements are used to add accurate modeling of mechanical phenomena. If a compressor or turbine element is added to the model, a mechanical shaft element is required.

The main focus for this chapter is the flow elements, which include the following:

- a) Ambients: Ambient elements are used as flow sources and sinks in a WAVE model and attach to the rest of the flow network via a single duct. They are most-commonly used to represent an infinite reservoir at standard atmospheric conditions.
- b) Cylinders: Cylinder elements are typically used to model the cylinders of a standard IC engine; however additional elements are included to model piston compressors and crankcases.
- c) Ducts: Ducts are used to represent all those sections of a pipe network where the flow can be treated as one-dimensional. Each duct is required to have a constant or linearly-varying diameter and thus is described by a diameter at each end, an overall length, and a discretization length.

- d) Injectors: WAVE fuel injectors can be attached to engine cylinders, ducts, and Y-junctions. Each injector can attach to one element.
- e) Orifices: An orifice element is treated as plane on the boundary between two ducts or as an interface between WAVE and an external model. Thus, there is no volume associated with orifice elements.
- f) Turbo Junctions: Turbo junction elements are used to represent the complex machinery of turbines, superchargers, and turbo-compressors. They have no volume, but change the condition of the flow across a planar boundary.
- g) Valves: Valve junctions are placed between two ducts (or, for a valved connection, between a duct and a Y-junction) in the flow system and represent variable area orifices.
- h) Y-junctions: Y-junctions are volumes to which one or more ducts can be connected. They are often used to simulate Y or T type branches in the flow system. The volume and geometry of the junction as well as the relative orientation of the ducts in a 3-D space are user inputs, required to define the junction. The contribution of the momentum flux from each duct is considered in the solution of the momentum equation, as is the effect of partial or complete stagnation in the plenum. Flow passing through the junction in a straight line from one duct to another will incur head loss only from changes in area and boundary friction. Pressure change due to stagnation occurs only when there is an angular deflection of the flow and increases smoothly from zero for no angular deflection to complete stagnation for 180° deflection. The flow path through the Y-junction is accounted for in this model; i.e., that distance should not be included in the lengths of the attached ducts.

### 3.3.1. Discharge Coefficient

At points of abrupt area changes there is a need to modify the geometrical area of the junction by a discharge coefficient. This coefficient is defined as the ratio of the orifice effective area to the orifice geometrical area. It will typically have two different values depending on the flow direction. The discharge coefficient has a great impact on the gas velocity from the ambient to the duct connected.

Discharge coefficient values can be inserted for the flow of a specific end of the duct into the adjoining element. This is typically set to "AUTO" to allow Wave to calculate the coefficient based on area ratios (normally in the range of 0.6 to 1.0). The coefficient decides the pressure drop ratio between the two connected elements. It can be calculated with the following formula:

$$C_D = 1 - \left( 1 - \left( \frac{D}{D_1} \right)^4 \right) * \left( 0.2 + 0.2 \left( 1 - \left( \frac{D}{D_2} \right)^4 \right) \right)$$

Where  $C_D$  is the discharge coefficient,  $D$  is the orifice diameter in mm,  $D_1$  is the upstream diameter in mm and  $D_2$  is the downstream diameter in mm.

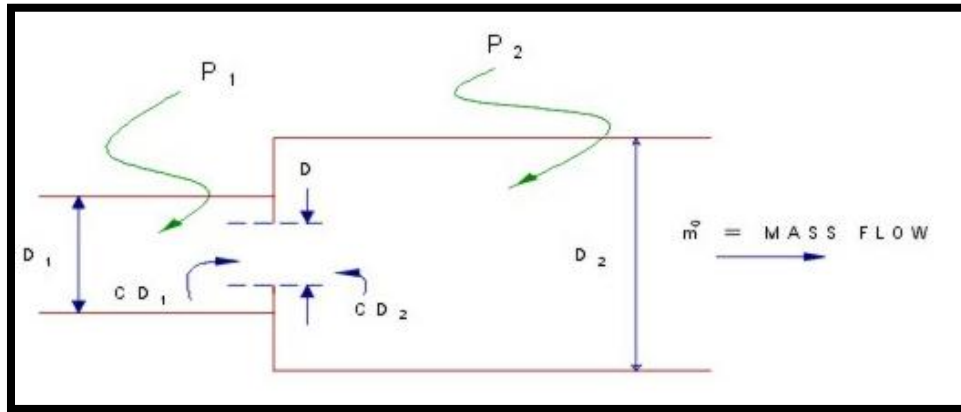


Figure 16 Reference Geometry for Discharge Coefficient Calculation

Based on (Gilani, 2012) the AUTO option for the program was tested. Compared to the manual calculations and based on the air intake speed diagrams, no value divergence was observed. Hence, the program can be utilized with the AUTO setting regarding the discharge coefficient.

### 3.3.2. Friction correlation

Friction caused by the piston motion inside the engine is modelled with a polynomial based modified version of the Chen-Flynn friction model, which is based on maximum cylinder pressure and piston speed. The correlation has a constant term (for accessory friction), a term which varies with peak cylinder pressure (for load dependence), a third term linearly dependent on mean piston velocity (for hydrodynamic friction) and a fourth term quadratic with mean piston velocity (for windage losses).

The program has the following inputs:

**ACF:** **Constant portion** of the Chen-Flynn friction correlation. If the friction is to be entered directly, this input field should be used and the BCF, CCF, and QCF terms should be set to zero.

**BCF:** Term which varies linearly with **peak cylinder pressure** in the Chen-Flynn friction correlation.

**CCF:** Term which varies linearly with the **piston speed** in the Chen-Flynn friction correlation. This is to account for hydrodynamic friction in the power cylinder.

**QCF:** Term which varies **quadratically with the piston speed** in the Chen-Flynn friction correlation. This is to account for windage losses in the power cylinder.

All the inputs above are used to calculate the friction through the following formulas:

$$FMEP = A_{cf} + \frac{1}{n_{cyl}} \sum_{i=1}^{n_{cyl}} [B_{cf}(P_{cyl})_i + C_{cf} * (S_{fact})_i + Q_{cf} * (S_{fact})_i^2]$$

$$S_{fact} = RPM * \frac{stroke}{2}$$



There are three other types of mean effective pressure necessary to provide and include in the model. These are Pumping, Indicated and Brake Mean Effective Pressure. The pumping losses (PMEP) are calculated separately. The engine indicated performance (IMEP) represents the software calculated performance and the BMEP is the sum of IMEP and FMEP.

There is no sensor for PMEP to be used in Wave. If, however, there is interest in evaluating BMEP or IMEP it is optional to attach a sensor to the model.” If it is attached to a Cylinder element, it will report the work from that cylinder alone. If it is attached to the Engine, it will report the work from all cylinders and crankcases plus the work from gear driven superchargers and power turbines minus friction losses.

### 3.3.3. Discretization length

Discretization is the practice of taking the modeled geometric system and dividing the large single volume into smaller sub-volumes. In each of these sub-volumes, fundamental equations will be solved at each timestep for the conservation of mass and energy. At the boundaries between each volume, the equation for conservation of momentum is solved. Using this method, scalar quantities, such as pressure and temperature, are stored at the cell center (middle of the volume) while vector quantities, such as mass-flow and velocity, are stored at cell boundaries (edges of the volume).

The purpose of discretization is to achieve better resolution of changes in the calculated state of the fluid. For example, the more elements along the length of a duct, the easier it is to model a traveling pressure

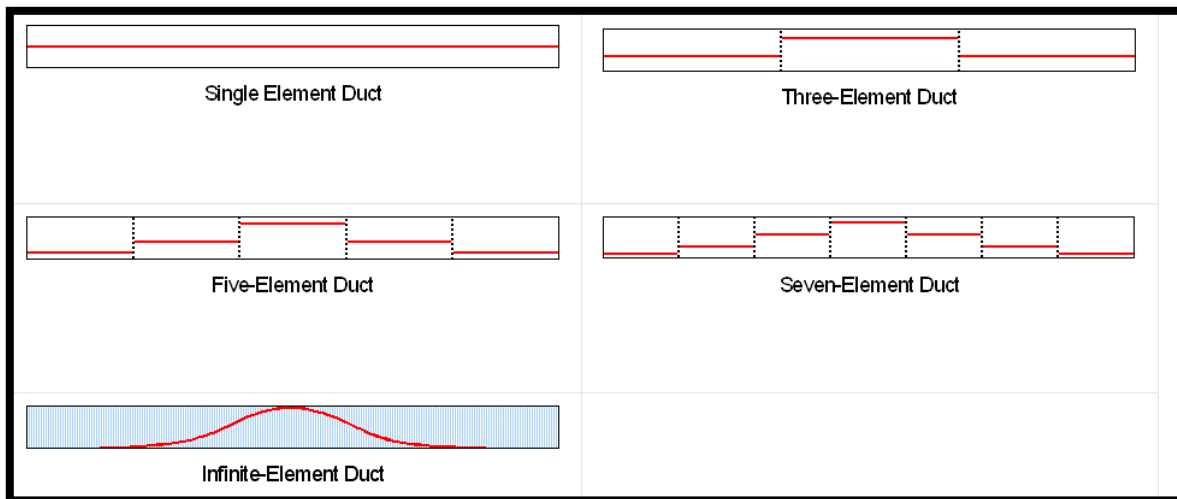


Figure 17 Discretization Length Basic Explanation with Different Number of Elements

wave. Higher discretization, i.e. more elements/sub-volumes, means better resolution of results hence higher accuracy. However, this also slows down the simulation. Discretization creates a trade-off in price (computational time) vs. performance (accuracy).

Higher discretization slows the simulation in two ways. More elements mean more calculations as each fundamental equation is solved on a per-element basis but more importantly, WAVE is an explicit solver with a variable time step size. During a WAVE simulation, the Courant condition is used for every sub-volume to determine the maximum allowable time step size.

Time step size is linearly related to discretization. The smaller the elements, the smaller the time step, and therefore more time steps needed to complete the simulation. A single small element in the system could limit the time step size for the entire model.

WAVE automatically discretizes each duct within a model when the user provides a discretization length. The final sub-volume size is determined as a function of both overall length and discretization length. The discretization length represents the desired sub-volume size. It is used by WAVE to divide the duct into a number of equal-length sub-volumes whose lengths are as near the discretization length as possible. To achieve the best combination of speed and accuracy, it is recommended that the discretization length is set equal for all ducts of similar temperature within a system. This is because the time step size is also related to the instantaneous speed of sound (which itself is a function of gas temperature). The hotter a duct is, the larger the discretization length must be to maintain the same time step size.

### 3.3.4. Heat Transfer Model

Heat transfer sub-models are used to calculate the convective heat transfer coefficient in the engine. The great amount of heat produced has a big impact on the engine efficiency, friction and wear. Several simulation models exist for evaluating the heat transfer coefficient, one of the most common in engine research being the Woschni model. The original model for heat transfer assumes simple heat transfer from a confined volume surrounded on all sides by walls representing the cylinder head, cylinder liner and piston face areas exposed to the combustion chamber.

Unfortunately, Wave does not have the opportunity to manually insert the Woschni heat transfer coefficient. The only choice is to provide the software with input regarding the model type and heat transfer multipliers and let the program calculate automatically. The Woschni heat transfer coefficient is defined by the following formula:

$$h_g = 0.0128D^{-0.20}P^{0.80}T^{-0.53}v_c^{0.8}C_{enht}$$

The Woschni's modified correlation will be used in this project and most likely set to be calculated automatically since the option of manually inserting the Woschni correlation is, as mentioned earlier, not provided by Wave but only the ratio.

### 3.3.5. Combustion Model

Combustion occurs in the cylinder element and relies on the amount of fuel delivered into the model. Typically, it is prescribed, following a heat release curve that is scaled by the actual amount of fuel delivered and fitted between the combustion start point and duration. These parameters can all be controlled to make the model's behavior match measurements.

Fuel is added to the model by injectors, or, in special cases, by adjusting the fluid composition in intake ambients. Fuel introduced into ducts and ambients is treated as fully premixed. Fuel introduced into the cylinder is treated as a spray and follows a mixing schedule.

The basic engine model is a time-dependent simulation of in-cylinder processes, based upon the solution of equations for mass and energy. The mass equation accounts for changes in in-cylinder mass due to flow through valves and due to fuel injection. A separate calculation is made for fluxes of air, vaporized fuel, liquid fuel and products of combustion. The liquid fuel is assumed to have mass but to occupy only a very small volume (very high density compared to the gases). The energy equation is based on the first law of thermodynamics (Principle of conservation of energy) and equates the change of internal energy of in-cylinder gases to the sum of enthalpy fluxes in and out of the chamber, heat transfer, and piston work.

The terms “burn rate” and “heat-release rate” are often used interchangeably. There are however distinct differences between the two that are important in respect to their usage in WAVE. Burn rate can be defined as the rate at which the fuel mass in the cylinder is consumed in the combustion process to become products of combustion. Regardless of the final state of the air/fuel mixture (emissions products, free radicals, burned air, etc.), the initial fresh air and fuel no longer exist in their natural states when combustion has completed.

Heat release rate itself can have many different meanings but is most often intended as “apparent heat release rate”, which is usually calculated using analysis methods from a measured in-cylinder pressure trace. It is labeled “apparent” as the analysis methods of the in-cylinder pressure measurement cannot perfectly account for the heat transfer through the chamber walls and the unknown instantaneous specific heat ratio during the combustion event. For premixed combustion of fuel-lean or stoichiometric mixtures, the heat release profile should be fairly close to the fuel burn rate profile.

The approach for this thesis will be to define the combustion profile by the Wiebe function. Wiebe is widely used, simply using the combustion duration. A curve simply represents the fuel mass burned in the cylinder. The Wiebe function is empirical constructed and is used to describe the heat release during combustion approximately but quite accurately. The Ricardo Wave program uses the function below to calculate the mass fraction of burned fuel ( $W_n$ ) as a fraction of crank angle:

$$W_n = 1 - \exp\left(-AWI \left(\frac{\theta}{BDUR}\right)^{WEXP+1}\right)$$

Where, AWI represents the internally calculated parameter to allow BDUR to cover the range of 10-90%, BDUR represents the User-entered combustion model (10-90%), WEXP refers to the user-entered exponent (controlling the shape of the Wiebe curve) and  $\theta$  the degrees past start of combustion. The user can also select the profile control terminate value for the SI Wiebe combustion model to be fully defined. The control terminate value refers to efficiency and will not be tampered with.

As stated by (Gilani, 2012), to be able to transform maximum amount of chemical energy into thermal energy and then produce kinetic energy it is crucial that the combustion starts, peaks and ends at the right position of the crankshaft. Since the compression ratio and air/fuel mixture remain constant throughout the rpm range in the program’s simulation setup, the amount of time it takes to combust can be considered constant as well. Therefore, it is necessary to adjust the initiation of the combustion regarding to the crankshaft position, earlier with higher rpm. The location of 50% burn point and the combustion duration will therefore not be set as constants but as a variable depending on rpm.

All the forementioned data will be set as variables which provide the software with new data for each case hence altering the behavior of the curve. Varying the 50% burn point simply shifts the entire curve forward or backward, Varying the 10-90% duration will extend the total combustion duration, making the profile extend longer or compress shorter. Varying the Wiebe exponent will shift the curve to burn mass earlier or later. All the values for the CA50 and BDUR variables for each case can be found in tables 8 and 9. The figure below shows the SI Wiebe combustion model in Wave.

Properties		
Location of 50% Burn Point	{CA50}	deg
Combustion Duration (10%-90%)	{BDUR}	deg
Exponent in Wiebe Function	2.0	
Profile Control	Terminate at	1.0

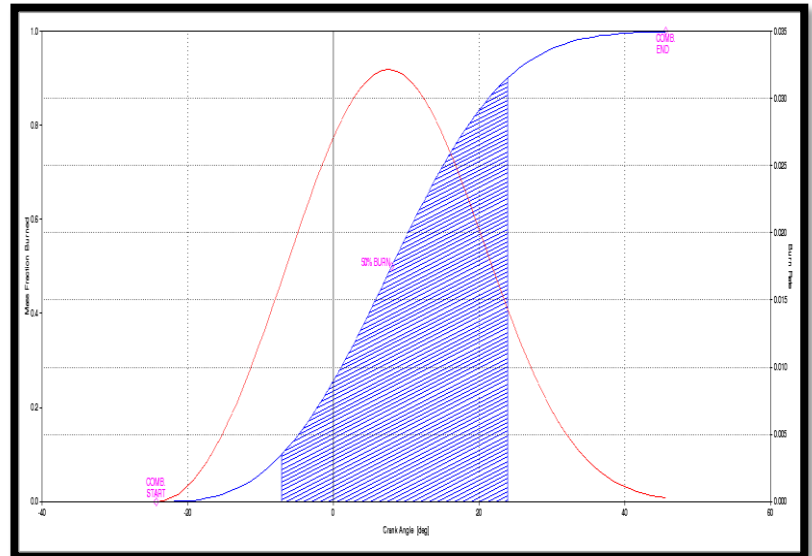


Figure 18 SI Wiebe Combustion Model in WAVE and Table of Properties

### 3.3.6. Complex Y-Junction

The complex Y-junction (collector) is a more flexible option to the simple Y-junction with more possibility to control and adjust. It is however more complicated to use. It is a single computational cell in the flow network and is best applied if one of the following conditions applies:

- The volume is duct-like. In this case complex Y-junctions will represent more accurately the junction volume as well as the flow path length through it.
- The volume has perforated walls (such as inside silencers) or connects to many parallel passages (such as heat exchanger or catalyst brick).
- The volume is elongated or of non-uniform size – the distance across the junction or its cross-sectional areas are different from different sides (such as an air cleaner).

A complex Y-junction must be attached to one or more ducts. The complex Y-junction shape is not required to be provided; this enables to construct all shapes of junctions but is a rather complicated input to measure hence there is some specific distances required for Wave to be able to approximately represent the junction. By providing the number of ducts connected to the junction together with DELX, DIAB, pressure, flow direction, duct shape, diameter and angle in between the ducts the matrix for the system can be solved.

The Y-junction diameter is required to calculate flow velocity. Through this value, Wave calculates the Reynolds number hence this value affects the heat transfer between the gas and the wall. Another important parameter is the volume. This is the primary variable used in calculation of mass transfer (not the diameter), and thus is equivalent to the discretization of a duct in its effect on overall solution speed. Further important variables that affect the y-junction include the X,Y,Z angles. The orientation angles specify the direction in which a duct enters

or leaves a specific y-junction. The defined angles are specific only to that particular junction, i.e. the orientation of the openings only need to be correct relative to each other and not the any global coordinate system. The 3 angles are calculated using direction cosines for a Cartesian coordinate system.

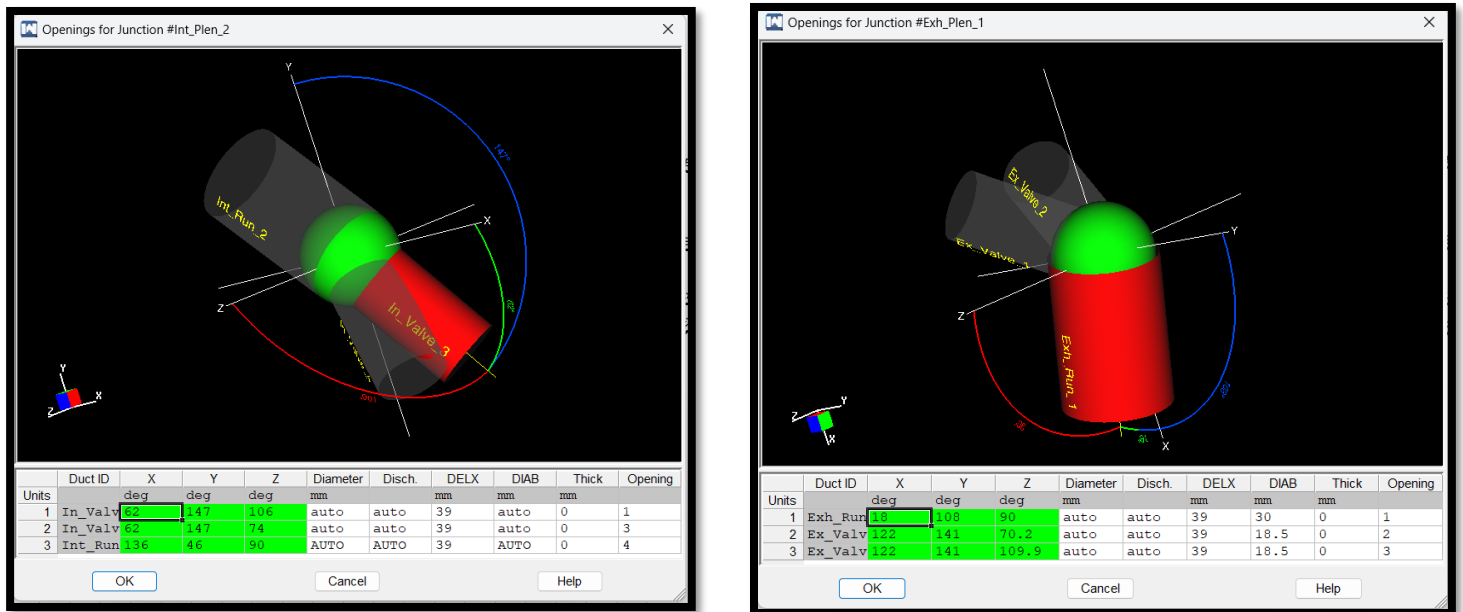


Figure 19 Complex Y-Junction Illustration of Intake (Left) and Exhaust (Right) of the Yamaha R6 Engine

The X, Y, and Z values define the angle between the duct and each of the respective axes. A positive angle does not give a rotation in a particular direction, so the correct definition of all three angles (regardless of sign) is required to ensure that there is only one possible opening orientation. The DELX variable represents the characteristic length of the y-junction relative to the opening, typically taken to be the distance across the volume from the opening to the opposite side. The DELX is used to calculate the total distance traveled by gas through the volume. A duct also has a DELX value, but is known as the “Discretization Length” (dx). In a complex y-junction, one-half of the DELX value for one opening (A) plus one-half the DELX of another opening (B) represents the total flow length from opening A to opening B through the volume as the figure shows below:

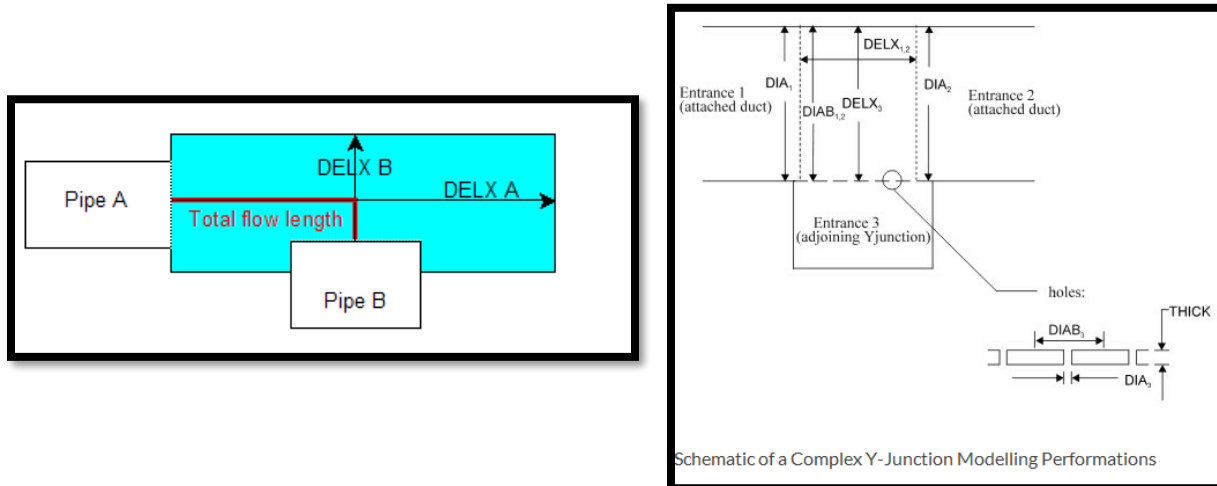


Figure 20 Complex Y-Junction Modeling Dimensions

The variable DIAB represents the Expansion diameter of Y-junction opening. Used to determine area ratios for flow losses entering and leaving the Y-junction. If set to “AUTO”, this value will be calculated by the code as the Y-junction’s “Diameter” (not the individual opening’s “Diameter”) divided by the square root of the “Count” of the attached duct. This dimension also affects the momentum transfer in the Y-junctions between the individual openings and the dissipation of the momentum flux into heat.

Finally, is the thick variable which accounts for the thickness of the implicit orifice at the boundary between the Y-junction and attached duct. Sharp edged orifices have zero thickness, but square orifices have a thickness that should be accounted for.

## 4. Engine Selection – Specifications Identification

### 4.1. Engine Choice-Engine Specifications

As previously stated, the competition rules require the use of an engine with a maximum capacity of 710 cm<sup>3</sup>. Based on market research and previous competitions, a trend formed that led practically every team to use bike or racing bike engines. Some of them went through the process of building their own engine which in our case was considered an unviable option. Hence, thorough research was made into motorbike engines. The majority of these engines are oversquare (the diameter of the cylinders is larger than the stroke of the pistons) and high-revving, which is in line with the racing philosophy of the competition.

At the same time, they have an integrated gearbox, which is designed for their torque value, whilst they are usually serial type, which makes the gearchanges quick and the handling on the driver's side simple and effortless. Finally, these motors are designed to be anchored on the frame of the bike without elastic mounts, and thus carry loads, which is similar to our application. An important parameter for the operation of an engine is also the number of cylinders. The number of cylinders simultaneously affects maximum rpm (and therefore the horsepower), vibrations, weight and the cost, both of the engine itself and of all its peripherals. Another aspect to keep in mind is whether or not forced induction is utilized. Commercial engines are rarely turbocharged, so the design and customization would have to be done by the team,

which was deemed inconvenient. The final decision was made from the team to use a Naturally aspirated (NA) engine with the help of a decision matrix which can be seen below. The goal matrix display at chapter 1 was also utilized in order to rate accordingly each type of engine based on the team's needs. A scale of 1 through 5 was used with 5 being an excellent score and 1 correspond to poor performance.

*Table 2 Engine Type Evaluation Table*

	Power	Torque	Cost	Market Availability	Reliability	Weight	Total
1 Cyl. NA	2	3	5	5	2	5	22
4 Cyl. NA	4	2	3	5	4	3	21
1 Cyl. Forced Induction	2	5	2	1	1	4	15
4 Cyl. Forced Induction	5	3	1	1	1	1	12

The table above demonstrates a clear advantage for naturally aspirated engines. Aside from the apparent size, weight, and simplicity advantages, there are numerous very genuine performance benefits to using a single-cylinder engine. Motocross bikes are designed for tracks with short straights and tight corners, so the power requirements are much like an FSAE track. Therefore drivability, especially out of corners, is great because of high torque and diminished emphasis on gear changes. One of the most important benefits is the cost. Being a first-year team, managing a very tight budget and maximizing performance out of every part was the key in order for the project to succeed. In a one-cylinder engine, because there are less parts to manufacture (i.e. one intake vs. four) and everything on the car being smaller means less material cost. The engine is also easy to tune because there is no need to balance the air flows to the cylinders and easy to maintain with only one spark plug to change.

However, there are also drawbacks, like diminished throttle response. Four-cylinder powered cars are much faster on the course straights as well. Also, comparing drivetrain component sizes like gears and clutches, single cylinder engines can actually have the same or larger components than multi-cylinder engines. A single-cylinder engine gives only one power stroke per revolution (two-stroke cycle) or two revolutions (four-stroke cycle). Hence, the torque pulses are widely spaced, and engine vibration and smoothness are significant problems.

Multicylinder engines are invariably used in automotive practice more often. As rated power increases, the advantages of smaller cylinders in regard to size, weight, and improved engine balance and smoothness point toward increasing the number of cylinders per engine. An upper limit on cylinder size is dictated by dynamic considerations: the inertial forces that are created by accelerating and decelerating the reciprocating masses of the piston and connecting rod would quickly limit the maximum speed of the engine. The increased frequency of power strokes with a multicylinder engine produces much smoother torque characteristics. Multicylinder engines can also achieve a much better state of balance than single-cylinder engines. Four-cylinder in-line engines are the most common arrangements for automobile engines up to about 2.5-liter displacement. It provides two torque pulses per revolution of the crankshaft and primary inertia forces are balanced.

Based on the forementioned data, the team turned towards finding a 4-cylinder naturally aspirated engine. With the help of one of its sponsors, it managed to acquire a Yamaha YFZ-R6 engine of the 2006-2007 model year (YZFR6V©). It is a four-stroke transverse in line 4 cylinder with Dual Over-Head Camshafts (DOHC) with 4 valves per cylinder. It is a Naturally aspirated engine, water cooled with a mechanical pump and a gearbox with 6 gears. This engine unit will form the basis of the team’s first race car and it will be the one simulated through the 1D modeler. Some basic data from the constructor about the engine can be found on the table below.

*Table 3 Yamaha R6 2006 Engine Specifications*

Make Model	Yamaha YZF R6
Year	2006
Engine Type	Liquid-cooled 4-stroke DOHC
Displacement	599cm <sup>3</sup>
Cylinder Arrangement	Forward-inclined parallel 4-cylinder
Bore*Stroke	67.0 X 42.5 mm
Compression ratio	12.8:1
Recommended fuel	Premium unleaded gasoline
Lubrication System	Wet Sump
Transmission type	Constant mesh 6-speed
Max Power (BHP)	125 to 133 hp @ 14500 rpm
Max Torque (BT)	59 to 68 Nm @ 12000rpm
Wrist Pin Offset	0.5 mm
Weight	54 kg

## 4.2. Real life Measurements

The data presented in the previous chapter were all gathered through the manufacturer’s manual. All the forementioned values will be considered as constants when they will be inserted into the program. In addition to the constants, further measurements were made with the help of Xaris Kontonassios, the previous head of the Engine & Powertrain Sub team. These measurements include valve profiles and diameters, the head cylinder ducts and junctions as well as the intake runner and throttle body. All these data were collected and will be used into the program and to the final geometry design. All the measurements were made using the necessary tools such as a micrometer and a thickness gauge.

At first, the intake manifold flanges were measured. These will be used in the final intake assembly as the connection point between the intake and the engine block.



*Figure 21 Yamaha R6 2006 Stock Intake Flange*

*Table 4 Yamaha R6 2006 Intake Flange Data*

D IN circle	46.00 mm
D1 OUT (ellipse)	38.50 mm
D2 OUT (ellipse)	33 mm
L total	24.00 mm
L circle	9.50 mm
L ellipse	14.50 mm



Then, the throttle body was measured, with the main emphasis to the inside diameters, the total length and the injector placement.

Table 5 Yamaha R6 2006 Intake Throttle body Data



Figure 22 Yamaha R6 2006 Throttle Body

Duct diameter before throttle	Throttle Diameter	Throttle Shaft Diameter	Duct diameter after throttle
42 mm	40 mm	5 mm	39 mm
Total Length	Length before Throttle	Length after Throttle	Injector placement (From throttle)
90 mm	49 mm	41 mm	19 mm

Next, the head cylinder was measured. It was split into 2 different sections, the intake and exhaust. Each port was then split into different dimensions such as Length and Diameter and the volume of each port was calculated in order for the value to be inserted into the software. The schematic below illustrates the different values that were collected.

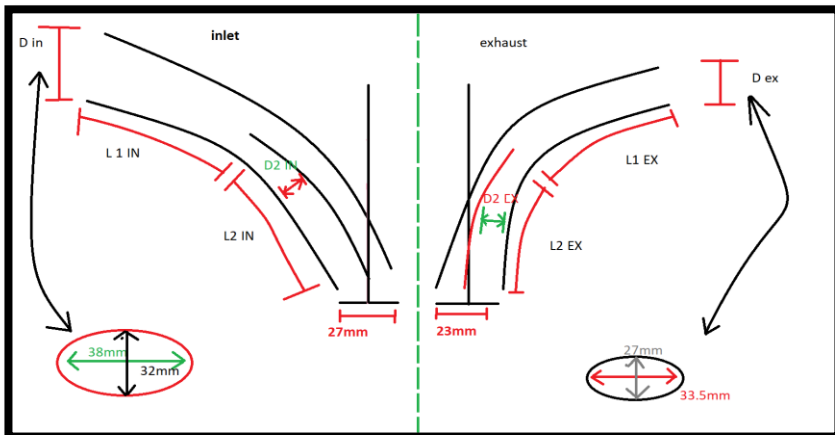


Figure 23 Schematic of Intake and Exhaust Port Geometrical Analysis



Figure 24 Intake Ports of the Yamaha R6 Cylinder Head

Table 6 Intake Valve Port Data for Ducts and Y-Junction

INLET		Y-JUNCTION INTAKE (Figure 19 Illustration)									
Diam. In Major	38 mm	DUCT ID	X	Y	Z	DIAM	DISCH COEF	DELX	DIAB	THICK	
Diam. In Minor	32 mm	UNITS	deg	deg	deg	mm	-	mm	mm	mm	
D2 In (Major)	24 mm	1	InductionValve1	62	147	74	auto	auto	39.0	auto	0.0
L1 In	50 mm	2	InductionValve2	62	147	106	auto	auto	39.0	auto	0.0
L2 In	45 mm	3	IntakeRunner	136	46	90	auto	auto	39.0	auto	0.0
L Total	95 mm										
Intake Plenum Volume	0.098 Lt										
Valve Diam.	27 mm										

Table 7 Exhaust Valve Port Data for Ducts and Y-Junction

EXHAUST		Y-JUNCTION EXHAUST (Figure 19 Illustration)									
Diam. Ex Major	33.5 mm	DUCT ID	X	Y	Z	DIAM	DISCH COEF	DELX	DIAB	THICK	
Diam. Ex Minor	27 mm	UNITS	deg	deg	deg	mm	-	mm	mm	mm	
Diam.2 Ex (Major)	19 mm	1	ExhaustValve1	122	141	70.2	auto	auto	39.0	auto	0.0
L1 Ex	23 mm	2	ExhaustValve2	122	141	109.9	auto	auto	39.0	auto	0.0
L2 Ex	17 mm	3	ExhaustRunner	18	108	90	auto	auto	39.0	auto	0.0
L Total	40 mm										
Runner Port Diam.	45 mm										
Runner Port L	9.5 mm										
Exhaust Plenum Volume	0.042 Lt										
Valve Diam.	23 mm										

Finally, the intake and exhaust valves need to be studied. More specifically the valve lift profiles which need to be inserted into the program to ensure correct operation of the model. The valve opening was measured relative to the camshaft angle at first and then was corresponded to crank angle to insert to the program. The valve diameters as well as the lash values were also recorded. The resulted diagrams can be viewed below whilst the Table Data used can be found in the Appendix.

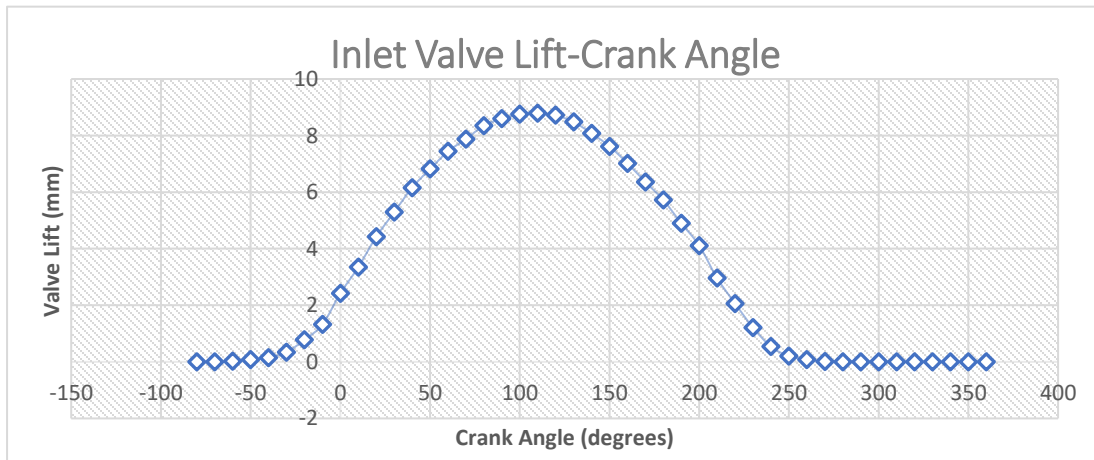


Figure 27 Intake Valve Lift - Crank Angle Diagram



Figure 26 Top View of Yamaha R6 Cylinder Head



Figure 25 Exhaust Ports of Yamaha R6 Cylinder Head

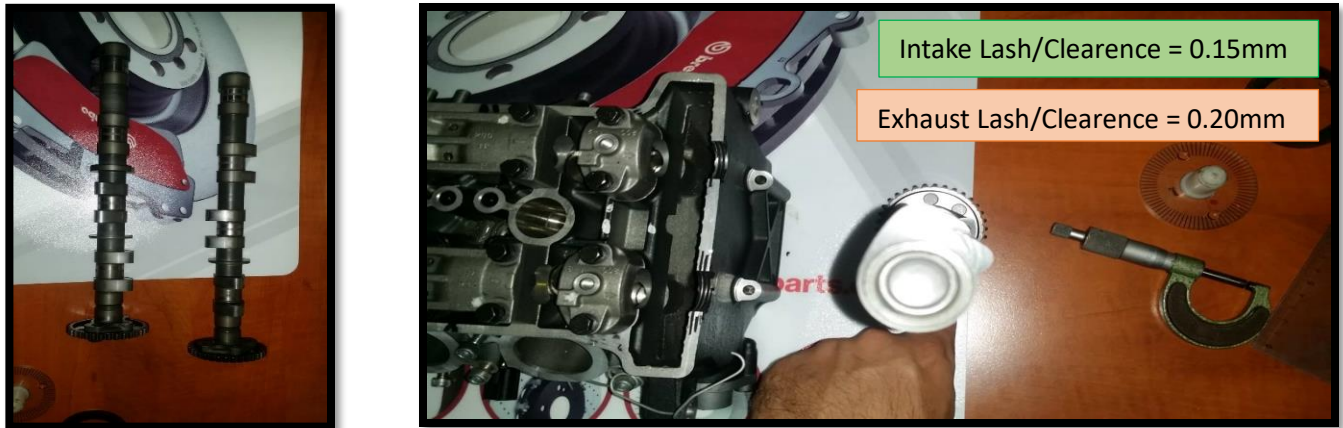


Figure 28 Intake and Exhaust Camshafts of Yamaha R6 Cylinder Head

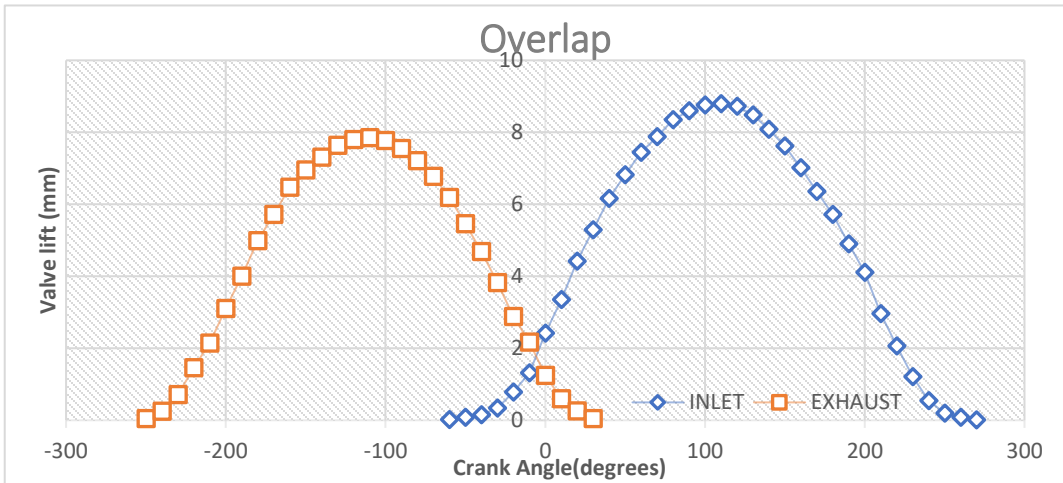


Figure 30 Valve Overlap Diagram

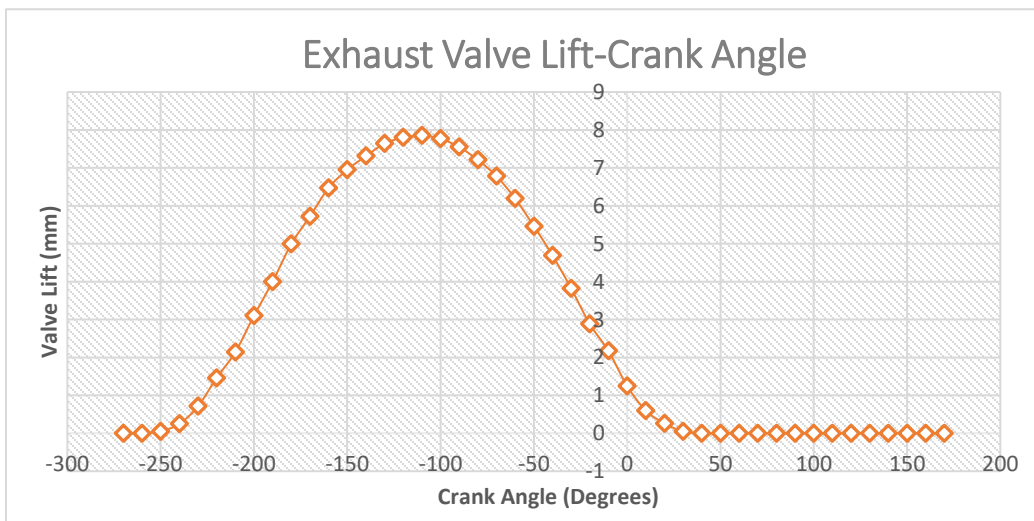


Figure 29 Exhaust Valve Lift-Crank Angle Diagram

### 4.3. Data insert into Engine Model

Before attempting to construct the Yamaha R6 engine model in Wave by adding components it was required to provide the software with some general information. All units in the simulation control were defined in the SI system with [mm] as the basic unit for length. The basic fuel available in the FSAE Series is unleaded gasoline with octane rating of 98 RON. Fuel in reality can vary in quality. The simulation was therefore implemented on a special laboratory fuel called **indolene**. This fuel has an equal amount of energy value as the 98 RON unleaded which is a liquid test fuel and should therefore correspond well to reality. It is also used according to the US Federal Test Procedure for vehicle certification as it allows for perfectly reproducible results due to low sulfur content and lack of additives. Another setting that needs to be altered is the duration of the simulation. A number of 50 engine cycles, is enough to achieve convergence. The code is configured to assume that convergence has been achieved when for 2 consecutive cycles it has results that differ by less than 1% in the values of fluid pressure and velocity in each computational cell at the end of each cycle. In case of convergence, it stops running the specific case regardless of whether it has completed 50 cycles.

#### 4.3.1. Simulation Controls

The goal for the program is to make a fully customizable model so that changes in basic dimensions and geometry can be made immediately and easily. This makes it much easier to optimize the design, since virtually all the basic characteristics of the intake assembly remain undefined. Below, the simulation control options can be observed that include all the options and parameters used for the final simulation.

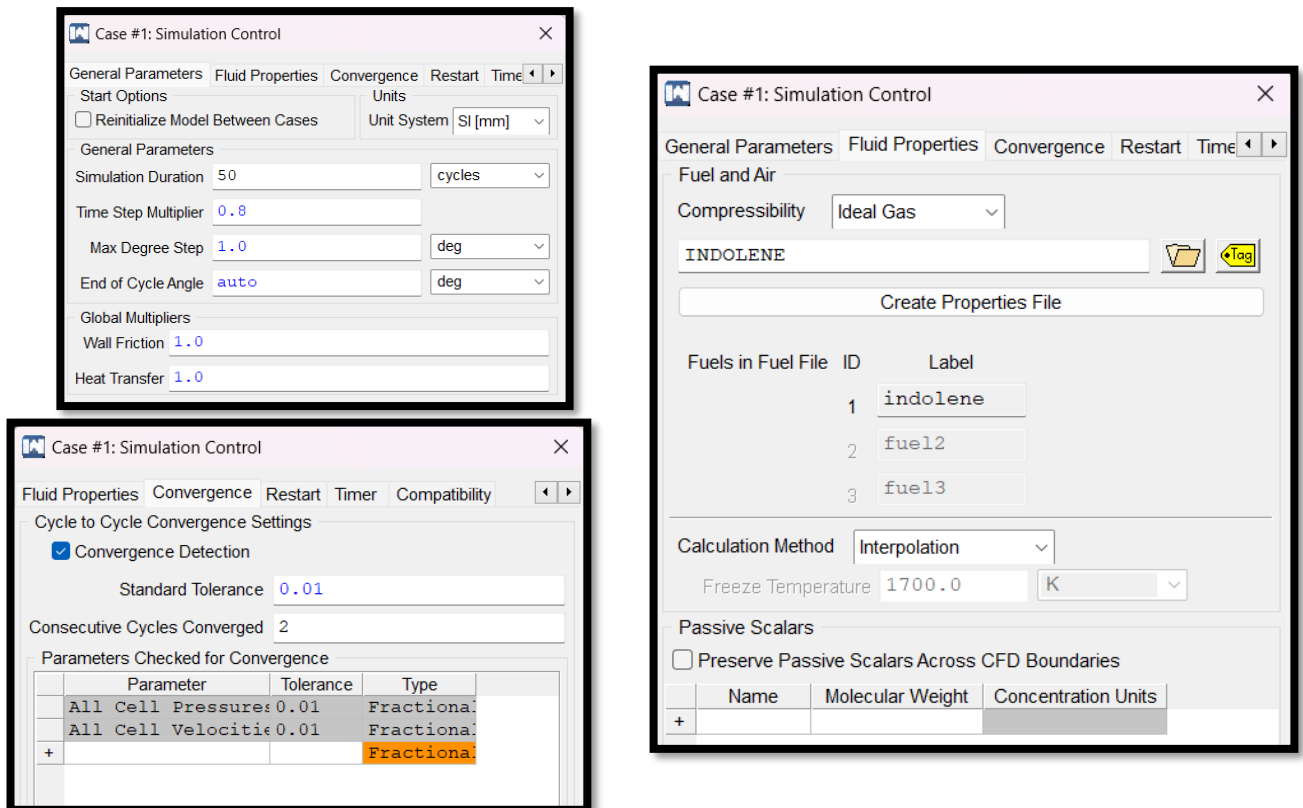


Figure 31 Simulation Control Settings for Ricardo Program

### 4.3.2. Intake Ambient

As the general parameters have been defined, the next step is to feed in geometric characteristics data as well as specify the initial and boundary conditions. Navigating through the canvas to the Tools menu, the air composition can be changed to 21% Oxygen and 79% Nitrogen. Below, the settings for the ambient element which is simulating the environment conditions can be seen. The “auto” diameter adjust automatically to the connected duct. Value of 1.0 [bar] and 300 [K] and a composition of 100% fresh air represent the environment adequately. The discharge coefficient [Cd] was set to “auto”.

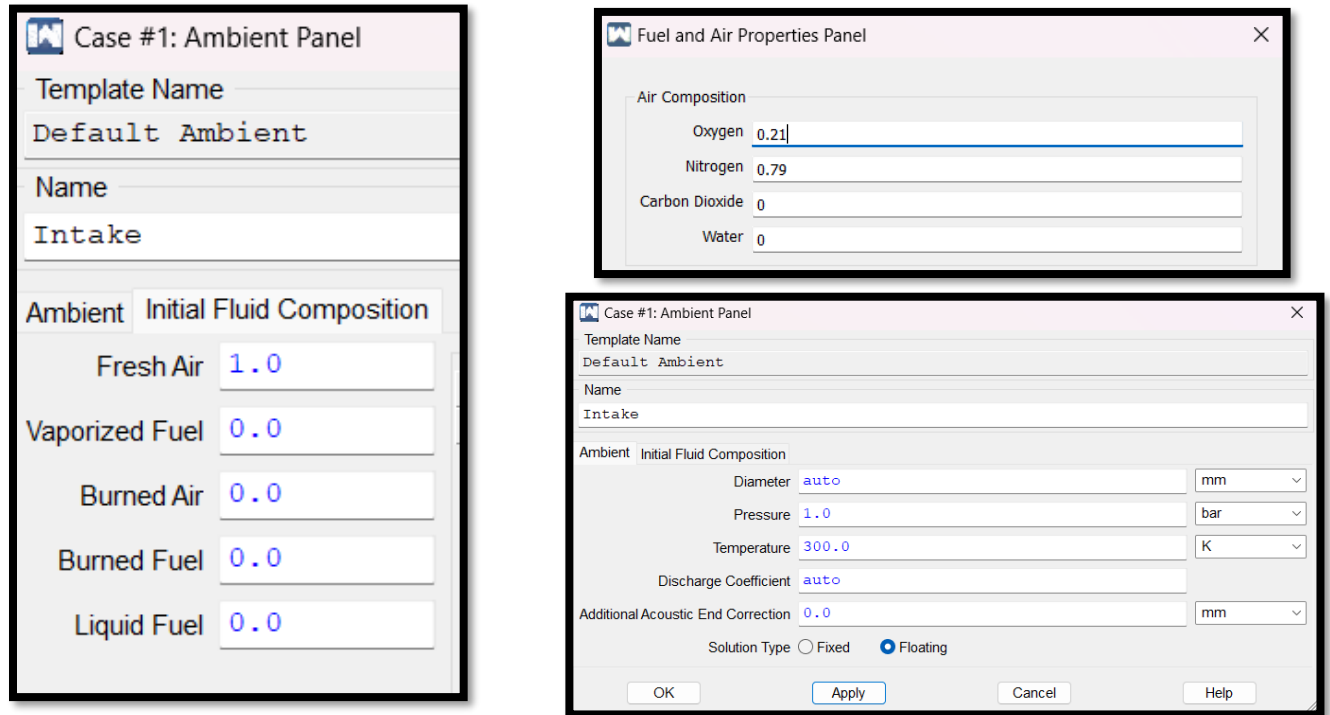


Figure 32 Ambient Settings for Ricardo Program

### 4.3.3. Ducts (Valve ports)

This chapter will cover the basic settings for the ducts that represent the valve ports. The discretization length was set to 30 mm. This is the program's default discretization length. Since this is a multi-cylinder engine, solving time is an issue, so no changes were made to this setting. The accuracy is much needed in the intake part of the model and so lower values will be used for those parts. The total length of the duct In\_Valve\_1 is 45 mm which is 1.5 times the discretization length. Wave would automatically divide the duct into several equal lengths but for this example the total length corresponds to the discretization length.

The entire engine head is made of aluminum, therefore the roughness height for In\_Valve\_1 and every other duct which represents the valve ports was set to 1.5  $\mu\text{m}$ , which is an average value for new aluminum. The discharge coefficient for the left and right end of duct1 was set to “auto” as well as for all the other orifices and ducts since automatic calculation of the discharge coefficient returns back a trustworthy result.

The Wall friction and wall heat transfer inputs are only multipliers of the standard calculation and were kept as default since normal conditions applied. Regarding the initial conditions, with the help of constants different initial conditions could be simulated in order to study the engine operation under different circumstances. The atmospheric pressure and the surrounding temperature have a great impact on the outcome and needed to be very accurate. The default wave pressure value was raised notably in 1.01 bar. The temperature of injected air was more difficult to determine. The air intake is just millimeters away from the combustion chamber. Furthermore, engine packing at the vehicle's rear has proven to be a difficult undertaking, requiring the engine and intake system to be extremely tight. As a result, the intake air temperature fluctuates several degrees throughout operation and is more likely to remain higher. For the simulation to correspond accurately to the real engine, the initial intake temperature was set to 305K = 32°C which is higher than the Wave default value.

Multipliers		Coefficients	
Wall Friction	1.0	Left Discharge	auto
Wall Heat Transfer	1.0	Right Discharge	auto
		Pressure Loss	<input checked="" type="radio"/> Fixed 0.0
			<input type="radio"/> vs. Reynolds Number <span>Edit Profile</span>

Dimensions	Coefficients	Initial Conditions	Body Forces
Pressure	{In_P}		bar
Temperature	{In_T_Int}		K
Wall Temperature	{Wall_Temp}		K

Figure 33 Coefficients and Initial Conditions for Valve Port Ducts

Name	Connectivity	
In_Valve_1	Left ID Int_Plen_1	Right ID cyl1
Side View	Top View	3D View
Duct Data	Attachments	Structure Initial Fluid Composition
Dimensions	Coefficients	Initial Conditions Body Forces
Shape	Circular	Discretization Length 30.0 mm
Circular	Rectangular	Overall Length 45.0 mm
Left Diameter 27.7 mm		Roughness Height 1.5 um
Right Diameter 27.7 mm		Count 1.0
		Bend Angle 0.0 deg
		Maximum Taper Angle 0 deg

Figure 34 Duct (Intake Valve Port Settings) for Ricardo Program

Similarly, the exhaust ports were simulated using ducts with the main difference being the initial temperature which was raised to 310K= 37°C. The initial conditions used here simulate a cold engine that has been not been operational for a several amount of time.

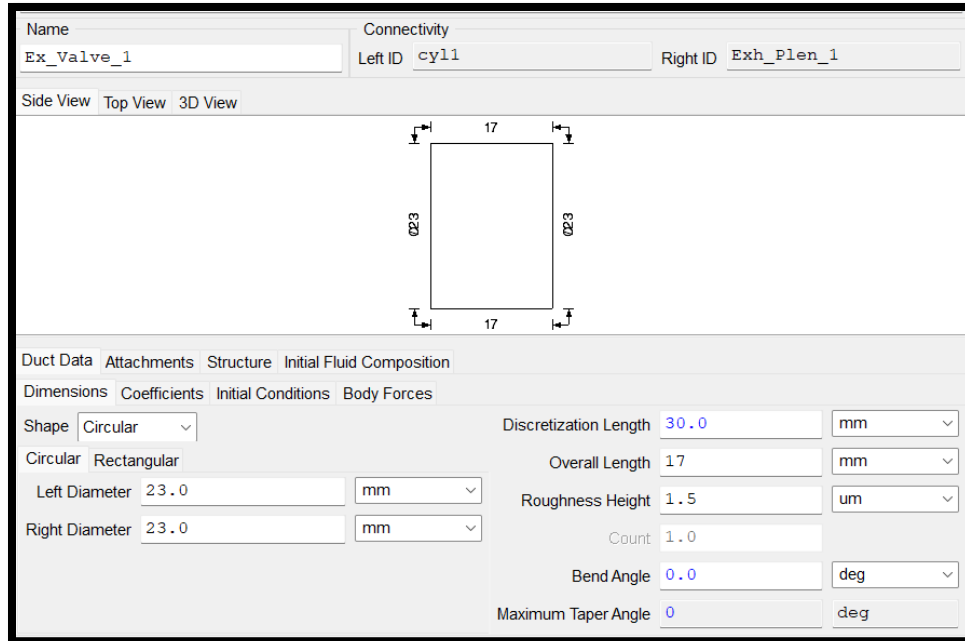


Figure 35 Duct (Exhaust Valve Port Settings) for Ricardo Program

As it can be seen by the above figures, Wave gives the option to alter the shape of the duct between circular and rectangular. The schematic shown in the previous paragraph illustrates the shape of the valve ports which is elliptical. This can also be confirmed through the photos. Since elliptical shape is not optional in Wave this has to be compensated for. To overcome this issue, since the program only uses the effective area to run the simulation, the ducts were selected into the program as circular and an appropriate value of diameter was chosen to simulate the same effective area as the one in the real engine. The schematic above also illustrates that in order to simulate the ports accordingly, each port was split into three different elements into the program. The first part was simulated as a complex Y-junction and the second part as two separate ducts. These ducts connect with the valves of the cylinder.

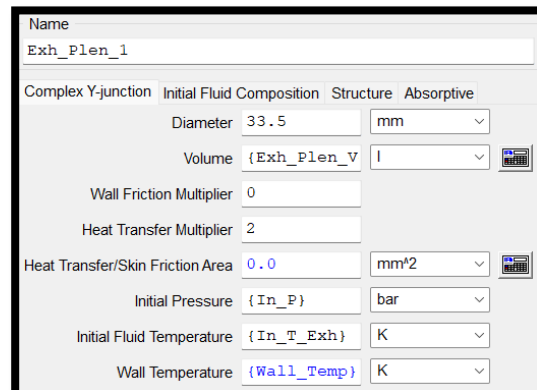
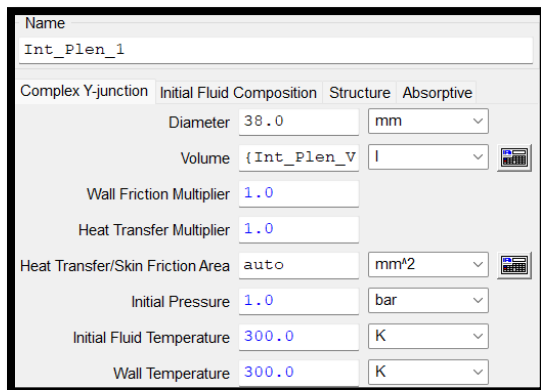


Figure 36 Intake and Exhaust Valve Y-junction Settings

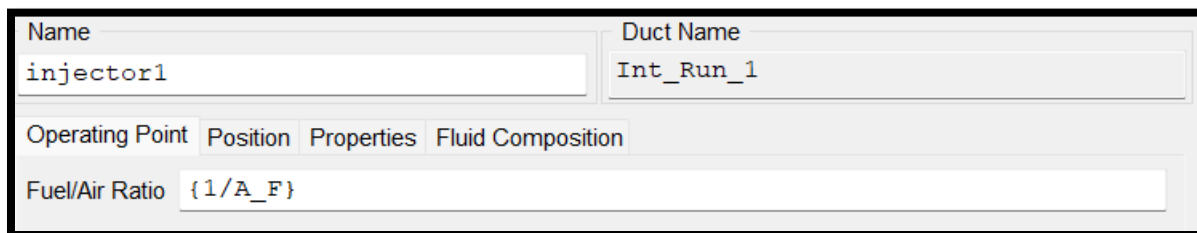
For the complex Y-junctions, the volume was calculated with the measured data of the ports as well as taking into consideration the throttle body flange for the intake and the exhaust runner port for the exhaust flange. The settings for the openings for each complex Y-junction can be found on the table in the previous paragraph.

#### 4.3.4. Fuel Injectors

The Yamaha R6 Engine utilizes port fuel injection with eight fuel injectors. Four of them are considered to be the primary and the other four the secondary ones. The primaries are placed to the throttle body with a certain angle in order to achieve a better air fuel mix. For the needs of the 1D simulation, the primary ones are only going to be simulated since the secondary ones are not going to be utilized in the final car since the team had only the primary ones at their disposal. The lack of the secondary injectors was resolved through the aftermarket ECU that was used in the vehicle.

The advantages of port fuel injection are increased power and torque through improved volumetric efficiency and more uniform fuel distribution, more rapid engine response to changes in throttle position, and more precise control of the equivalence ratio during cold-start and engine warm-up. Fuel injection allows the amount of fuel injected per cycle, for each cylinder, to be varied in response to inputs derived from sensors which define actual engine operating conditions. Following the goals that were mentioned at the start of this thesis, in order to achieve maximum durability and reliability of the power unit, the placement of the injectors onto the final intake assembly was to remain as close to the one used by the manufacturer as possible. Hence, the injector angle and distance from the intake port was measured and inserted into the software. These angle and distance values will remain the same for the stock engine model that is simulated at this time of the thesis as well as for the modified model in the later stages.

The primary injectors used are the DENSO 297500-0640. Due to limited data from the manufacturer, the inserted values used were kept close to the default ones of the program. Firstly, the fuel to air ratio is inserted. For the 1D software, constants have been used again for easier and faster changes of values. The air to fuel ratio is equal to the stoichiometric value of 14.7 and so the inverse fraction represents the fuel to air ratio which is directly calculated by the program.



The screenshot shows the configuration interface for an injector in the Ricardo program. It features two input fields at the top: 'Name' with the value 'injector1' and 'Duct Name' with the value 'Int\_Run\_1'. Below these is a row of tabs: 'Operating Point', 'Position', 'Properties', and 'Fluid Composition'. The 'Fluid Composition' tab is active, showing a 'Fuel/Air Ratio' field with the value '{1/A\_F}'.

Figure 37 Injector Settings for Ricardo Program

The next option to define was the injector position. Based on the 4-throttle body data retrieved from the previous paragraph, we can simulate into the program the whole throttle body. Each throttle-body consists of two ducts and the throttle valve. The imported data for the ducts and the throttle can be seen in the figures below.



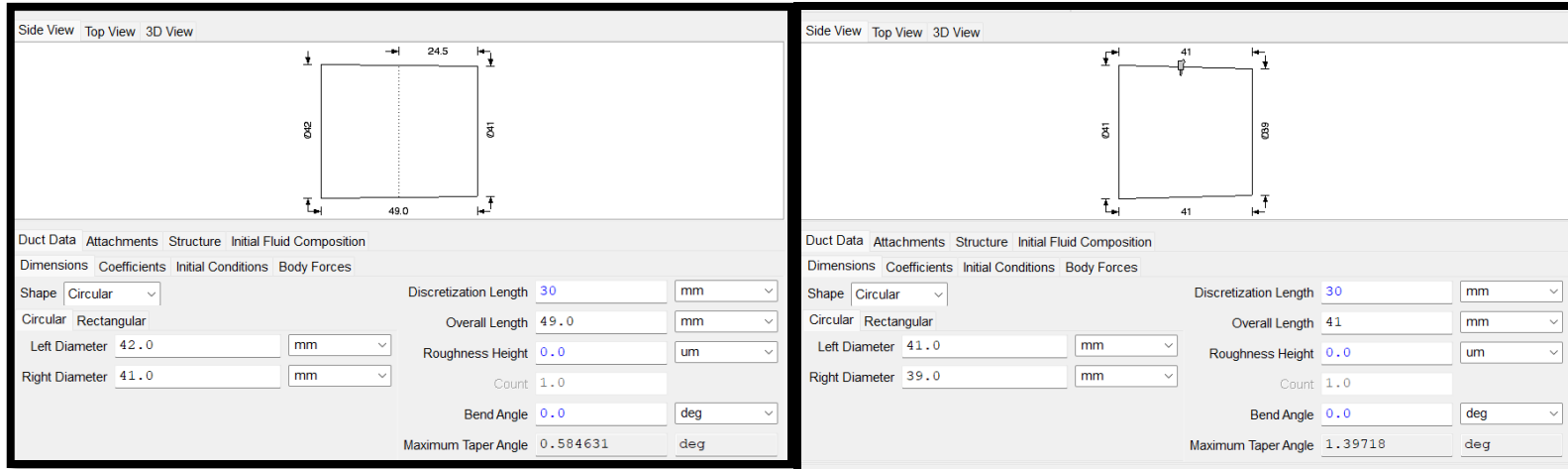


Figure 38 Duct Data and Injector Placement on Duct Port

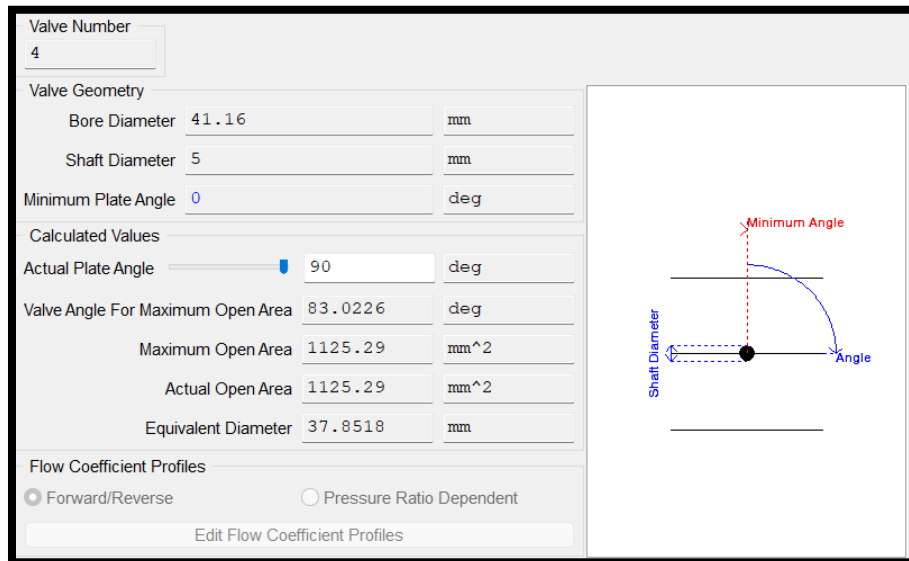


Figure 39 Throttle Valve Settings for Ricardo Program

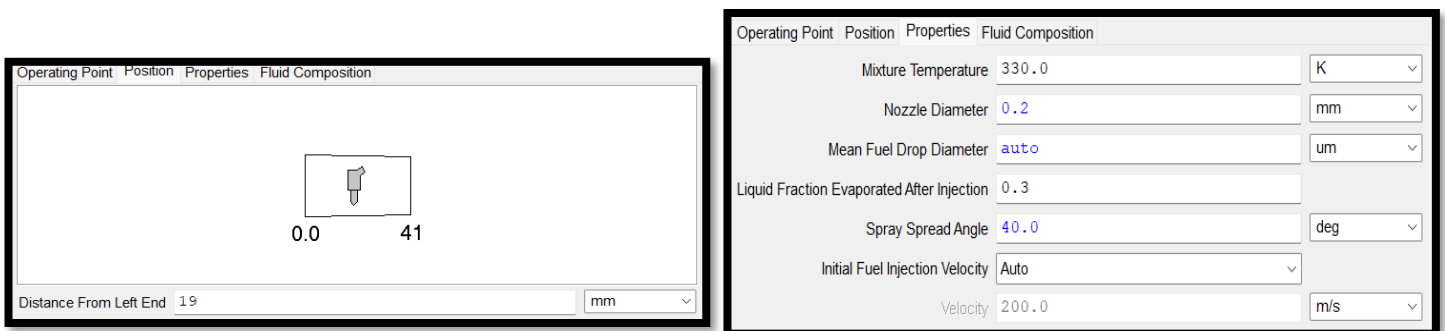


Figure 40 Injector Properties for Ricardo Program

Some basic properties for the injectors include the fuel mixture temperature which was raised compared to the default value in order to simulate the possible higher standard temperatures of the power unit. The temperature used is 330 K. All the other variables were kept as default except the evaporated fraction. This, refers to the fraction of any liquid injected which evaporates immediately after injection.

WAVE's standard convection model does not account for liquid evaporation in the flow network, with exception of inside the engine cylinders. Because some fuel evaporates between the injector and the cylinder (typically about 20%-30% in gasoline port-injected engines), an amount which will evaporate immediately can be specified upon being injected. The highest value of the recommended ones was chosen for this simulation.

#### 4.3.5. Cylinder - Engine

In order to fully simulate the engine into the program, Wave utilizes the cylinder element and the engine general panel. Through these panels, all the engine data in the engine choice table that were presented before can be inserted into the program. The Wave software provides an extended engine database that provides a wide variety of useful data regarding values that were impossible to measure from the team members or they were unapproachable after communication with the manufacturer. Some of these values include the friction correlation factors and the conduction settings for the engine components. The software menu after inserting the engine data is represented by the figures below.

The screenshot shows the 'Configuration' and 'Friction Correlation' panels of the Ricardo Wave software. The 'Configuration' panel includes fields for 'No. of Cylinders' (4), 'Strokes per Cycle' (4), 'Engine Type' (Spark Ignition), and 'Displacement' (0.599363). The 'Friction Correlation' panel includes fields for 'ACF' (0.3), 'BCF' (0.005), 'CCF' (325.0), and 'QCF' (0.2). The 'Firing Order and Relative TDC' table is also visible.

	1	2	3	4
Cylinder	1	2	4	3
TDC	0.0	180.	180.	180.

The screenshot shows the 'Operating Parameters' panel of the Ricardo Wave software. It includes fields for 'Engine Speed' (SPEED), 'Reference Pressure' (1.0), and 'Reference Temperature' (298.0).

Figure 41 Engine Settings and Geometrical Data for Ricardo Program

The Ricardo Wave program provides the user with a sample engine of a 600cc 4-cylinder motorbike exactly like the one used by the team. This model was used as reference for the thermal conductivity values for the cylinder walls, cooling and valves. The values used can be seen below.

Cylinder Walls Cylinder Cooling Valves

Properties

	Units	Piston	Cylinder Head	Cylinder Liner
Mean Thickness	mm	5	10	7
Thermal Conductivity	W/m/K	140	150	160
Total Volume	mm <sup>3</sup>	17628.3	35256.5	62619.8
Volumetric Heat Capacity	J/m <sup>3</sup> /K	3.e6	3.e6	3.e6
Coolant-Side Area	mm <sup>2</sup>	3525.65	3525.65	8945.69

Thermal Resistance Between Piston and Liner 0.005 K/W

Cylinder Walls Cylinder Cooling Valves

Boundary Conditions

Piston Fixed Head Fixed Liner Fixed

Properties

	Units	1	2	3	4
Piston Oil Temperature	K	{T_Oil}	{T_Oil}	{T_Oil}	{T_Oil}
Piston Oil-Side Heat Transfer Coefficient	W/m <sup>2</sup> /K	{Coolant_Piston}	{Coolant_Piston}	{Coolant_Piston}	{Coolant_Piston}
Cylinder Head Coolant Temperature	K	{T_Coolant}	{T_Coolant}	{T_Coolant}	{T_Coolant}
Cylinder Head Coolant-Side Heat Transfer Coefficient	W/m <sup>2</sup> /K	{Coolant_Head}	{Coolant_Head}	{Coolant_Head}	{Coolant_Head}
Cylinder Liner Coolant Temperature	K	{T_Coolant-12}	{T_Coolant-12}	{T_Coolant-12}	{T_Coolant-12}
Cylinder Liner Coolant-Side Heat Transfer Coefficient	W/m <sup>2</sup> /K	{Coolant_Liner}	{Coolant_Liner}	{Coolant_Liner}	{Coolant_Liner}
Fraction of Engine Friction which Heats Piston		0.3	0.3	0.3	0.3
Fraction of Engine Friction which Heats Liner		0.3	0.3	0.3	0.3

Cylinder Walls Cylinder Cooling Valves

	Units	Intake	Exhaust
Conduction Model		on	on
Valve Thickness	mm	2.5	2.5
Seat Width	mm	2	2
Thermal Conductivity	W/m/K	50	50
Volumetric Heat Capacity	J/m <sup>3</sup> /K	3.e6	3.e6
Thermal Contact Conductance	W/m <sup>2</sup> /K	2000	2000

Figure 42 Cylinder and Valve Settings for Ricardo Program

Finally, the cylinder settings can be seen in the cylinder element model below and the valve profiles which have been showcased before can be inserted into the software.

Name: cy11 Cylinder Number: 1 Number of Valves: 4

Edit Engine General Properties

Geometry Initial Conditions Valves Sub-Models Initial Fluid Composition

Liner Head Piston

Bore: 67.0 mm

Stroke: 42.5 mm

Clearance Height: 0.5 mm

Geometry Initial Conditions Valves Sub-Models Initial Fluid Composition

Liner Head Piston

Surface Area Multiplier: 1.6

Surface Area: 5641.04 mm<sup>2</sup>

Figure 43 Piston and Cylinder Settings for Ricardo Program

Geometry Initial Conditions Valves Sub-Models Initial Fluid Composition

Liner Head Piston

Surface Area Multiplier 1.0

Surface Area 3525.65 mm<sup>2</sup>

Connecting Rod Length 90.5 mm

Wrist Pin Offset 0.5 mm

Compression Ratio 12.8

Name cyl1 Cylinder Number 1 Number of Valves 4

Edit Engine General Properties

Geometry Initial Conditions Valves Sub-Models Initial Fluid Composition

Piston Top Temperature {PISTON\_TEMP} K

Cylinder Liner Temperature {LINER\_TEMP} K

Cylinder Head Temperature {HEAD\_TEMP} K

Intake Valve Temperature {IV\_TEMP} K  Same as Head Temperature

Exhaust Valve Temperature {EV\_TEMP} K  Same as Head Temperature

Swirl Ratio 0.0

Figure 45 Piston and Cylinder Settings for Ricardo Program

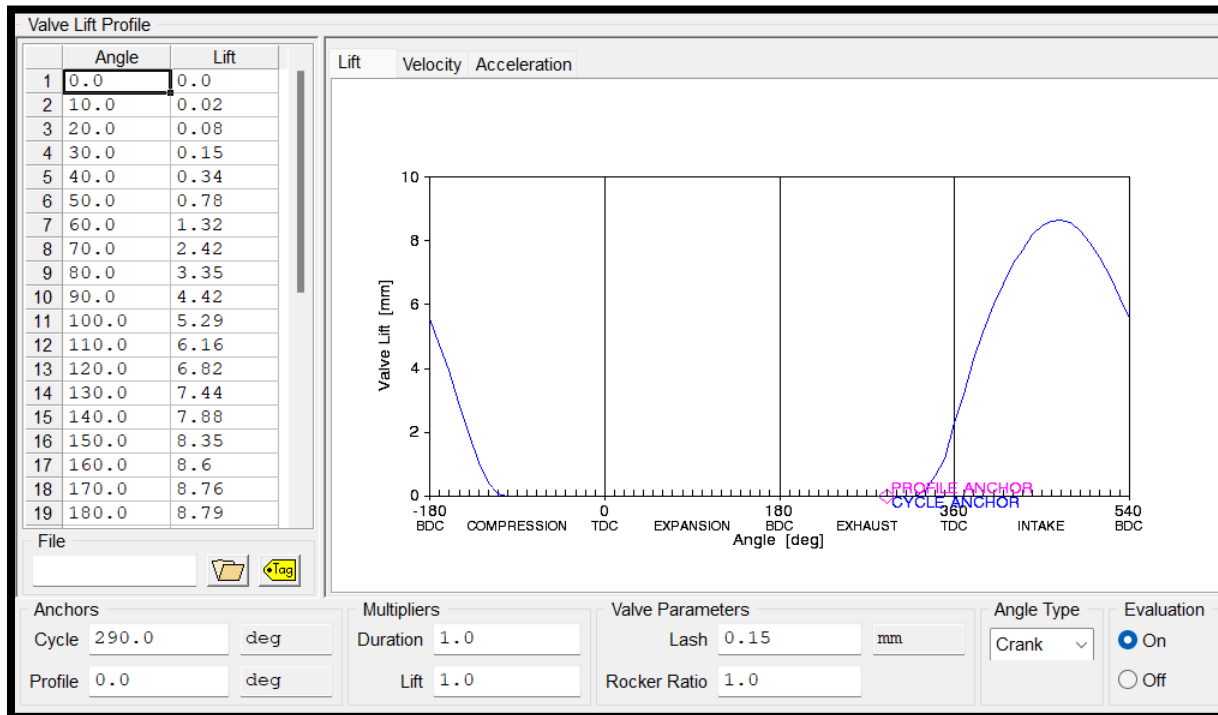
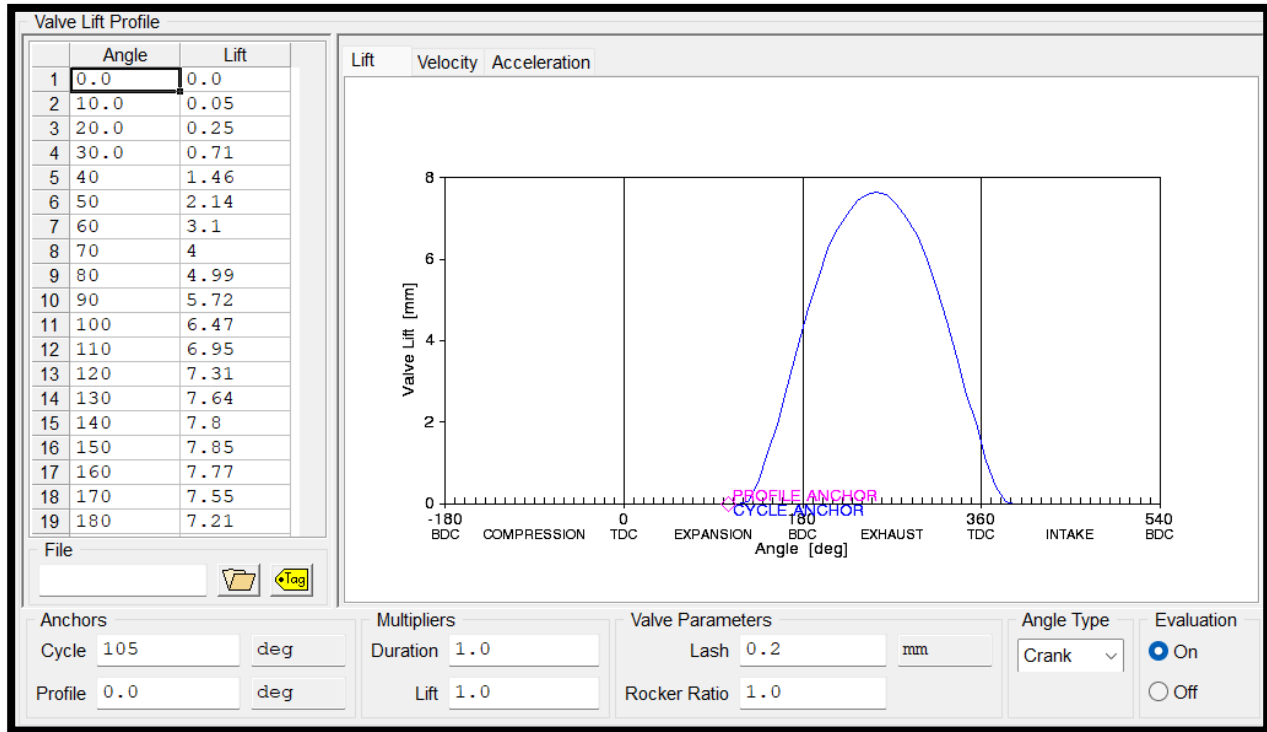
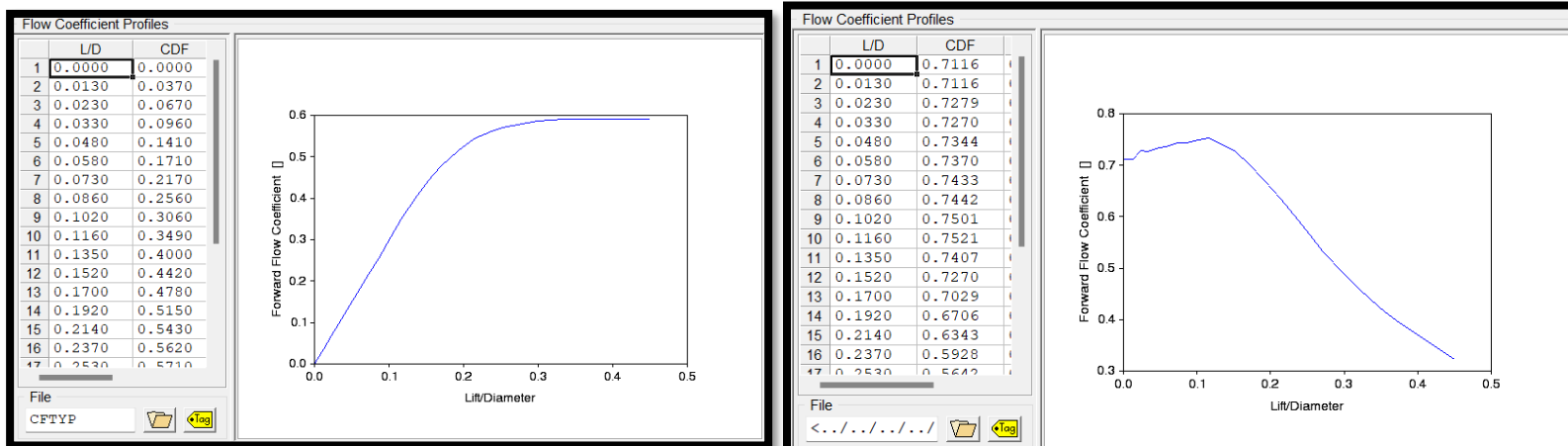


Figure 44 Intake Valve Lift Profile



The valve's profile data have been manually gathered from the Yamaha R6 engine. The data were gathered while the engine was cold, therefore it was necessary to add "hot lash". The hot lash moves the entire valve lift curve down to simulate the thermal expansion of the camshaft and valve when the engine was simulated to run hot. Wave automatically take the user provided hot lash value in account when the engine is hot. Measuring the lash can be done with a thickness gauge. Recommended camshaft clearance for this particular engine is between 0.12 - 0.19 mm for the intake valve when cold and 0.16 - 0.23 mm for the exhaust valve according to the manufacturer's manual. The lash values were selected as 0.15 and 0.2 for intake and exhaust respectively. Moreover, the flow coefficient profiles for each valve were inserted. A typical valve coefficient profile was used that the program provides as default.



$Coefficient\ of\ discharge\ (C_d) = Coeff.\ of\ flow/velocity\ (C_v) \times Coeff\ of\ contraction\ (C_c)$

where

$C_d$  = actual discharge/theoretical discharge

$C_c$  = Area of vena contracta (minimum diameter of flow)/ area of orifice

$C_v$  = actual velocity at vena contracta/theoretical velocity

With Coeff. of flow/velocity ( $C_v$ ), the Coeff of discharge ( $C_d$ ) can be calculated, once  $C_c$  is known. The given diagrams of flow coefficient can be seen above for the intake (left) and the exhaust (right).

### 4.3.6. Variables

Throughout this chapter, all the settings for the main program were presented as well as all the given values used for each parameter. As mentioned before, with the help of variables we can simulate better each case and alter the values of each parameter to get a more representative result of the real engine model. The program provides a table where each variable can be named and numerical values can be assigned for each case. For this study, each case will represent a different number of rpm (revolutions per minute). As the rpms increase, all the values will alter accordingly to the table. The rpm increase step is 500 rpm in order to get a much more detailed view of all the needed diagrams and manage a wider variety of data points. The variables table can be seen below.

Table 8 Variables Table for each case in the Ricardo Program

Status	Name	Units	Case 1	Case 2	Case 3	Case 4	Case 5	Case 6	Case 7	Case 8	Case 9	Case 10	Case 11	Case 12	Case 13	Case 14
Title			Run	Run	Run	Run	Run	Run	Run	Run	Run	Run	Run	Run	Run	Run
1	SPEED	rpm	1000	1500	2000	2500	3000	3500	4000	4500	5000	5500	6000	6500	7000	7500
2	pi		3.141592	3.14159265	3.14159265	3.14159265	3.14159265	3.14159265	3.14159265	3.14159265	3.14159265	3.14159265	3.14159265	3.14159265	3.14159265	3.14159265
3	_session_name		Complete	Complete R	Complete R	Complete R	Complete R	Complete R	Complete R	Complete R	Complete R	Complete R	Complete R	Complete R	Complete R	Complete R
4	_version		2019.1	2019.1	2019.1	2019.1	2019.1	2019.1	2019.1	2019.1	2019.1	2019.1	2019.1	2019.1	2019.1	2019.1
5	A_F		14.7	14.7	14.7	14.7	14.7	14.7	14.7	14.7	14.7	14.7	14.7	14.7	14.7	14.7
6	BDUR	deg	17	17	18	18	19	19	20	20	21	21	22	22	23	23
7	CAS0	deg	15	15	14	14	13	13	12	12	11	11	10	10	8.8	8.8
8	Coolant_Head	W/m^2/K	5000	5000	5000	5000	5000	5000	5500	5500	6000	6500	6500	7000	7000	7000
9	Coolant_Liner	W/m^2/K	1000	1000	1000	1000	1000	1000	1000	1100	1200	1300	1500	1600	1700	1700
10	Coolant_Piston	W/m^2/K	1100	1100	1100	1100	1100	1100	1200	1300	1300	1400	1400	1500	1500	1500
11	EV_TEMP	K	350	350	355	355	360	00	365	365	365.5	365.5	366	366	368	368
12	Exh_Diam	mm	36	36	36	36	36	36	36	36	36	36	36	36	36	36
13	Exh_Fin_Leng	mm	400	400	400	400	400	400	400	400	400	400	400	400	400	400
14	Exh_Plen_Vol	l	0.042	0.042	0.042	0.042	0.042	0.042	0.042	0.042	0.042	0.042	0.042	0.042	0.042	0.042
15	Exh_Primary_Leng	mm	120	120	120	120	120	120	120	120	120	120	120	120	120	120
16	Exh_Secondary_Leng	mm	600	600	600	600	600	600	600	600	600	600	600	600	600	600
17	HEAD_TEMP	K	520	253	526	531	537	542	550	559	565	572	580	585	587.5	587.5
18	Heat_Trans_Mul		1.5	1.5	1.5	1.5	1.5	1.5	1.5	1.5	1.5	1.5	1.5	1.5	1.5	1.5
19	In_P	bar	1.05	1.05	1.05	1.05	1.05	1.05	1.05	1.05	1.05	1.05	1.05	1.05	1.05	1.05
20	In_T_Exh	K	310	310	310	310	310	310	310	310	310	310	310	310	310	310
21	In_T_Int	K	305	305	305	305	305	305	305	305	305	305	305	305	305	305
22	Inj_Dist	mm	{Int_Run	{Int_Runne	{Int_Runne	{Int_Runne	{Int_Runne	{Int_Runne	{Int_Runne	{Int_Runne	{Int_Runne	{Int_Runne	{Int_Runne	{Int_Runne	{Int_Runne	{Int_Runne
23	Int_Plen_Vol	l	0.098	0.098	0.098	0.098	0.098	0.098	0.098	0.098	0.098	0.098	0.098	0.098	0.098	0.098
24	Int_Runner_Diam	mm	42	42	42	42	42	42	42	42	42	42	42	42	42	42
25	Int_Runner_Leng	mm	150	150	150	150	150	150	150	150	150	150	150	150	150	150
26	IV_TEMP	K	300	300	305	305	310	310	312	312	313	313	314	314	315	315
27	LINER_TEMP	K	400	430	450	480	510	520	540	540	555	555	570	570	575	575
28	PISTON_TEMP	K	450	455	460	465	470	480	500	505	515	520	530	535	540	545
29	Plen_Vol	l	3	3	3	3	3	3	3	3	3	3	3	3	3	3
30	T_Coolant	K	363	363	363	363	363	363	363	363	363	363	363	363	368	370
31	T_Oil	K	363	363	363	363	363	363	363	363	363	363	363	363	363	363
32	THROTTLE_ANGLE	deg	45	45	45	45	45	45	45	45	45	45	45	45	45	45
33	Wall_Temp	K	300	300	300	300	300	300	300	300	300	300	300	300	300	300

Table 9 Variables Table for each case in the Ricardo Program

Status	Name	Units	Case 15	Case 16	Case 17	Case 18	Case 19	Case 20	Case 21	Case 22	Case 23	Case 24	Case 25	Case 26	Case 27	Case 28	Case 29
Title			Run	Run	Run	Run	Run	Run	Run	Run	Run	Run	Run	Run	Run	Run	Run
1	SPEED	rpm	8000	8500	9000	9500	10000	10500	11000	11500	12000	12500	13000	13500	14000	14500	15000
2	$\pi$		3.14159265	3.14159265	3.14159265	3.14159265	3.14159265	3.14159265	3.14159265	3.14159265	3.14159265	3.14159265	3.14159265	3.14159265	3.14159265	3.14159265	3.14159265
3	_session_name		Complete R	Complete R	Complete R	Complete R	Complete R	Complete R	Complete R	Complete R	Complete R	Complete R	Complete R	Complete R	Complete R	Complete R	Complete R
4	_version		2019.1	2019.1	2019.1	2019.1	2019.1	2019.1	2019.1	2019.1	2019.1	2019.1	2019.1	2019.1	2019.1	2019.1	2019.1
5	A_F		14.7	14.7	14.7	14.7	14.7	14.7	14.7	14.7	14.7	14.7	14.7	14.7	14.7	14.7	14.7
6	BDUR	deg	23.8	23.8	24.5	24.5	25.2	25.2	26	26	27	27	28	28	29	29	30
7	CAS0	deg	7.6	7.6	6.4	6.4	5.2	5.2	4	4	2.9	2.9	1.8	1.8	0.8	0.8	0
8	Coolant_Head	W/m^2/K	7500	7500	8000	8000	8500	8500	9000	9000	10000	10000	11000	11000	12000	12000	13000
9	Coolant_Liner	W/m^2/K	2000	2000	2300	2300	2500	2500	2800	2800	3050	3050	3300	3300	3500	3500	3700
10	Coolant_Pistor	W/m^2/K	1900	1900	2100	2100	2400	2400	2500	2500	2600	2600	2900	2900	3000	3000	3100
11	EV_TEMP	K	370	370	372.5	372.5	375	375	376	376	377	377	378.5	378.5	380	380	381
12	Exh_Diam	mm	36	36	36	36	36	36	36	36	36	36	36	36	36	36	36
13	Exh_Fin_Leng	mm	400	400	400	400	400	400	400	400	400	400	400	400	400	400	400
14	Exh_Plen_Vol	l	0.042	0.042	0.042	0.042	0.042	0.042	0.042	0.042	0.042	0.042	0.042	0.042	0.042	0.042	0.042
15	Exh_Primary_Len	mm	120	120	120	120	120	120	120	120	120	120	120	120	120	120	120
16	Exh_Secondary	mm	600	600	600	600	600	600	600	600	600	600	600	600	600	600	600
17	HEAD_TEMP	K	595	595	607.5	607.5	620	620	625	625	630	630	632.5	632.5	635	635	636
18	Heat_Trans_Mul		1.5	1.5	1.5	1.5	1.5	1.5	1.5	1.5	1.5	1.5	1.5	1.5	1.5	1.5	1.5
19	In_P	bar	1.05	1.05	1.05	1.05	1.05	1.05	1.05	1.05	1.05	1.05	1.05	1.05	1.05	1.05	1.05
20	In_T_Exh	K	310	310	310	310	310	310	310	310	310	310	310	310	310	310	310
21	In_T_Int	K	305	305	305	305	305	305	305	305	305	305	305	305	305	305	305
22	Inj_Dist	mm	(Int_Runne)	(Int_Runne)	(Int_Runne)	(Int_Runne)	(Int_Runne)	(Int_Runne)	(Int_Runne)	(Int_Runne)	(Int_Runne)	(Int_Runne)	(Int_Runne)	(Int_Runne)	(Int_Runne)	(Int_Runne)	(Int_Runne)
23	Inj_Plen_Vol	l	0.098	0.098	0.098	0.098	0.098	0.098	0.098	0.098	0.098	0.098	0.098	0.098	0.098	0.098	0.098
24	Int_Runner_Dis	mm	42	42	42	42	42	42	42	42	42	42	42	42	42	42	42
25	Int_Runner_Ler	mm	150	150	150	150	150	150	150	150	150	150	150	150	150	150	150
26	IV_TEMP	K	316	316	317	317	318	318	318	318	319	319	320	320	320	320	321
27	LINER_TEMP	K	580	580	587.5	587.5	595	595	597.5	597.5	600	600	608	608	615	615	620
28	PISTON_TEMP	K	550	555	565	570	580	580	582.5	582.5	585	585	590	590	595	595	598
29	Plen_Vol	l	3	3	3	3	3	3	3	3	3	3	3	3	3	3	3
30	T_Coolant	K	373	373	378	380	383	383	388	390	393	393	393	393	394	394	393
31	T_Oil	K	363	363	363	363	363	363	363	363	363	363	363	363	363	363	363
32	THROTTLE_ANGLE	deg	45	45	45	45	45	45	45	45	45	45	45	45	45	45	45
33	Wall_Temp	K	300	300	300	300	300	300	300	300	300	300	300	300	300	300	300

The table also includes the variables that are going to be used for the intake development and so some of them are going to be discussed more extensively in the following chapters.

## 5. Stock Engine Ricardo Model

The purpose of these first series of simulations was to verify that the gathered data produce a simulation with comparable results to the real stock Yamaha R6 engine by comparing simulation output results to the manufacturer numbers. At first, the original concept to check the simulation data was to place the engine onto a hydraulic dynamometer which the university had in its disposal.

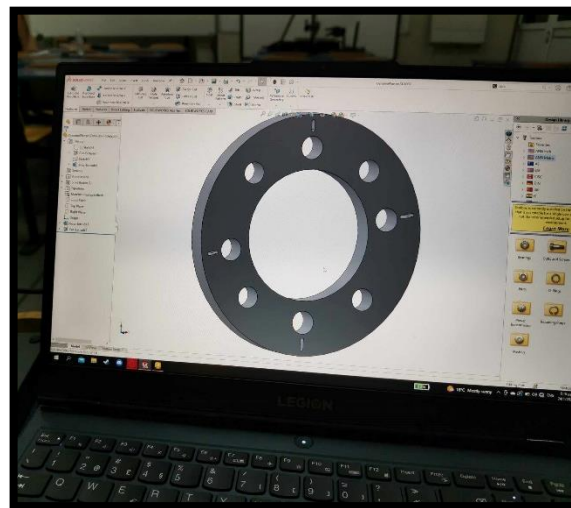


Figure 48 Hydraulic Dynamometer Flange Design

The team detached the engine that was previously mated to the dynamometer and started gathering dimensions to manufacture the needed flange in order to properly mount the R6 engine in its place. The flange was manufactured and the engine was attached to the dynamometer. However, due to time constraints and lack of experience of use with the particular machine, the team opted not to dedicate any more time to this process. Instead, it was decided that the data validation of the simulation would be done through the 0.6l default motorbike engine example the Ricardo Wave software provides, along with the max power and torque values given by the manufacturer. Basically, the diagram behavior would directly be compared to the stock engine model with the max power and torque values based on the manufacturer data. It should be pointed out, that the values for the R6 engine that are being compared are brake horsepower and brake engine torque, since all the friction losses and the drivetrain losses are taken into consideration. Moreover, in table 3, which includes all the stock engine data, a range of peak power and torque values are given and not specific ones. That is because after a lot of in-depth research into the Yamaha R6 bibliography, the 2006 model appears to have different power and torque values depending on the reference which is being used. In addition to that, the manufacturer every year made minor tweaks which made the power output numbers change as little as 2-3 units.

The most common seen values for the motorbike range between 130-133 bhp and 65-68 Nm of torque. With the above values making up the maximum points of the diagram, the diagram behavior was the next parameter to be decided. The diagram below showcases a 2006 Yamaha R6 engine dyno. It can be observed that the torque and power values are lower than the ones stated by the manufacturer. Based on the previous statements the diagram will only aid at the general understanding of the diagram behavior and will not be used to directly compare numerical values.

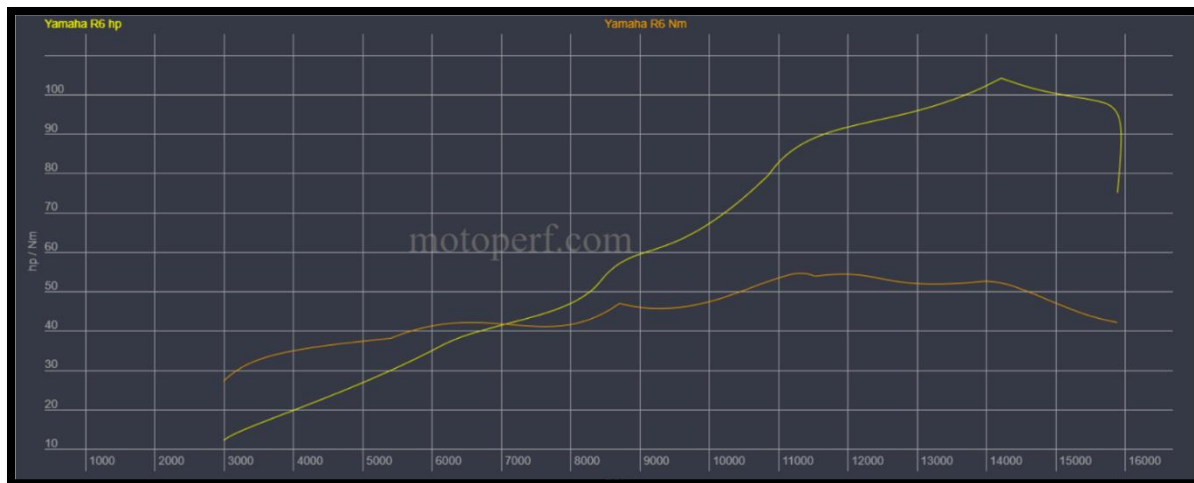


Figure 49 Yamaha R6 Engine Dyno Diagram

From the above figure, we can identify some key behaviors. Firstly, maximum power occurs at 14250 - 14500 rpm and max torque around 11000-11500 rpm. Power seems to raise abruptly, almost nearly throughout the rpm range whilst torque follows a much flatter curve that doesn't reach high torque values below 9000 rpm. Below 5000 rpm the engine is very unresponsive. Between 3000 rpm and 5000 rpm the YZF-R6 produces less than 40Nm of torque. After 5000 rpm, torque picks up a little and



although the midrange seems to remain flat, it raises again at 8000rpm, then it drops and then recovers slightly and slowly builds up. Basically, the diagram shows good performance and behavior after the 9000rpm value whilst it suffers from ups and downs throughout the midrange with several peaks of torque at relatively low numerical values. This behavior is justified since this particular motorbike engine was developed to mainly work at very high rpm and compete in motorsport competitions.

Having grasped the general idea of the engine diagram, the Ricardo default diagrams of the 0.6l motorbike engine can be assessed and compared directly to the stock engine. The diagrams as created by the software appear below.

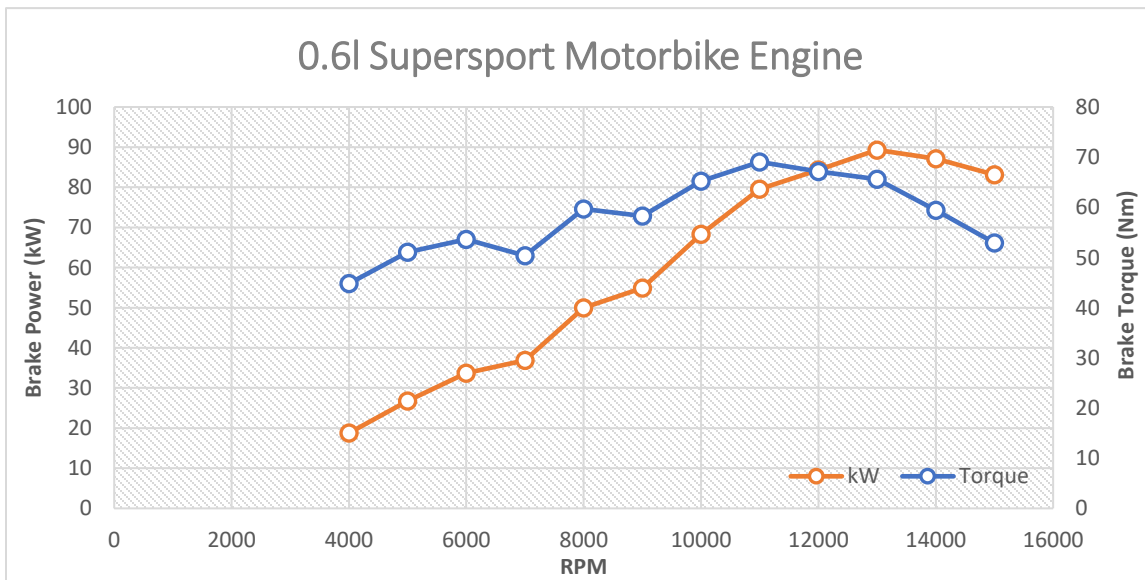
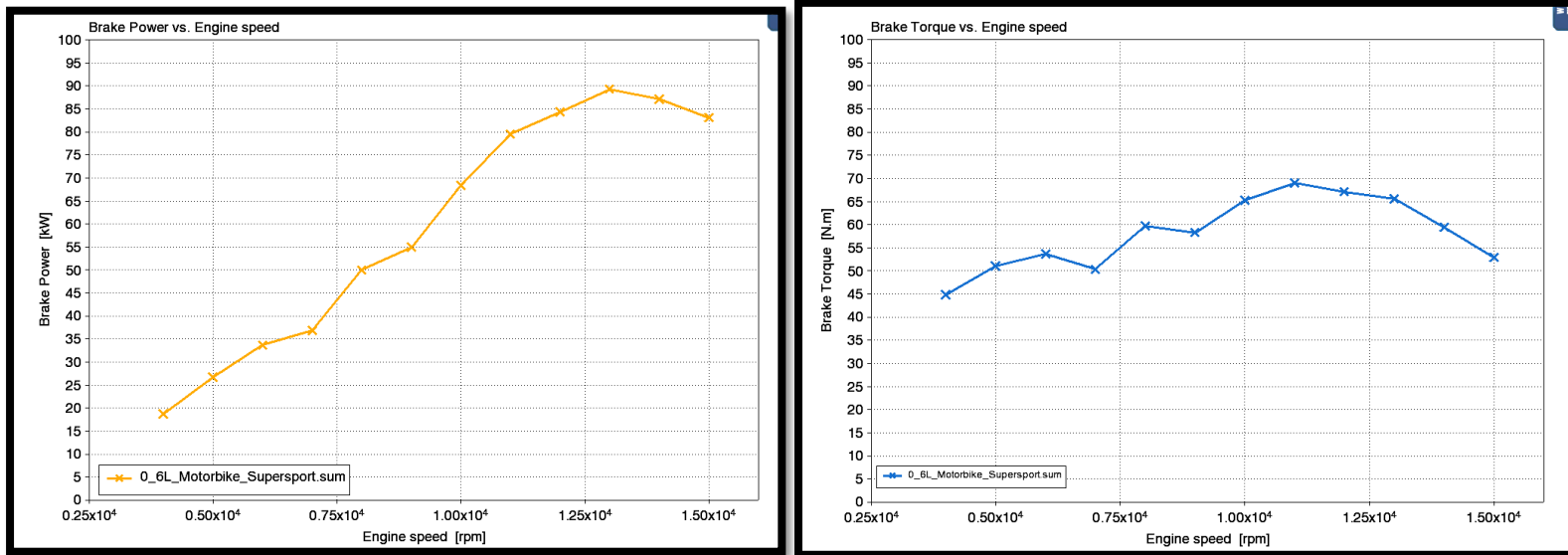


Figure 50 Brake Power and Torque Diagrams of a 0.6L SuperSport Motorbike Engine

The data available from the Ricardo stock engine model begin from 4000 rpm and end up to 15000 rpm. Observing the behavior of the torque and horsepower diagrams, similar characteristics can be underlined. Ignoring the apparent difference that appears in the torque values which are slightly higher to the stock engine diagram, we can generally observe a very similar behavior with a torque curve that only raises significantly after 8500-9000 rpm and a horsepower curve that increases its values almost linearly. Comparing the maximum values between manufacturer and Engine Model, a decrease of 8.2% in horsepower and an increase of 1.4% in torque can be observed for the model.

Having a difference of less than 10% between the max values and having the behavior of the diagrams generally matching the one from the manufacturer, the model was considered to be representing the engine well and could become the reference for the team's effort to replicate it.

### 5.1. Model Overview

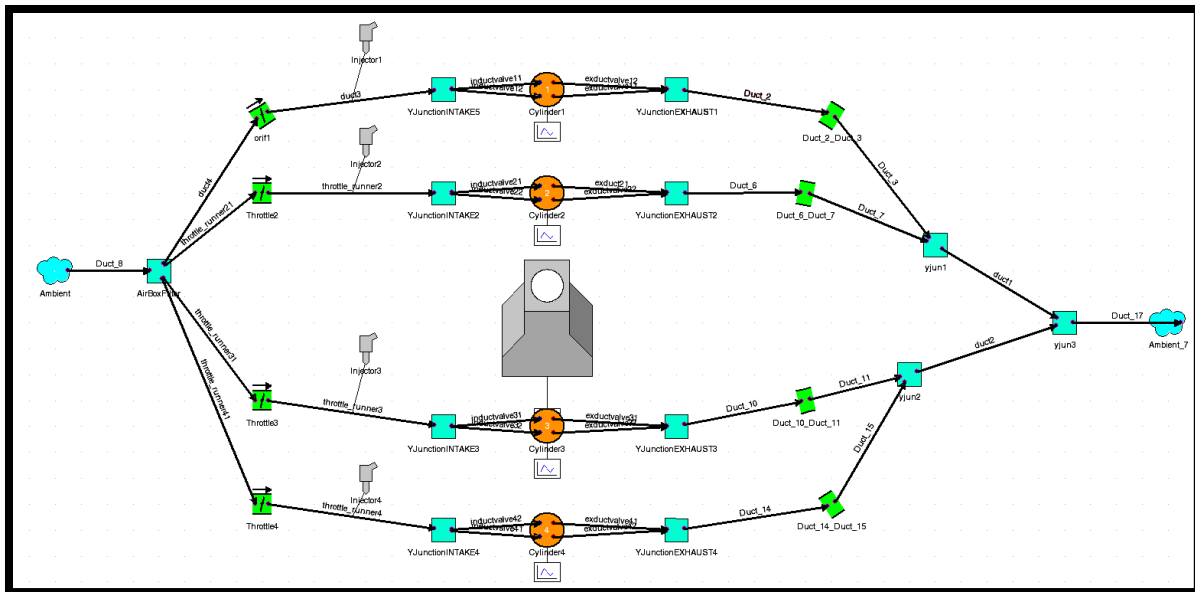


Figure 51 Simulated Model of Stock Engine made by the Team (Throttle Body)

In the figure above the final wave model of the stock R6 engine can be seen made by the team. This model has 4 throttle valves. All the basic numerical values discussed in the previous chapters are utilized and can be seen on the canvas. An important aspect to note is the exhaust runners for the stock model. As mentioned, before it is not showcased here in this thesis in depth, however it should be mentioned that the stock exhaust runners were simulated based on information and dimensions the team found through the manufacturer. The team did not own at any point the stock exhaust so taking measurements in a similar way to the ones from the engine was deemed impossible. Therefore, a simple 4-2-1 exhaust arrangement was conceived to simulate the stock one. This exhaust model was altered again for the final modified engine model where the modified exhaust designed and manufactured by the team was simulated. Another point to note is the Y-junction in the start of the duct. It simulates the air filter box used in the motorbike which was found to be 1.4l.

The model was at this stage ready to run through an input check and was set to prepare the requested data for post-processing. The log was printed in real-time to be examined and an output file was also

printed with the fully detailed log. The log was an important source of information for troubleshooting the simulation. Simple informational messages start with I\*\*\*, warning messages with W\*\* and finally, failure message which cause Wave to abort the simulation are marked with F\*\*\*.

## 5.2. Run Data – Diagrams

Below, the horsepower and torque diagrams can be seen as they were produced by the R6 team's model.

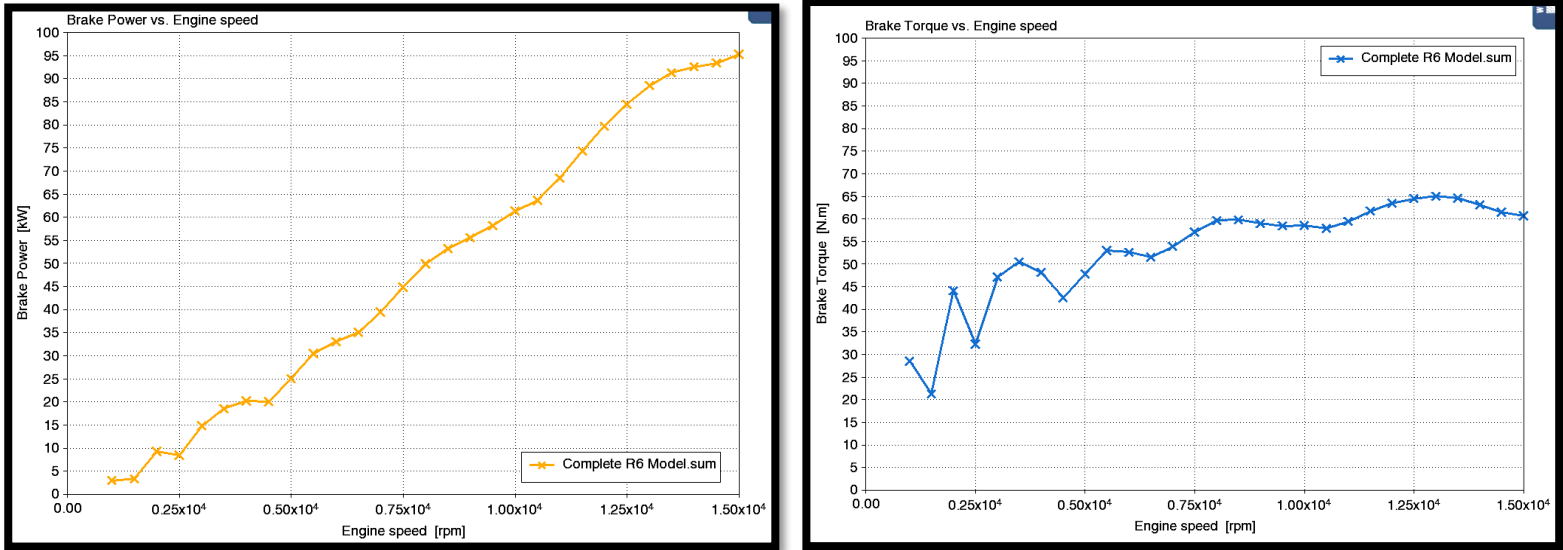


Figure 52 Power and Torque Diagrams of the Team's Model

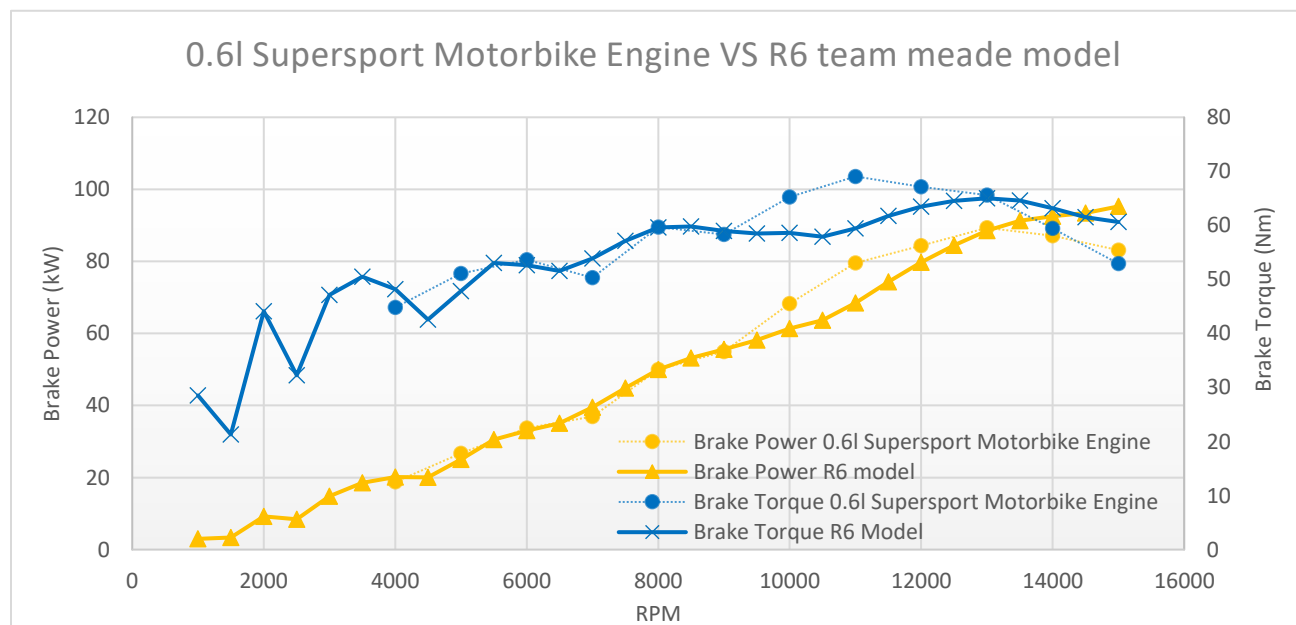


Figure 53 Comparison between Team's Model and 0.6L SuperSport Model

### 5.3. Comments

Comparing the maximum values to the ones of the manufacturer in a similar way to the Ricardo tutorial model, a decrease of 3% of brake power and 5.8% of brake torque can be observed. In the diagram above, the Ricardo tutorial values are put together with the team's model for a direct comparison. In the team's model, both power and torque present a decrease compared to the manufacturer values. In the tutorial, the power was slightly higher and the torque was lower, nearly 10%, than the manufacturer suggested. In the diagram behavior, similar patterns can be identified for both models. Due to the wider rpm range used by the team, direct comparison can only be made for the mid-range rpm and the higher rpms. In the lower values, the torque diagram of the R6 model showcases sudden changes, even though the model criteria are satisfied and the model converges according to the log. This behavior can be justified from the engine's main purpose which is to operate at high rpm as mentioned before. This can also explain the reason the Ricardo tutorial does not include these values and why the dyno diagram from the stock motorbike starts from 3000 rpm and above. The main focus of the diagrams now shifts to the medium range of rpm which shows similar behavior from the two models till the 9500-rpm mark. From that value and above, the R6 model retains lower power and torque values while retaining a smoother transition to the higher rpms. At maximum rpms, the team's model reaches the highest values out of the two. Regarding the ups and downs of the dyno diagram, similarities can mostly be found with the diagrams from the tutorial mainly around the 10500 and 11000 rpm where the general max values seem to occur for the 0.6l SuperSport motorbike engine.

### 5.4. Final Results

All In all, both models responded well in regards to the manufacturer data and the reference dyno. Most differences could be explained and justified. The team needed one of these models to become its reference for the modifications that were going to be made to the model in order to make the engine rules compliant. Although the 0.6l SuperSport motorbike model seemed the most obvious choice out of the two, the team opted to continue with their model. One of the main reasons were the value deviations which were much closer and more consistent in the R6 model. Both power and torque showed a small decrease which could be taken into account afterwards in the later stages of the simulation. Another reason was the smoother curves which, as mentioned several times, are a key aspect of proper power output of an FSAE engine and make up an important design goal of the simulation. Hence, having a smooth curve as reference was considered important and valuable for the next steps. In conclusion the R6 model was selected to become the stock engine reference for the next modifications. It is important to note that all the upcoming changes were made onto the R6 model and for each step and modification data was collected in order to find the best possible solution. Finally, it should also be pointed out that the simulations never reflect fully the real engine and that the dynamometer which was mentioned at the start of the chapter will always give back more representative information. Based on the tools available and the time constrains the simulation began with the restrictor implementation.

## 6. Restrictor and Throttle-body Implementation

### 6.1. Restrictor Model Overview

One of the most important components of the intake assembly for the competition is the restrictor. As mentioned before in this thesis only some basic parameters and dimensions are going to be mentioned. The whole restrictor was studied, designed and optimized separately by another member of the team, Georgios Maniotis, who utilized the ANSYS fluent program. With the help of the program, the appropriate type of the restrictor was chosen as well as the basic dimensions such as the inlet and outlet diameters and the divergence and convergence angle. Sixty (60) different restrictors were produced and pressure and velocity data were collected. The main goal was to achieve the minimum pressure drop between inlet and outlet. The final dimensions that are selected can be seen in the table below:

Table 10 Restrictor Data Table

Din = 40mm	Dout = 40mm
Convergence ang. = 12deg	Divergence ang. = 6deg
Max velocity at throat = 197.83 m/s	Total Length = 127.046
Distance between restrictor and inlet = 42mm	

Having the dimensions in our disposal we can insert the above values into the software to simulate the restrictor properly. The Ricardo wave software provides this capability with some limitations regarding pressure losses. The Taper Angle ( $\theta$  angle as shown in figure 54) is automatically calculated in Wave Build. Because of the fundamental formulation of 1-D flow calculations, pressure loss due to flow separation along the length of a duct is not predicted. Flow along a 1-D duct element is assumed attached at all points. According to the Ricardo WAVE help page regarding modeling tapered ducts, a taper angle greater than approximately  $7^\circ$  will cause flow separation and create some pressure loss that is unaccounted for in a simple 1-D duct element.

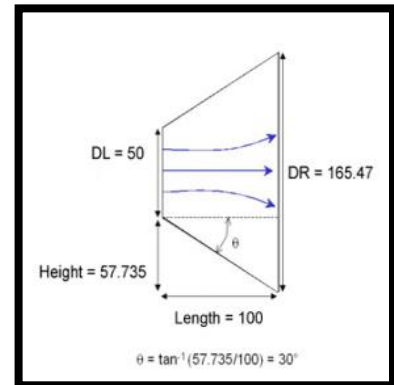


Figure 54 Taper Angle implementation in Ricardo Software

The main concerns with tapered ducts according to the software are the following: the length over which the taper occurs and whether flow separation occurs. As the taper angle increases, the overall length of the duct used to model the geometry decreases. If the overall length is shorter than the discretization length, the tapered duct becomes an undesirable modeling method as it will increase computational time by decreasing the timestep size to maintain stability. Flow separation will only occur with a sudden expansion, hence only if the flow passes through a severely tapered duct in an expanding direction.

Keeping all the above in mind, the program suggests a way to simulate more accurately the taper angle using an orifice element instead. When the primary flow direction passes through a sudden expansion it is more accurate to model the expansion, not as a tapered duct, but using an orifice to connect two ducts of different diameters. This will account for the pressure loss due to flow separation by using the ratio of the areas. It is also not unusual to encounter geometry details that may be classified as very

short ducts. Examples would be a very sharp cone or a bell mouth rounding of an entrance, as shown in the figure below. Such small geometry details all entail two- or three-dimensional flow behavior which can be accounted for only in a lumped fashion. This is accomplished using specific discharge coefficient values.

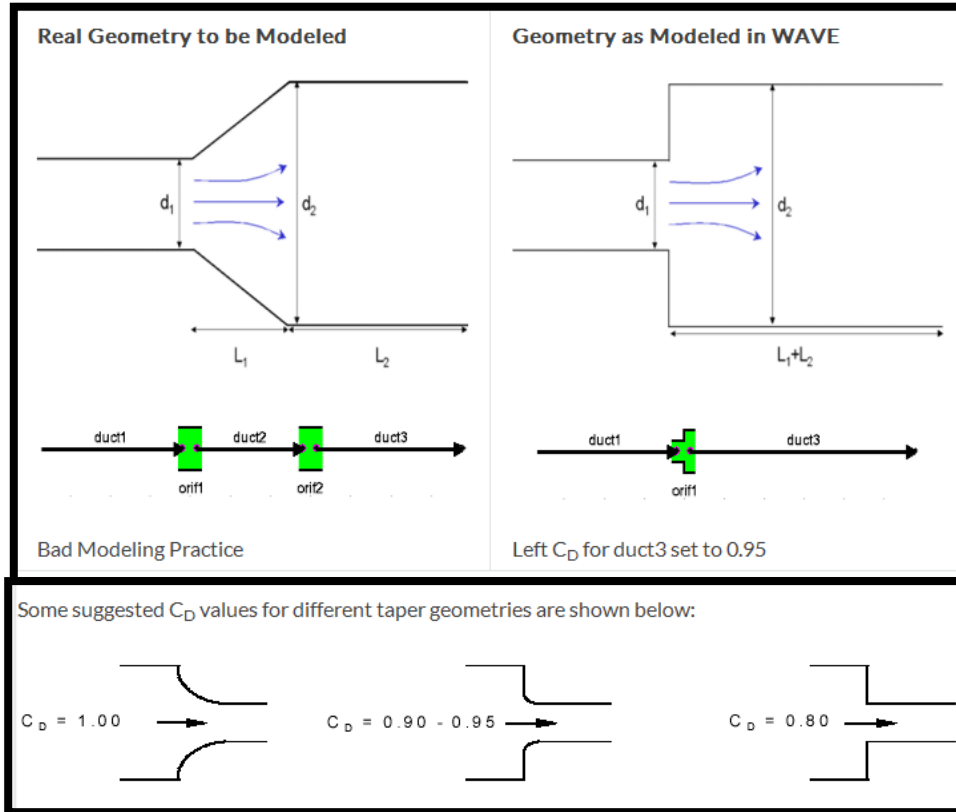


Figure 55 Bell-Mouth Modeling in Ricardo Software

Based on all the modeling propositions from the software, the restrictor was modeled accordingly. The Wave model of the restrictor can be seen in the figure below.

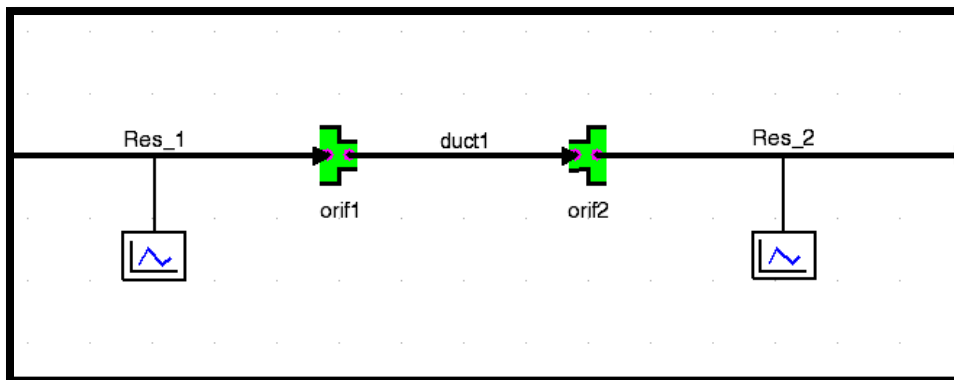


Figure 56 Team's Modeled Restrictor

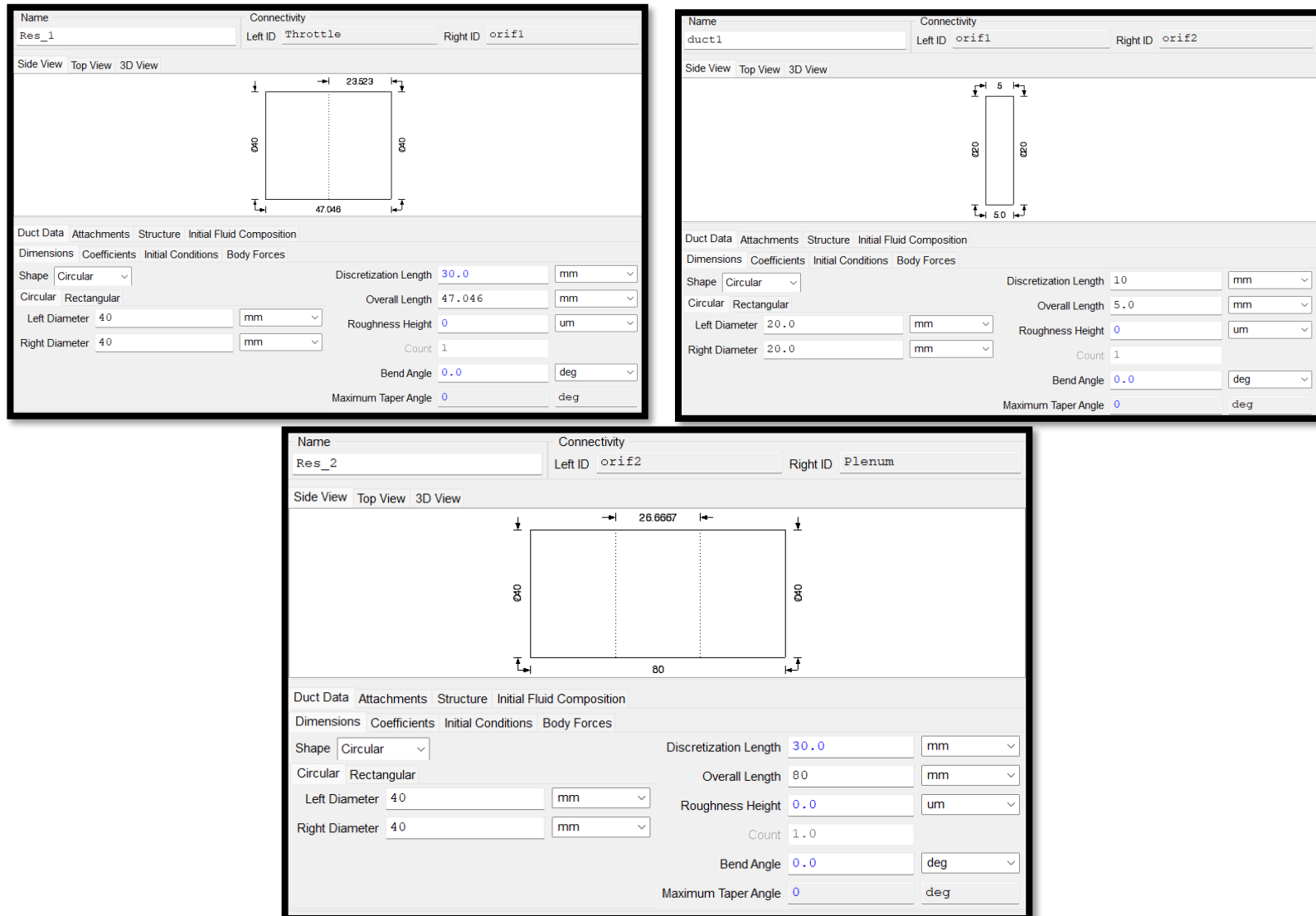


Figure 57 Duct Data used in Restrictor Model

## 6.2. Throttle-body Model Overview

One of the first aspects of the intake system along with the restrictor that must be considered is the throttle-body. The throttle plays a vital role in the drivability of the car, which in turn is crucial for the drivers being able to extract the full potential from the car.

When choosing a throttle body, it is important to consider several aspects. Firstly, the control type is a critical decision that must be made, as a throttle body can be manually actuated (usually by means of a cable attached to the throttle pedal) or electronically actuated in a drive-by-wire system, where a sensor on the throttle pedal relays torque requests to the ECU, which actuates the throttle body accordingly. Secondly, bore size must be considered as this will determine the manifold pressure for a given throttle valve position and engine speed, and be largely influential in determining the drivability of the car. Cost

and mass are considered also, as reducing mass and cost are both beneficial to the team. In order to make the whole intake system rules compliant, the throttle-body should be placed before the restrictor on the vehicle. Hence, the 4-throttle-body setup the R6 engine utilizes was considered inappropriate for this use. It was removed and the team designed and fabricated an alternative throttle-body. Its dimensions were mainly based on the bore sizes of the stock throttle-body and several spare parts from automotive solutions were used to make the whole assembly operational.

Regarding the Ricardo Wave software, the butterfly valve sub-model defines a rotating plate valve mounted on a shaft. The opening is controlled at the referencing location, directly via a defined fixed position or a controlling actuator, and not in the valve sub-model. Similarly to the 4-throttle model showcased earlier, the basic parameters of the new throttle-body can be inserted. The valve editor figure can be seen below.

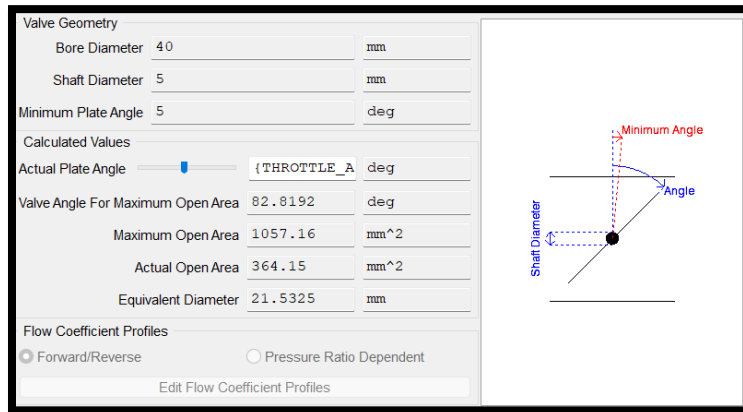


Figure 58 Throttle Valve Geometry Settings for Final Model

For this setup, several changes can be observed. Initially, the bore diameter was elected to be 40mm. The value resulted from the butterfly valve acquired from another automotive application. More specifically, both the shaft diameter and valve diameter were previously used in a commercial vehicle. The minimum plate angle refers to the point at which the valve is fully closed (i.e. no flow passes). The actual plate angle has to be equal or bigger than the given minimum plate angle. For this particular application it was considered to utilize a variable minimum plate angle which will vary between 5 and 8 degrees. For this model, the value of 5 degrees will be used unless is mentioned otherwise. It should also be mentioned that the actual plate angle has been assigned to a variable, THROTTLE ANGLE, making the model easier to test at a variety of occasions. The Wave model with the restrictor and the throttle-body implemented can be seen below.

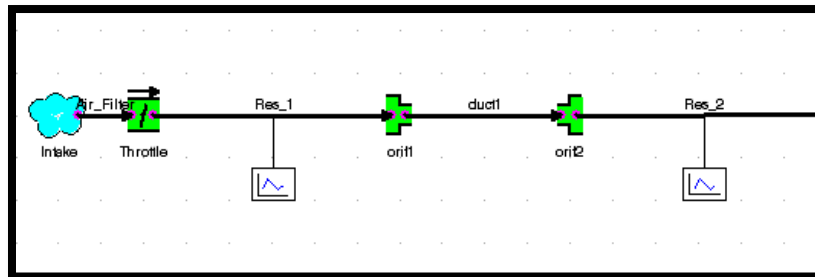


Figure 59 Final Intake System Model



## 7. Final Engine Model

Before any intake system concepts could be produced, it was firstly important to select the basic geometrical parameters. This would then largely determine the viability of different packaging concepts before significant time was invested in them, streamlining the design process. The two key factors that would influence concept generation were the runner length and plenum volume. Since it's the team's first participation at the competition, no previous data were available. Hence, it was of high importance to settle a steady foundation of data and knowledge from the very first year in order to keep the development of the engine and the car alive for many more competitions. To achieve this, the engine model was modified several times based on several variables used in the constants table. The main model consists from all the elements already mentioned in the thesis. From this point forward the analysis will be focused around the runner length and plenum volume. At first, the runner length and diameter are going to be calculated based on the tuning phenomenon mentioned at the theoretical part of this thesis. Several runner length values are going to be tested through the model to confirm the numerical evaluation. After that the plenum volume will be elected and together with the runners, the total dimensions are going to be specified.

In multi-cylinder engines, the construction of the intake manifold is intended to exploit the pulses from the air flow. The system must be properly designed to avoid pulses caused by different cylinders to meet at the same pipeline, because this leads to increased pressure drop and reduced volumetric efficiency. It is generally desirable that 2 or 3 of the cylinders that are in a different phase are connected to a common intake manifold. The most common and simplest form of the intake manifold will be implemented for this concept, which consists of a pulse damping vessel (plenum) from which separate pipelines begin and reach in each cylinder. Important design parameters are the following:

- **Low flow resistance**, i.e. the pressure drop along the intake should be as small as possible. This is achieved by minimizing the curvatures of the runners, as well as achieving good surface quality.
- **Uniform distribution** of air in the cylinders in order to accommodate all cylinders with equal amounts of mixture. This is achieved by symmetrical design of the intake manifold.
- **The length of the runners** to each cylinder should be such as to exploit the tuning phenomenon in them. Also, the runners must be small enough in diameter to accelerate the flow sufficiently at low engine rotational speeds, but also large enough not to strangle the flow when it reaches high speeds due to high engine speed.
- **Suitable size of plenum**. It must be large enough to provide enough air mass to each cylinder when it is in the intake phase, but small enough for reasons of air inertia. When the load changes, the throttle-valve angle changes and as a result the air supply changes. Due to inertia, however, the change in angle does not lead to an immediate engine response. The smaller the plenum, the less air there is in it, therefore less inertia and therefore a more immediate response.

## 7.1. Model Overview

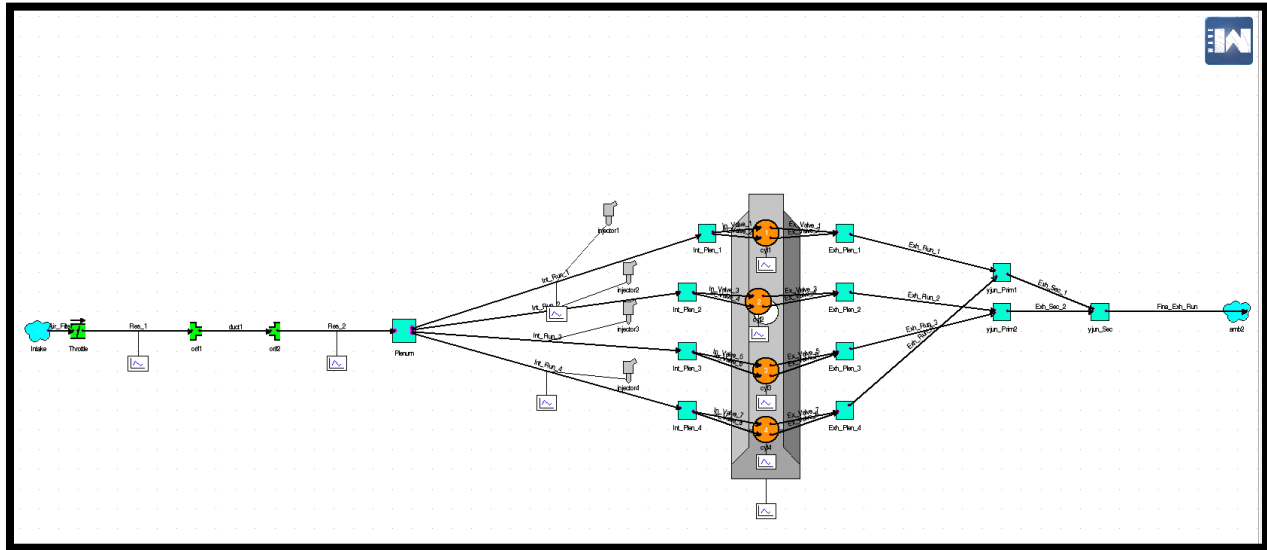


Figure 60 Final Team's Engine Model

The model above showcases the final R6 engine model the team used to gain data for the engine. This model utilizes only one throttle valve. It should be pointed out that the exhaust system used in the model above as mentioned before represents the final exhaust system that was manufactured for the final race car.

## 7.2. Runners

Based on the tuning and ramming phenomena analyzed before, the intake runners were the starting point for intake assembly development. The goal as mentioned before was to maximize the volume of air introduced into the engine cylinders at the target rpm to achieve maximum power and torque output. Based on several research from previous years, most race cars seemed to operate around the 7500-rpm mark. This target rpm was therefore chosen as point of interest for the rest of the study. To be able to tune the intake runner length to time the arrival of the pressure waves the rpm for which the ramming phenomenon is to be optimized for, have to be decided and the duration of the intake valve and speed of sound in air are required. Below are the basic values needed for the optimal runner length calculation.

Engine speed of interest: 7500 rpm	Intake valve open for 340 degrees	Speed of sound at 30°C is 349.08 m/s
------------------------------------	-----------------------------------	--------------------------------------

The following calculations will all be made using units in SI; hence the rpms are converted to 125 rps. Based on that, it can be calculated that one revolution takes about 0.008sec and the intake valve remains closed for  $720-340=390$  degrees. This value corresponds to 1.08 revolutions.

The time it takes between when the valve closes and when it opens again is:  $0.008 * 1.08 = 0.0086s$ . The wave moving at the speed of sound during that time will cover the distance of:  $0.0086 * 349.08 \approx 3.00m$  before the intake valve opens again.

Since the pressure wave has to travel back and forth, the optimum length for the intake runner when it comes to using the ramming phenomenon at 7500 rpm is half of the calculated length ( $\approx 1.5\text{m}$ ). A runner length of approximately 1.5m would be near impossible to fit in the car due to the space limitations.

To deal with this issue, one solution is to shorten the runner length at  $\frac{1}{2}$ ,  $\frac{1}{4}$  or  $\frac{1}{8}$  of the initial length. With this modification, the pressure wave will travel up and down the pipe several number of times before the intake valve opens again, however it still arrives at the valve at the same time. Reducing the runner length based on the forementioned values, the recommended runner lengths range between 750 to 187.5 mm. The range still seemed to be larger than expected. In order to limit the number of options and further aid the packaging issue, it was decided that the model will be tested for 10 different lengths ranging between 150mm to 240mm with a step size of 10mm.

The velocity of the flow and therefore momentum of the air entering the combustion chamber at different engine speeds can be also adjusted by varying the diameter of the intake runners. A small diameter runner will be beneficial at low engine speeds, as it will increase the velocity of the flow when the mass flow rate remains the same. This higher velocity will increase the momentum of the air, thus increasing the density of the air in the combustion chamber. Based on the intake port area from the R6 data gathered before, we can calculate the ideal Runner diameter for the given value.

$$D_{Runner} = \left( 2 \times \sqrt{\frac{A_{Runner}}{\pi}} \right) * 1000 = 44.7 \text{ mm where}$$

$$A_{Runner} = \text{Inlet Valve Area} = 41.5\text{mm (Rel. Length)} * 38\text{mm (Rel. Diameter)} = 0.00157 \text{ m}^2$$

Compared to the stock diameter of the engine intake port, the runner diameter calculated is higher. Taking into consideration the main purpose of the engine as mentioned before, a smaller intake diameter will aid the engine operation at lower rpm values which is very crucial for the competition. It was decided that the intake diameter would be verified after the runner length and plenum volume final dimensions. In order for the model to be operational, a smaller value of runner diameter was chosen of 42mm. After the program calculations, the intake runner diameter would be tested with a range of 5 different diameters ranging between 36mm to 44mm with a step size of 2mm.

### 7.3. Plenum

The plenum volume serves as ‘air storage’ that the engine can draw from during the intake stroke, and then refill as the engine goes through the rest of the four-stroke cycle. The plenum therefore effectively acts to damp the high frequency pressure oscillations of the engine and keep positive flow through the restrictor. Unlike the runner length, there is no direct way to directly calculate an ideal volume. However, through the power and torque diagrams created from the Ricardo program, the plenum volume behavior can be monitored in regards to power and torque output. For this thesis and in order to get back useful result, the plenum volume tested used values between 3 and 5 Liters with a 0.5L step size. From there, plenum volume was also elected based on packaging availability.

Based on (Wilson, 2019) and his research, a larger plenum volume will negate the effect of the restrictor more than a smaller plenum volume, which is apparent through the increased power output of larger plenum volumes. The issue with those larger plenum volumes however is that the pressure in the intake manifold will take longer to change with respect to changes in throttle position, resulting in a delayed throttle response, hence negatively affecting drivability. In order to verify these statements, further tests and comparisons were made with different volumes. The final output diagrams can be seen and are discussed thoroughly in the next chapter.

#### 7.4. Run Data – Diagrams

The components were at first added with a basic benchmark geometry and they were individually tested over a range of different geometry values to properly map out how each change affected the engine behavior. This process helped narrow down the range of possible optimums for each component. The initial dimensions of the elements were 3L plenum volume and 150mm runner length. Before running the simulation in Wave and proceeding to Wave Post for analysis, it was necessary to setup how the engine was supposed to run in terms of speed, load and what data was topical for Wave to sample. The information of interest were runner length and plenum volume. The engine speed was sweeping from 1000 - 15000 rpm in 500 rpm increments to simulate multiple steady-state test points in one speed sweep. All the data gathered for the diagrams have been simulated with 45° throttle body. Each steady state test point has its own case which implies 29 cases in total. Every diagram for each value of plenum volume and runner length can be found at Chapter 12. Indicatively, the diagrams shown below refer to a plenum of 3L and illustrate every possible combination with the available runner lengths.

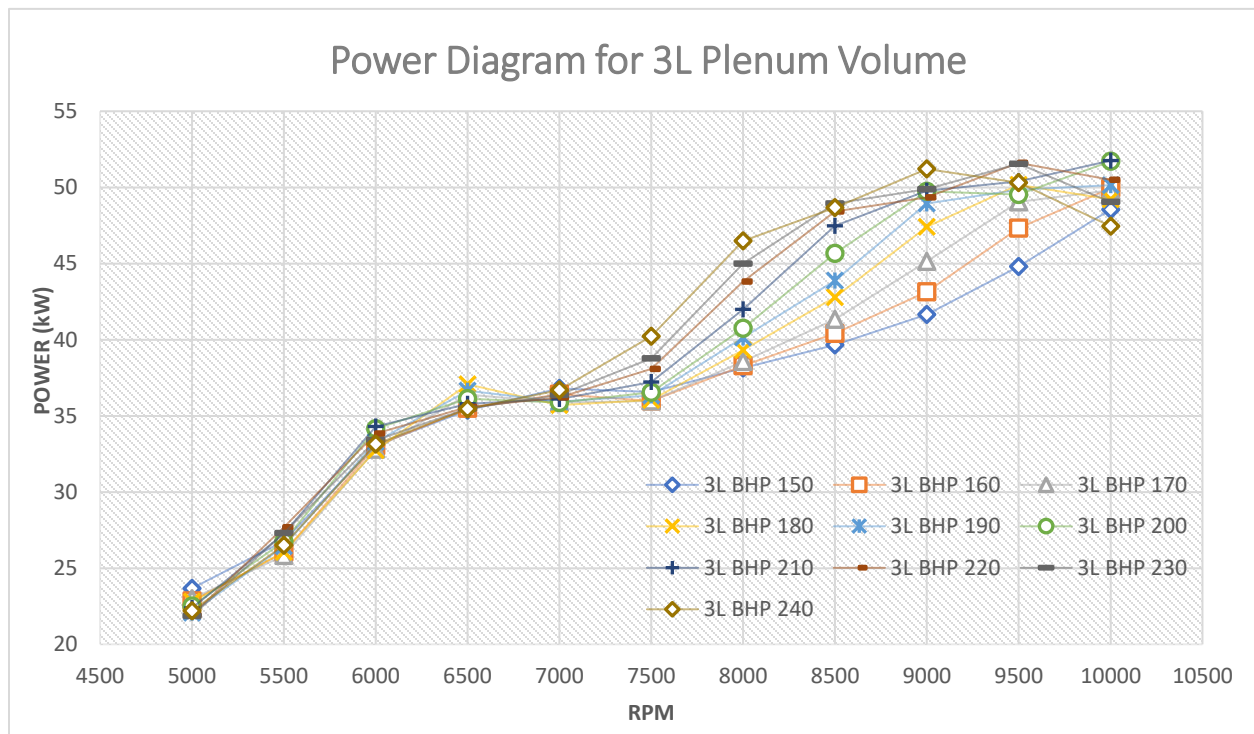


Figure 61 Power Diagram for 3L Plenum and Different Length Runners. The last number refers to the length of the tested runner in mm.

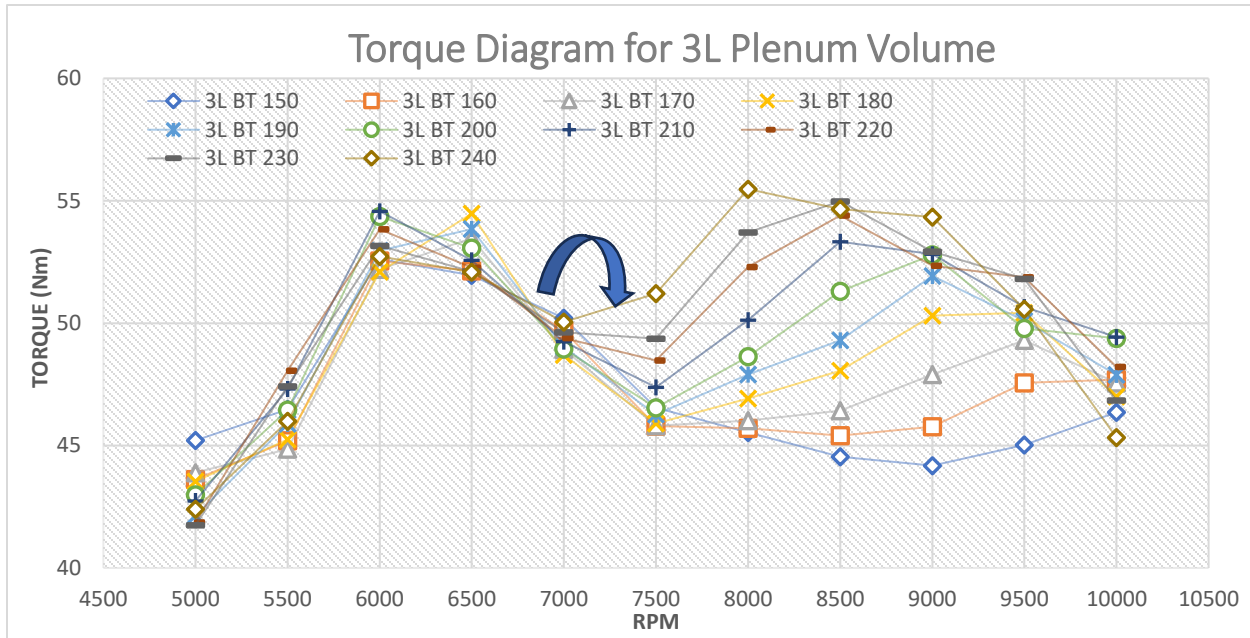


Figure 62 Torque Diagram for 3L Plenum and Different Length Runners. The last number refers to the length of the tested runner in mm.

Based on all the diagrams produced from the model, a similar behavior can be observed for power and torque output as the runner length increases. The two diagrams above are simplified and are focusing around the area of interest for the team. This diagram magnification also helps ignore the unpredictable behavior of the torque values at low rpm, mainly below 5000. In some cases, the model did not converge and hence the resulting form of the diagram cannot be evaluated accordingly. However, the same cannot be said for the medium and high rpm values. Through the diagrams, it is clear that both torque and power diagrams seem to show a pivot point at the 7000-rpm mark. More specifically, the longer runner length produces higher power and torque between the 7500 and 9000 rpm range. Especially for the torque diagram the change seems to become more abruptly compared to smaller runner lengths. In contrast, the longer runners seem to produce lower values of torque below the 7000-rpm mark. The differences in the power diagram are much smaller and can almost be considered neglectable between the runner length differentiations. It should also be mentioned that at even higher rpms (after 10000 rpm) the shorter runner lengths produce more power and the diagram behavior changes again, however this change can be seen clearer at the appendix diagrams and is not of great interest for this application.

The optimum runner length is not univocal but depending on what rpm range is valued. As can be seen in the figures above and in appendix 12.1 where all different runner length tested are presented, the characteristics of the power and torque over the rpm range changes. Unfortunately, the calculated driving range covers the swing point, forcing the optimum chosen runner length to be a compromise of more power below or over 7000 rpm.

Since longer runners are preferable if the engine speed range of peak power is between 7000 and 9000 rpm and shorter runner lengths are preferable if the rpm range for peak power is between 6000 and 7000 rpm the optimum runner length for this particular engine lies between the 200-240mm range.

Those runner length values also seem to produce the peak amount of torque at the rpms of interest even though the curve changes abruptly. The benchmark length of 150 mm runner length although more stable cannot offer the desirable values and presents a dip in the curve that does not help engine operation. Hence the optimal runner length value of 240mm is elected. Comparing the runner length value from the diagram data to the one from the equation, a significant differentiation can be acknowledged. Below, the power and torque diagrams can be seen for the standard plenum volume of 3L and 180mm and 240mm runner length.

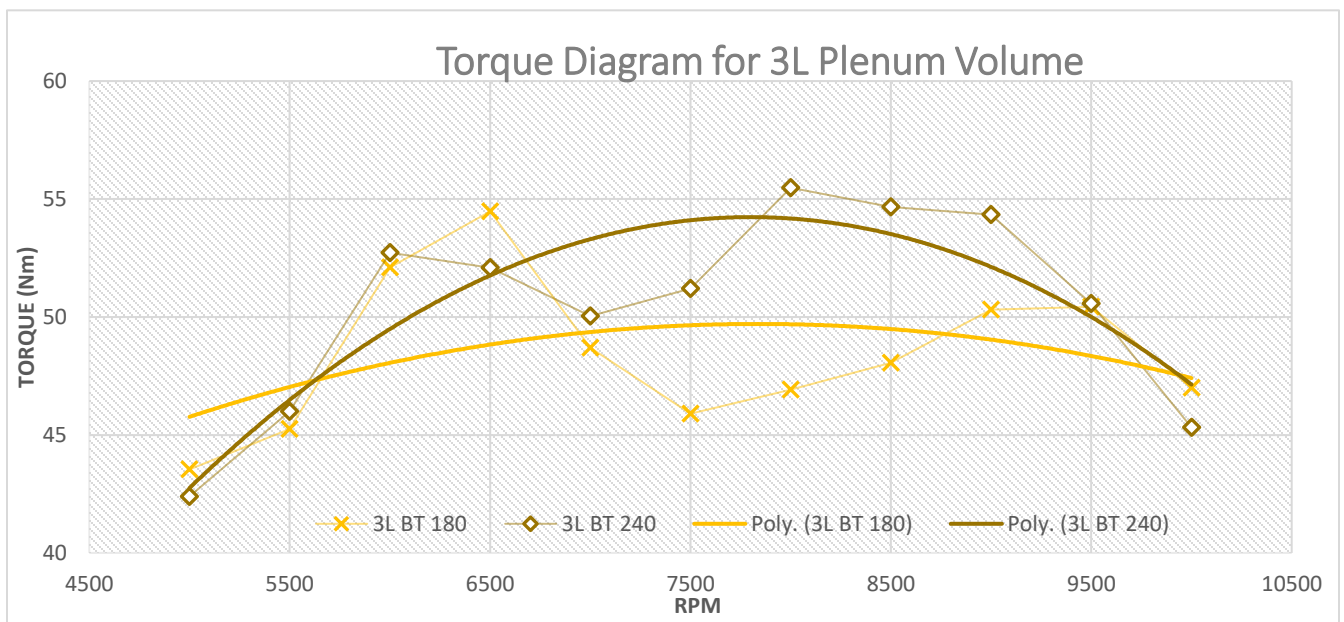
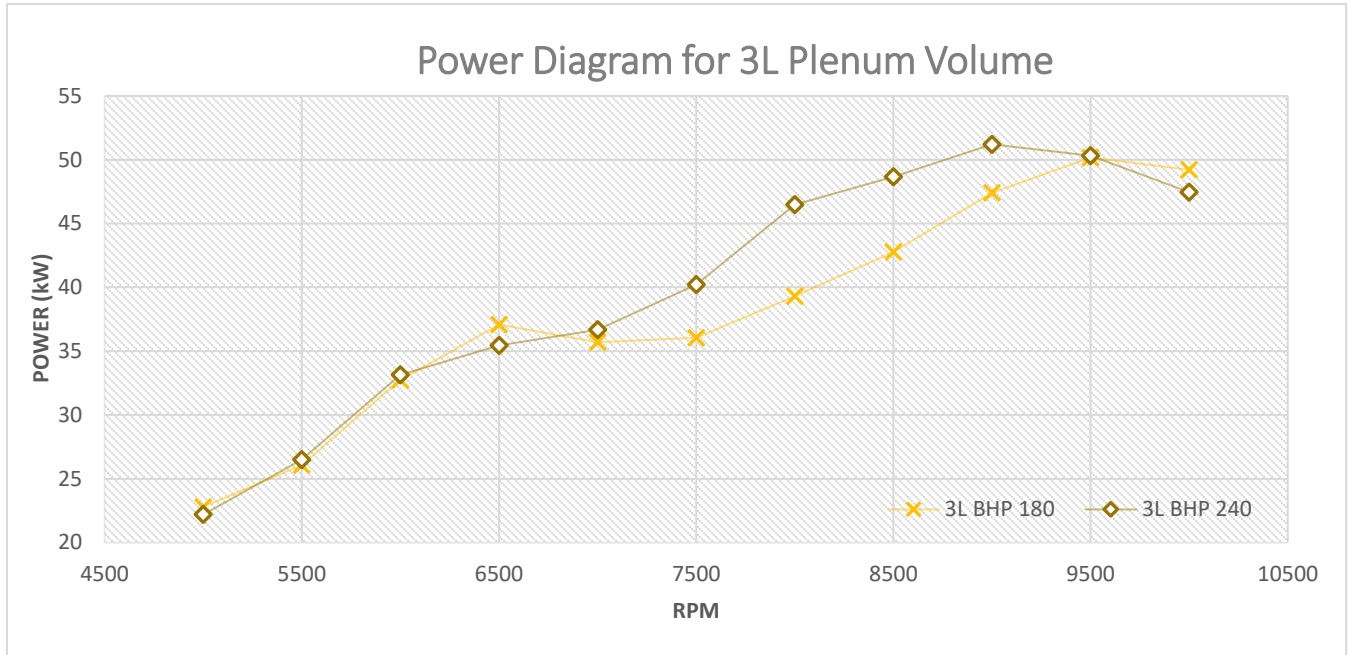


Figure 63 Comparison for 3L plenum and the two best runner options regarding torque and power. The last number refers to the length of the tested runner in mm.

Comparing the two runner lengths alone with each other clarifies the different affect they have to the engine. With the addition of a polynomial trendline to the torque curves, a more comprehensive visualization of the torque curves can be made. The longer runner retains a constantly upwards trajectory for the power curve whilst achieving higher torque values after the 7000-rpm mark. Based on the all the gathered data, the 240mm runner will be considered the optimum value.

Next step is to elect the plenum volume. A similar process is followed with the main difference being that the runner length now equals to 240mm.

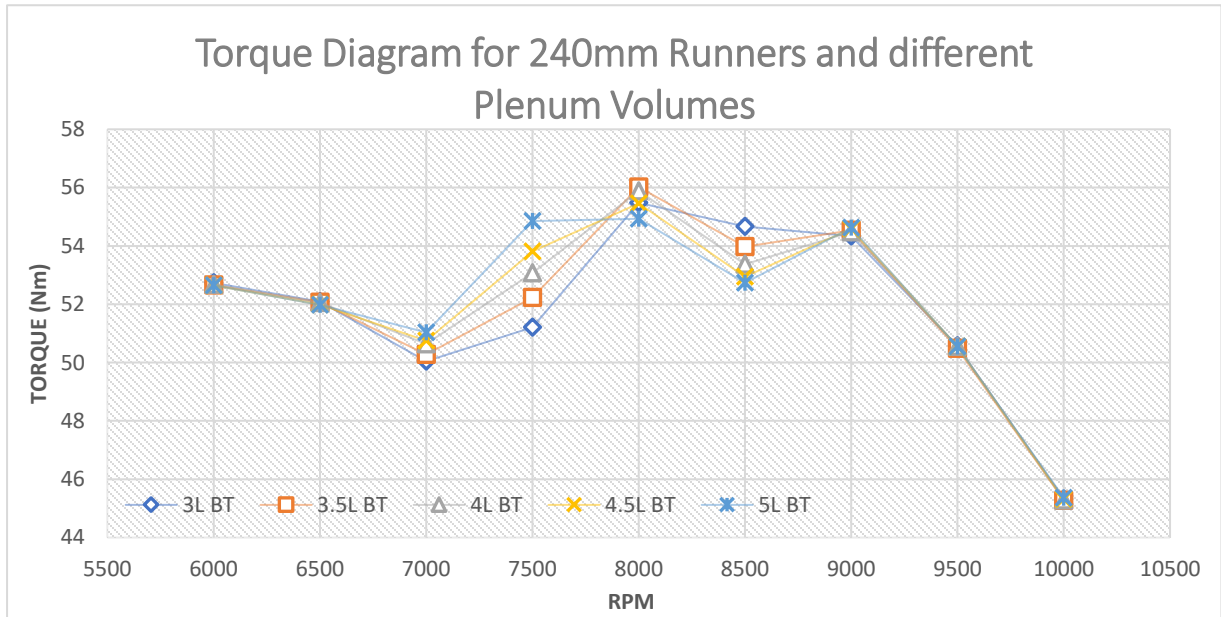


Figure 65 Torque Diagram for optimal runner option and different plenum volumes. The first number refers to the volume of the tested plenum in L.

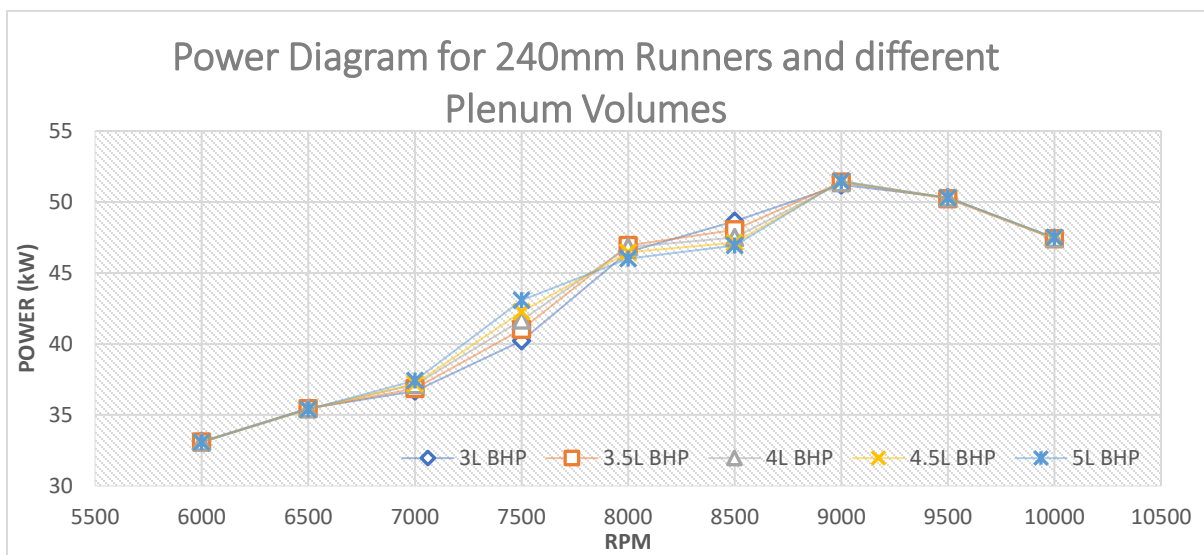


Figure 64 Power Diagram for optimal runner option and different plenum volumes. The first number refers to the volume of the tested plenum in L.

The two diagrams visualize the effect of plenum volume to power and torque output. The higher the volume, the more effective its size becomes at rpm values around the 7500 mark. Similarly, the smaller volumes become more useful and can extract the full potential of the engine at values above the 8000-rpm mark. The pivot point is still visible at both diagrams. The difference at volume is more apparent at the torque diagram which also is the one of higher importance to the team. Based on the diagrams alone, the higher values again seem to be the choice that best fits the car's needs. The 4.5L and 5L plenum volumes present the higher torque values of all although the 5l also has the most stable curve of the two. In addition to these diagrams, the maximum values of power and torque were studied at the whole range of rpms and for the 7500 value specifically.

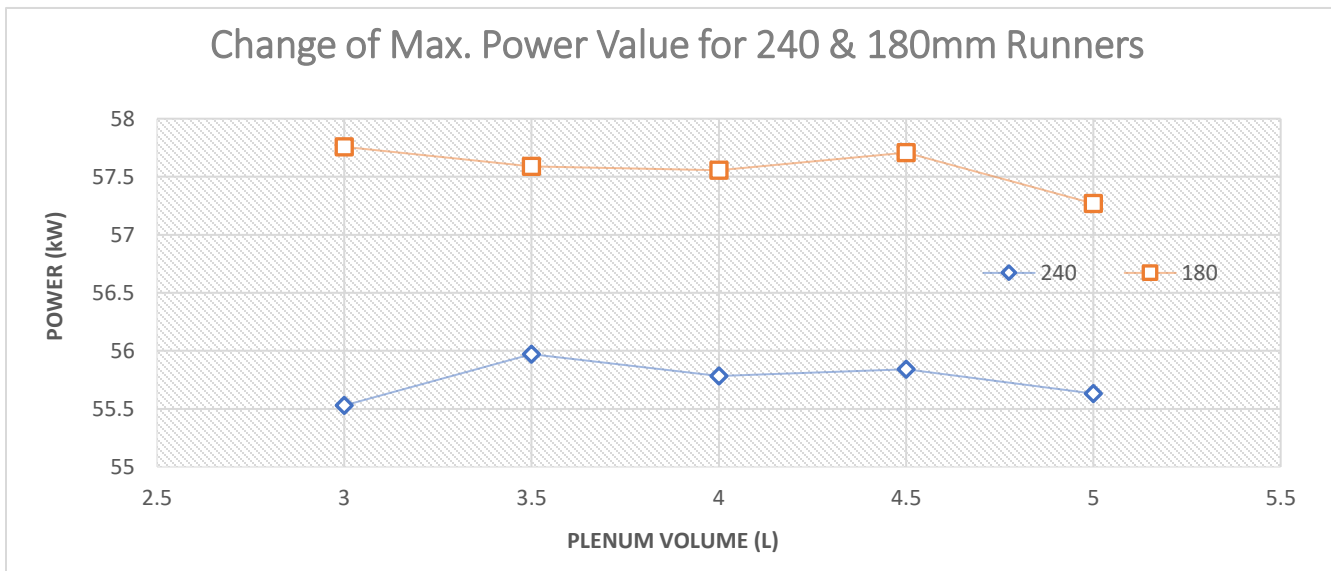


Figure 67 Peak Power Differential between the best runner options. The two numbers correspond to the different length in mm.

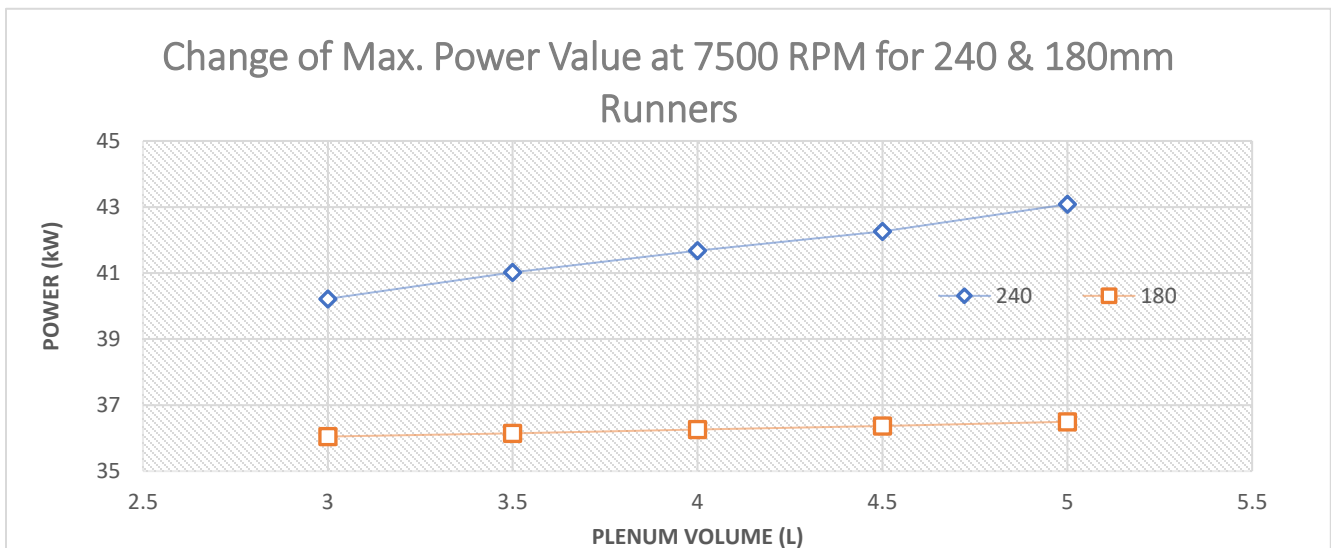


Figure 66 Max Power Differential at 7500rpm between the best runner options. The two numbers correspond to the different length in mm.



It can be observed that the 5L plenum presents the highest number of power output for the 7500 rpm for both runner lengths but ends up to have the lowest max value out of every volume that is being tested. Another interesting observation is the differences between max and min values for the two runner lengths. For the 240mm runner, a 6.6% difference between the 5L and 3L volumes can be seen. However, at the 180mm runner power peak stays almost identical along all the volumes with a mere change of 1.2% which can be considered neglectable. It is also very important to point out that the max power diagram is the only diagram where the 240mm runner is lagging behind the shorter counterpart. Biggest difference of max power is for the 3L plenum with a 3.8% difference and biggest difference for 7500 rpm power is 15.1% for 5L plenum and 10% for 3L plenum.

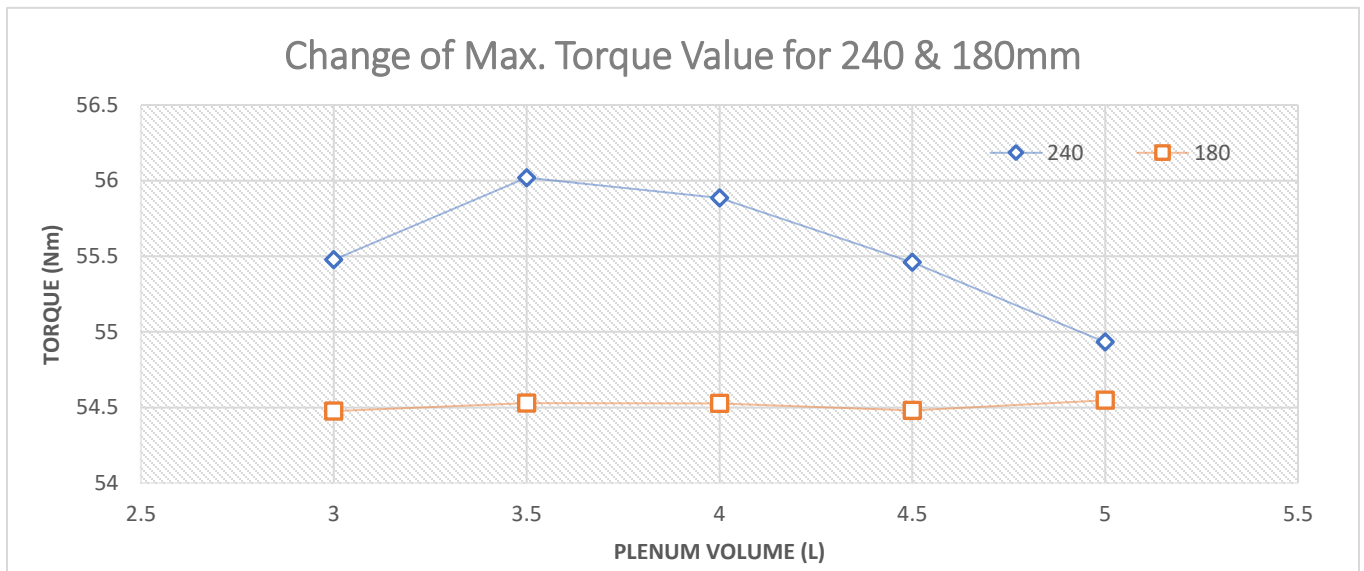


Figure 69 Peak Torque Differential between the best runner options. The two numbers correspond to the different length in mm.

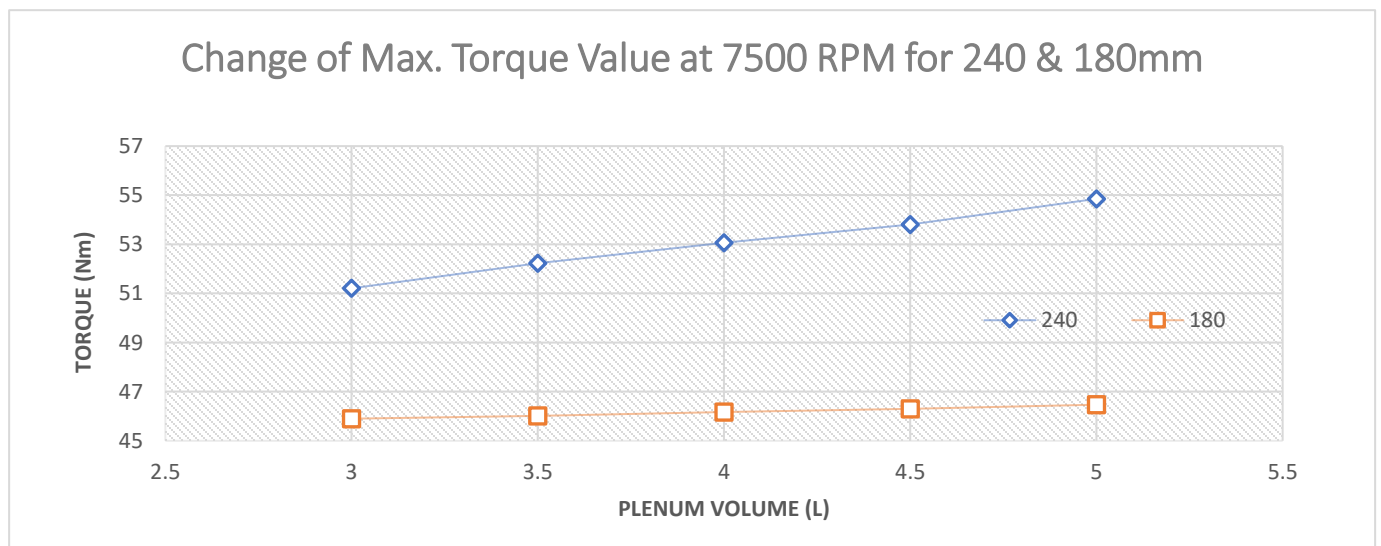


Figure 68 Max Power Differential at 7500rpm between the best runner options. The two numbers correspond to the different length in mm.

In contrast to the power diagrams, torque curves present higher values for the 240mm runner. Peak torque is reached at 3.5L whilst at the rpms of interest it seems that torque follows a linear upwards trajectory as plenum volume increases. The same cannot be said for the 180mm runner which again seems to have a more stable curve both for max torque values for the whole range of rpm as well as for the rpms of interest. The values are also lower compared to the ones of the 240mm runner, with 2.6% difference being the maximum for general max values and 14.9% the maximum for the 7500-rpm mark. It can be easily understood that the main difference lies at the 7500 rpm where the larger plenums operate better for both power and torque. The general max values present smaller differences that can be ignored for the final runner length and plenum volume selection. It is implied by the diagrams that the larger volume will have much better results where they are needed the most by the team. As plenum volume increases however, so does the mass and difficulty of packaging the system. The same goes for the runner lengths. The drivability can also be adversely affected. With consideration to throttle response and drivability a 5L plenum seems to be the best option to be utilized for the first-year vehicle.

Based on power and torque output, the best solution for the team involves a 5L plenum and 240mm runners. Before confirming the forementioned results, the volumetric efficiency and volumetric flow are also accessed for the 180 and 240mm runners and for every possible plenum volume. The volumetric efficiency diagram shows a significant increase in volumetric efficiency in the rpms of interest at higher values of plenum volume and runner length. As the volume and length increase, so does volumetric efficiency. More specifically, at the 7500 rpm, the highest volumetric efficiency value for 180mm runner length was almost 10% lower than the lowest value for the 240mm length. It should also be mentioned that for the 180mm runner, the highest value is achieved at 6500 rpm whilst for the 240mm it is achieved at 8000 rpm. The volumetric efficiency at that point is almost reaching the value of 1 but does not overcome it, that means that the tuning effect is not achieved but is really close. The values of volumetric efficiency were considered acceptable and the 5L plenum and 240mm runners were considered again to be the optimal solution.

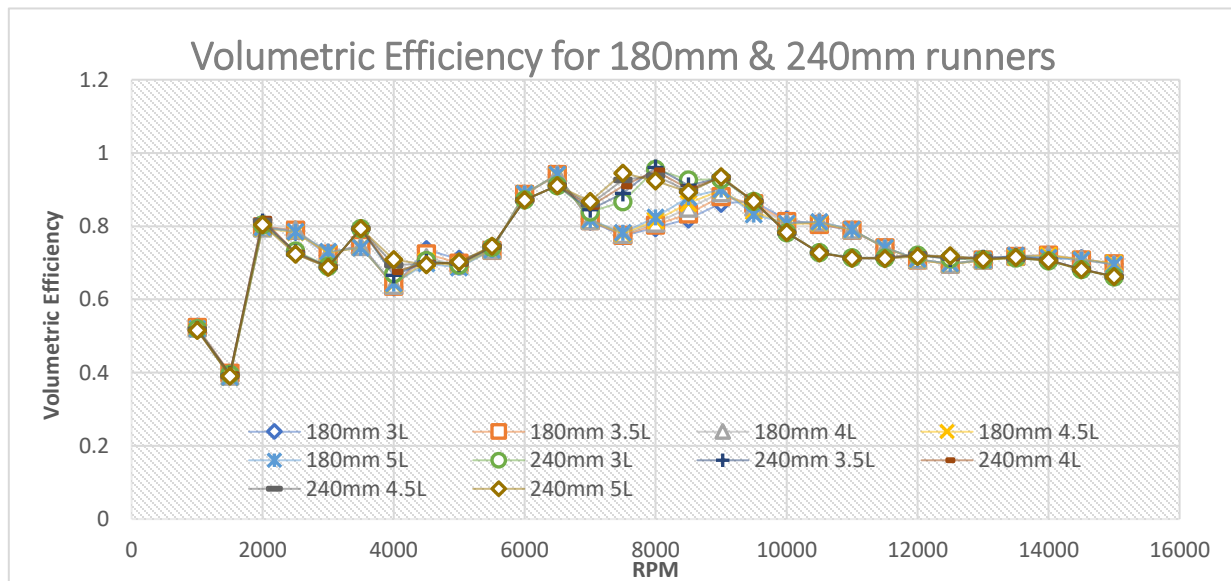


Figure 70 Volumetric Efficiency Diagram for a Range of Different Plenums Between the Best Runner Options. The first number corresponds to plenum volume in L whilst the last to runner length in mm.

Finally, with the help of the Ricardo software we can visualize the volumetric flow throughout the intake assembly for all the tested configurations to ensure proper airflow through the whole assembly for smooth power production. The bigger the plenum volume is made, less negative flow through the restrictor there is and the flow as a direct consequence is also transported more evenly through the restrictor which is preferable. Figure 71 shows volumetric flow vs distance as a real time operation showing how fast all fluids move through the entire system hence direction and magnitude of airflow. On the left side, the 180mm behavior is illustrated and, on the right, the 240mm accordingly. By observing the live animations of the figures below through the program, it can be noticed that a greater buffer of air created by a bigger plenum chamber decreases the tendency of negative flow through the restrictor.

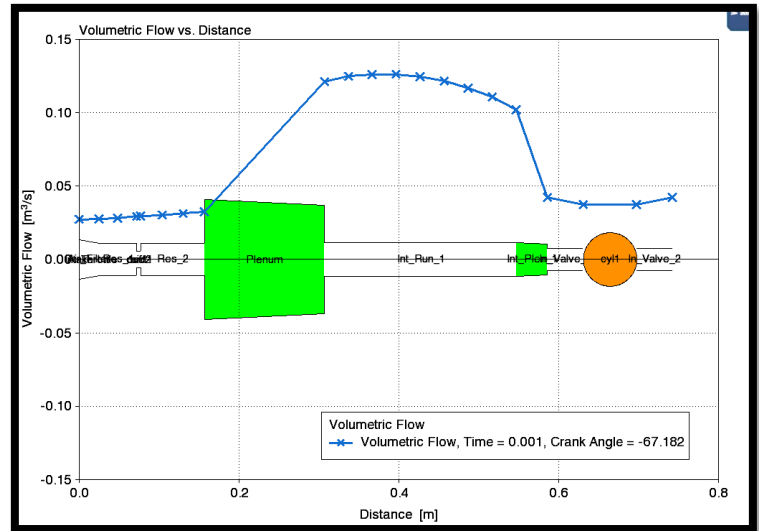
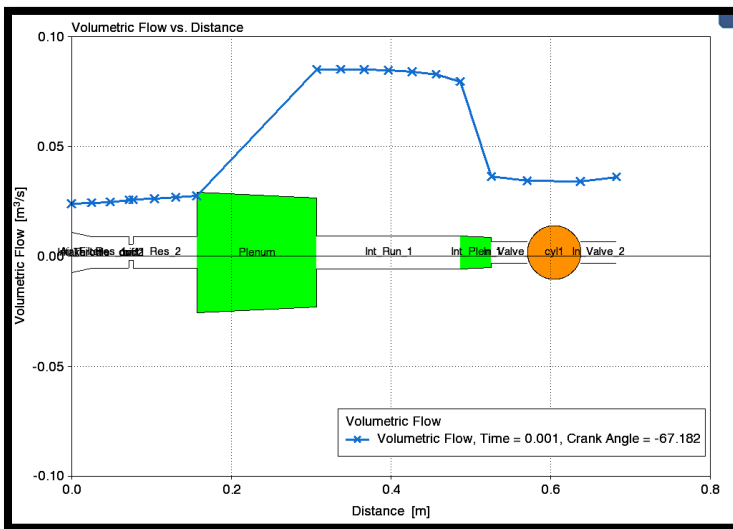


Figure 71 Volumetric Flow Along the Intake for 180mm (Left) and 240mm (Right) Runners

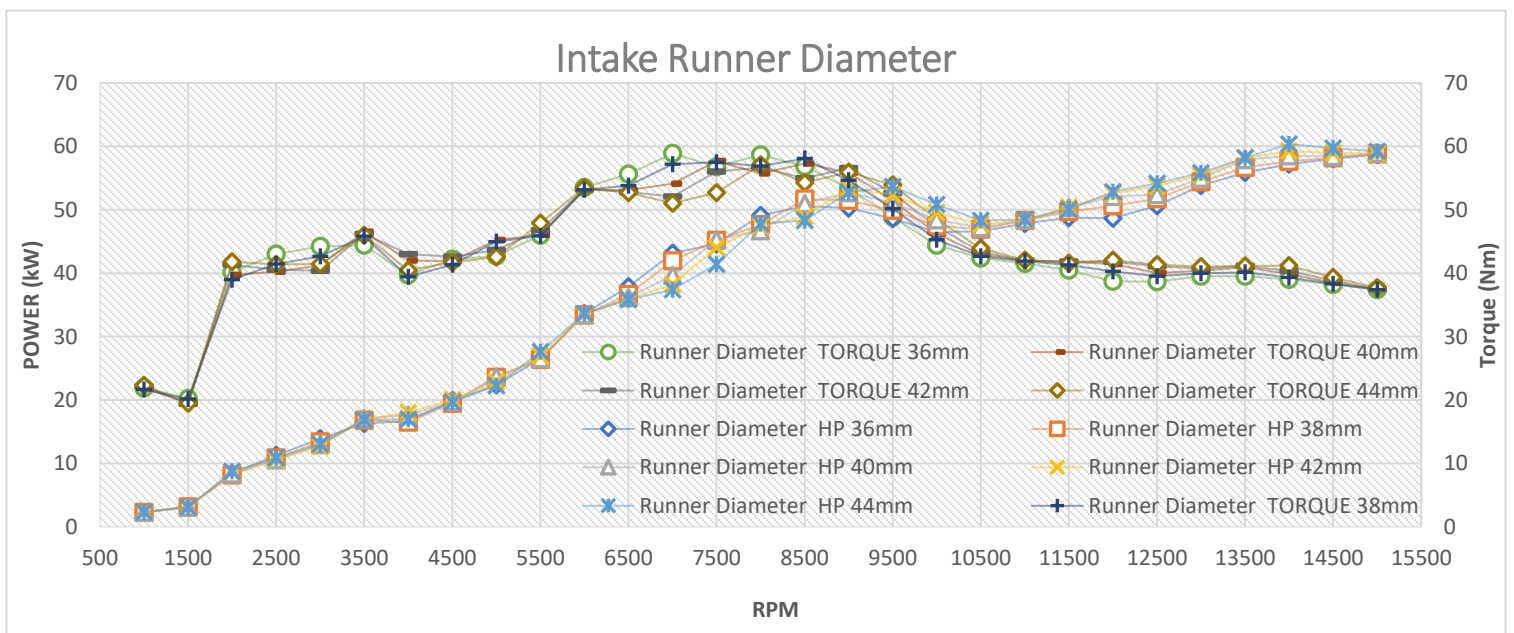


Figure 72 Comparison for Optimal Runner Diameter.

Finally, the runner diameter can be evaluated. The 5L plenum and 240mm runner diameter were kept as constants and the runner diameter was changed according to the forementioned steps. In the diagram above it can be observed that the higher diameters perform better at higher rpm values. In the zone of interest, all the runner diameter values apart from the 44mm are very similar in power and torque output. More specifically the maximum difference between the values does not go over 3%. It should also be noted that the 42mm runner always produces the lowest outputs whilst the 40mm the highest values. Although the differences between them could be considered minimal and almost neglectable, the 40mm runner has the slight edge. Hence, the 40mm runner was deemed to be the optimal choice for our application.

## 7.5. Final Results & Comments

With the approximate size of the plenum decided, its positioning relative to the intake port of the engine is dictated by the runner length. As discussed in the theoretical part of this thesis, runner length tuning in naturally aspirated concepts is particularly important when deciding the shape of the power and torque curves of the engine, as acoustic effects have a considerable influence on volumetric efficiency. A longer runner tends to result in a torque curve shifted towards lower engine speeds, and a shorter runner results in a torque curve shifted towards higher engine speeds. Ultimately, the final runner length and plenum volume choice would be determined by the packaging and the space available for the intake placement. The numbers elected by the Ricardo software make up the benchmark which the team will aim to accomplish. The final goal values are 5L for plenum volume and 240mm runner length. The final values although promising in the Ricardo software seemed to be larger than the ones expected and concerns were risen regarding the actual implementation of these values. In order for the team to be able to overcome any packaging issues that may arise, a general rule was put in effect which stated that the most suitable intake assembly that was going to be placed in the car was the one with the largest volume and runner length that could fit within the rule-mandatory boundaries. The final step before proceeding to the shape of the mentioned parts was to compare the data gathered from the software for the stock engine and the modified one to underline the performance changes and gains produced by the additional components and layout changes.

## 8. Model Data Comparison

In this Chapter the stock engine model is going to be compared with the race ready one in order to access and comment upon the most significant differences and changes. Another reason is to try to anticipate and foresee the engine behavior when that is going to be placed in the vehicle and fix any issues that may be found in the process.

### 8.1. Key Differences between Stock and Race engine

The starting point of this evaluation is the power and torque diagrams which are the basic point of comparison and have been the main theme and point of interest for this thesis. The diagram presents very similar behavior between the stock and modified engine up until the 8000-rpm mark, where the restrictor comes to effect. The choice of a similar throttle body diameter to the electronic 4-throttle assembly of the stock one seems to have kept the power and torque values very similar between the two different models. However, after the 8000 rpm mark the restricted air flow starts to show its effect to the engine.

Power and torque drop significantly since all cylinders have to be fed by the same 40mm throttle whilst passing through the 20mm restrictor. Peak power has taken a drop of 41.5% and peak torque a drop of 15.5%. At the 7500 rpm however, the drop is almost neglectable with both power and torque being just 3.9% lower than the stock numbers. Effectively, the simulations show that the engine has lost a lot of each high rpm power and has kept relatively close to the manufacturer numbers in the rpms that the team aimed for. The torque peak value also seems to have been affected the least from the changes made. Basically, the results taken from the diagram have been the ones that the team anticipated and hoped to see at the end of the software model development.

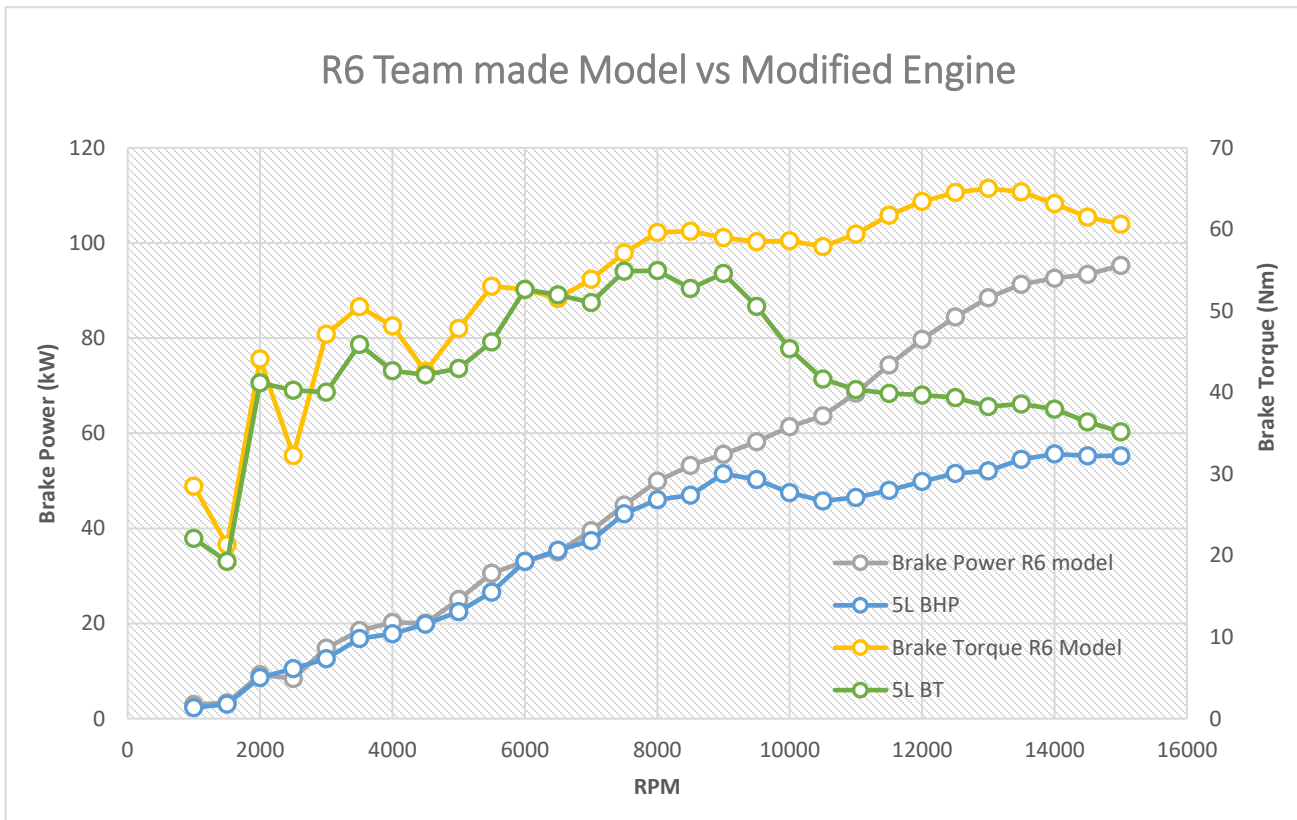


Figure 73 Comparison between Stock R6 Ricardo Model vs Modified Ricardo Model

Another important parameter tested is the volumetric efficiency. The stock engine model showed excellent efficiency mainly at higher rpms where the tuning effect takes place and the volumetric efficiency climbs above the value of 1. This behavior further confirms the racing focus of the engine. This behavior changes however when the FSAE modifications are installed. The volumetric efficiency now drops at the higher rpms making the engine almost inefficient at rpm values higher than 8500 rpm. The important characteristic of this diagram however is that the volumetric efficiency near the 7500 rpm remains almost the same or improves at some parts of the rpm range. Still, the volumetric efficiency does not improve further than the 0.96 value and so the tuning effect does not appear even after the modifications. Summing up, the volumetric efficiency of the engine seems to be a downgrade compared to the stock

engine even though at some rpms the values remain fairly similar. The tuning effect was not successful however the general behavior of the diagram made the team optimistic of a similar performance under real circumstances.

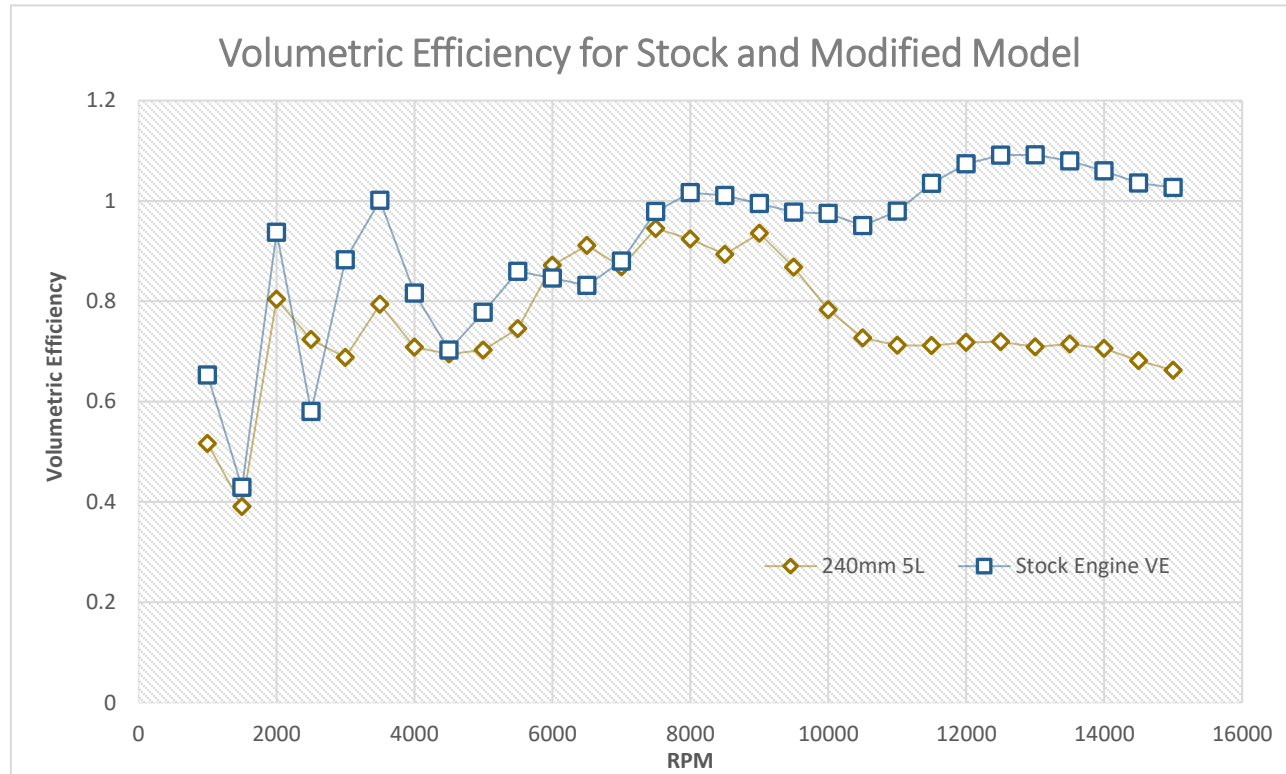


Figure 74 Comparison of Volumetric Efficiency Between Stock and Modified R6 Model

Finally, the break mean effective pressure and break specific fuel consumption are evaluated. As mentioned in the first chapters of this thesis, BMEP is purely theoretical and does not correspond to real engine pressure values. It is simply a tool to evaluate the efficiency of a given engine at producing torque from a given displacement. Based on the following diagram, a direct comparison between the modified and stock engine can be made. It is evident that the modified engine has generally lower BMEP values throughout the rpm range. Effectively, that means that the stock engine was more efficient at producing torque from its displacement. The most significant change can be seen at the higher rpm where again the restricted amount of air drops the BMEP values 5 units bar below the stock engine. It is important to note however that the BMEP values around the rpm range of interest remains relatively similar and in one or two cases the modified engine achieves slightly higher values. The difference is about 2% in the forementioned scenario and so it can be considered that the modifications have kept the engine's efficiency regarding torque output in a similar level to the original capabilities.

Regarding the BSFC, lower values correspond to a more fuel-efficient engine. The general diagram behavior indicates higher BSFC values at lower rpm which as the rpm increase drop and stabilize. More specifically, higher BSFC values correspond to worse fuel consumption due to higher friction heat losses. Looking into the diagram with more detail, it can be observed that the two engines present similar BSFC values across the rpm range. Some differences can be observed at higher rpms and some scattered points mostly at the mid-range. More specifically, the modified engine seems to have worse fuel consumption than the stock engine at higher rpms. The values actually do not seem to stabilize as mentioned before but increase as the rpm increase. At the 7500-rpm mark, the BSFC values remain more or less the same to the stock engine which means that the fuel consumption is going to be generally unaffected when the engine operates under those conditions.

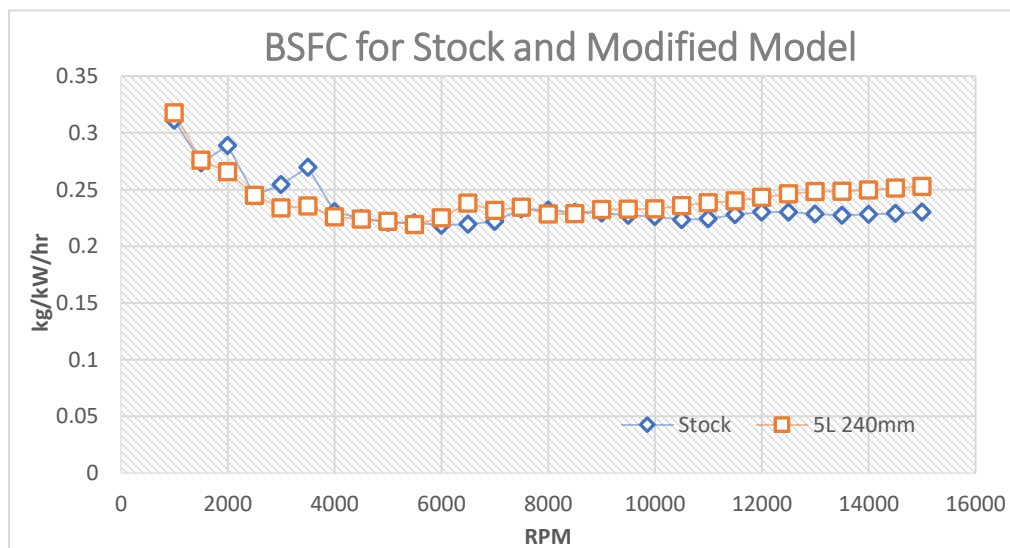
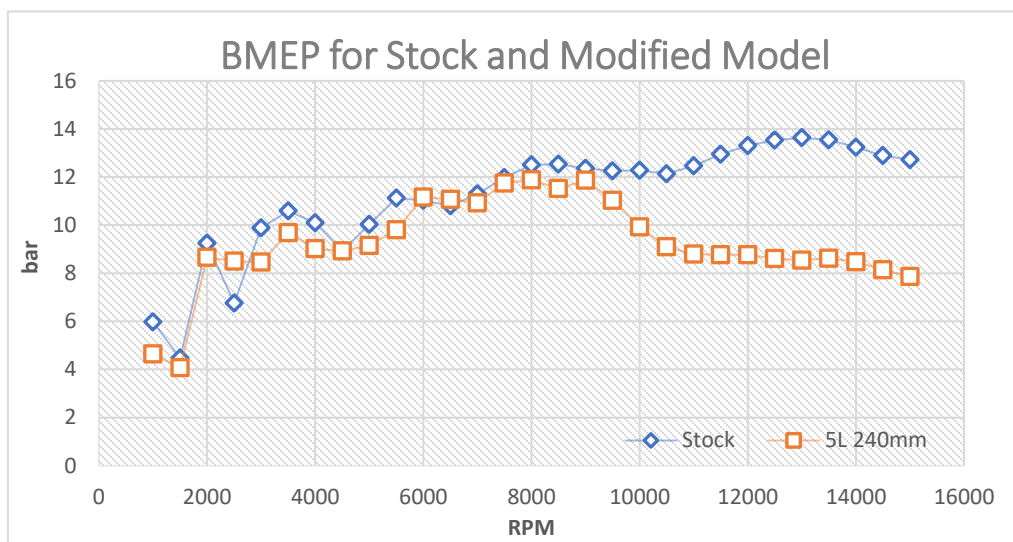


Figure 75 BMEP and BSFC Comparison Between Stock and Modified Model.

## 8.2. Goal Assessment

Before continuing to the final dimensioning of the whole intake assembly, an evaluation of the generated results was considered to be necessary in order to assess the success of the software model. Based on all the retrieved data and all the comparisons with the stock model, the modified engine seems to behave along the anticipated performance. The main key points include a power and torque diagram that greatly resembles the manufacturers both in the values themselves as well as to its general behavior. In every diagram mentioned in the thesis, the values above the 9000 rpm always showed the most significant changes that often corresponded to decreased performance and efficiency. This behavior is mainly caused by the restrictor which was also simulated in the model. These behaviors can confirm the proper implementation of the restrictor and the proper simulation of its effects. With the added modifications the engine has lost its high-end power and performance abilities and now it is mainly more efficient between the 6000-8000 rpm. With the 7500 rpm being the main operational point, means that the team has achieved its goal of ideal engine operation at the given rpm. In addition to all the above, the extra diagrams of volumetric efficiency, BMEP and BSFC further confirm that the modified engine has very similar behavior to the stock one up until the upper limit of the rpm range of interest. The volumetric efficiency is the only parameter where the team did not succeed its goal to achieve the tuning phenomenon. The produced values were acceptable however and within the anticipated range from the original ones. All in all, the Ricardo software produced valuable data for the upcoming practical tests and gave feedback in the model builder of the engine. It also gave a general preview and idea to the team of how the car's engine is going to behave under a wide range of different recommended modifications.

## 9. Final Dimensioning and CFD study

After the virtual engine model is concluded, the resulted values must be incorporated into the car design and comply with the component packaging. In addition to that, the given numbers alone of plenum volume and runner length are not enough to fully define the intake dimensions onto the vehicle. The final shapes and configurations need to be decided in order to further aid engine operation and car behavior.

### 9.1. General Limitations

As mentioned at the beginning of this thesis, the competition is based upon rules that dictate the basic packaging and dimensions of every vehicle taking part to the competition. The rule T 1.1.17 portrays the surface envelope on a default vehicle. The figures below illustrate the forementioned surface envelope in the team's car. Due to the 5L plenum size and 240mm runner length combined with the tight packaging chassis, placing the intake within the 'surface envelope' would prove a difficult task, and narrowed the choice down to two general concepts.



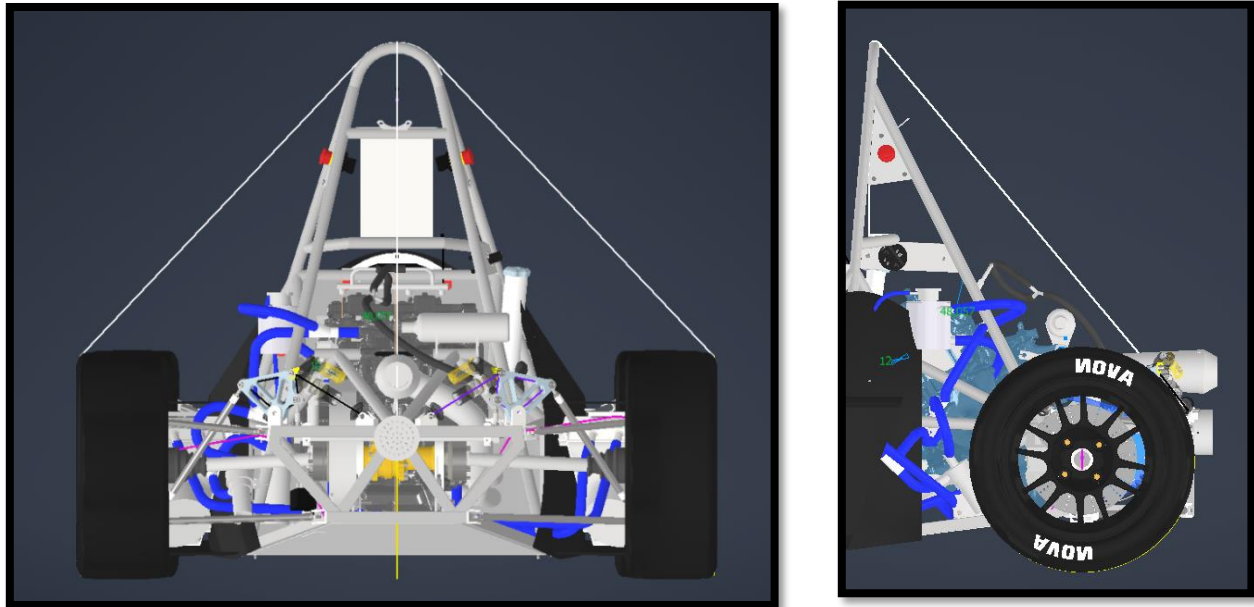


Figure 76 Envelope Visualization on Cad Software

The first option was a ‘side-mounted’ concept. This design has a lower Centre of Gravity (COG) but is asymmetric compared to the whole car which may be an issue since the car implements two sidepods and the exhaust manifold ends at the back in the middle of the vehicle. The side mounted concept mainly suffers from the air needing to turn through almost 180 degrees from entry into the air filter to the intake ports. The mounting of the system should also be a headache since most car components such as the cooling and fueling system use the available space for their mounting and the sidepods utilize most tubing for their mountings and cover most of the useful space.

The second option is a ‘top mounted’ concept. This concept initially seems promising for the symmetry that it offers and straight flow path for clean air from the throttle to the plenum. Another positive is the ease of mounting the intake. Since no electronic throttle is being used this year the whole throttle assembly with the air filter is lighter and a mounting on the roll hoop by some types of brackets could prove reliable enough. This concept however has a higher center of gravity (COG) than the side-mounted one although due to the minimal weight of the assembly it does not have a significant effect on the car. Finally, the most important disadvantage comes from packaging the runners of the required length. A sharp bend would be required to turn the air approximately 90 degrees into the intake port and the pressure drop through there would be considerable. Based on the given circumstances, the available space and taken into consideration all the forementioned data, the top mounted option was elected.

## 9.2. Final Design Choices and Dimensions

Having the final intake assembly part dimensions and the final concept of the assembly placement onto the car, the final step to complete the intake study was to manage the packaging accordingly to get the most out of the assembly. The volume of 5L had to be distributed accordingly to fully take advantage of the available space whilst leaving enough space for the 240mm runners without creating any 90° bends or abrupt direction changes.

The starting point of the design consisted of 4 different geometries which were tested and evaluated based on **pressure distribution**, velocity lines and **turbulence elimination** in order to maximize the **utilization of air energy**. A total of 56 designs were tested which were based on 3 initial basic geometries of the sphere, disk and cone as well as the final produced shape which was a combination of the advantages of all of the above. The design evaluation was carried out with the help of the ANSYS program. The program setup and parameter choice are going to be further explained in the next paragraph.

Before proceeding in the ANSYS optimization it was realized that the space available for the assembly placement was considerably limited. The surface envelope was in every case limiting the available space and the volume eligible was smaller than the one calculated. The runners elected were also much larger than the space available. The space available also forced the intake runners to incorporate some degree of bending in order to fit within the foreseen envelope. In order to face the problem that arose, it was decided to look back at the produced diagrams and find the dimensions appropriate for our fitment. The re-dimensioning of the assembly consists of a 3.5L plenum and 200mm runners. The plenum volume was the largest amount of volume possible to fit within the envelope. It also produced higher max values for power and torque but gives its peak at the 8000-rpm mark which is slightly higher than the team's goal. At the 7500-rpm mark it responds reasonably well and the compromise made at that value of rpm, would further strengthen the vehicle 500 rpm higher. Regarding engine operation, the rpm difference was deemed to be manageable and the vehicle control was thought to remain within the anticipated limits. Although, only under real-time testing could this be properly assessed.

Having made the proper adjustments for the intake to fit within the envelope, next step was to begin experimenting with the final shape. As mentioned before, a plethora of different shapes were evaluated until the final general shape was produced.

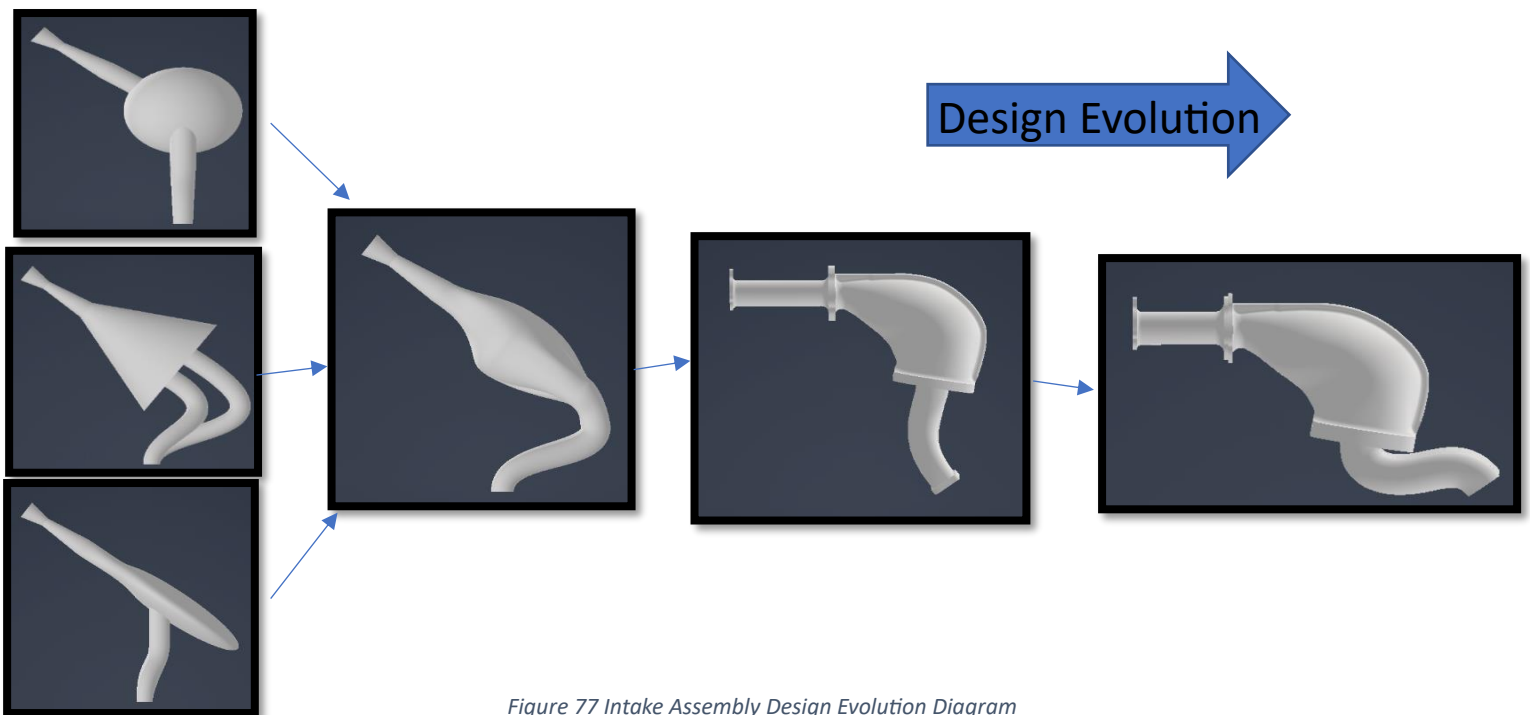


Figure 77 Intake Assembly Design Evolution Diagram

### 9.3. Basic Parameters for ANSYS Study and ANSA pre-processing

In order to access further the different shapes generated and manufacture the best possible solution the ANSYS fluent program was utilized. The basic goals that were set for the program aim at:

- suitable runner's design for proper air outlet speeds to the combustion chamber
- uniform mixing of air with fuel,
- maximizing air supply to the cylinders
- suitable plenum design for achieving progressive power and torque output at acceleration.

The ANSYS program was used and more specifically the Computational Fluid Dynamics software. With the help from the Aerodynamics sub-team, the basic program parameters were set for each different assembly to be tested. The final table with the complete number of parameters and constants used can be seen below.

Table 11 Basic parameters for Ansys software

Solver	Viscous Model	Inlet Zone	Outlet Zone	Wall Zone
Pressure-Based	Standard k-epsilon (2eqn)	<b>Velocity Magnitude:</b> 36m/s	<b>Gauge Pressure:</b> 83000 Pa	Wall Motion: Stationary Wall
Absolute Velocity Formulation	Standard Wall Functions	<b>Initial Gauge Pressure:</b> 101325Pa	<b>Pressure Profile Multiplier:</b> 1	Shear Condition: No slip
Steady Time		<b>Reference Frame:</b> Absolute	<b>Backflow Direction:</b> Normal to Boundary	Wall Roughness: Standard
Mesh Display	Material	<b>Turbulence Specification Method:</b> Intensity and Viscosity Ratio	<b>Backflow Pressure:</b> Total Pressure	Roughness Constant: 0.5
<b>Zones:</b> Inlet, Outlet, Wall-Volume	<b>Fluid, Name:</b> Air	<b>Turbulent Intensity:</b> 5%	<b>Turbulence Specification Method:</b> Intensity and Viscosity Ratio	
	<b>Density:</b> 1.225 kg/m <sup>3</sup>	<b>Turbulent Viscosity Ratio:</b> 10	<b>Turbulent Intensity:</b> 5%	
			<b>Turbulent Viscosity Ratio:</b> 10	

Wall Zone	Reference Values for Reference Zone Volume		Solution Methods: SIMPLE Scheme	Solution Controls Under Relaxation Factors:	Residual Monitors, For all Residual equations:	Solution Initialization: Standard Initialization
<b>Wall Motion:</b> Stationary Wall	<b>Area:</b> 1m <sup>2</sup>	<b>Temperature:</b> 288.16 K	<b>Gradient:</b> Least Squares Cell Based	<b>Pressure:</b> 0.3 <b>Density:</b> 1	<b>Monitor:</b> Check	<b>Reference Frame:</b> Relative to Cell Zone
<b>Shear Condition:</b> No slip	<b>Density:</b> 1.225 kg/m <sup>3</sup>	<b>Velocity:</b> 36m/s <b>Viscosity:</b> 1.7894e-05 kg/(m s)	<b>Pressure:</b> Second Order <b>Momentum:</b> Second Order Upwind	<b>Body Forces:</b> 1 <b>Momentum:</b> 0.7	<b>Check Convergence:</b> Check	<b>Initial Values:</b> 101325 Pa
<b>Wall Roughness:</b> Standard	<b>Enthalpy:</b> 0 J/Kg,	<b>Ratio of Specific Heats:</b> 1.4	<b>Turbulent Kinetic Energy:</b> First Order Upwind	<b>Turbulent Kinetic Energy:</b> 0.8	<b>Absolute Criteria:</b> 0.001	<b>X Velocity:</b> -0.12095 m/s <b>Y Velocity:</b> -4.933776e-15 m/s <b>Z Velocity:</b> 35.9998 m/s
<b>Roughness Constant:</b> 0.5	<b>Length:</b> 1m <b>Pressure:</b> 101325 Pa	<b>Yplus:</b> 300	<b>Turbulent Dissipation Rate:</b> First Order Upwind	<b>Turbulent Dissipation Rate:</b> 0.8 <b>Turbulent Viscosity:</b> 1	<b>Plot:</b> Check <b>Print to Console:</b> Check	<b>Turbulent Kinetic Energy:</b> 4.86 m <sup>2</sup> /s <sup>2</sup> <b>Turbulent Dissipation Rate:</b> 14552.7 m <sup>2</sup> /s <sup>2</sup>

Name	Contents	Color	Mesh Parameters	Quality Criteria	Status
<input checked="" type="checkbox"/> <b>Meshing_Scenario_1</b> <input checked="" type="checkbox"/> restrictor <input checked="" type="checkbox"/> plenum <input checked="" type="checkbox"/> runners <input checked="" type="checkbox"/> Default_Session	8		CFD parameters	Fluent Strict	✓ <b>Comple...</b>
<input checked="" type="checkbox"/> <b>Volume_Scenario_2</b> <input checked="" type="checkbox"/> Default_Session	1		CFD parameters	Fluent Strict	<b>Empty</b>

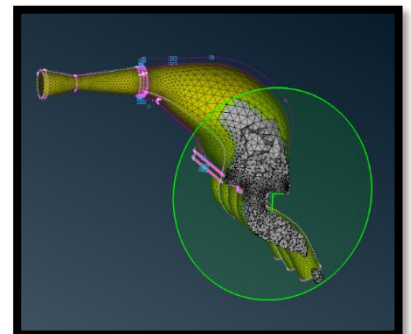


Figure 78 Batch Meshing Scenarios for Different Intake Parts and Meshing Visualization from Cut Plane.

With all the basic parameters being set for the solver-software, the results file is then being withdrawn and inserted into the BETA CAE META program for the post processing. It should also be mentioned that the ANSA Pre-processing software was used before the data were inserted into the ANSYS software to prepare the geometry for the simulation and to produce the meshing of the intake assembly components. The basic meshing parameters are shown in figures 78 & 79. The meshing for each part was triangular shaped and the total number of elements for the whole assembly surpassed 1800000 (1842739). All the BETA CAE programs used were operated with the help of the aerodynamics sub team.

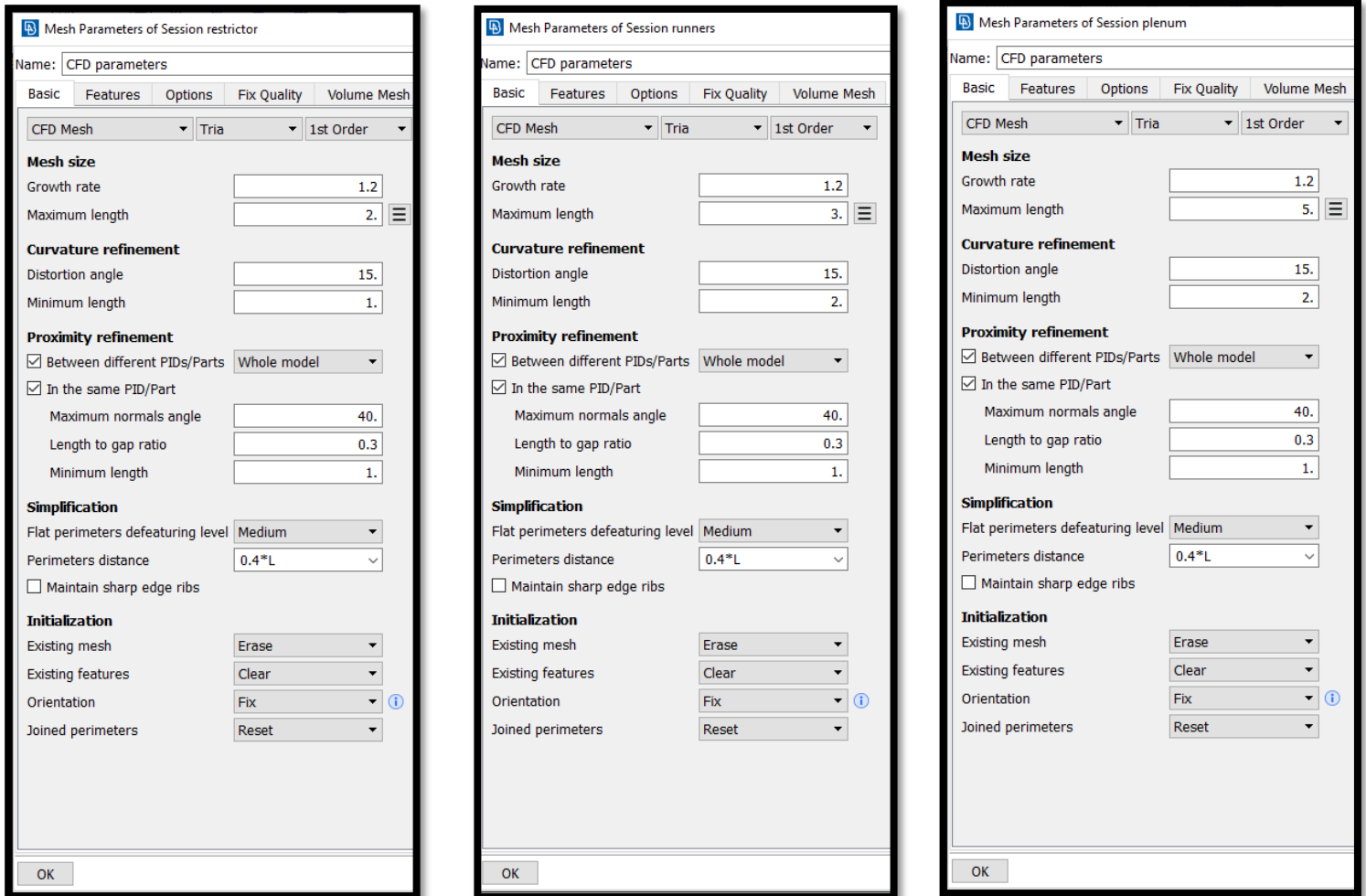


Figure 79 Basic Mesh Parameters for Each Intake Part. Restrictor, Inlet and Outlet (Left), Runners (Middle), Plenum (Right).

All the data inserted into the ANSYS program that can be seen in table 11 were derived from the Ricardo simulations. The goal of the ANSYS software was to visualize and form accordingly the runner bends and plenum shape to take advantage of the air supply at the 7500-rpm. Based on the data gathered from the software, air velocity at the entry point is 36m/s and so this is the velocity that will be used in the inlet of the intake assembly. Regarding the outlet of the runners, data were gathered through the Ricardo program for pressure values at different crank angles for each runner. As each cylinder reaches the intake stroke the pressure value for the corresponding runner is used in the outlet. That value would be the lowest out of all the runners at that particular time. In the Appendix the diagrams of pressure vs Crank angle for every runner can be found. The values of pressure used can be found within the red lines, inside the Intake stroke. The Volumetric flow data for each cylinder were derived from the solver in the outlets of the runners and the flow paths inside the intake were observed. The team's efforts mainly focused on comparing the volumetric flow data from the 1D program to the ones from the ANSYS solver in order to ensure correct operation and manufacture a good operational shape. The volumetric flow values at the end of each runner were also compared with each other to confirm a uniform apportionment of the initial inserted air volume. Finally, the plenum was a major component of interest for the team because, as mentioned before, it determines throttle response and air distribution of the whole intake assembly.

### 9.4. Meta Analysis

After the ANSA pre-processing was completed and the solver was finished, the produced results were inserted into the META software and the visualization of the flow, pressure distribution and vorticity began. This process was repeated for the several different geometries produced and the results were assessed separately and with comparisons between each other. In this paragraph some basic key characteristics and findings are going to be discussed and some basic diagrams for the final intake shape are going to be presented.

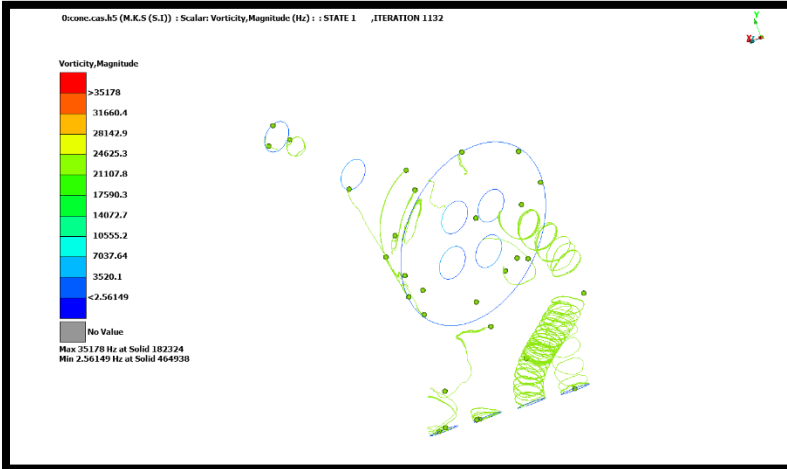


Figure 81 Vorticity Magnitude Diagram for Cone Geometry

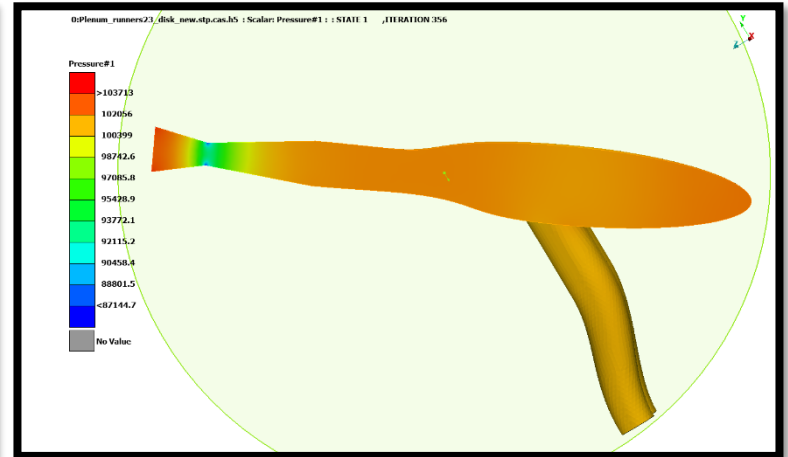


Figure 82 Pressure Diagram for Disc Geometry

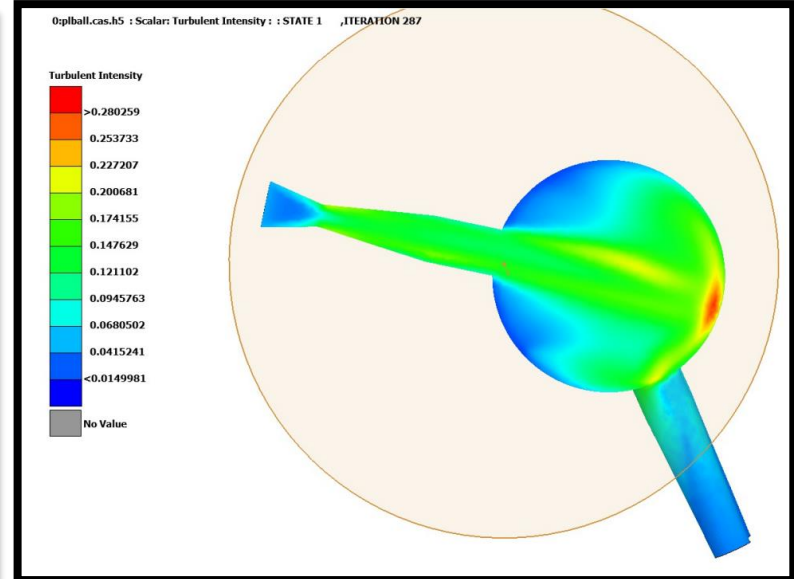
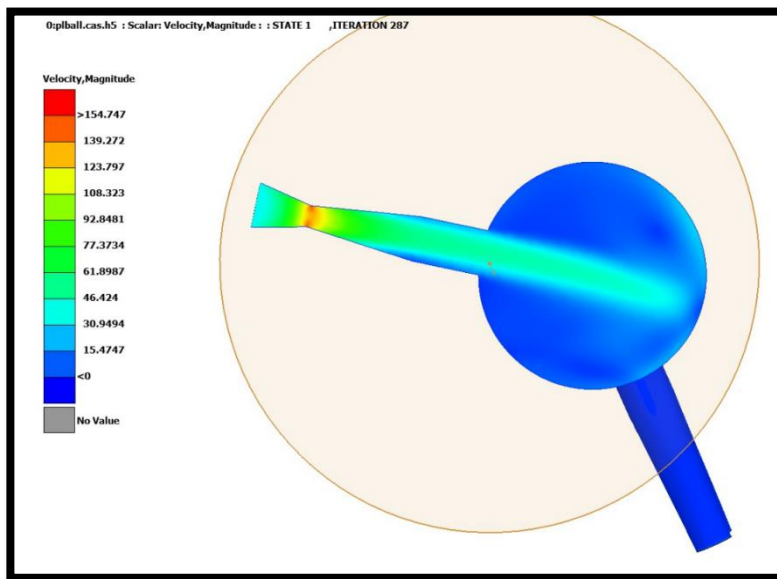


Figure 80 Velocity Magnitude (Left) and Turbulent Intensity (Right) for Ball Geometry

As mentioned before, the flow study begun with 3 basic geometric shapes, a disc, a ball and a cone as shown in figure 80. An initial study was carried out upon these

shapes and gradually the shapes evolved and changed based on the disadvantages the team could point out from the diagrams produced. Some basic characteristics for each one can be seen below. In all the tests performed the restrictor was also implemented to properly simulate the conditions of operation.

**Cone:** This was the design that was evolved the least out of them all. Increased turbulent energy was observed at the edges of the shape. Due to its shape air velocity was lower than the other geometries. The pressure distribution was slightly better than the rest and the air-flow was observed to follow a strange path where only two of the four runners were fed with more air volume than the others. The turbulent kinetic energy was also higher even at some of the runners themselves.

**Ball:** This design fared better to the cone in terms of overall results and performance. The dynamic pressure was higher than the cone and the max value of the turbulent kinetic energy was lower. The pressure was also more evenly distributed apart from the rear most area of the ball-plenum. At that point abrupt changes in pressure and velocity were observed which however were considered solvable with a small adjustment in the runner placement. The middle part of the plenum also showed some considerable viscosity values.

**Disc:** This geometry proved to be the most promising out of the three and became the base for the final intake assembly where all the modifications were incorporated. The Disc geometry showed relatively uniform pressure and the highest velocity out of all the geometries. The turbulent kinetic energy was lower than the others and the only drawbacks seemed to be the width of the plenum and the rear most part of it because of the high-pressure concentration that was created. This however was later fixed with the runners being placed at that point compared being placed at the middle like the initial design.

The three geometries with their advantages were converted into one shape. The runners were moved to the back of the geometry, the plenum lost the large width of the disc but kept the roundness and the slim opening and combined them with the one from the ball geometry. The basic shape of the plenum was to operate like a diffuser. The geometry started with a slim opening and gradually opened up to reach a semi-round part and then converged towards the runner fitment section. With this design combination, the air moved through the assembly to feed the runners with air whilst almost simultaneously, some air streamlines that were not fed to the engine were recycled into the plenum following the round bottom section until they reached the front part of the plenum where they get mixed with the freshly entered air. This cyclic operation was meant to take place every time as the engine operates. After making the required changes to the geometry to incorporate all the forementioned changes, the final design proves to be again much larger than anticipated. Some changes on the general shape approach were needed in order for the available space to accommodate the assembly. The changes made included a significant bend to the plenum of about 90 degrees. The plenum kept its roundness and simultaneously became a surface that the streamlines followed along from the moment they inserted into the assembly till they reached the runners at the bottom. Roundness was also implemented at the top part of the runners to further aid the feeding of fresh air to the engine. The runners were placed next to each other as close as possible and the recycling of the air seemed to work as it was described previously without any problems. The final intake assembly can be seen in the right most picture of the evolution diagram. The runners also incorporated significant bend angles at two points throughout their length. One is right after the plenum connection point and the latter is at the end about 30-40mm before the engine connection point. These bend angles

were necessary as it will be mentioned later into the thesis for the injector placement and in order to make the assembly rules-compliant. It was believed however that the bends could prove helpful at making a more uniform mixture that could later be crucial for more efficient combustion. The figures below portray the pressure, viscosity and velocity distribution throughout the geometry.

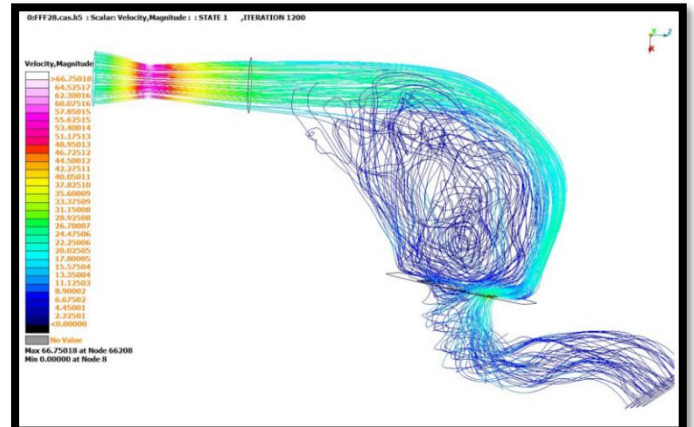
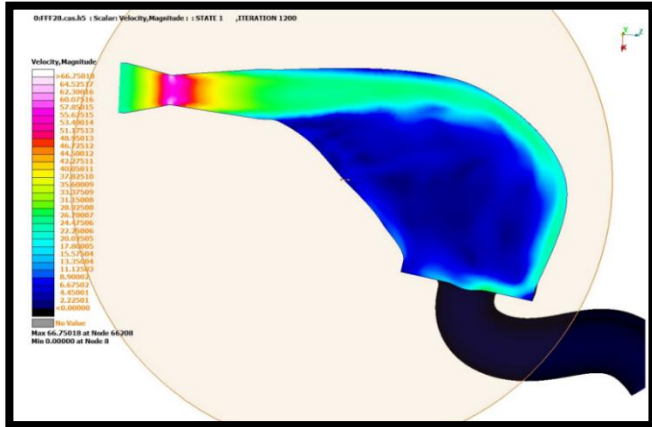


Figure 85 Velocity Diagram for Final Intake on a Selected Plane (Left) and with Flow Line Visualization (Right)

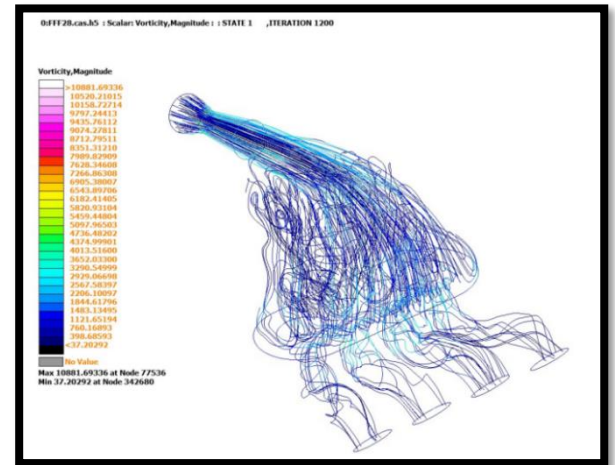
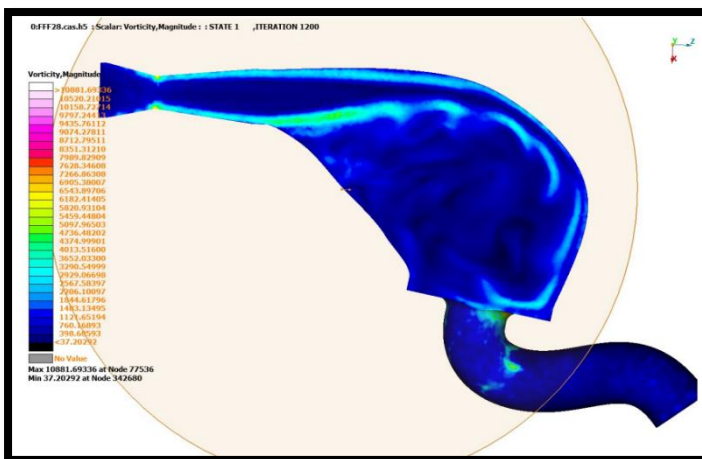


Figure 84 Vorticity Diagram for Final Intake on a Selected Plane (Left) and with Flow Line Visualization (Right)

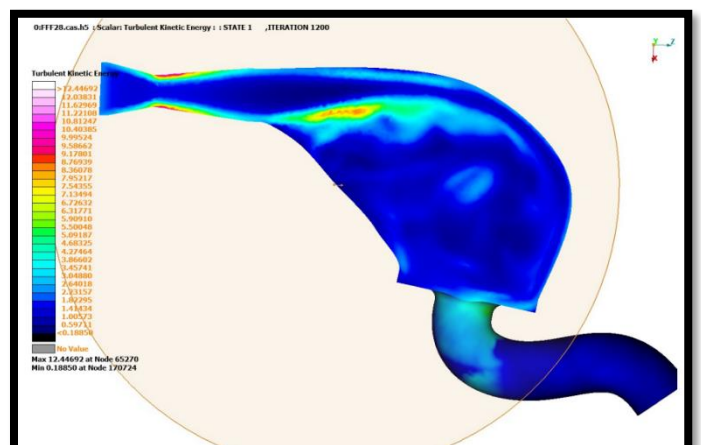
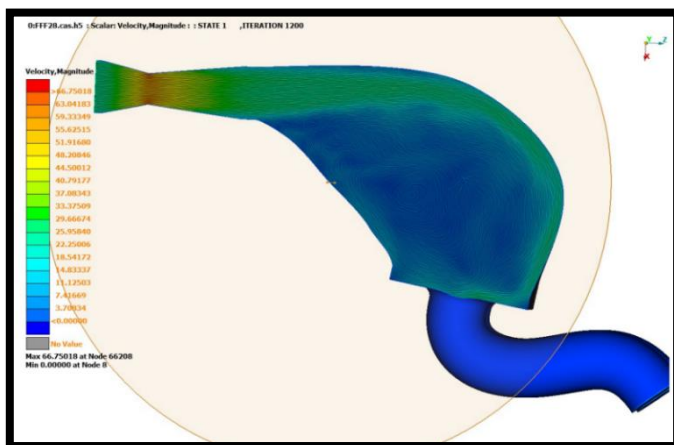


Figure 83 Velocity Magnitude Diagram for Final Intake on a Selected Plane (Left) and Turbulent Kinetic Energy on a Selected Plane (Right)



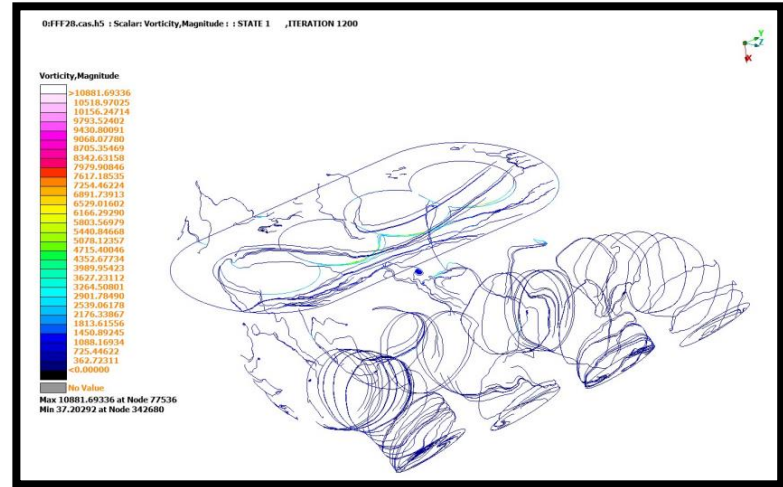


Figure 86 Total Pressure on a Selected Plane (Left) and Vorticity Magnitude with Flow Line Visualization (Right)

The final plenum shape was further analyzed with the help of the post analysis data from the above diagrams. From the velocity figures, it looks like the shape is tangentially directing the flow into the runners whilst maintaining a decent amount of its velocity. The mid part of the plenum has the lowest velocity values and from the streamline diagram the lines follow an uneven pattern. The pressure distribution also seems to be fairly even through the plenum and runners whilst staying close to environmental pressure values. Vorticity and turbulent kinetic energy diagrams further confirm the anticipated air behavior in the intake assembly. Points of interest are the connection between plenum and restrictor where the air flow detachment happens and air vortexes are created. More specifically, the vorticity figure illustrates the recycling of the flow that it was mentioned before at the design phase of the intake. The connection between the plenum also looks to present relatively higher turbulent kinetic energy values due to the abrupt change of direction. The dissipation rate also makes the energy losses seem even more apparent at the points mentioned above. Finally, the vorticity magnitude figure illustrates that each runner experiences varying swirl frequencies. Swirl helps to promote rapid combustion by aiding fuel mixing in the combustion chamber. Most notably, cylinders 1 and 3 appear to have more intense vorticity compared to the others. This may have to do with the tangential flow of the air through the plenum. The air volume throughout the 4 runners was almost identical which means that the evenly distributed flow was achieved.

## 10. Manufacturing, FEA Analysis and vehicle placement

### 10.1. Manufacturing Method

Having made the ideal design into the 3D software and having optimized it with the help of the CFD software, the team had to decide upon the manufacturing method of the parts. It quickly became obvious that in order to manufacture such complicated design with the help of traditional methods would be almost impossible or very expensive. The solution to these problems seemed to be 3D printing, a relatively new and already widespread method of manufacturing. The primary advantages of selecting 3D printing are a reduced manufacturing time and a greater freedom of geometry. Having almost limitless geometry boundaries, allows for the creation of shapes that reduce pressure losses through the system guided by the CFD analysis results and 1D simulation. This will allow for a system with higher

volumetric efficiency, giving increased power and efficiency. It also enables the production of a system which meets stress and deflection goals for the least mass possible by using FEA to guide structural design, increasing the performance of the car by decreasing mass that sits higher in the vehicle. It is also time efficient compared to a more conventional fabricated intake because a lot of man-hours from manufacturing are saved. These are man-hours that can be spent on further designs and improvements to the system, or on further testing and calibration once it is received. The freedom of geometry attainable with 3D printing is also possible to achieve with a composite intake, but the tooling cost, material cost and additional hours of manufacturing time make the method financially and practically unviable.

Although there are many advantages to 3D printing the intake system, there are disadvantages that must be considered as well. First and foremost is the manufacturing cost. The high price of 3D printing materials and equipment for manufacturing a large object such as the intake system cannot be ignored and affects heavily the team's resources. Moreover, because of the geometrical freedom offered by the method, a far greater amount of time must be spent on the design of the system to utilize fully its potential. This requires learning and utilizing complex surfacing techniques in CAD, ensuring that the CAD is perfect and mates up with everything perfectly, because the system cannot be test fitted and checked during the manufacturing process in the same way that a conventionally fabricated system could be. FEA simulations must be setup and run to guide the structure of the system, to ensure that the mass is kept to a minimum, and CFD analysis should also be used to guide the internal geometry of the system. All of the above result in a much more complex and demanding design process than a traditional system. The repairability of the system is decreased too, as a major failure cannot have a quickly solution manufactured using simple hand tools or a welder. Moreover, a failure at the competition without any extra parts could prove devastating for the team's goals throughout the competition.

Overall, the advantages of the 3D printing method were considered to be of higher importance to the team taking into consideration the tight manufacturing time constraints and limited human resources available as well. The potential performance increase and reduced manufacturing time seemed to be worthy of the increased complexity of design and decreased repairability.

## 10.2. Material Choice

With 3D printing as the chosen method, the 3D printing technique must also be decided on. Many types of 3D printing are available, each one with their own advantages and disadvantages. Viable options considered for the manufacture of the intake were Fused Deposition Modelling (FDM), Stereolithography (SLA) and Selective Laser Sintering (SLS). FDM printing uses the extrusion of a melted filament to build a part, with the printhead and extrusion nozzle moving in the X and Y direction, and the print bed moving in Z. SLA printing utilizes a resin bath, which is cured layer-by-layer using UV light. SLS utilizes a 'powder bed' in which the raw material is kept. SLS printing sinters the material together using a laser beam. The figures below illustrate the differences between each printing method. In the graphic representation below the SLA method is at the top left, SLS at the top right and FDM at the bottom.

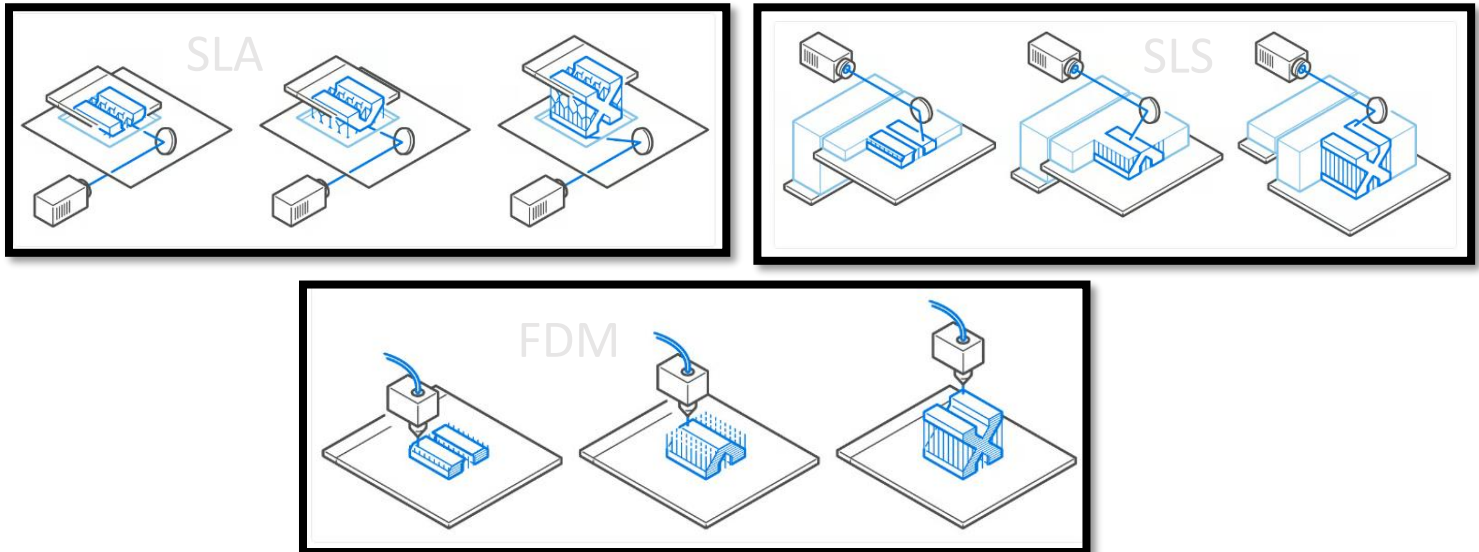


Figure 87 Different 3D Printing Methods Available for the Intake Assembly

One undesirable trait of 3D printed materials is that almost all of them have some level of anisotropy. This is due to the way that they are manufactured, which is one layer at a time. This manufacturing process results in less effective bonding between print layers. Hence, the mechanical properties, such as tensile strength, Young's Modulus and elongation at break of the printed product are often worse in the print (Z) direction than in the print plane (X&Y). FDM printed materials are affected most heavily by this, and hence are generally not recommended to be used in structural applications. SLS and SLA also display some anisotropic properties, but to a lesser degree. These must be compensated for in some way during the structural analysis of the system, to ensure that its strength is not over-estimated. A more isotropic material is hence ideal for the intake system, where stresses are applied in all directions and print orientation is assumed to be unknown.

Another consideration is the way that the part is printed and whether the geometry involves overhangs. Methods that create free-standing parts, such as FDM and SLA, require support structure to be printed to support the part during the printing process. This structure then must be removed after the print and is often time consuming and difficult. It also effects the surface quality. Methods that utilize a powder bed, such as SLS, do not require a support structure because the un-sintered powder provides support for the part and is simply blown out of the finished product.

Due to the intake system comprising of very large and enclosed volumes, printing without support structure will reduce post processing time and increase surface quality. SLA printed parts, as well as requiring support structure, tend to be quite brittle and are also not recommended for structural applications. This then meant that the ideal printing method of choice was the SLS. With SLS printing as the chosen method, the next consideration made was for material type. Due to the requirements of the intake system including interfacing with the engine and delivering the air/fuel mixture to the combustion chamber, the material must have a high temperature resistance and must be chemically stable in 98RON and E85 fuels. The material must also have a high specific stiffness and specific strength, to assist with keeping the part as light as possible. However, the partner of the team during that time was dealing with technical issues in their SLS printers. That meant that a solution with similar capabilities had to be found. After some thorough

conversations, some test samples were decided to be made with the FDM method using a new material with promising technical capabilities. The material was called PAHTCF15 (Polyamide High Temperature with 15% Carbon Fiber). With this formulation, it brings more dimensional stability and allows to work under 150°C continuous temperatures with a peak temperature of 180°C in comparison to a standard PA. 15% carbon fiber reinforcement makes it stiffer thus making it a great choice for demanding applications such as the intake assembly. The figure below shows its mechanical properties in detail.

Mechanical Properties   Conditioned specimens				
Print direction	Standard	XY	XZ	ZX
		Flat	On its edge	Upright
Tensile strength	ISO 527	62.9 MPa / 9.1 ksi	-	19.1 MPa / 2.8 ksi
Elongation at Break	ISO 527	2.9 %	-	0.8 %
Young's Modulus	ISO 527	5052 MPa / 733 ksi	-	2455 MPa / 356 ksi
Flexural Strength	ISO 178	125.1 MPa / 18.1 ksi	121.9 MPa / 17.7 ksi	56.0 MPa / 8.1 ksi
Flexural Modulus	ISO 178	6063 MPa / 879 ksi	6260 MPa / 908 ksi	2190 MPa / 318 ksi
Flexural Strain at Break	ISO 178	No break	3.6 %	4.0 %
Impact Strength Charpy (notched)	ISO 179-2	5.1 kJ/m <sup>2</sup>	5.3 kJ/m <sup>2</sup>	1.6 kJ/m <sup>2</sup>
Impact Strength Charpy (unnotched)	ISO 179-2	21.9 kJ/m <sup>2</sup>	20.4 kJ/m <sup>2</sup>	2.8 kJ/m <sup>2</sup>
Impact Strength Izod (notched)	ISO 180	6.5 kJ/m <sup>2</sup>	5.8 kJ/m <sup>2</sup>	-
Impact Strength Izod (unnotched)	ISO 180	16.3 kJ/m <sup>2</sup>	15.1 kJ/m <sup>2</sup>	4.1 kJ/m <sup>2</sup>

Figure 88 Mechanical Properties for PAHTCF15 Material

Looking at the mechanical properties, the team seemed intrigued to test the capabilities of this material until the SLS printers were operational. It would also make up for a good comparison between the two printing methods and the final products. The team was also ensured by the partner for top quality results. In order to ensure its fuel resistance and chemical reaction the team performed a series of tests. 4 small rectangular test pieces were printed from the same material. These pieces were then weighed and split up into 4 separate tests. The first one remained as it was printed and it was kept at a dry place with no humidity. The other 3 were submerged in 98RON gasoline for 3 different time durations. The time durations were 12, 24 and 48 hours. After each time mark was reached, the pieces were transferred in the same storage space as the first non-submerged part until the 48 hours passed. At that point, all the pieces were gathered, weighed again to write down the difference and the test began. Each piece was carefully placed on a clamp as it is shown in the figures below. Then, gradually the clamp was closed until each piece reached the breaking point. The pieces were placed next to each other and the results were assessed. As it can be seen again from the figures below, the piece that stayed outside of the fuel presented the least amount of deformation with a small difference however to the one that stayed 12 hours submerged. The 24-hour piece showed the most permanent deformation whilst the 48 hour was split into two parts and it is not included in the figure. The dry piece also presented the biggest amount of resistance to each change in dimensions.



*Figure 89 Process of Assessing the PAHTCF15 Material with the Help of Test Pieces*

Having assessed the results of the test, some questions arose relative to the materials capabilities to withstand the fuel that would be constantly sprayed from the injectors inside the cylinders and on the inside surface of the runners. The most worrying part of the test was that the 48-hour piece broke almost instantly and keeping in mind the long test period and the difficulties of constantly drying that part of the intake to prevent it from braking was a serious issue. The test however had the test pieces fully and constantly submerged, conditions which would never correspond to the real operation and were considered extreme. Hence, the printing of the intake began with the PAHTCF15.

With the printed parts getting delivered the results did not look promising. The figures below illustrate the problems that were observed. Layer detaching was noticed in every part that was printed. The phenomenon is much more visible from the side view on the upper gasket. The red circles indicate the particular point where the layers did not join properly, causing the flange to get inclined and displaced inwards. This point is quite critical as a screw passes through it and is secured with a nut on this flange. At the same time, the printed plenum was checked using a vacuum pump in order to simulate the existence of vacuum internally. What was observed, after it was properly sealed between the two flanges, is that the plenum could not hold vacuum internally but communicated with the atmospheric air through small holes that could not be perceived by the eye that were located on the outside curvature. These holes appear to have been created by discontinuities in the print or by insufficient joining of the different layers. As a solution to this problem, the team considered to get externally coated with a special high-temperature resin all the printed parts.

The team was also quite concerned about the quality of the internal surface of the runners. The relevant photo below shows in more detail the quality of the print at the main air entry point. Especially at that point of radii the smoothest possible surface was needed as it is the main entry point. At the runner flange, the different layers seem to be offset to each other making a stairs effect. A change in table orientation with less inclination was believed that may eliminate the steps at the base. Finally, regarding the plenum, it was observed that all flat surfaces had the best quality and were easily manageable. However, the inner surface had similar problems to those in the runner's photo mentioned earlier. Again, orientation problems seemed to have affected this part as well.

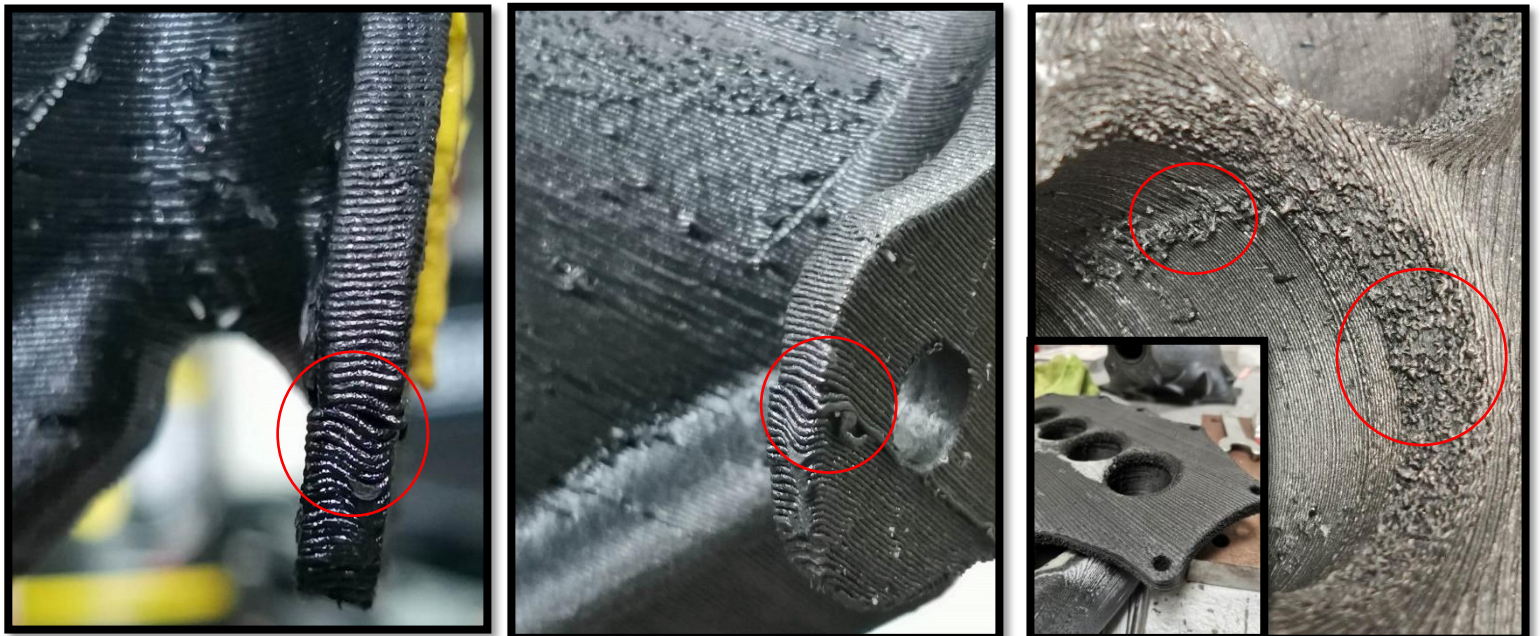


*Figure 90 Issues of PAHTCF15 Components After Printing*

After all the observations and having assessed the final FDM printed parts, it was clear that the surface quality and the severity of the problems that arose was too much for the team to handle. The scenario of an FDM printed intake was then almost instantly abandoned and the team turned towards SLS materials to find a solution which could take immediate effect. Through this process however several design changes were made that enhanced the final design and made it more printable and manageable. Other improvements were made to the curves and general geometries of the two components. Some minor changes were also made to improve printing without significantly changing the main curves.

With the necessary changes made, the SLS printing method was looked into in more detail. The material that was elected was the HP 3D High Reusability PA 12. Some of the advantages of the material regardless of the printing method itself were the excellent chemical resistant to oils and greases, the heavy engineering by the manufacture that makes the material production orientated as well as the watertight properties and robust thermoplastic properties. The mechanical properties of the material can be seen in the figure below.

Technical specifications <sup>8</sup>			
Category	Measurement	Value	Method
General properties	Powder melting point (DSC)	187 °C/369 °F	ASTM D3418
	Particle size	60 μm	ASTM D3451
	Bulk density of powder	0.425 g/cm <sup>3</sup>	ASTM D1895
	Density of parts	1.01 g/cm <sup>3</sup>	ASTM D792
Mechanical properties	Tensile strength, max load <sup>9</sup> , XY	48 MPa/6960 psi	ASTM D638
	Tensile strength, max load <sup>9</sup> , Z	48 MPa/6960 psi	ASTM D638
	Tensile modulus <sup>9</sup> , XY	1700 MPa/247 ksi	ASTM D638
	Tensile modulus <sup>9</sup> , Z	1800 MPa/261 ksi	ASTM D638
	Elongation at break <sup>9</sup> , XY	20%	ASTM D638
	Elongation at break <sup>9</sup> , Z	15%	ASTM D638
	Flexural strength (@ 5%) <sup>10</sup> , XY	65 MPa/9425 psi	ASTM D790
	Flexural strength (@ 5%) <sup>10</sup> , Z	70 MPa/10150 psi	ASTM D790
	Flexural modulus <sup>10</sup> , XY	1730 MPa/251 ksi	ASTM D790
	Flexural modulus <sup>10</sup> , Z	1730 MPa/251 ksi	ASTM D790
	Izod impact notched (@ 3.2 mm, 23°C), XYZ	3.5 kJ/m <sup>2</sup>	ASTM D256 Test Method A
Thermal properties	Heat deflection temperature (@ 0.45 MPa, 66 psi), XY	175 °C/347 °F	ASTM D648 Test Method A
	Heat deflection temperature (@ 0.45 MPa, 66 psi), Z	175 °C/347 °F	ASTM D648 Test Method A
	Heat deflection temperature (@ 1.82 MPa, 264 psi), XY	95 °C/203 °F	ASTM D648 Test Method A
	Heat deflection temperature (@ 1.82 MPa, 264 psi), Z	106 °C/223 °F	ASTM D648 Test Method A
Recyclability	Refresh ratio for stable performance	20%	
Certifications	USP Class I-VI and US FDA guidance for Intact Skin Surface Devices, RoHS <sup>11</sup> , EU REACH, PAHS		

Figure 92 Mechanical Properties for PA12 Material

In a similar way to the FDM material, a similar test was held. This time the tensile strength of the pieces was tested in order to evaluate not the fuel resistance but whether a coat of resin was increasing the mechanical properties of the intake parts. The pieces were design based on the ASTM D638-14, Type IV standard in order to evaluate the results as scientifically as possible. 10 pieces were manufactured. From

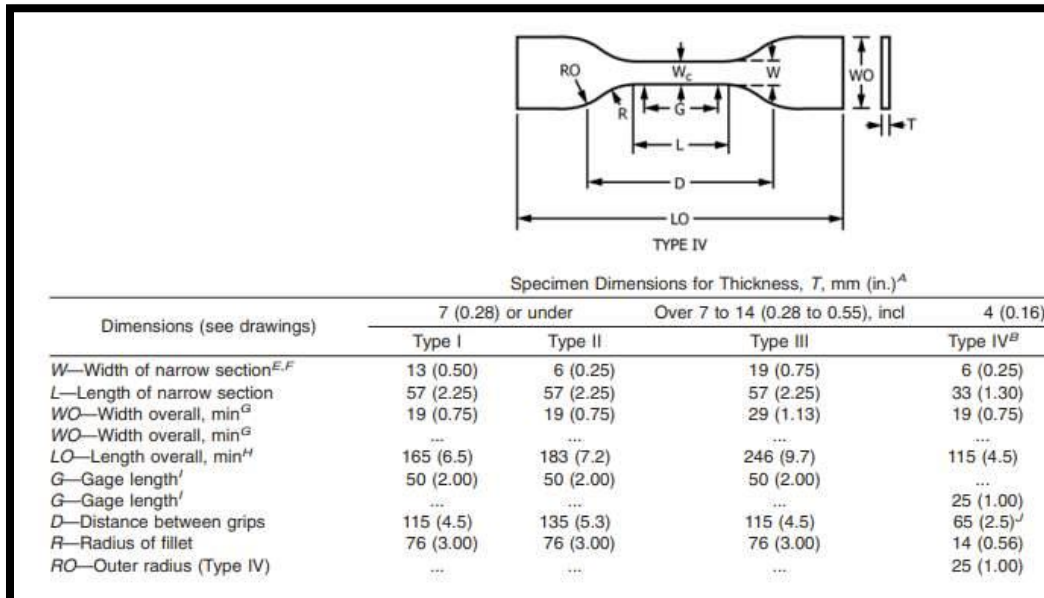


Figure 91 ASTM D638-14 Test Piece Dimensions

them, 5 were submerged into the resin and were put onto the tensile machine. The other 5 were put into the machine instantly after they were made. The resin-submerged parts were also kept at environmental conditions to dry before the test. The results of the tensile test showed similar behavior with minimal differences with the resin counterparts fairing much worse than the standard parts. Hence, the decision was made not to use the resin.

Another parameter that the team checked was the surface roughness. SLS printed parts have considerably higher roughness values than that of aluminum or carbon fiber. The surface finish of the HP PA12 was able to be significantly improved through sanding, after the parts were printed as part of the post processing of the parts. Moreover, it was found that the accuracy of the printing method was accurate enough for printed O-ring bores to work as expected with no post-machining required.

### 10.3. FEA Analysis

Before moving forward to the final manufacturing of the intake, a structural analysis had to be made in order to ensure the structural integrity of the assembly. Due to the limited time available in the design period, it was decided that a simplified FEA setup would be pursued, allowing more time for iteration and analysis. The SolidWorks program was utilized for the structural analysis. The printed portion of the intake system is mounted through ten different points. This includes two bolted connections to a soft mount to the chassis at the top flange of the restrictor and eight rubber boots connecting the intake runner to the inlet port of the engine. In the interest of time constraints, these were all modelled as fixed supports that likely over-simplified the model.

For meshing within SolidWorks, a solid, blended curvature-based mesh was used, as this combination can easily fit more complex geometry with fewer elements, facilitating faster simulations. The mesh was further refined around mounting points and any other areas of interest, with a general mesh sizing varying between 15 and 0.75. The final number of elements created was 319614. The figure on the right contains some further information regarding the meshing settings.

Study name	Static 1 (-Default)
Details\Mesh type	Solid Mesh
Mesher Used	Blended curvature-based mesh
Jacobian points for High quality mesh	16 points
Max Element Size	15 mm
Min Element Size	0.75 mm
Mesh quality	High
Total nodes	543757
Total elements	319614
Maximum Aspect Ratio	4,153.8
Percentage of elements with Aspect Ratio < 3	84.6
Percentage of elements with Aspect Ratio > 10	0.937
Percentage of distorted elements	0.000313
Number of distorted elements	1

Figure 93 Meshing Parameters for FEA Model

A custom material had to be created within the SolidWorks software before simulation could begin. The values were used from the HP datasheet and included a Tensile strength of 48MPa, a yield strength of 30 MPa and Young's Modulus of 2050 MPa. The Poisson's ratio used was 0.4, based on the Poisson's ratio of other SLS printed Nylon-12 materials. It was assumed that the generous safety factor and conservative approach to design would compensate for the anisotropy of the material and a relative and approximate result could be produced.

The boundary conditions for the structural analysis included the remote load which simulated the air filter weight on the intake and, the pressure inside the plenum which was retrieved from the Ricardo software



at the rpm where the highest vacuum was seen. This was done in order to approach with the simulation the most realistic scenario possible. Finally, a preliminary safety factor of 1.5 was targeted for the system. The conservativeness of the safety factor was a result of the uncertainties of implementing the SLS manufacturing method for the first time, and the simplifications made when setting up the model in SolidWorks. The figures below illustrate the equivalent stress, displacement and Safety Factor of the geometry.

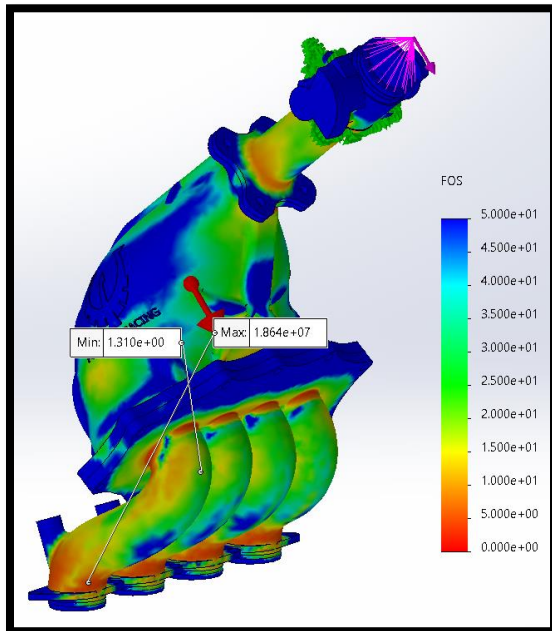


Figure 94 Factor of Safety Visualization on Intake Assembly

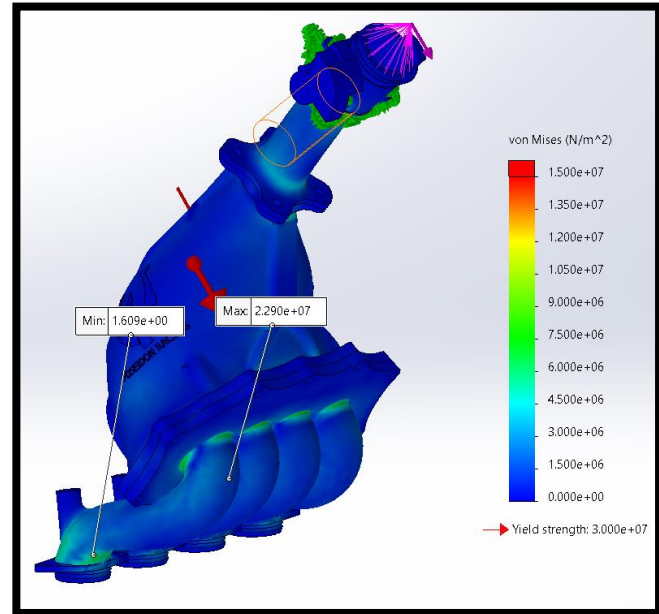


Figure 95 Equivalent Stress Visualization on Intake Assembly

Looking into the stress diagram, the maximum stress value of 22Mpa was considered to be acceptable. However, due to the anisotropic behavior of the material the team wanted to incorporate as many ways as possible to ensure a robust assembly. Hence, to add stiffness to the structure, ribs throughout the plenum were implemented. The overall thickness of the plenum was also increased by 2mm. This would add weight to the whole assembly, but through simulations the mounting points seemed more than adequate to tolerate the extra weight. Worth noting is that while the results suggest a lot more refinement is still available, due to a lack of trust in the accuracy of the simulation due to highly simplified and likely inaccurate material and model setups, this was chosen as the finishing point of the simulation.

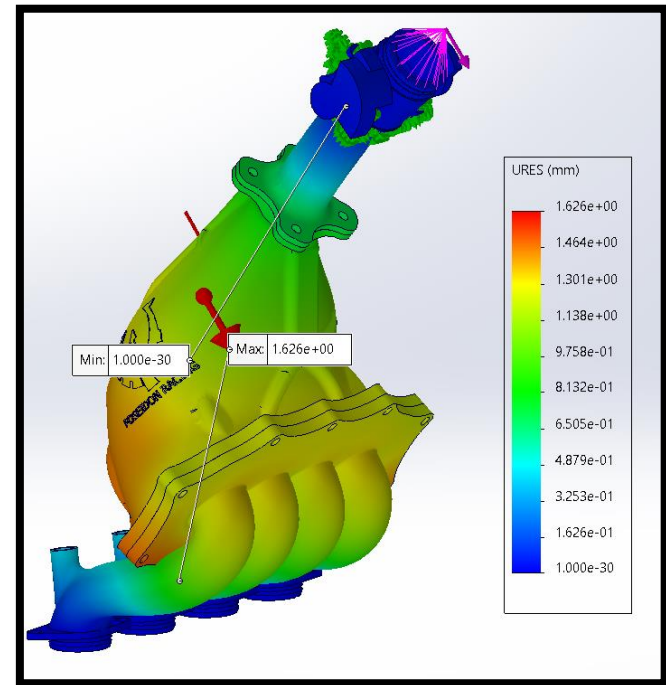


Figure 96 Deformation Visualization on Intake Assembly

#### 10.4. Final Assembly and First Tests

After the manufacturing phase was concluded and decided upon, the final assembly was ready to be produced. In the figure below the whole assembly of the intake can be seen in the 3D design program Inventor.

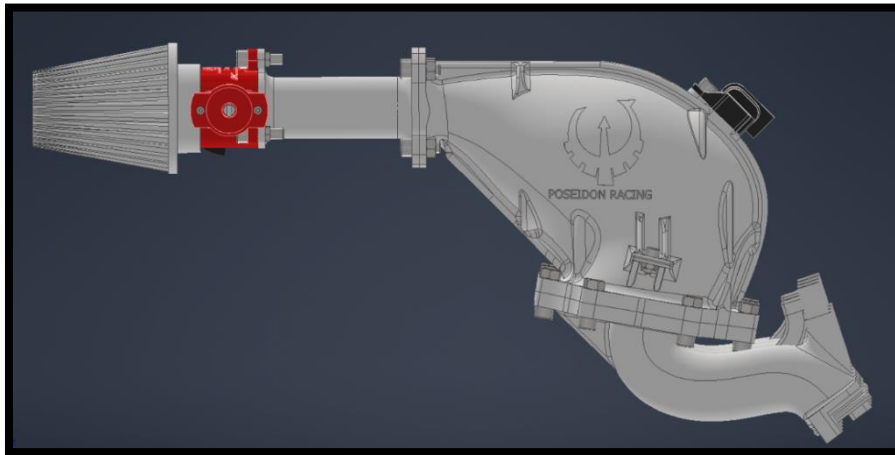


Figure 97 Final Intake Assembly in Cad Software

The final assembly includes the air filter, throttle-body subassembly, restrictor, plenum, runners, O-rings, fuel injectors, MAP Sensor and every nut and bolt the system utilizes. The 3D-printed parts were redesigned before the final assembly due to tolerance issues mainly around the bolt holes, O-ring grooves and sensor base fitting in order to achieve the best possible fitment and achieve an airtight package. After the final parts were completed, the files were transferred to the team's partner, 3D-Hub for printing. The figures below showcase the final products during the post processing of the parts and their placement on the test bench made by the team during the testing phase before they were installed onto the race car. More particularly, the ribs can be identified from the bottom figures with the middle part being the thickest



Figure 98 Post Processing and Testing of Final Manufactured Assembly on Engine

out of them all splitting the plenum into two sections. All the flanges from all the parts were printed excellently having a relatively smooth surface and inspiring confidence for their rigidity and uniformity. In addition to that a lot of detail has been spent in the “runners” part redesign. This part was decided to host the fuel rail supports for the vehicle. Careful measurement and design of the part was carried out in order to come as close as possible to the manufacturer’s dimensions. This was a very crucial goal for the team because no modifications were made to the engine apart from the runners. The injectors themselves remained unchanged and the team attempted to keep every dimension of the injector’s placement as close to the stock engine as possible in order not to intervene with the fuel spray allocation during operation. To achieve this goal, careful dimensioning was needed when designing the base placement. With the help of the SLS 3D-printing method all the dimensions and annotations needed were managed to be achieved and the final product operated accordingly and the fitment with the rubber hoses of the throttle body was the one that the team anticipated. All the bolts of the assembly were placed and were torqued down with care in order to achieve the airtightness that the team was aiming for without damaging the surface of the part. Regarding the plenum part, the surface quality and annotations were in the same level as already mentioned. A problem however later arose at the testing phase when the intake was placed onto the engine test-bench. It was noticed by team-members that when the throttle was valve changed position rapidly, went from fully open to fully closed conditions, the plenum part seemed to inflate. Most notably at the bottom section near the ribs and the main flange. This inflation was fairly worrying for the team especially when the conditions at the competition demanded several abrupt changes of the throttle valve for a long amount of time. In order to overcome the Vacuum effect issue, a new outer cell design was implemented to the plenum to further strengthen the rigidity of the part. The pattern that was placed in the outside surface can be seen in the figure next to this paragraph.

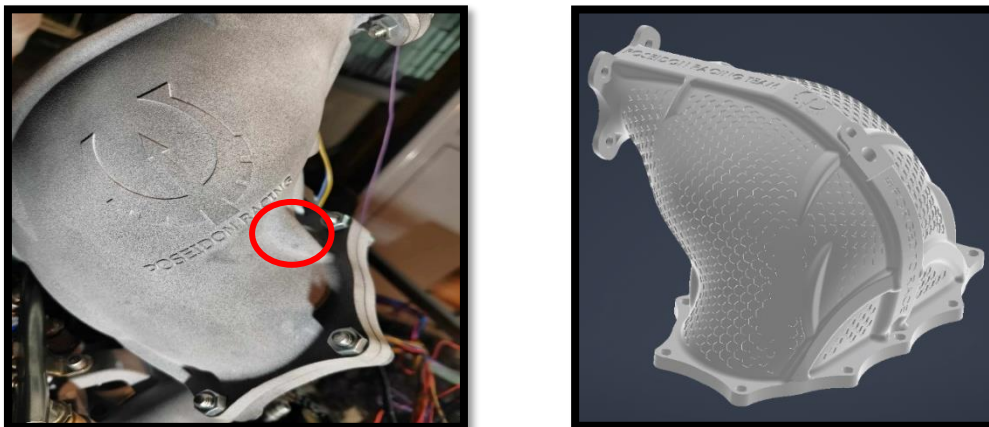


*Figure 99 Plenum Redesign on Cad Software and Issue Area*

## 11. Results

### 11.1. Competition Results

Poseidon Racing Team participated in Formula Student East with the final manufactured vehicle named “Orion - PR23”. The team managed to deal with the strict process of scrutineering and with all the difficulties that came up and claimed the 10th position in the overall standings whilst claiming 5th place

at the endurance event. More specifically, the team performed better at the static events. It managed to get 11<sup>th</sup> place at the Business Plan, 10<sup>th</sup> at Cost and Manufacturing, 6<sup>th</sup> at Design Event which justifies the 7<sup>th</sup> Static place Overall. In the Dynamic events did not fare as well. The car managed a 12<sup>th</sup> place at acceleration completing the 75m in 6.3sec from stop and finishing with a speed of 78Km/h. The Skid Pad and Autocross event were not managed to be completed whilst the Endurance gave the best finishing result of 5<sup>th</sup> place. The Dynamic Overall place was 11<sup>th</sup> which combined with the Static Overall gave the 10<sup>th</sup> Final position for the whole competition.

In the Design Event the Sub-Team managed to achieve a score 16/20 for the Understanding of the Concept, the Design and Concept itself, the Manufacturing & Assembly and finally the Validation and Refinement. The Sub-Team was praised for its goal setting method and the goals themselves, the understanding for all the systems the Design and Concept process for the whole intake, its manufacturing and assembly as well as the validation and calibration efforts. The lack of A Dyno test and the lack of some documentation to support the presentation were the only drawbacks for the Design Event.

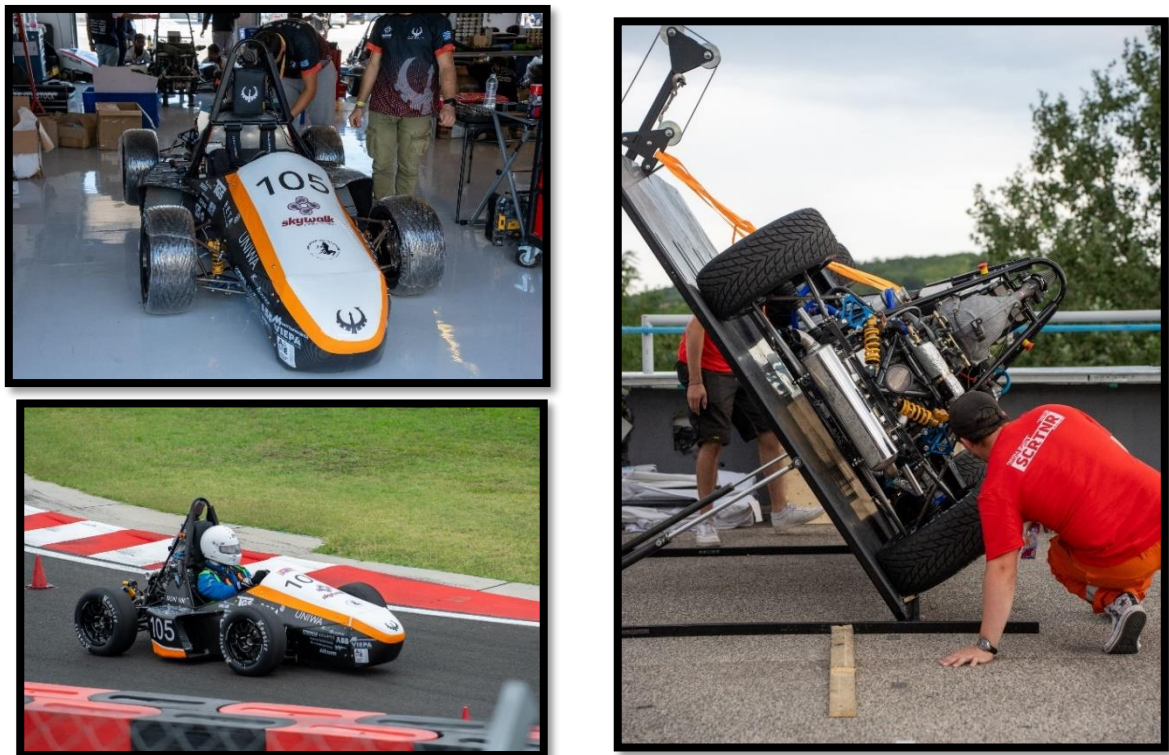


Figure 100 The PR-23 Race car During the Dynamic and Static Events of the Competition

## 11.2. Acknowledgments – Comments

The aftermath of the competition was a successful first year with lots of positive feedback not only for the Intake assembly that this thesis was mainly focused around but for the whole vehicle and the team. Hard work, proper goal assessment, time and resources management, good engineering practices formed the basic idea for the team's first try at making a fast FSAE race car. There are still plenty of points to fix however

in order to make the car even faster and the team better prepared for the next one. Regarding the Intake and Engine assembly there are several points where the car could be improved or can be changed to enhance the performance of the vehicle. Firstly, is the validation process. As it was mentioned several times, the team even though prepared to use a hydraulic dyno for data validation did not manage to do so due to time constrains. Testing the car in real time and under different loads with different gears could make the car better optimized for the track and the conditions it had to face. It would also aid the ECU-Tuning which in this years' case, was made onto the test bench without load until the engine was placed onto the car and only then Engine tuning begun under real circumstances. Fuel mapping, proper throttle valve position, idle rpms and redline were all elected after lots of hours of driving. The dyno would make everything easier and more convenient. In the end a dyno run was carried out with the help of one of the team's sponsors, GEARTECH Engineering after the competition had ended. All the forementioned issues were dealt with and critical changes were made including a correction in valve timing. Proper tuning for every gear was also carried out and a final power and torque diagram was able to be produced.

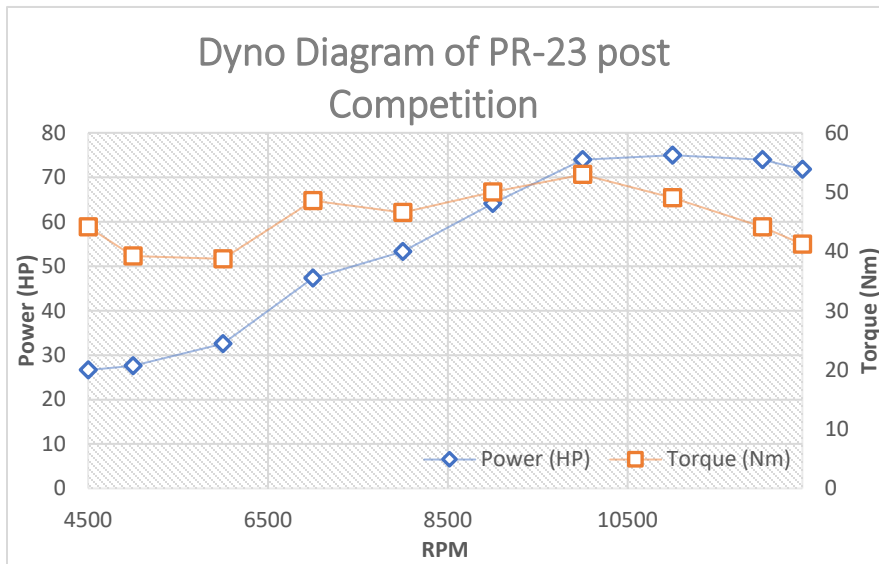


Figure 101 Dyno Diagram for PR-23 Post Competition

The dyno run for the car was carried out using a load bearing dyno. This type of dyno uses a load application mechanism to the engine which is fully controlled either via an electric motor (eddy current) or hydraulically with oil. In this type of dyno, the driven wheels are removed and therefore it is normal to give back slightly higher horsepower values. Since no further information is available regarding the diagram in figure 49, no direct comparison can be made in order to assess the modifications done to the vehicle. Just by observing the two diagrams' similarities can be found in their behavior with the diagram in figure 101 showing smaller values and losing power and torque after the 10000-rpm mark. Evaluating the dyno diagram on its own the car seems to show a relatively steady torque curve around the 7500-rpm value with the power increasing significantly as the rpms increase. The final peak produced values for power and torque are 75 HP at 11000rpm and 53Nm at 10000rpm respectively.

Another important aspect of the car's performance was the exhaust muffler. The original choice of muffler was not rules compliant and it had to be changed a long way along the tuning phase of the engine. This meant that all the tuning specifications and settings had to be changed or adjusted to this single change in order to make the car drivable again and compliant with the maximum decibel value. In essence, with the muffler change made the car could compete but the performance was heavily affected hence the relatively high values for the acceleration event. After the competition the muffler was replaced with the original one and the car was instantly better in performance.

At the dynamic events, with either exhaust mufflers installed, it was noticed by the drivers that the car was slow to react at the throttle pedal change. That meant that whenever the driver wanted to fully accelerate the engine was slow to respond hence making the car unpredictable and relatively difficult to drive out of slow speed corners. In the high-speed corners, the car fared much better with the torque being plenty when the car was already above a certain number of rpms. This can be evaluated in two ways.

One solution could be to further lower the point of peak torque in the diagram. This could help in low-speed corners. Another change could be to make an even smaller plenum that could fit in the given space. The team already knew that due to packaging the best solution for the car with the Ricardo data was not installed. Some modifications could also be made in the engine itself. Some racing camshafts could enhance the valve timing and extend the valve overlap hence extracting more power out of the engine which as mentioned before was kept stock to prevent any reliability issues.

Some further modifications could also be made in the model of the 1D program. The aim of the volumetric efficiency that exceeded the value of 1 could not be achieved. Perhaps with further testing and with a much more detailed model more potential of the engine can be extracted. Another possibility for the team is to further enhance the flow model with simulating the piston movement and inserting the engine data in a solver such as the ANSYS IC simulation.

One of the largest concerns with the intake concept was reliability. With plenty km of racing completed so far, Orion's intake system has performed reliably and without issue, confirming the viability of using SLS printed components.

Finally, it should be mentioned that all the diagrams produced by the Ricardo model display a different behavior compared to the one anticipated. Mainly, the power diagram in figure 61 displays a better performance in higher rpms for longer length runners whilst the shorter runners appear to be the best solution for lower rpms. This data does not fully correspond with most papers regarding intake manifolds for FSAE vehicles however the dyno data after the competition proved that most problems mentioned before were not mainly caused by mistakes in intake dimensioning but rather in the exhaust modifications and other inconveniences that were produced from other mechanical components. The Intake assembly showed potential and can be further improved upon for the next year's competition.

## 12. Appendix

### 12.1. Ricardo Diagrams

Below, all the data diagrams can be seen from the Ricardo software for every value of plenum volume and for each runner length.

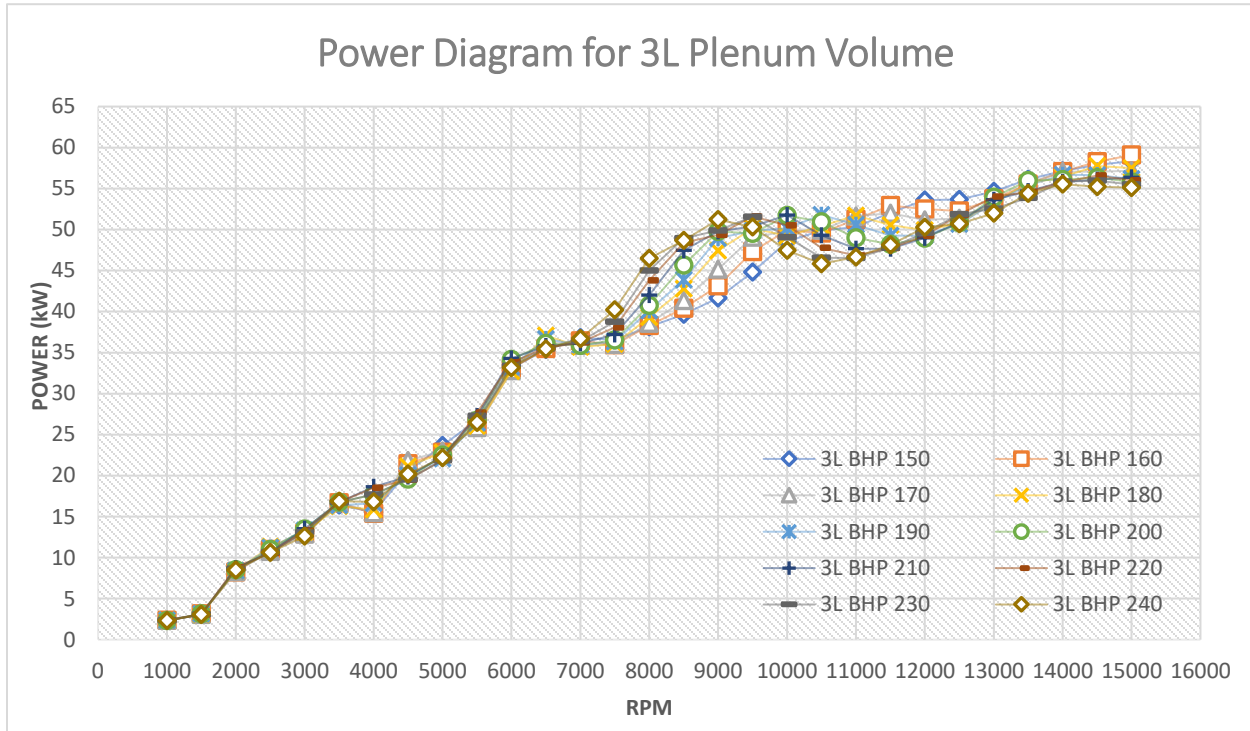


Figure 103 Power Diagram for 3L Plenum and Different Length Runners. The last number refers to the length of the tested runner in mm.

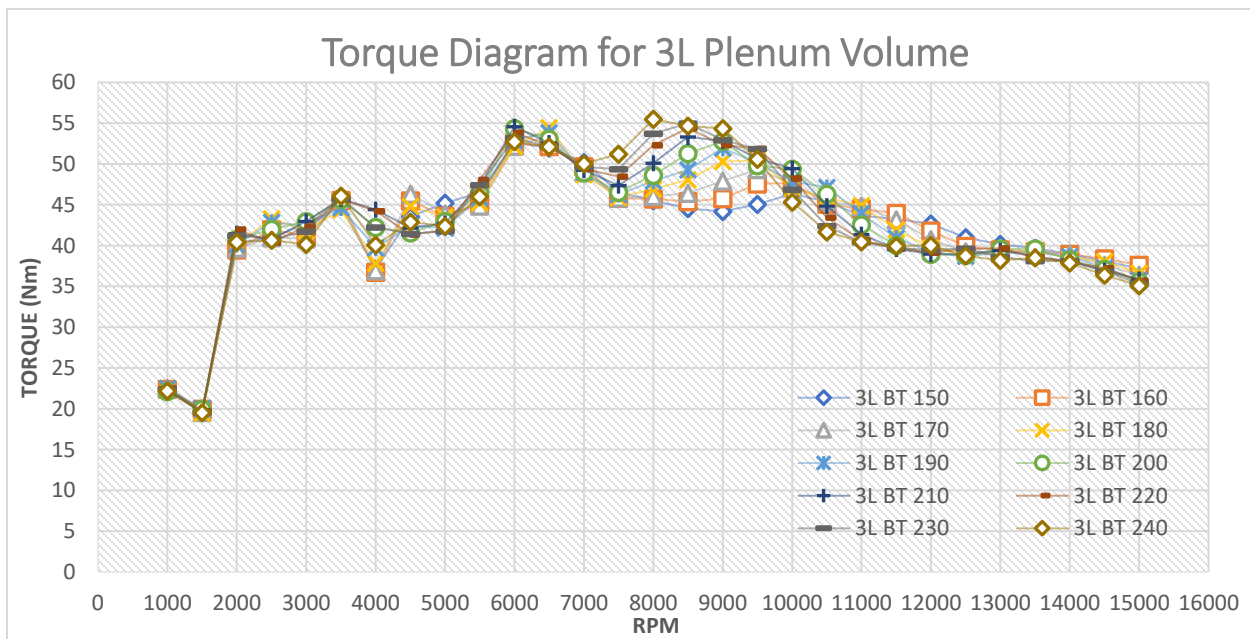


Figure 102 Torque Diagram for 3L Plenum and Different Length Runners. The last number refers to the length of the tested runner in mm.

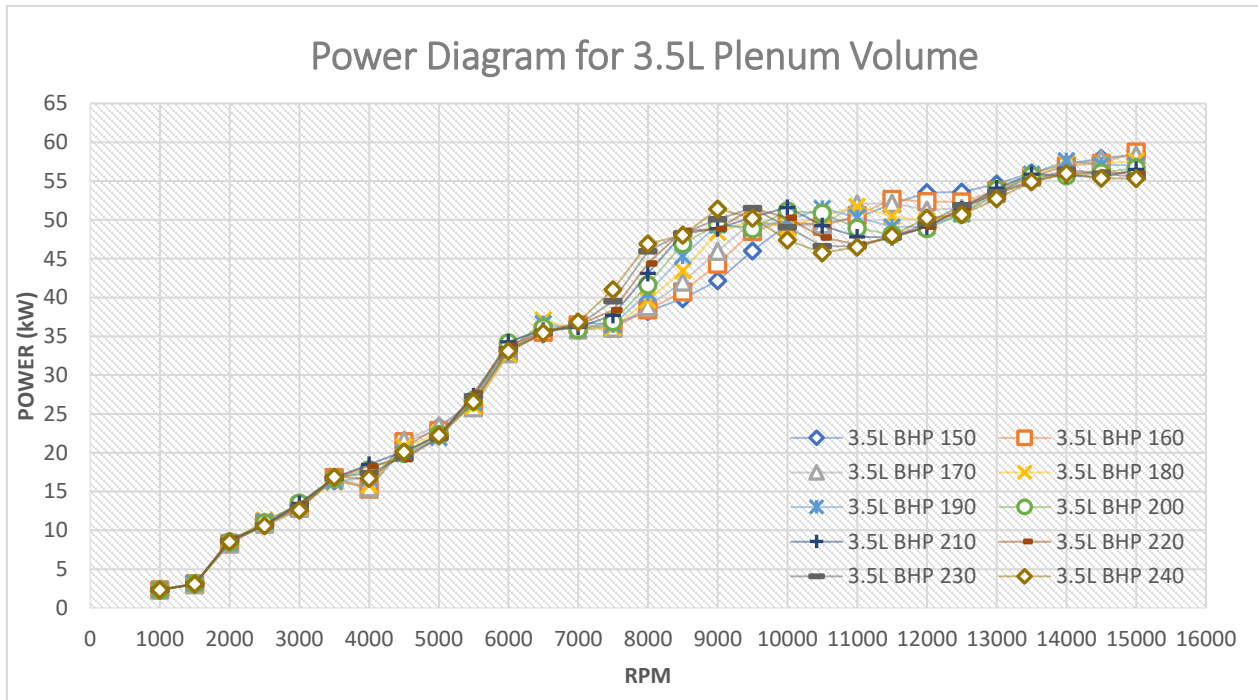


Figure 104 Power Diagram for 3.5L Plenum and Different Length Runners. The last number refers to the length of the tested runner in mm.

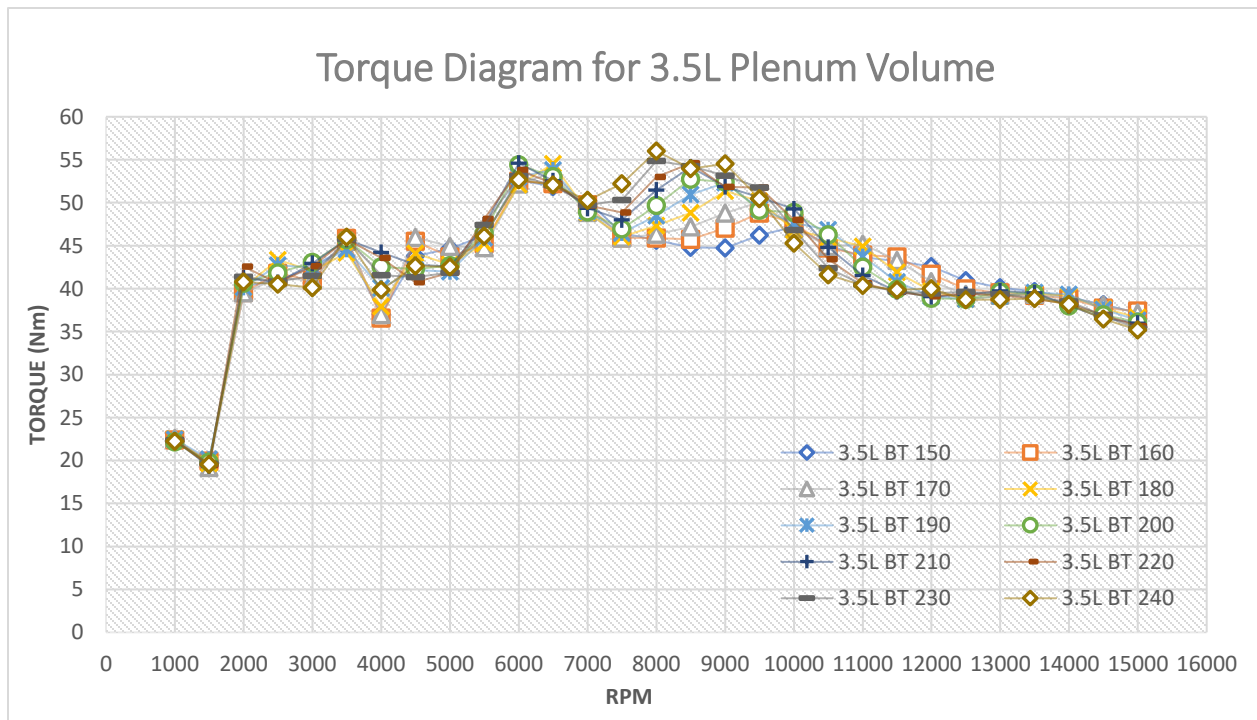


Figure 105 Torque Diagram for 3.5L Plenum and Different Length Runners. The last number refers to the length of the tested runner in mm.



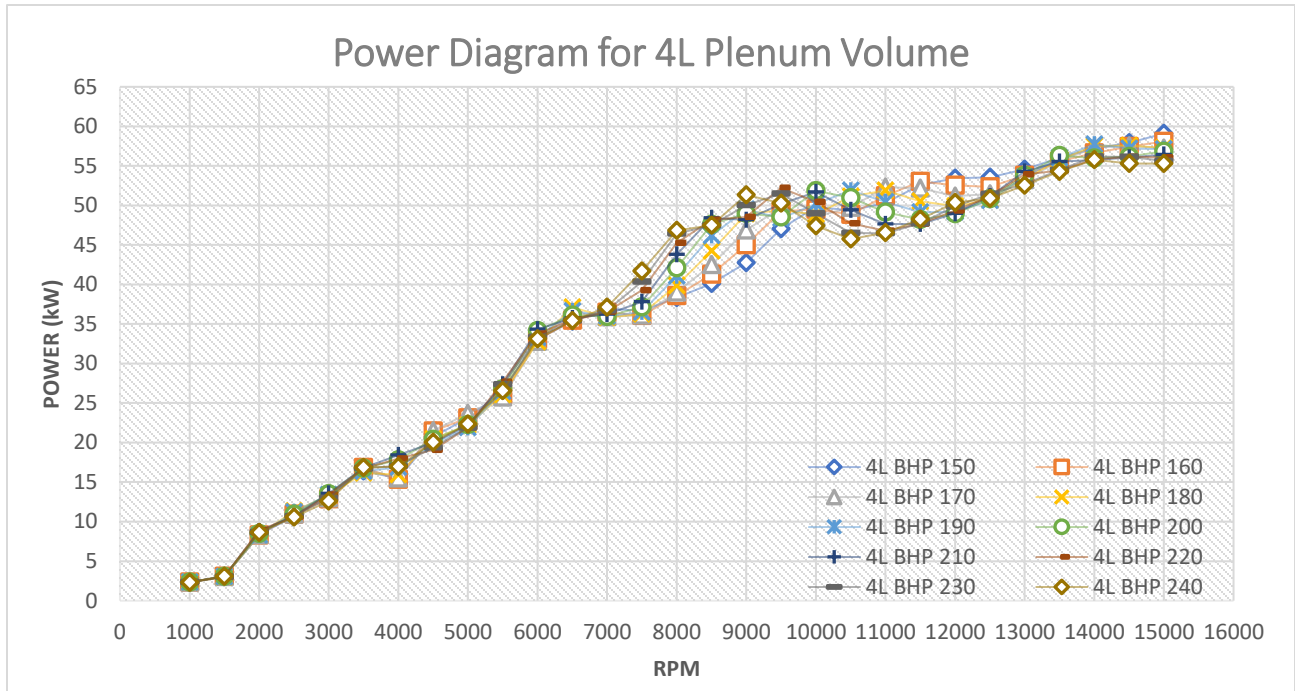


Figure 106 Power Diagram for 4L Plenum and Different Length Runners. The last number refers to the length of the tested runner in mm.

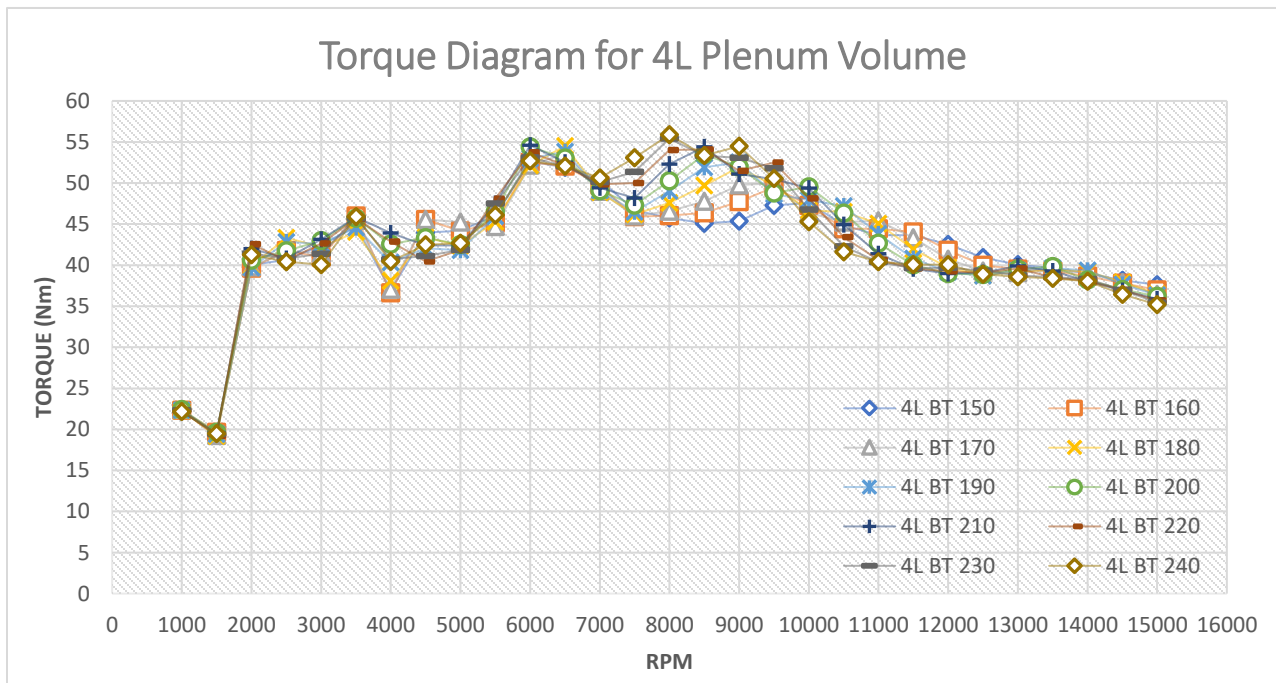


Figure 107 Torque Diagram for 4L Plenum and Different Length Runners. The last number refers to the length of the tested runner in mm.

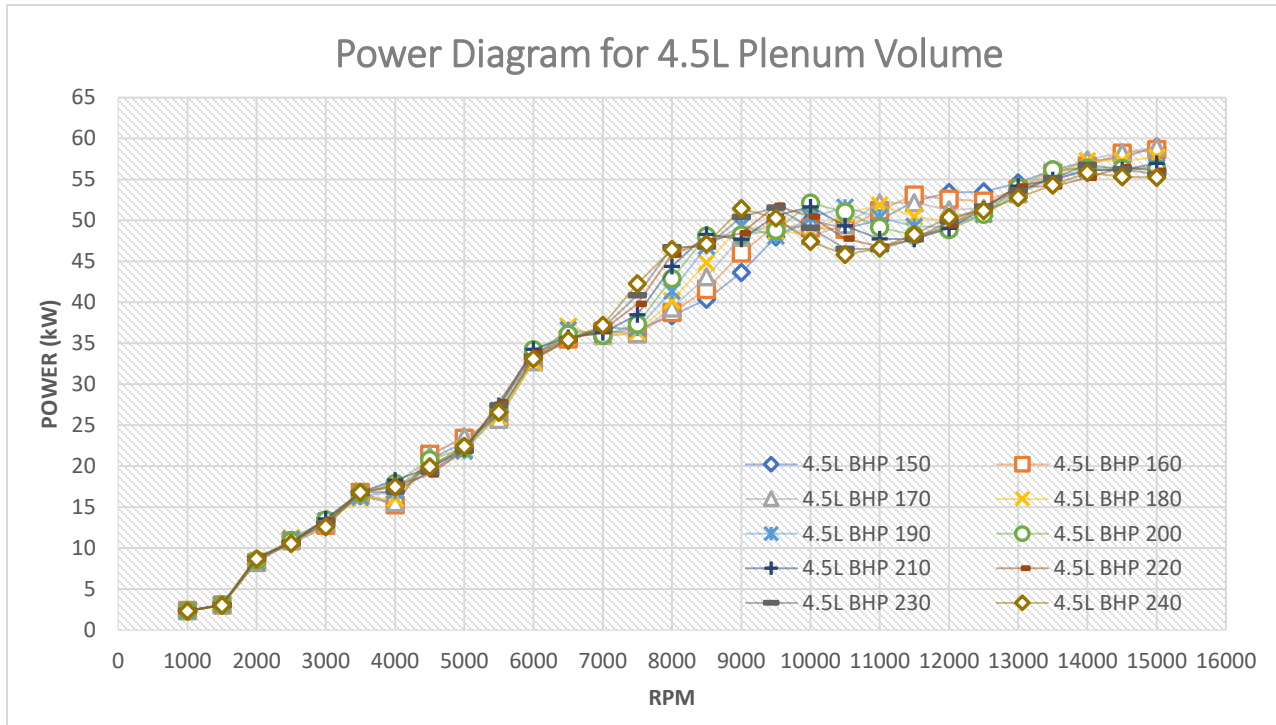


Figure 108 Power Diagram for 4.5L Plenum and Different Length Runners. The last number refers to the length of the tested runner in mm.

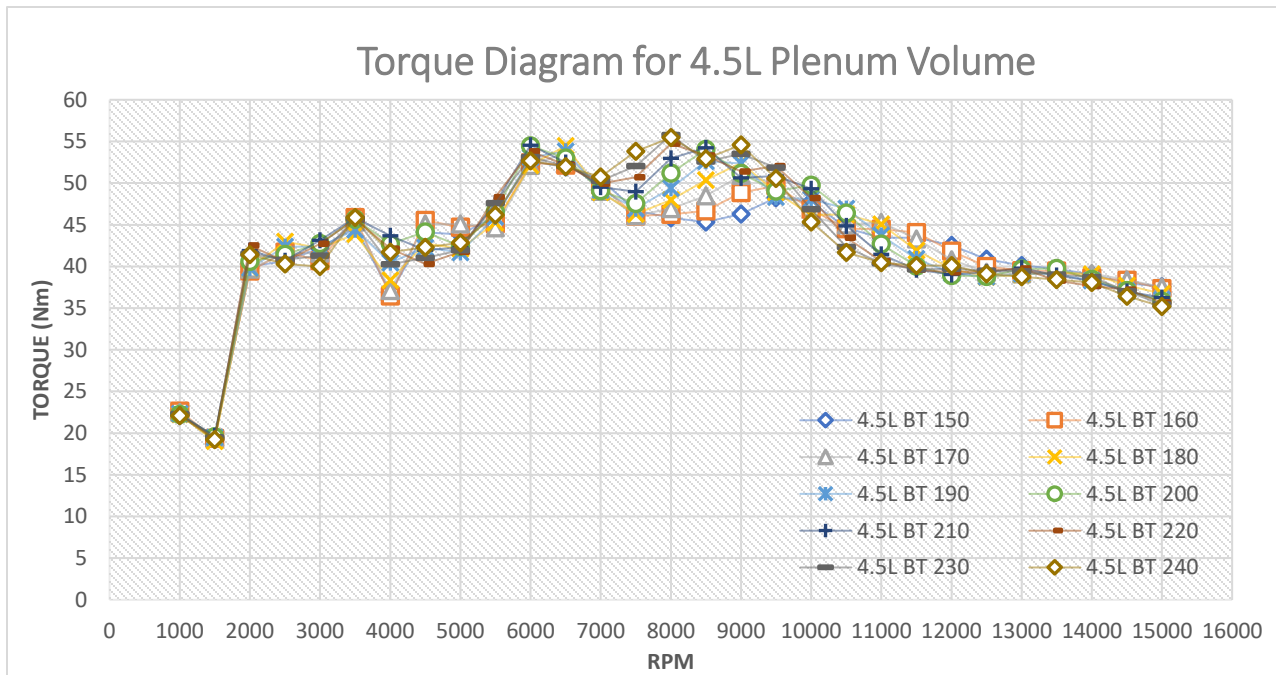


Figure 109 Torque Diagram for 4.5L Plenum and Different Length Runners. The last number refers to the length of the tested runner in mm.

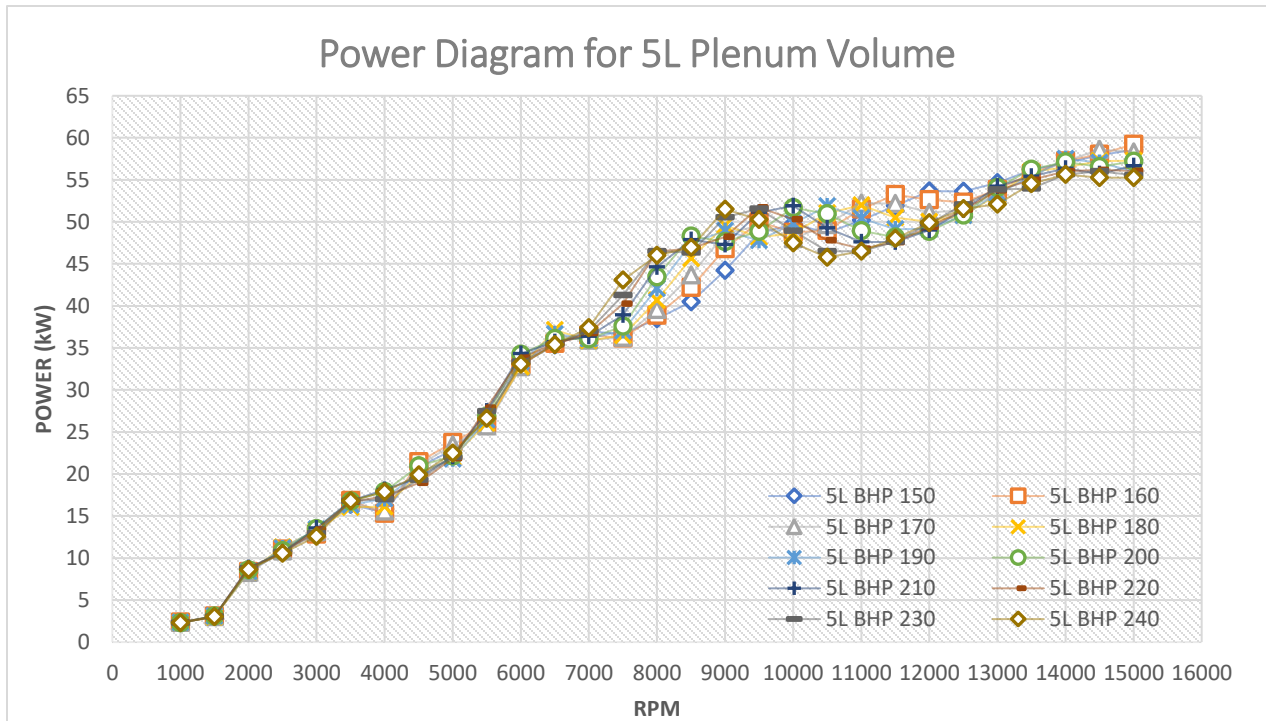


Figure 111 Power Diagram for 5L Plenum and Different Length Runners. The last number refers to the length of the tested runner in mm.

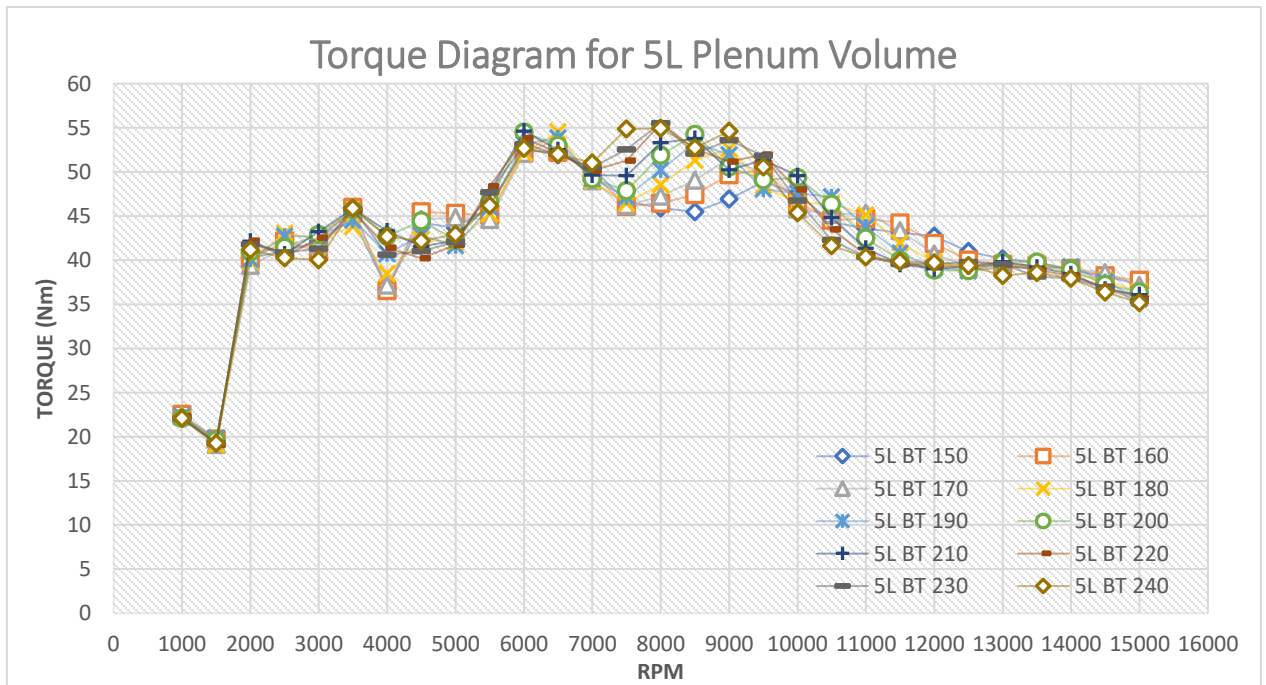


Figure 110 Torque Diagram for 5L Plenum and Different Length Runners. The last number refers to the length of the tested runner in mm.

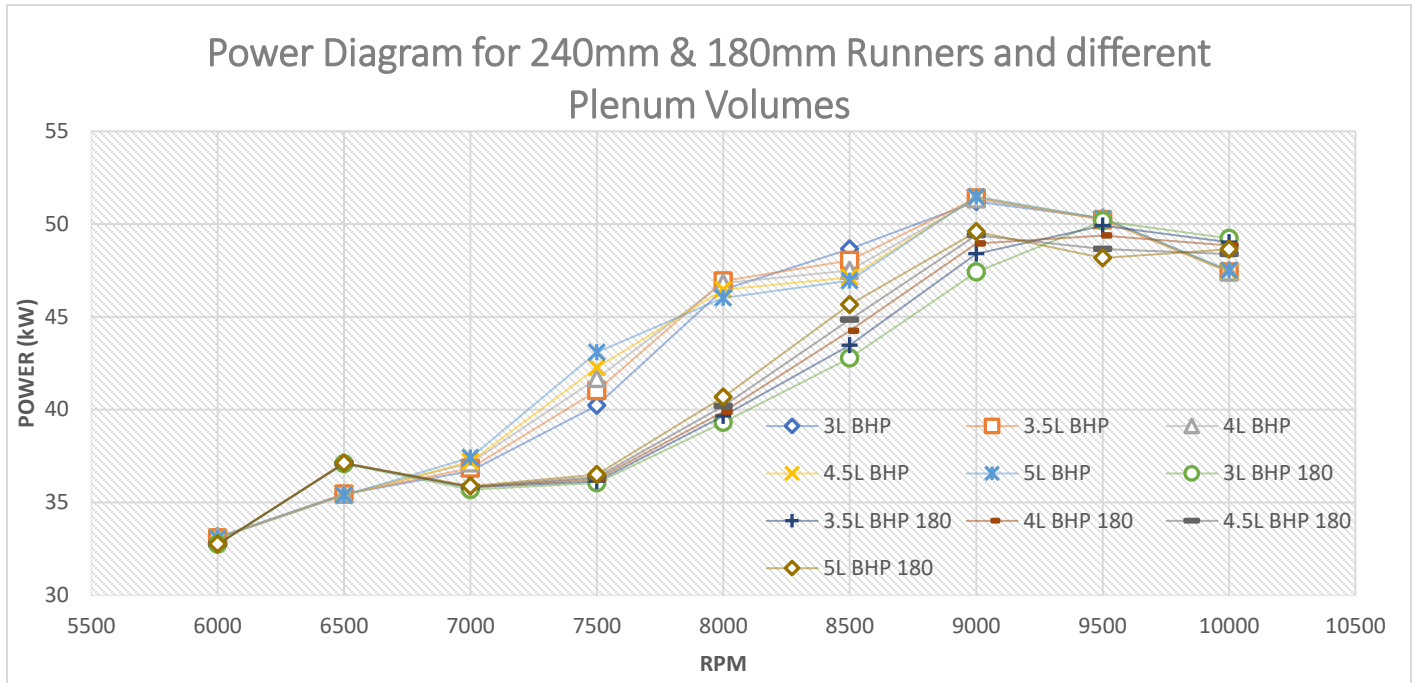


Figure 112 Power Diagram for 240mm and 180mm Runners and Different Plenum Volumes

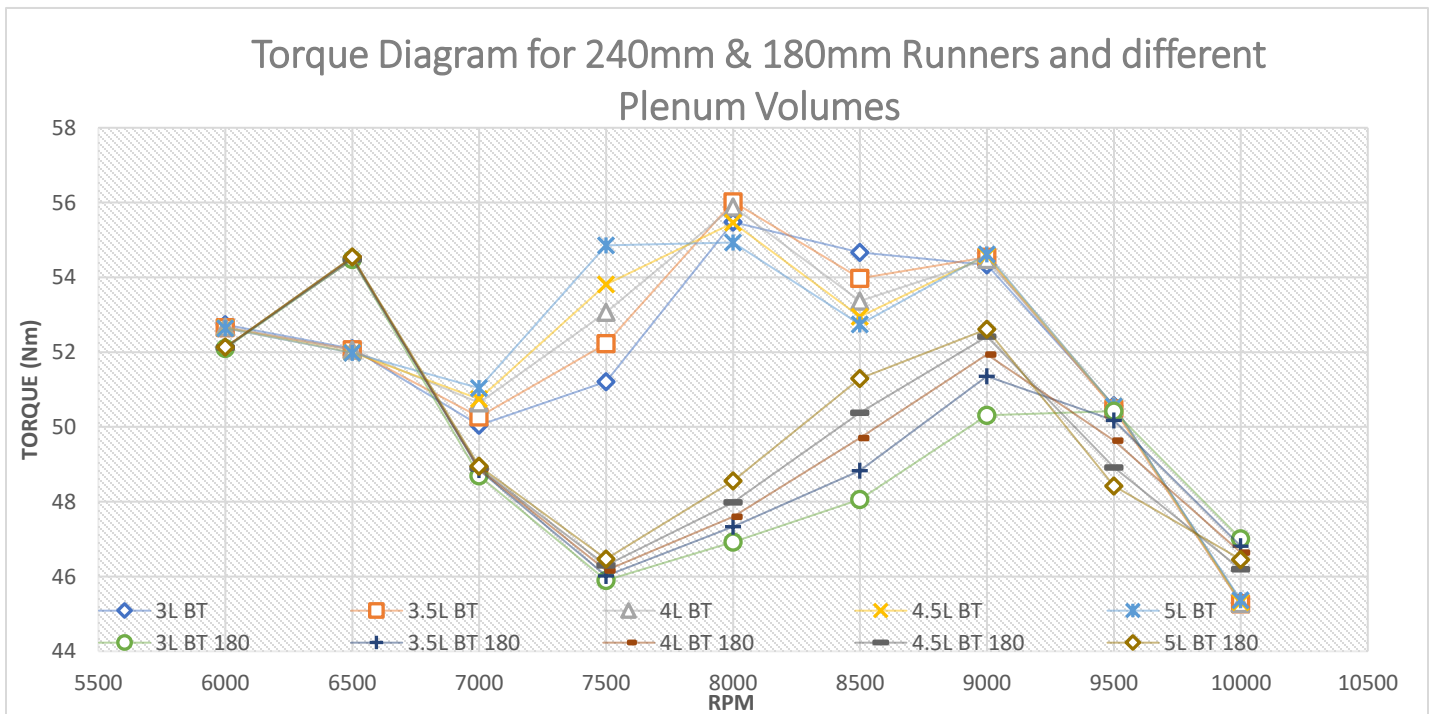


Figure 113 Torque Diagram for 240mm and 180mm Runners and Different Plenum Volumes

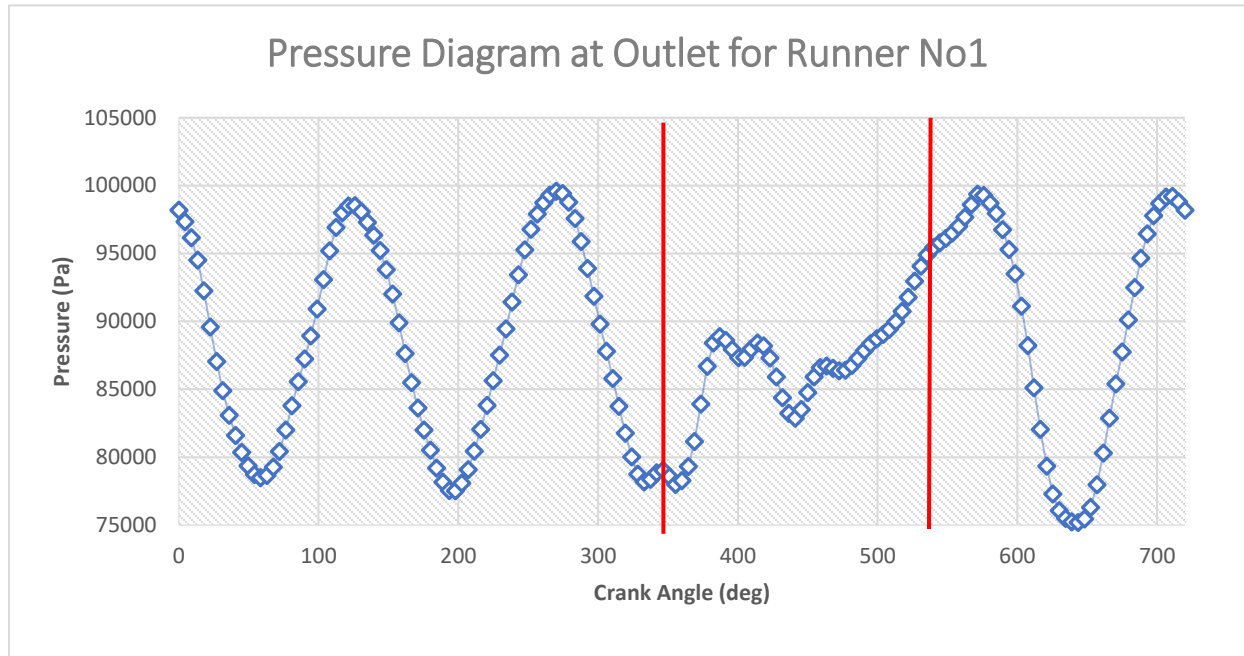


Figure 114 Pressure Diagram at Runner No1. The Red Vertical Lines Indicate the Intake Stroke.

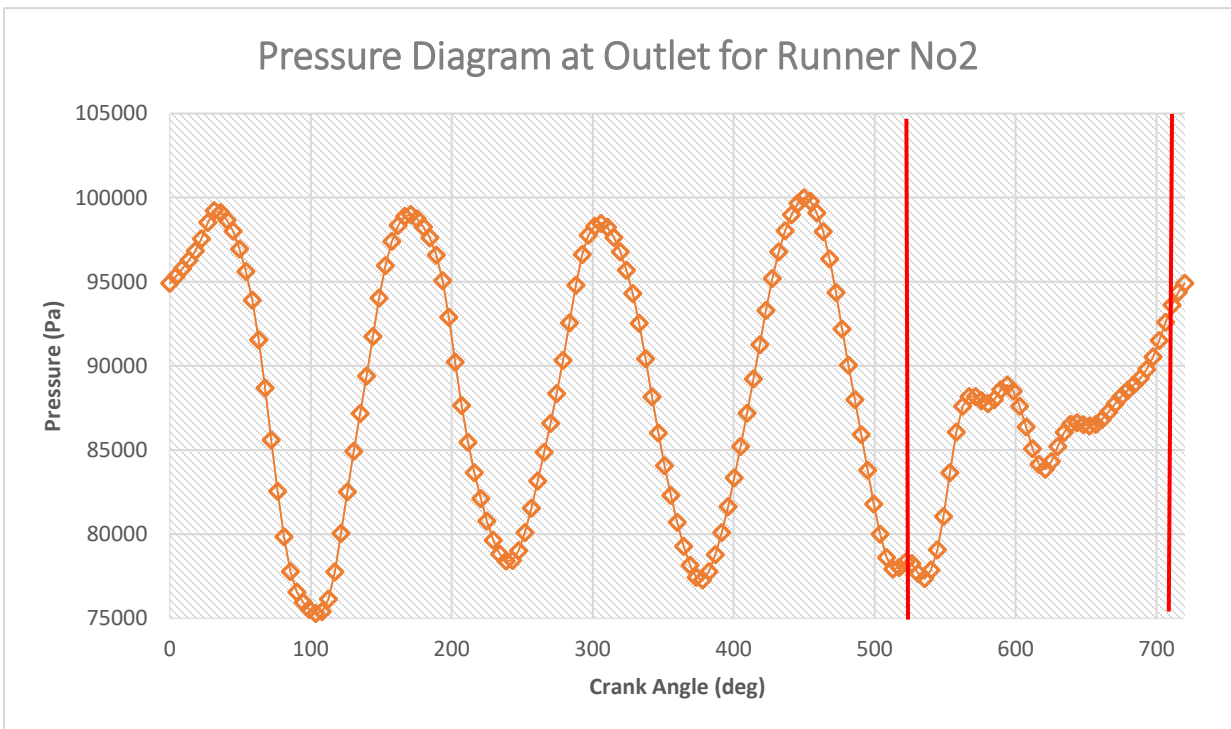


Figure 115 Pressure Diagram at Runner No2. The Red Vertical Lines Indicate the Intake Stroke.

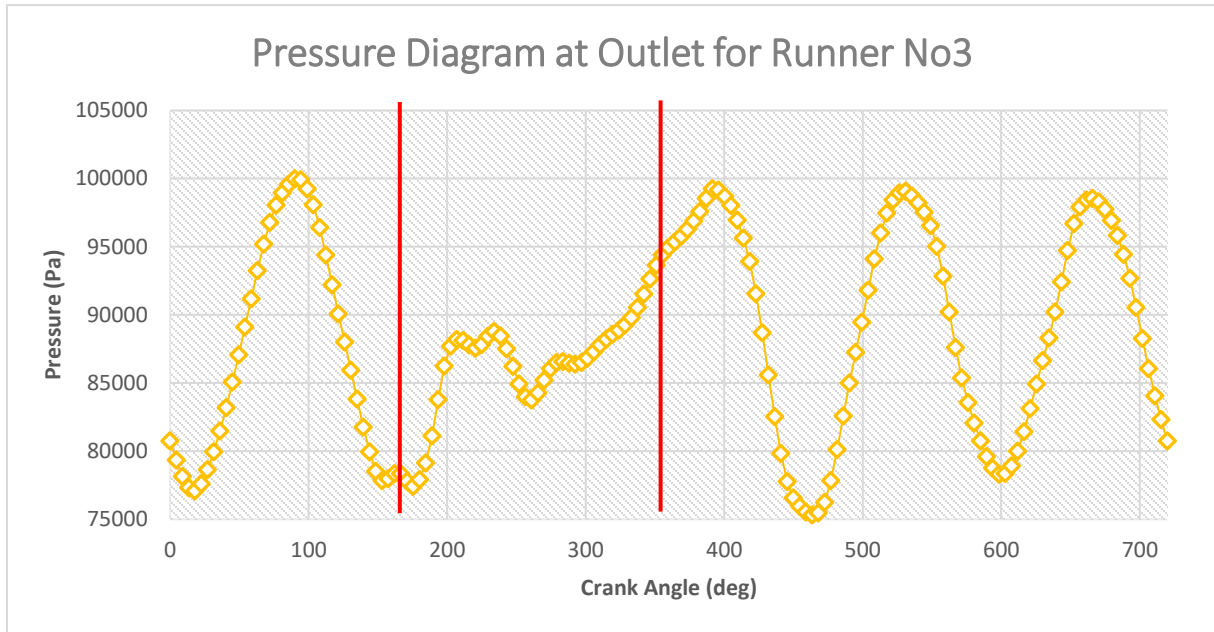


Figure 117 Pressure Diagram at Runner No3. The Red Vertical Lines Indicate the Intake Stroke.

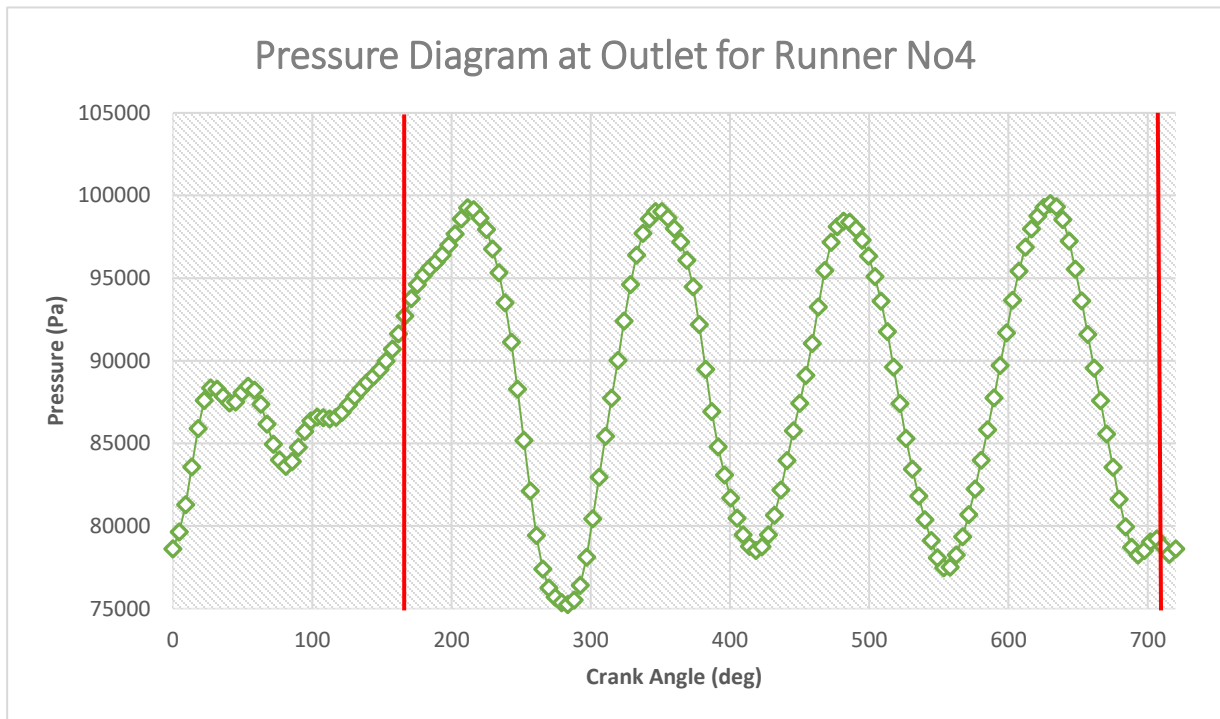


Figure 116 Pressure Diagram at Runner No4. The Red Vertical Lines Indicate the Intake Stroke.

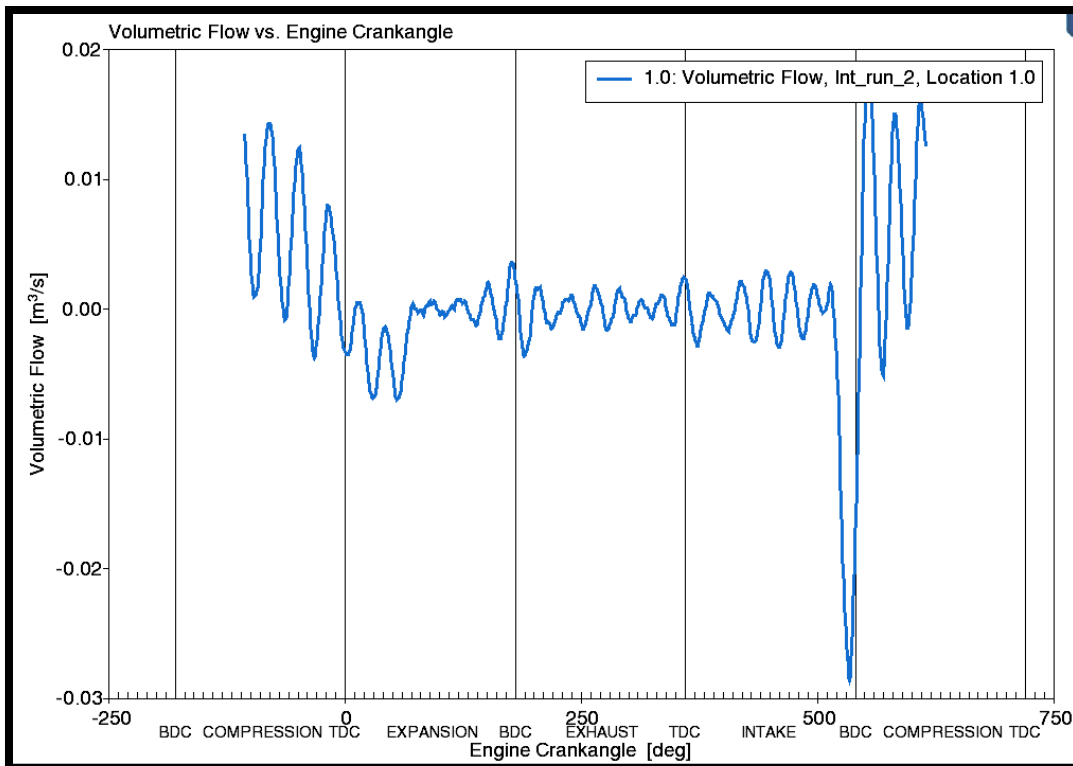
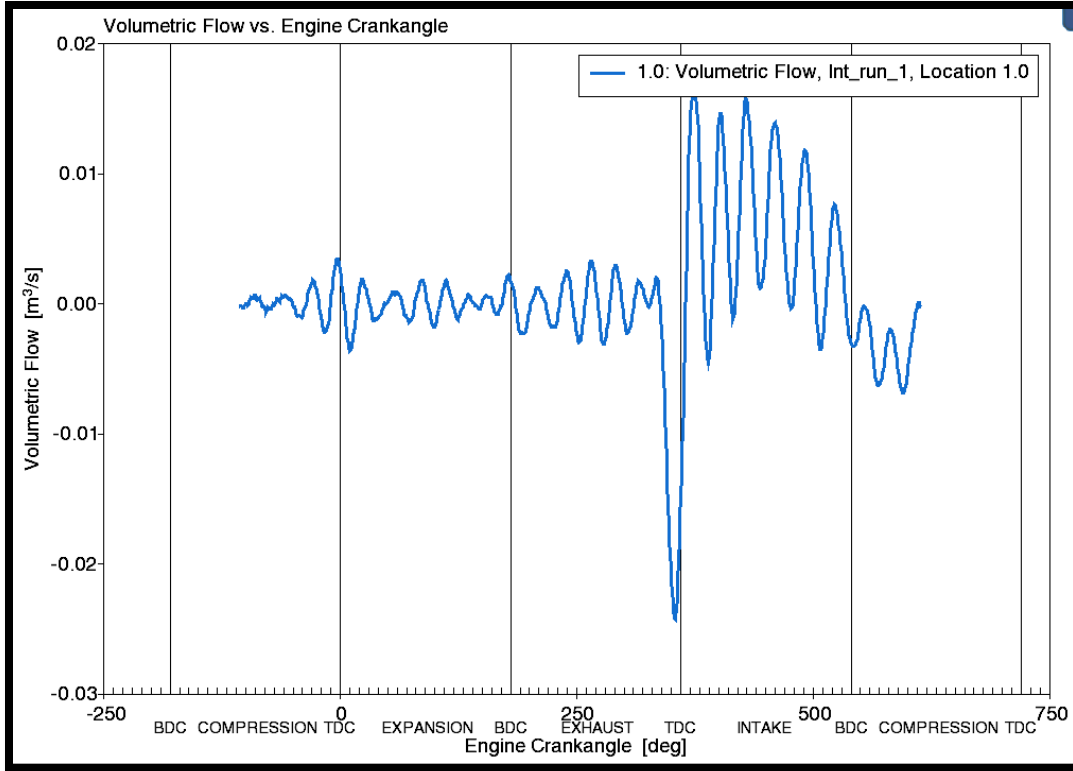


Figure 118 Volumetric Flow vs Crank Angle for Runners 1 (Above) and 2 (Below)

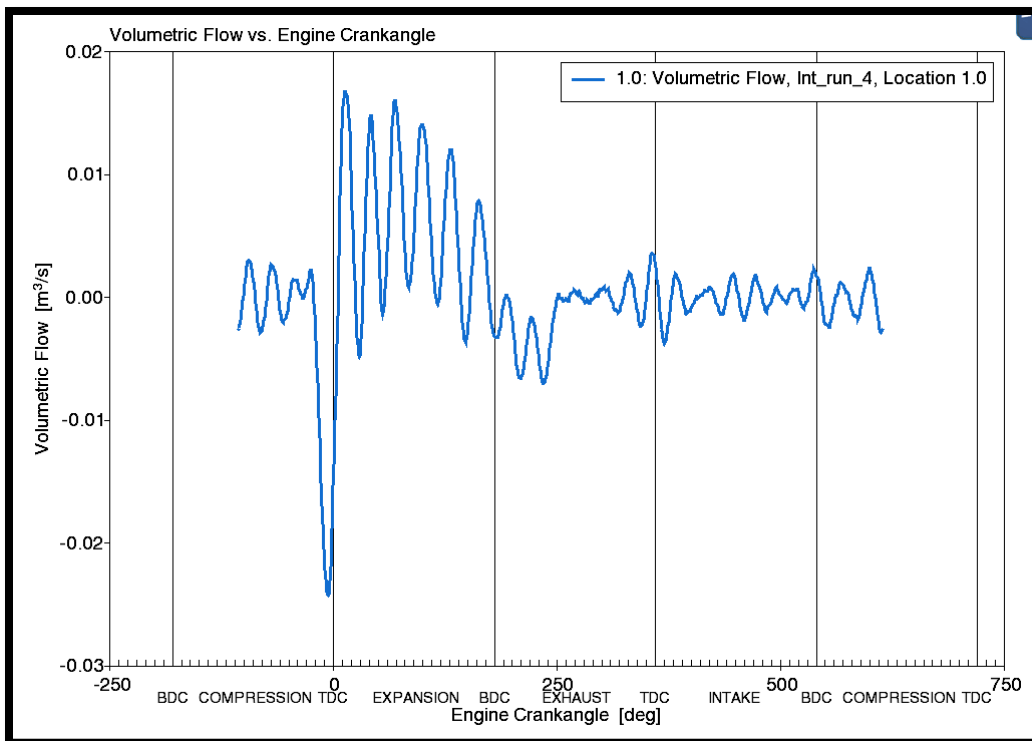
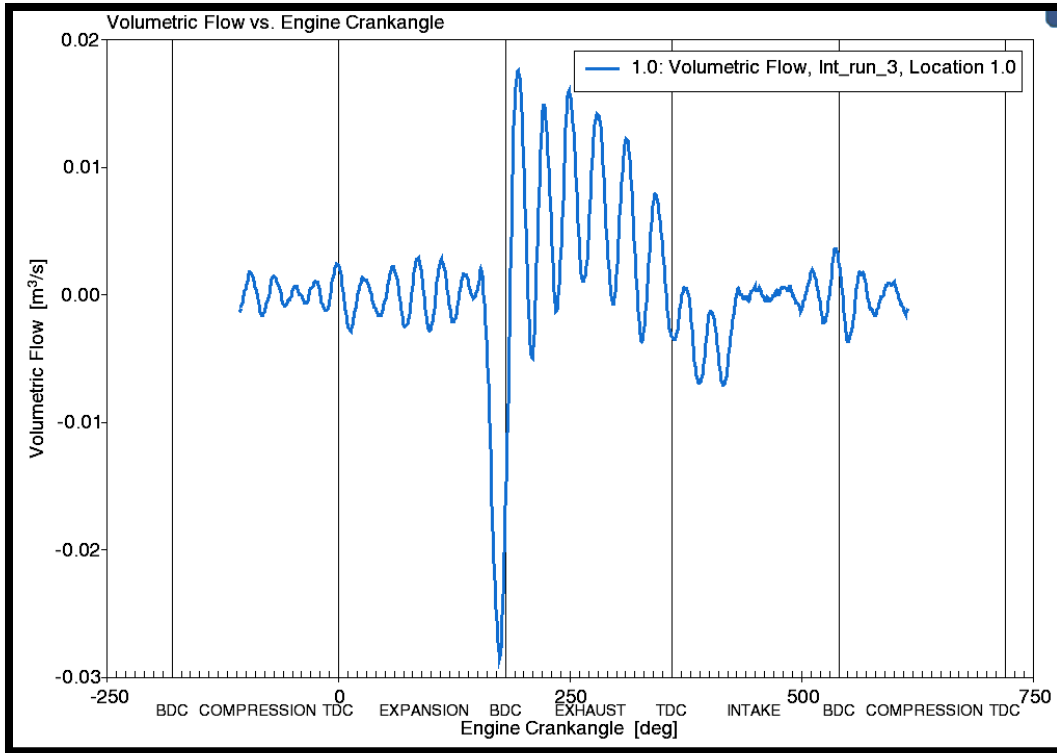


Figure 119 Volumetric Flow vs Crank Angle for Runners 3 (Above) and 4 (Below)



## References

- A. A. Boretti, M. B. (2018). *Numerical Optimization of a Racing*. Bologna, Modena: Society of Automotive Engineers.
- Aaron Khan, D. C. (2014). *Final Report*. Melbourne: University of Melbourne.
- Air-Composition and Molecular Weight*. (n.d.). Retrieved from The Engineering Toolbox:  
[https://www.engineeringtoolbox.com/air-composition-d\\_212.html](https://www.engineeringtoolbox.com/air-composition-d_212.html)
- BCN3D. (2024). *BCN3D-Filaments-Technical-Data-Sheets*. Retrieved from BCN3D:  
<https://www.bcn3d.com/wp-content/uploads/2020/02/BCN3D-Filaments-Technical-Data-Sheet-PAHT-CF15.pdf>
- Formula Student Germany*. (n.d.). Retrieved from Formula Student Germany:  
<https://www.formulastudent.de/about/concept/>
- Formula Student Germany*. (n.d.). Retrieved from FSG:  
[https://www.google.com/url?sa=t&rct=j&q=&esrc=s&source=web&cd=&ved=2ahUKEwiT-8DUuPGDAxVt9gIHHZ8KABIQFnoECAOQAQ&url=https%3A%2F%2Fwww.formulastudent.de%2Ffileadmin%2Fuser\\_upload%2Fall%2F2023%2Frules%2FFS-Rules\\_2023\\_v1.1.pdf&usg=AOvVaw185zAHRDCYAPo6LnIj4r5e](https://www.google.com/url?sa=t&rct=j&q=&esrc=s&source=web&cd=&ved=2ahUKEwiT-8DUuPGDAxVt9gIHHZ8KABIQFnoECAOQAQ&url=https%3A%2F%2Fwww.formulastudent.de%2Ffileadmin%2Fuser_upload%2Fall%2F2023%2Frules%2FFS-Rules_2023_v1.1.pdf&usg=AOvVaw185zAHRDCYAPo6LnIj4r5e)
- Gilani, R. (2012). *Engine Simulation Model for a Formula SAE Race Car*. SE-971 87 Luleå Sweden: Department of Engineering Sciences and Mathematics Division of Product and Production Development Luleå University of Technology.
- Heywood, J. B. (1988). *Internal Combustion Engine Fundamentals*. R. R. Donnelley & Sons Company .
- Heywood, J. B. (2021). *Βασικές Αρχές Μηχανών Εσωτερικής Καύσης*. Athens: Εκδόσεις Παπασωτηρίου Επιστημονική Επιμέλεια Ανδρέας Θεοδωρακάκος .
- Hosein, F. (2016). *Modelling, Simulation and Validation of a Top/Central-Fed Air-Intake System for a FSAE Restricted 600cc Four-Stroke Engine*. London: City University.
- HP Development Company, L. (2017, November). *Cimquest Resource Center* . Retrieved from Cimquest-inc: <https://cimquest-inc.com/resource-center/HP/Materials/HP-PA12-Datasheet.pdf>
- Kori Lutenbacher, B. M. (2012). *FSAE Engine Selection: Four or One Cylinder*.
- Len Hamilton, J. S. (January 2009). *The Effects of Intake Plenum Volume on the Performance of a Small Naturally Aspirated Restricted Engine*. Lucerne, Switzerland: Journal of Engineering for Gas Turbines and Power.
- Mark Claywell, D. H. (2006). *Investigation of Intake Concepts for a Formula SAE Four Cylinder Engine Using 1D/3D (Ricardo WAVE-VECTIS)*. Twin Cities: University of Minnesota.
- MotorCycleSpecs*. (n.d.). Retrieved from YamahaR62006:  
[https://www.motorcyclespecs.co.za/model/yamaha/yamaha\\_r6%2006.htm](https://www.motorcyclespecs.co.za/model/yamaha/yamaha_r6%2006.htm)

*Poseidon Team*. (n.d.). Retrieved from Poseidon Team: <https://poseidonteam.gr/Distinctions-en.html>

*Realis Reaching net zero emissions*. (2023). Retrieved from Realis-simulation: <https://www.realis-simulation.com>

*Realis Simulation*. (2023). Retrieved from Wave- combustion and emissions: <https://www.realis-simulation.com/products/wave/wave-combustion-and-emissions/>

*Realis Simulation announced as the new name for Ricardo Software*. (2022, November 1). Retrieved from Realis-simulation: <https://www.realis-simulation.com/insights/press-releases/realis-simulation-announced-as-the-new-name-for-ricardo-software/>

*SAE International*. (n.d.). Retrieved from FORMULA SAE:  
<https://www.fsaeonline.com/page.aspx?pageid=c4c5195a-60c0-46aa-acbf-2958ef545b72>

*SAE International* . (n.d.). Retrieved from SAE International : <https://www.sae.org/about/>

SGSash. (2013). *What is Horsepower? Torque? An Explanation You Can Actually Understand*. Retrieved from ONPOINT DYNO + RACE SERVICE: <https://www.onpointdyno.com/what-is-horsepower-torque-an-explanation-you-can-actually-understand/>

Singh, A. P. (May 2014). *Intake Manifold Design Using Computational Fluid Dynamics*. PUNJAB (INDIA): LOVELY PROFESSIONAL UNIVERSITY.

*Types of 3D printers - 3D printing technology*. (2024, February 23). Retrieved from All3dp.com: <https://all3dp.com/1/types-of-3d-printers-3d-printing-technology/>

*Wikipedia*. (n.d.). Retrieved from Formula Sae: [https://en.wikipedia.org/wiki/Formula\\_SAE](https://en.wikipedia.org/wiki/Formula_SAE)

Wilson, S. (2019). *Design and Manufacture of an SLS Printed Intake Using ETC for FSAE*.

*Yamaha*. (n.d.). Retrieved from Yamaha: <https://www.yamahapubs.com/>

*YAMAHA R6 (2006 - 2007) Review*. (n.d.). Retrieved from MotorCycleNews:  
<https://www.motorcyclenews.com/bike-reviews/yamaha/r6/2006/#specs>

*Yamaha R6 2006-2007*. (n.d.). Retrieved from Motoperf.com:  
<https://motoperf.com/motorcycles/Yamaha-R6-2006-143545>

*Yamaha YZF-R6 Top Speed & Acceleration*. (n.d.). Retrieved from Motostatz:  
<https://motostatz.com/yamaha-ymzf-r6-acceleration/>

Γεώργιος, Ζ. (2024, April 22). *Geartech Engineering*. Retrieved from Geartech Engineering  
Δυναμομετρήσεις: <https://www.geartech.gr/geartech-content.asp?nid=12>

Καββαθάς, Κ. (2006-2008). Retrieved from Καββαθάς WebSite:  
[https://www.kavvathas.gr/show.php?cat\\_id=148&page\\_id=736](https://www.kavvathas.gr/show.php?cat_id=148&page_id=736)

Λιαμπας, Σ. (2012). *Πειραματική Διευρυση Χαρακτηριστικών Λειτουργίας Κινητήρα FSAE*. Θεσσαλονίκη.

Λώρενς, Β. Α. (2011). *ΣΧΕΔΙΑΣΜΟΣ ΚΑΙ ΚΑΤΑΣΚΕΥΗ ΜΟΝΟΘΕΣΙΟΥ ΑΓΩΝΙΣΤΙΚΟΥ ΟΧΗΜΑΤΟΣ ΠΡΟΔΙΑΓΡΑΦΩΝ FORMULA SAE*. ΑΘΗΝΑ: ΕΘΝΙΚΟ ΜΕΤΣΟΒΙΟ ΠΟΛΥΤΕΧΝΕΙΟ.

Μαρινόπουλος, Ν. Ι. (2012). *Caroto*. Retrieved from Ισχύς & ροπή, παράλληλοι βίου... [blog]:  
<https://www.caroto.gr/2012/05/13/power-torque-internal-combustion-engine/>

Μιλτιάδης, Χ. Ν. (2011). *Μοντελοποίηση και σχεδιασμός κινητήρα οχήματος formula SAE*. Θεσσαλονίκη.